NANOSTRUCTURED MATERIALS BASED ELECTRODES FOR BIOFUEL CELLS

Xing-Hua Xia, Yan-Yan Song, Cui-Hong Wang and Jin-Hua Yuan*

Key lab of Analytical Chemistry for Life Science, Department of Chemistry, Nanjing University, Nanjing 210093, China

Introduction

Combination of biologically active components (enzymes, antibodies, nucleic acids and cells) with nanomaterials with unique properties has been promising for biosensing, genome analysis, bioelectric devices, biofuel cells. [1,2] To realize these applications, high stability and function density of the immobilized biologically active components are usually required. We recently focused on the preparation and characterization of biointerfaces based on assembly of nanostructured materials with rigid structure, good conductivity, good biocompatibility and larger active surface area. Glucose oxidation and direct electron transfer of hemoglobin were used as model to demonstrate importance of such materials for construction of functional electrodes for glucose biosensor and biofuel cells with high function density.

Experimental

Biocompounds (Sigma) were used without further purification. All the other chemicals were of analytical grade. Solutions were prepared with distilled water (>18 MΩ, Purelab Classic Co., USA).

All electrochemical experiments were carried out on a CHI650 Electrochemical Workstation (CH Instrument, U.S.A.). A traditional three-electrode system involving a Pt sheet as counter electrode, a saturated calomel electrode (SCE) as reference, and an ordered macroporous noble metal film (Pt or Au) as working electrode was used. The geometric area of the working electrode was controlled by a Viton O-ring and determined to be 0.19 cm^2. All potentials in this paper refer to the SCE.

Morphology of the 3D Au films was examined on a scanning electron microscope (Hitachi SEM-X650, Hitachi Ltd., Tokyo, Japan) at an acceleration voltage of 20 kV. High-resolution SEM micrographs (HRSEM) were also measured on a Semi-in-lens Field Emission SEM-4700 (Hitachi, Japan). Structural characterization was performed by means of X' Pert Pr X-ray diffraction (Philips). Attenuated total reflection (ATR) spectra were recorded on a Tensor 27 Fourier transform infrared spectrometer (Bruker, Germany) equipped with a multi-reflection ZnSe prism and a DTGS detector.

Preparation of ordered noble metal Macroporous Film electrodes. Monodispersed SiO_2 spheres were synthesized on the basis of Stöber method. [3] The vertical deposition technique [4] was used to self-assemble the silica spheres on gold/Cr/glass slides, forming (111) close - packed crystals. Before metal deposition, the silica colloidal crystals were sintered at 200 °C under nitrogen atmosphere for 2 h. Then, the silica template was immersed into a solution containing gold or platinum salt for 1h prior to electrolyzing in order to allow the solution to penetrate throughout the template. Using the silica template on gold slides as the working electrode, electrochemical deposition of gold in the spaces between silica beads was carried at 0.3 V (vs. SCE) until the required charge has been passed. This deposition potential was chosen to guarantee that the deposition be realized within the interspaces of the silica template without damaging its highly ordered structure. Thickness of the macroporous metal films was controlled by the charge used during the electrodeposition step. After the deposition, the silica template was etched for ca. 5 min using 5% aqueous HF to leave behind a highly ordered macroporous metal film. These films were characterized with AFM or SEM. Electrochemical cleaning of the electrode was performed using cyclic potential scan in a solution of 0.5 M H_2SO_4 at a scan rate of 100 mV/s. From the hydrogen region for Pt or the reduction peak for Au materials, the active surface areas were measured by assuming that a monolayer of AuO requires 0.386 mC or a monolayer of H_{ad} requires 0.21 mC per square centimer.[5,6]

Results and Discussion

The prepared platinum or gold macroporous film is of similar structure consisting of interconnected periodic hexagonal array of monodispersed pores. **Figure 1** shows the film structure of the 3D macroporous Pt film. X-ray diffraction result showed that the macroporous catalyst mainly consisted of (111) and (200) crystalline orientations. The average particle size of the Pt deposited in 200 nm hole size was calculated to be ca. 5.36 nm from a (111) X-ray diffraction peak of Pt fcc lattice in terms of the Scherrer equation. By controlling the deposition time, we obtained 3D macroporous Pt films with different surface roughness factor (R_f: ratio of the real active surface area which can be determined by the charge for hydrogen adsorption to the geometric area).

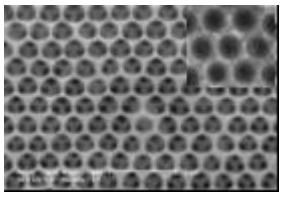

Figure 1. SEM photograph of a 3D macroporous Pt film prepared as described in the text.

The electrocatalytic activity of the Pt film electrode towards the oxidation of glucose in PBS was investigated. As shown in **Figure2**, there are two current peaks for the electrooxidation of glucose. The first current peak should be due to the electrosorption of glucose to form an adsorbed intermediate, releasing one proton per glucose molecule. The second current could be due to the direct oxidation of glucose on the Pt film electrode. In addition, it is clear that the electrocatalytic activity of the Pt film electrodes increases with the decrease in pore size. Understanding of this phenomenon is undertaking.

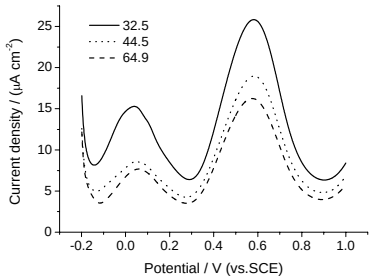

Figure 2. Current density-potential curves of the Pt film electrodes with pore size of 200 nm (solid curve), 320 nm (dotted curve) and 500 nm (dashed curve) in a solution of PBS+50 mM glucose at a scan rate of 2 mV/s.

Due to the high electrocatalytic activity of the Pt film electrode towards the oxidation of glucose, in principle, such electrodes can serve as suitable anode for implantable biofuel cells. In addition, it can be used as glucose sensor for evaluation of the glucose level in human body. Therefore, detection potential and solution PH for glucose sensing using a Pt film electrode with pore size of 200 nm was optimized. It was found that the optimal solution pH and the detection potential are 9.18 and 0.5 V vs SCE, respectively. Further

experiments were performed using 0.05 M phosphate buffer solution at pH 9.18.

Under the above optimal experimental conditions, amperometric response of the 3D Pt film electrode with a pore size of 200 nm is linear in glucose concentration in the range from 10^{-2} mol L^{-1} to 10^{-6} mol L^{-1} with a detection limit of 10^{-7} mol L^{-1} and a sensitivity of 31.3 mA cm^{-2} mM^{-1} estimated at a signal-to-noise ratio of 3, indicating that our sensing material can give higher sensitivity for glucose detection. The response of the normal interferents to glucose detection was evaluated. **Figure 3** shows the response of a 3D inverse opal Pt film electrode (pore size: 200 nm) and a directly deposited Pt electrode to glucose upon addition of 0.2 mM UA, 0.2 mM AP, and 0.1 mM AA. It was found that under the optimal detection conditions, negligible interference form these interferents was observed. The present results showed that increase in surface roughness factors can significantly increases the selectivity for glucose detection. This is due to the fact that the electrochemical reaction for glucose is kinetic controlled, while the reactions of interferents are diffusion controlled. The current for the latter is only determined by the geometric area. While in the former case, the current is significantly enhanced by increasing the real surface area. The results demonstrate that the present 3D inverse opal Pt film electrode is promising for fabrication of non-enzymatic glucose biosensors. In addition, the Pt film electrode can be easily cleaned with modulated potential cycling; they are promising for implantable biofuel cells and glucose biosensors.

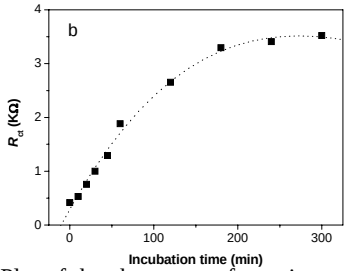

Figure 3. Plot of the charge transfer resistance R_{et} against incubation time. The data were obtained from electrochemical impedance measurements using ferricyanide as probe.

When look at the macroporous film electrode with high resolution SEM, we observed that the structures were consisted of Pt nanoparticles. Such nanoparticles are good biocompatible sites for immobilization of biocompounds, e.g., proteins, enzymes. For this proposes, we fabricated 3D gold film electrode and studied the immobilization and direct electron communication of hemoglobin on the film electrode via the gold nanoparticles as electron relays. Such electrodes have many advantages such as stable structure, high conductivity and high active surface area which is important for obtaining high function density. In addition, the structure provides suitable microenvironment for the immobilization of biocoumpounds whose bioactivity is fully retained. Attenuated Fourier infrared spectroscopic measurements showed that hemoglobin can be easily immobilized on such gold film structure. Appearance of the FTIR features for the secondary structure of the polypeptide chain demonstrates that the immobilized hemoglobin on gold film electrode retains its bioactivity.

We used the sensitive electrochemical impedance technique to probe the adsorption kinetics of hemoglobin (Hb) on gold film electrode using ferricyanide as probe. As shown in **Figure 3**, at the beginning, the Hb coverage increased with the adsorption time almost linearly (<180 min) and then its coverage reached a relative stable value with longer adsorption time (>180 min). This result demonstrated that a saturated monolayer of Hb with coverage of 87.4% was formed at the adsorption of 180 min. This monolayer of Hb on gold film electrode is stable within one month if stored at 4 ^{o}C.

Direct electron transfer between the adsorbed Hb and gold film electrode was characterized with cyclic voltammetry. **Figure 4** shows the cyclic voltammograms (CVs) of a 3D macroporous gold film electrode in PBS with pH 7.0 in the presence (curves b and c) and absence of Hb (curve a). Without Hb in the solution, there is no current peak in the scanned potential window. Addition of 0.2 mg ml^{-1} Hb into the PBS solution, a well-resolved pair of quasi-reversible redox peaks appeared (curve b) due to the direct electron communication of the adsorbed Hb and the gold film electrode. The anodic and cathodic peak potentials located at 0.27 V and 0.09 V (*vs* SCE), respectively. The observed direct electron transfer of the Hb can be due to the fact that the gold nanoparticles of the macroporous gold film electrode are effective adsorption sites that can penetrate easily to the active center of the Hb molecules. In addition, the gold nanoparticles of the macroporous structure would provide multiple adsorption sites for Hb molecules, retaining the bioactivity of the adsorbed Hb. Thus, it is possible to achieve fast direct electron transfer between the heme site of immobilized Hb and the electrode surface. The increased peak current with the increase of Hb concentration (compare curves b and c) demonstrated that more Hb molecules adsorbed on the electrode surface, indicating that concentrated Hb solution facilitated the adsorption of Hb on the electrode surface.

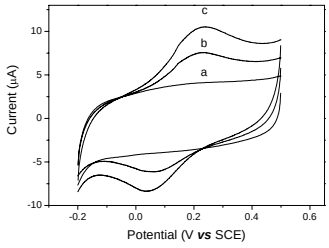

Figure 4. Plot of the charge transfer resistance R_{et} against incubation time. The data were obtained from electrochemical impedance measurements using ferricyanide as probe.

Conclusions

The as prepared 3D macroporous noble metal film electrodes are promising for construction of implantable glucose biofuel cells and glucose biosensor as well. In addition, such structured materials are stable and biocompatible and suitable for construction of bioelectronic devices with high function density via nanoparticles as electron relays for direct electron transfer.

Acknowledgement. This work was supported by grants from the National Natural Science Foundation of China (NSFC, No. 20125515; 20375016; 20299030) and the Doctoral Fund of Education Ministry of China (20020284021).

References

(1) Daniel, M.C.; Astruc, D. *Chem. Rev*. **2004**, *104*, 293.
(2) Shipway, A. N.; Katz, E.; Willner, I. *ChemPhysChem* **2000**, *1*,18.
(3) Stöber, W.; Fink, A.; Bohn, E. *J. Colloid Interface Sci.* **1968**, *26*, 62.
(4) Jiang, P.; Bertone, J. F.; Hwang, K. S.; Colvin, V. L. *Chem. Mater*. **1999**, *11*, 2132.
(5) Kozlowska, H. A.; Conway, B. E.; Hamelin, A.; Stoicoviciu, L. *J. Electroanal. Chem.* **1987**, *278*, 429.
(6) Xia, X. H.; Iwasita, T. *J. Electrochem. Soc.* **1993**, *140*, 2559.

DIRECT METHANOL FUEL CELLS WITH MEDIATED BIOCATALYTIC CATHODES

Nicholas S. Hudak and Scott Calabrese Barton

Department of Chemical Engineering, Columbia University, 500 W. 120th St., Suite 801, New York, NY 10027, Fax: 2128543054, nsh2001@columbia.edu

Abstract

The oxygen-reducing enzyme laccase can be used with a redox polymer mediator as the cathode catalyst in direct methanol fuel cells (DMFC). The biocatalyst has several advantages over precious-metal catalysts, including selectivity and low manufacturing cost. A biocathodic DMFC has demonstrated successful operation with 10 M methanol at the anode and air-saturated buffer solution at the cathode or with a mixed-reactant feed supplied to both electrodes. In order for the biocatalytic cathode to be used in a conventional DMFC, it must operate on gas-phase air. Sufficient catalytic activity, electron and ion transport, and hydration must be maintained in the presence of gaseous reactants. These properties will be studied along with the effect of any added solid electrolyte phase.

FABRICATION AND ELECTROCHEMICAL CHARACTERIZATION OF GLUCOSE OXIDASE-IMMOBILIZED CARBON ELECTRODE

Ying-Ying Horng[1], *Chia-Liang Sun*[2], *Li-Chyong Chen*[2], *Kuei-Hsien Chen*[2,3], *and Chia-Chun Chen*[1,3]

1. Department of Chemistry, National Taiwan Normal University, Taipei, Taiwan
2. Center for Condensed Matter Sciences, National Taiwan University, Taipei, Taiwan
3. Institute of Atomic and Molecular Sciences, Academia Sinica, Taipei, Taiwan

Abstract

We demonstrated the synthesis and related electrochemical properties of enzyme, glucose oxidase (GO_x), modified carbon cloth electrodes which are mediated by gold nanoparticles (Au NPs) in this report. The Au NPs with an average diameter of 4 nm are used as a significant electron relay or mediator for the alignment of the GO_x on the carbon support. Meanwhile, the GO_x is immobilized by flavin adenin dinucleotide cofactor on Au NPs. Therefore, the biological catalysts, GO_x, become much more stable on conductive carbon supports. Moreover, cyclic voltammetry are used to study the electrochemical behavior in a three-electrode system. The results show that immobilized GO_x is able to maintain its specific enzyme activity in the presence of glucose. Furthermore, the dependence of current density and the redox potential in the corresponding reaction is also investigated. As a consequence, under optimal condition, good electrochemical behavior and large current can be achieved, thereby indicating the potential application in biofuel cells.

ELECTRICITY GENERATION FROM FOOD AND ANIMAL WASTEWATERS USING MICROBIAL FUEL CELLS

SangEun Oh[1], Jungrae Kim[1], Booki Min[1], and, Bruce Logan[1,2]

[1]Department of Civil and Environmental Engineering,
[2]The Penn State Hydrogen Energy (H_2E) Center, Penn State University, University Park, PA, 16802, U.S.A.

Introduction

Wastewater containing high-strength organic contaminants is produced daily from industrial, animal, and agriculture procedures. For example, Approximately 20,000 food processing industries in the US annually produce 1.4 billion liters of wastewater (*1*). Agriculture manures are annually generated at 5.8×10^7 ton (*2*). Aerobic wastewater treatment costs can be very high for these wastewaters. However, recent approaches for dealing with these wastewaters not only consider treatment but also generate useful energy such as hydrogen or methane from the organic matter in the wastewater (*3,4*).

Recently, a new technology of using a microbial fuel cell (MFC) has been developed to generate electricity directly from marine sediments, anaerobically digested sludge, and domestic wastewater (*5-11*). Logan (2004; ref. *3*) compared the relative economic potential of hydrogen, methane, and electricity production through MFCs from a single large food processing plant and found that it was most economical when all the organic matter could be recovered directly as electricity in an MFC. A laboratory-scale MFC generated 10 to 16 mW/m^2 based on placing an anode electrode in a marine sediment (anaerobic) and a cathode electrode in the overlying seawater (aerobic) (*5,6,8*). Tender et al. (2002; ref.*7*) obtained over 25 mW/m^2 of power by in situ use of MFCs in marine sediments in the field (*7,8*). Domestic wastewater was also used as the source of a biocatalyst and substrate in MFC operations (*9-11*). A single chamber MFC continuously generated 26 mW/m^2 (maximum power density) while removing up to 80 % COD of wastewater (*9*). Liu et al. (2004; ref. *10*) generated more power (146 ± 8 mW/m^2) using an air-cathode MFC, that lacked a proton exchange membrane, in a batch mode operation. A flat plate MFC generated continuous power of 72 ±1 mW/m^2 at 1.1 h hydraulic retention time (HRT; 0.39 mL/min) with a COD removal rate of 2.4 mg/L-min (42 % removal) (*11*). It is also known that electricity can be generated in MFCs from typical fermentation end products such as acetate and butyrate (*10-13*), but actual waste streams or solutions containing a variety of these chemicals have not been directly tested.

In this study, we investigated the potential of producing electricity from food processing and animal wastewaters using a MFC.

Methods

MFC construction. Electricity generation from food processing and swine wastewaters was measured using two different MFC systems: a two chambered aqueous cathode system, and a one-chambered direct air cathode system. The two-chambered system was constructed by joining two media bottles (310 mL capacity, Corning Inc. NY) with a glass tube containing a proton exchange membrane (PEM; Nafion™ 117) clamped between the flattened ends of the glass tubes fitted with two rubber gaskets (6.2 cm^2 cross section) as described previously (*13*). The surface area of proton exchange membrane was A_{PEM}=6.2 cm^2, and the anode and cathode had equal projected surface areas of $A_{An}=A_{Cat}$=22.5 cm^2. A one-chambered MFC (28 mL capacity) was constructed and operated as previously reported (*10*), and did not contain a PEM (117 Ω external resistance; $A_{PEM}=A_{Anode}=A_{Cathode}$=7.1 cm^2). For both systems, the anode electrode was made of Toray carbon paper (without wet proofing; E-Tek) and the cathode electrode was coated with a Pt catalyst (0.5 mg/cm^2, 10% Pt; De Nora North America, Inc.) on one side. The systems were inoculated with anaerobic dewatered sludge (1g; 85% water content) or swine wastewater. The pH of the wastewaters was adjusted to pH=7.0 using 2M NaOH or 2M HCl. Maximum power density was determined by changing the circuit resistor and measuring power output over a complete batch cycle of operation.

Samples. A wastewater sample was taken from a cereal processing unit at a food processing plant that is known to be high in COD (Cereal). The animal wastewater was collected from the Pennsylvania State University Swine Farm. The wastewater was used to inoculate the chamber without any modifications. Raw or wastewater diluted with ultrapure water (Milli-Q system; Millipore Corp., New Bedford, MA) was used as the medium.

Calculations and analysis. Voltage (*V*) produced by the MFC was measured using a multimeter with a data acquisition system with power (*P=IV)* normalized by the cross sectional area (projected) of the anode. Power (*P*) was calculated according to *P=IV (I=V/R)*, where *I* (A) is the current, *V* (V) the voltage, and *R*(Ω) resistance. The Coulombic efficiency, *E* (%), was calculated as $E=(C_{Ex}/C_{Th})\times100$, where $C_{Ex,}$ is the total coulombs calculated by integrating the current measured at each time interval (*i*) over time as $C_{Ex}=(\sum_{i=1}^{T}V_i t_i)/R$. C_{Th} , the theoretical amount of coulombs that is available from COD (*i*=c) or propionate (*i*=p) oxidation, was calculated as

$$C_{Th}=\frac{F\ b_i\ S_i v}{M_i} \qquad (2)$$

where *F* is Faraday's constant (96,485 C/mol-e$^-$), *b* the number of moles of electrons produced per mol of substrate (b_c=4, b_p=10), *S* the acetate concentration, *M* the molecular weight of the substrate (M_c=32, COD basis; M_p=74.08), and *v* the liquid volume (L). The concentrations of several solvent compounds (acetone, ethanol, propanol, and butanol) and organic acids (acetate, propionate, and butyrate) were determined by gas chromatography (Varian Star 3400) as described previously (*14*). Glucose was analyzed using the phenol-sulfuric acid method for reducing sugars (*15*). Alkalinity, chemical oxygen demand (COD), Total suspended solids (TSS), and ammonia were determined according to Standard Methods (*16*).

Results and Discussion

Food processing wastewater. The in-plant stream obtained from the cereal processing wastewater contained a COD of 8920 (Cereal) mg/L. The diluted wastewater (10×) was first tested for electricity generation using the two chambered MFC. Following inoculation and start up, the reactor was switched to the diluted Cereal wastewater (TCOD=892 mg/L; SCOD=595 mg/L). The voltage increased rapidly to 0.29 V within 5 hr, and voltage was gradually decreased over the next 400 h as the organic matter in the reactor was degraded (Fig. 1A). The maximum power density was 81±7 mW/m^2 of electricity (power normalized to the surface area of the anode carbon paper electrode) during the first 200 h. This power density is close to the maximum believed to be possible with this system. For example, with acetate as the substrate, the maximum power with this system was found to be 88 mW/m^2 (*13*). Coulombic efficiencies were 27.1% and 40.5% based on TCOD and SCOD, respectively. The open circuit potential (OCP) was 776 mV, and the individual electrode potentials (based on a Ag/AgCl reference electrode) were 298 mV and -478 mV for cathode and anode, respectively.

An analysis of the reactor contents during electricity generation demonstrated that sugars were rapidly reduced, resulting in the formation and release into solution of many volatile acids and alcohols typical of fermentation processes. Sugars were reduced within 50 h from 230 mg/L to <20 mg/L (Fig. 1B). The main volatile acid was acetic, which reached a concentration of 166 mg/L followed by propionate. After 50 h of reaction, the concentrations of these two volatile acids slowly decreased over the next 400 h to <20 mg/L.

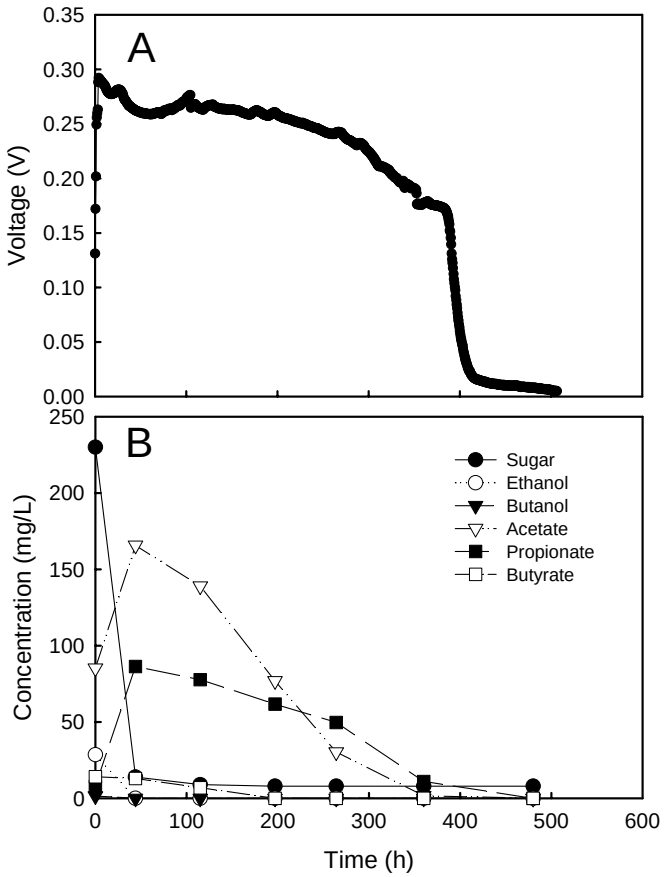

Figure 1. (A) Electricity generation by a two-chambered MFC using cereal wastewater, (B) Sugar, organic acid, and alcohol concentrations in the liquid in the anode bottle over time.(480 Ohm Resistor; liquid Volume: 250 mL; A_{PEM}: 6.2 cm^2 ;A_{Anode}=$A_{Cathode}$: 22.5 cm^2)

A power density curve taken following stable power generation indicated a maximum power density of 371± 10 mW/m^2 (150 Ω resistor). This maximum power density is less than that obtained using glucose (494±21 mW/m^2, ref.*10*) or acetate (506 mW/m^2, ref.*17*) in the same system, demonstrating that breakdown of the organic matter limited power densities generated by the system. However, this maximum power density was much larger than the power achieved using domestic wastewater in this system (28±3 mW/m^2, ref.*9*). It is therefore clear from the experiments with the biohydrogen reactor effluent that hydrogen generation can be successfully linked with electricity generation in a MFC.

Swine wastewater. The raw wastewater had a pH of about 7.1 ± 0.2 (n = 3) and an average chemical oxygen demand (COD) of 8300 ± 167 mg/L (n = 9). Voltage was slowly developed over two weeks after the MFC was loaded with the raw animal wastewater. After two sequential loadings of the wastewater into the chamber, power generation reached a maximum value of 213 mW/m^2 and then stabilized to average of 182 ±1 mW/m (voltage = 357 ±1 mV with 1000 Ω). The initial COD concentration of the animal wastewater of 8320 ±191 mg/L was reduced to 6090 ±60 mg/L (COD removal = 27%; CE = 8%) after 44 hr of operation. From the above results, we realized that bacteria in the animal wastewater were a suitable biocatalyst for generating power and degrading organic matter present in the wastewater. Power generation was measured as a function of different circuit resistances after achieving stable power generation with the 1000 Ω resistor. The circuit resistances loaded between two electrodes ranged from 2 Ω to 200 kΩ. The maximum power density was 261 mW/m^2 (Voltage = 191 mV with 200 Ω) with current density of 1.4 A/m^2.

To investigate if sufficient bacteria attached on the surface of the anode electrode, the anode chamber was filled with autoclaved animal wastewater (diluted by 1/10) for power generation. Power was produced from the sterilized wastewater in a similar manner to that obtained with raw wastewater based on maximum power (82 or 84 mW/m^2 with autoclaved wastewater; 77 or 79 mW/m^2 with raw wastewater). The Coulombic efficiency was about 20 % with raw wastewater, and 17 % with autoclaved wastewater. Thus, microorganisms attached on the electrode clearly were responsible for generating power, and the level of power generation was reproducible.

Acknowledgement. This research was supported by National Science Foundation Grants BES-0331824 and BES-0124674, United States Department of Agriculture grant 68-3A75-3-150, a seed grant from The Huck Institutes of the Life Sciences at Penn State, and the Stan and Flora Kappe endowment.

References

(1) Elitzak, H. Food Marketing, **2000**, 23(3):27-30. http://www.ers.usda.gov/publications/foodreview/septdec00/FRsept00e.pdf
(2) Dentel, S.K., Strogen, B., Sharma, A., and Chiu, P. *Proceedings*, IWA Conference on Resources from Sludge, Singapore March 2-3, **2004**.
(3) Logan, B.E. *Environ. Sci. Technol.* 2004, 38, 160A – 167A.
(4) Angenent, L.T., Karim, K., Al-Dahhan, M.H., Wrenn, B.A., and Domíguez-Espinosa, R. *TRENDS in Biotechnology*, **2004**, in press.
(5) Bond, D.R., Holmes, D.E., Tender, L.M., and Lovley, D.R. *Science* **2002**, 295, 483-485.
(6) Reimers, C.E., Tender, L.M., Ferig, S., and Wang, W. *Environ. Sci. Technol.* **2001**, 35, 192-195.
(7) Tender, L.M., Reimers, C.E., Stecher, III H.A., Holmes, D.E., Bond, D.R., Lowy, D.A., Pilobello, K., Fertig, S.J., and Lovley, D.R. Nat. Biotechnol. **2002**, 20(8), 821-825.
(8) Delong, E.F. and Chandler, P. Nat. Biotechnol. **2002**, 20, 788 - 789.
(9) Liu, H., Ramnarayanan, R., and Logan, B.E. Environ. Sci. Technol. **2004**, 38, 2281-2285.
(10) Liu, H. and Logan, B.E. Environ. Sci. Technol. **2004**, 38, 4040 – 4046.
(11) Min, B. and Logan, B.E. Environ. Sci. Technol. **2004**, 38(21), 5809-5814
(12) Bond, D.R.; Lovely, D.R. *Appl. Environ. Microbiol*. **2003,** *69*, 1548-1555.
(13) Oh, S. E.; Min, B.; Logan, B. E. *Environ. Sci. Technol.* **2004**, 38, 4900-4904.
(14) Logan, B.E., Oh, S.E., Van Ginkel, S.W. *Environ. Sci. Technol.* **2002**, **36** (11), 2530-2535.
(15) Dubois, M., Gilles, K.A., Hamilton, J.K., Rebers, P.A., and Smith F. Analytical Chemistry **1956**, 28(3),351-356.
(16) APHA; AWA; WPCF. American Public Health Association: Washington, DC, **1992**.
(17) Liu, H.; Cheng, S.-A.; Logan, B.E. *Environ. Sci. Technol.* **2005**, *39(2)*, 658-662.

BIOCONVERSION OF CELLULOSE INTO ELECTRICITY USING RUMEN MICROORGANISMS AS BIOCATALYSTS IN A MICROBIAL FUEL CELL

Hamid Rismani-Yazdi, Ann D. Christy, Burk A. Dehority, and Olli H. Tuovinen

Dept. of Food, Agricultural, and Biological Engineering
Ohio State University, 590 Woody Hayes Dr.
Columbus, OH 43210

Introduction

The diversity of biocatalyst microorganisms investigated in microbial fuel cells to date is limited and includes pure cultures such as *Shewanella putrefaciens*, *Escherichia coli*, *Geobacter sulfureducens*, and *Rhodoferax ferrireducens* as well as mixed consortia from municipal and industrial wastewater. Simple sugars, volatile fatty acids, and starch have been used as electron donors.[1] The scope of the study was to investigate the feasibility of using rumen microorganisms as biocatalysts and cellulose as the electron donor in a microbial fuel cell. Cellulose can not be easily dissolved or hydrolyzed under natural conditions due to its complex structure. Microorganisms in rumen of mammalian herbivores have great potential in the biodegradation of cellulosic materials due to their cellulolytic enzymes and their high cellulolytic activities.[2] For this study, rumen microbes and crystalline cellulose were evaluated for electricity production in a microbial fuel cell.

Materials and Methods

Microorganisms. Strained rumen fluid from a canulated cow was used as a biocatalyst. All cultures were incubated at 22±2ºC unless otherwise stated. Cellulose medium contained (per liter) 450 mg K_2HPO_4, 450 mg KH_2PO_4, 900 mg NaCl, 900 mg $(NH_4)_2SO_4$, 119.25 mg $CaCl_2{\cdot}2H_2O$, and 90 mg $MgSO_4$ plus 160 ml clarified rumen fluid (centrifuged for 5 min at 5000 *g*).[3] Crystalline cellulose (7.5 g/l) (Sigmacell-20, Sigma, St. Louis, MO) was ball milled for 24 h before it was used as the sole source of carbohydrate and electron donor. The medium was flushed with O_2-free CO_2. The pH was adjusted to 6.8 with NaOH, 4 g Na_2CO_3 was added, and CO_2 was flushed for an hour before autoclaving in a sealed round bottom flask. To determine the cellulolytic activity of the attached biofilm at the surface of the electrode in the anode compartment, biomass was scraped off and used to inoculate the cellulose media in culture tubes. Tubes were then incubated anaerobically at 39ºC and cellulose degradation was determined by visible decrease of cellulose in the media compare to uninoculated control. Where indicated, bacterial growth was inhibited with 2,000 IU of penicillin-G (Sigma) and 130 IU of streptomycin sulfate (USB Corporation, Cleveland, OH) per ml of media.

Microbial fuel cell and operation. A two-compartment biofuel cell was constructed as described by Bond and Lovley.[4] The working volume of the two chambers was 400 ml with 200 ml headspace. A proton-exchange membrane (Nafion 117; Electrosynthesis, Lancaster, NY) was used to separate anode and cathode compartments. Plain graphite 71 by 49 by 6 mm (83.98 cm^2) was used as the electrode. Chambers were autoclaved prior to the experiment. The anode compartment was gassed vigorously with O_2-free CO_2 passed through a hot copper column and filled with 360 ml cellulose medium and was inoculated with strained rumen fluid (10% vol/vol). The catholyte in the cathode compartment was 400 ml of 50 mM $K_3Fe(CN)_6$ solution in 100 mM K_2HPO_4 buffer flushed with air.[1] The power output of the fuel cell was monitored by measuring the voltage across a known resistance (1000 Ω) using a data acquisition unit. The power density, P (W/m^2) was calculated according to $P=V\times I/A$, where V is the voltage (V), I, ($I=V\times R$) is the current (A), and A is the surface area (m^2).

Results and Discussion

To study the role of rumen microorganisms as biocatalysts in a microbial fuel cell for electricity generation, strained rumen fluid was inoculated (10% vol/vol) anaerobically into the anode chamber. The final volume of anolyte was 400 ml. Cellulose was provided as the sole carbohydrate and electron donor. Electron flow commenced immediately after the inoculation and then declined gradually (**Fig. 1**). When the cell voltage reached below 0.2 V, after 97 h operation, the anolyte was removed and replaced anaerobically with 10 mM acetate and subsequently with fresh cellulose medium followed by reinoculation (10% vol/vol) with strained rumen fluid. Thereafter, the voltage rapidly increased and reached a consistent maximum of 0.58 ± 0.02 V, and a stable power production of 40 mW/m^2 was obtained over a period of about 82 h. At the end of these incubations, the anode was removed from the chamber and attached biofilm was scraped off. Inoculation of the cellulose medium in the culture tube with extracted biomass and its incubation at 39ºC revealed that electrode-attached microorganism were cellulolytic and hydrolyzed cellulose. Visual inspection clearly showed a loss of cellulose during the bioreactor run.

Penicillin and streptomycin were added to the cellulose medium in the anode chamber to inhibit bacterial growth. The effect of the antibiotics on electricity generation is shown in **Fig. 2**. The antibiotic amendment decreased the power output, demonstrating the involvement of bacteria in transferring electrons to the electrode while oxidizing cellulose and metabolites. Since the voltage did not reach the baseline, it was inferred that rumen fungi or bacteria were present that were resistant to the antibiotics. It is possible that anaerobic rumen fungi were involved in electron transfer to the electrode because eukaryotes are not affected by penicillin or streptomycin antibiotics. Microscopic observations of the anode contents from the antibiotic-treated chamber confirmed the presence of zoospores. Further experiments are needed to verify whether rumen fungi can transfer electron to the electrode directly or via secreting electron-transfer mediators. Stirring the anode contents at 300 rpm did affect the electricity production. The voltage obtained in the stirred fuel cell was higher than in the unstirred bioreactor.

Thus this work shows that it is possible to couple degradation of cellulose with generation of electricity, exploiting rumen microbial inoculum in a microbial fuel cell (MFC). By exploiting rumen microorganisms as biocatalysts in a mediator-less MFC, it was possible to generate as much as 40 mW/m^2 with cellulose as the substrate. Cellulose is a linear polymer of glucose connected through β-1,4-linkages and is usually arranged in microcrystalline structures which can be difficult to dissolve or hydrolyze under natural conditions. These results suggest that rumen microorganisms can generate electricity, evidence for the potential of rumen microorganisms as biocatalysts in microbial fuel cells while degrading cellulosic wastes.

Power generation was directed by both electrode-attached and suspended microorganisms. No external mediator was used in these experiments. These results add to the diversity of biocatalysts that can be used in microbial fuel cell applications. More research is needed to determine the optimal bioprocess conditions for these microorganisms to enhance their maximum power density outputs.

Acknowledgements

Partial support for this work was received from the Ohio Agricultural Research and Development Center, College of Food, Agricultural, and Environmental Sciences, at the Ohio State University.

References

1. Rabaey, K.; Boon, N.; Siciliano, S. T.; Verhaege, M.; Verstraete, W. *Appl. Environ. Microbiol.*, **2004,** *70*, 5373-5382.
2. Hu, Z.; Wang, G.; Yu, H. **Biochem. Eng. J.**, **2004**, *21*, 59-62.
3. Dehority, B.A., Rumen Microbiology, Nottingham University Press: Nottingham, U.K., **2003**.
4. Bond, D.R.; Lovley, D.R. *Appl. Environ. Microbiol.*, **2003**, *69*, 1548-1555.

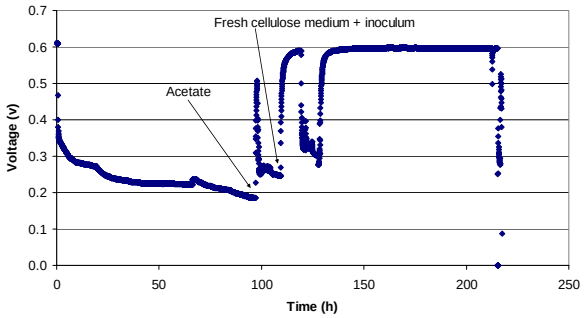

Figure 1. Electricity generation with rumen microorganisms. The bioreactor contained 7.5 g cellulose/l and 10% (vol/vol) strained rumen fluid as inoculum at pH 6.8 and at 22±2°C. At 97 h, 10 mM acetate was added. The anode solution was replaced with fresh cellulose media and inoculum at 110 h. The experiment was terminated at 215 h.

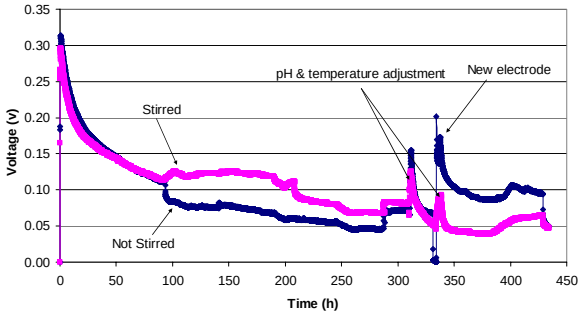

Figure 2. Electricity generation with rumen microorganisms. Initially, two bioreactors contained 7.5 g cellulose/l and 10% (vol/vol) strained rumen fluid as inoculum at pH 6.8 and at 22±2°C. The media contained penicillin-G 2,000 IU/ml and streptomycin 130 IU/ml. Stirring (300 rpm) was introduced to one bioreactor at 93 h. The pH was adjusted from 5.6 to 6.8 and the temperature was increased to 39°C at 310 h and 332 h. The anode was replaced with a new electrode at 332 h.

Biological Fuel Cells Exploiting the in situ Oxidation of Hydrogen Synthesized via Heterotrophic, Photo-heterotrophic and Photosynthetic Microbiological Activity

Uwe Schröder, Miriam Rosenbaum, Juliane Niessen, Falk Harnisch, Fritz Scholz*

Institut für Chemie und Biochemie, Universität Greifswald, Soldmannstr. 16, 17489 Greifswald, Germany

Introduction

To exploit the metabolic activity of microorganisms for electricity generation basically two major approaches can be followed, (i) the production of biohydrogen and biogas[1-3] combined with the subsequent conversion to electricity in conventional fuel cells or via combustion, and (ii) the direct electricity generation in microbial fuel cells.[4-6] Biofuel cells mostly exploit hetero-fermentative and metal-reducing microbes as biocatalysts. For biohydrogen production dark fermentative (e.g., *Clostridia*) as well as phototrophic hydrogen producing microorganisms (green algae, non-sulfur purple bacteria and cyanobacteria) are used. Our work aims to combine these approaches by means of microbial fuel cells that exploit heterotrophic (dark fermentation), photo-heterotrophic (photo-fermentation) or purely photosynthetic hydrogen synthesis for direct electricity generation via the in situ oxidation of the microbially produced hydrogen. Such integration shows a number of potential advantages. Thus, the combustion of biohydrogen in a conventional fuel cell requires the gas to be separated from the biomass, as well as its extensive purification. The separation of the hydrogen gas from microbial cultures is considered to be an important issue since large fractions of the gas remain dissolved in the microbial medium – promoting the possible growth of hydrogen consuming microorganisms and thus lowering the hydrogen yield. Additionally, high hydrogen partial pressures are known to limit the microbial hydrogen synthesis, which may act as a negative feedback inhibition of hydrogen production. A proposed method for the hydrogen removal is the purging with an inert gas, e.g., nitrogen. This procedure, however, is expensive and produces highly diluted hydrogen. With the concept of the direct electrochemical depletion of hydrogen from the bacterial solution by the implementation of electrocatalytic anodes into the microbial cultures these issues can be circumvented. It requires, however, the development of anodes that are resistant against biofouling and deactivation in the complex microbial environments. In 2003, we have presented a novel microbial fuel cell concept that is based on the anaerobic decomposition of glucose by *Escherichia coli*. Current densities much above all known systems have been reached.[7] The achievement is based on an anode composed of a layered composite consisting of platinum, allowing the electrocatalytic oxidation of hydrogen, overlaid by the conductive polymer polyaniline (PANI) that prevents poisoning and that also shows catalytic activity towards fuel oxidation. The further improvement of the anode concept and its adaptation to different microbial and substrate conditions has led to the development of a range of composite materials that allow higher stability and higher performance than the original Pt-PANI.[8] For the studies of the present communication, the following composites were used: Pt-Poly(tetrafluoroaniline) (**Pt-PTFA**), and Pt-Poly(3,4-ethylenedioxythiophene) (**Pt-PEDOT**)

One disadvantage using dark fermentation for hydrogen production and electricity generation is the incomplete substrate oxidation combined with the formation of organic acids (e.g., lactate, acetate, formate, succinate, propionate, butyrate) and alcohols. This limits the maximum substrate conversion efficiency to 4 mol hydrogen per mol glucose. Photo-heterotrophic non-sulfur purple bacteria may help solving this problem and increasing the substrate conversion efficiency, since they use the remaining organic acids as resource for photobiological hydrogen production in a second step utilizing dark-fermentation products (as illustrated in Scheme 1). With such a two-step MFC an increased hydrogen (and thus coulombic) yield is possible.[9]

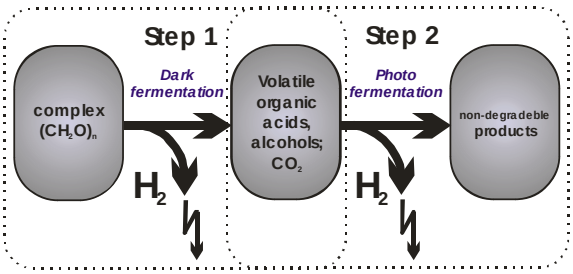

Scheme 1. Schematic illustration of the application of fermentation and photo-fermentation in a two-step microbial fuel cell system

Experimental

Metabolic analysis. Metabolic substrate diminution and non-gaseous fermentation product formation were followed using HPLC. The HPLC was equipped with a Rezex™ ROA-Organic Acid column in combination with the SecurityGuard™ cartridge AJO-4490. The chromatograms were recorded with 0.005 N sulfuric acid as the eluent; the detector was a differential refractometer. CO_2 and H_2 quantification was performed volumetrically, the separation of H_2 from CO_2 being achieved by absorption of CO_2 in NaOH solution.

Electrode preparation. For anode preparation, platinum mesh electrodes, platinum sheet electrodes, carbon cloth or paraffin impregnated graphite electrodes were electrochemically platinized in a stirred acidic solution containing 20 mM H_2PtCl_6 (Fluka) at a potential of –0.6 V for 500 s. The electrodes were subsequently coated with conductive polymers, e.g., polyaniline (Pt-PANI), poly(tetrafluoroaniline) (Pt-PTFA) or poly(3,4-ethylenedioxy-thiophene) (Pt-PEDOT) using oxidative electro-polymerization.

Electrochemical instrumentation. Two types of electrochemical experiments were used in this study for potentiostatically controlled and fuel cell experiments. For the potentiostatic experiments sealed (and for photobiological experiments illuminated) glass jars served as electrochemical cells hosting a working electrode, a reference and a counter electrode in a conventional three-electrode arrangement. The counter electrodes were graphite rods separated from the bacterial solution by a Nafion 117 perflourinated membrane. Silver | silver chloride electrodes, sat. KCl, 0.195 V vs. SHE, served as reference electrodes. The experiments were carried out using PGSTAT 20 and 30 potentiostats (Ecochemie, Netherlands). For the current measurement a permanent potential of 0.2 V was applied to the working electrode in order to oxidize microbial hydrogen under conditions similar to those present in a microbial fuel cell. Control experiments confirmed that varying the applied potential between 0.1 and 0.3 V did not noticeably affect the experimental results. Fuel cell experiments were carried out using a self-made simplified fuel cell models. The monitoring of redox potentials and currents under different external resistance loads was performed with a data acquisition system (Keithley Integra 2700 digital multimeter equipped with 7700 multiplexer, Keithley Instruments, Inc., Cleveland, USA) interfaced to a personal computer. The fuel cell setup was thermostatically controlled.

Results and Discussion

Dark fermentative processes that involve the microbial production of hydrogen from various substrates were used for electricity generation. As biocatalyst either single strains (e.g., *Escherichia coli* for glucose fermentation, *Clostridium butyricum* and

Clostridium beijerinckii for starch and molasses fermentation, or *Clostridium cellulolyticum* for cellulose fermentation), or microbiological consortia, isolated from heat-treated soils, were exploited. Whereas the use of single strains usually requires a careful selection of suitable microbe–substrate combinations, bacterial consortia allow flexible substrate utilization. Additionally, such consortia are generally more robust than cultures of single strains.

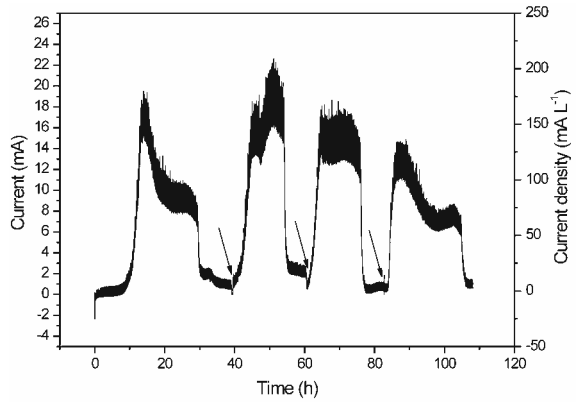

Figure 1. Current generation (semi batch) in a culture inoculated with heat-treated soil. Anode: Pt-PTFA composite (Mesh electrode, 100 cm^2). Substrate: glucose. E_{anode}= 0.2 V.

For the in situ hydrogen oxidation we currently use layered composite materials consisting of platinum covered by conductive polymer layers, which prevent deactivation of the electrocatalyst. Depending on the microbial environment, different polymers are used. Whereas fluorinated polyanilines (PTFA) are applied in MFCs using dark fermentation (*Clostridia*, *E. coli*, bacterial consortia (see **Figure 1**)) and photosynthesis (green algae *Chlamydomonas*, see **Figure 2**), poly(3,4-ethylenedioxythiophene), PEDOT, is used in MFCs exploiting the purple bacterium *Rhodobacter sphaeroides* for photo-fermentative substrate utilization.

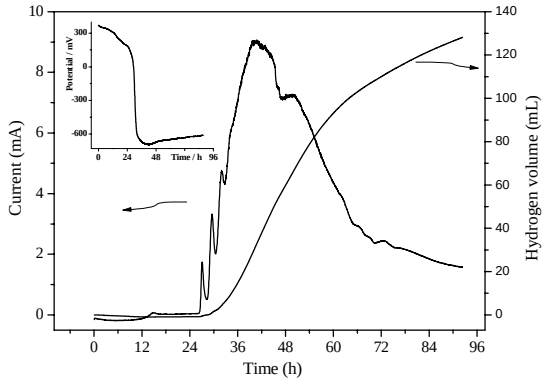

Figure 2. Left Y Axis: Current generation of a culture of the green alga *Chlamydomonas reinhardtii* CC125 in TAP-S, measured at a Pt-TFPA mesh electrode. E_{anode}= 0.2 V. The culture (550 ml) was sealed and constantly illuminated with fluorescence light. ϑ = 22°C. **Right Y Axis**: Total volume of the microbially produced and electrochemically oxidized hydrogen, calculated following Equ. 1. **Inset Figure**: Redox potential of a culture of *Chlamydomonas reinhardtii* CC125, grown in a TAP medium and transferred (1:10 v/v) into TAP-S. [9]

In the case of the anaerobic growth of the green alga *Chlamydomonas reinhardtii* under sulphur deprivation, hydrogen is produced as the sole electron donor for electrochemical oxidation. Thus the charge, produced during a "green solar cell" experiment, can be directly translated into the volume of photosynthetic hydrogen (**Equation 1**). A comparison of the results of the in situ oxidation of photosynthetic hydrogen (**Figure 2 and Table 1**) with literature values indicates a promotion of the photosynthetic hydrogen by the electrochemical hydrogen depletion from the microbial culture.

$$V_{H_2} = \frac{\int I\,dt}{z \cdot F} \cdot V_{n/32°C} \qquad \textbf{Equation 1}$$

Table 1. Normalized data of the hydrogen production by *Chlamydomonas reinhardtii* under different conditions (25 °C, 1,013 bar, 1 L culture volume).

Reference	*Duration of experim. / h*	*Final H_2-yield/ ml L^{-1} culture*
Our work [9]	***90***	***235****
Melis et al. [11]	*130*	*114***
Kosourov et al. [12]	*140*	*162***

*calculated from the electrochemical data; **volumetric data

The exploitation of photoheterotrophic microorganisms like the purple bacterium *Rhodobacter sphaeroides* offers a means for increasing the yield of microbial fuel cells by establishing a two-step MFC (see **Scheme 1**) consisting of a primary, fermentative part and a secondary photo-fermentation. As we can show for the example of glucose, degraded by *Escherichia coli K12* to produce H_2, lactate, acetate, formate, succinate and ethanol in a first step, the remaining organic acids can be utilized via photo-fermentation – increasing the coulombic yield by nearly 50%.

Acknowledgement

This work was supported by the US Office of Naval Research, (ONR project N00014-03-1-0431), by the Deutsche Forschungsgemeinschaft (DFG) and by the support by the Fonds der Chemischen Industrie.

References

(1) Reith, J. H.; Wijffels, R. H.; Barten, H., Eds. Bio-methane and Biohydrogen; Dutch Biological Hydrogen Foundation (http://www.ecn.nl/_files/bio/Bio-methane_and_Bio-hydrogen.pdf): Petten, 2003.
(2) Levin, D. B.; Lawrence, P.; Love, M., *Int. J. Hyd. Energy*, **2004**, 29, 173-185.
(3) Akkerman, I.; Janssen, M.; Rocha, J.; Wijffels, R. H., *Int. J. Hyd. Energy*, **2002**, 27, 1195-1208.
(4) Katz, E.; Shipway, A. N.; Willner, I. In *Handbook of Fuel Cells – Fundamentals, Technology and Applications*; Vielstich, W., Gasteiger, H. A., Lamm, A., Eds.; Wiley, 2003; Volume 1: Fundamentals and Survey of Systems.
(5) Logan, B. E., *Environ. Sci. Technol.*, **2004**, *38*, 160A-167A.
(6) Shukla, A. K.; Suresh, P.; Berchmans, S.; Rajendran, A., *Current Science* 2004, *87*, 455-468.
(7) Schröder, U.; Nießen, J.; Scholz, F., *Angew. Chem. Int. Edn.*, **2003**, 42, 2880-2883.
(8) Nießen, J.; Schröder, U.; Rosenbaum, M.; Scholz, F., *Electrochem. Commun.*, **2004**, 6, 571-575.
(9) Rosenbaum, M.; Schröder, U.; Scholz, F., *Appl. Microbiol. Biotechnol.*, **2005**, *in press*, published online: 5 Februar 2005.
(10) Nießen, J.; Schröder, U.; Scholz, F., *Electrochem. Commun.*, **2004**, 6, 955-958.
(11) Melis, A.; Zhang, L.; Forestier, M.; Ghirardi, M.L.; Seibert, M., *Plant Physiol.*, **2000**, 122, 127-135.
(12) Kosourov, S.; Tsygankov, A.; Seibert, M.; Ghirardi, M.L., *Biotechnol. Bioeng.*, **2002**, 78, 731-740.

PHOTODEPENDENT HYDROGEN EVOLUTION BY PHOTOSYSTEM I ENTRAPPED IN HYBRID ORGANO-SILICATE GLASSES

Hugh O'Neill, Barbra R. Evans and Elias Greenbaum

Chemical Sciences Division
Oak Ridge National Laboratory
Oak Ridge, TN 37831-6194

Introduction

Photosystem I (PSI) is one of three major photosynthetic energy transducing protein complexes found in thylakoids of higher plants, cyanobacteria and algae. The primary function of this transmembrane multisubunit complex is to convert electromagnetic energy into the electrochemical energy required for metabolic cellular processes. At the core of PSI is a pair of chlorophyll a molecules known as P700. After absorption of a photon, the photochemistry of P700 induces a charge separation ($P700^+A_0^-$) in the reaction center by rapid electron transfer to peripheral iron sulfur complexes (F_A and F_B) via the intermediates A_0, $A_1$and F_x.[1] The photochemical reaction is completed within 100-150 ns and generates approximately a 1 volt potential difference over a distance of 6 nm.[2] In vivo, electrons are transferred to ferredoxin and eventually used to reduce $NADP^+$ to NADPH. The $P700^+$ is re-reduced by plastocyanin with electrons that originate from water via the Photosystem II complex. The quantum yield of this photochemical reaction is close to 100%.[3]

In an interesting variant to the natural metabolic pathway protons can be used as a terminal electron acceptor for PSI using platinum catalysts.[4, 5] The platinization reaction takes place at ambient temperature and physiological pH according to the following reaction:

$$PtCl_6^{2-} + 4e^- + h\nu \rightarrow Pt\downarrow + 6Cl^-$$

The platinization of PSI is achieved by photochemical deposition of metallic platinum from sodium hexachloroplatinate in solution (Fig. 1). The electrons are photogenerated by PSI with Na ascorbate as a sacrificial pool of reductant. The photochemistry of platinum deposition and catalyst formation precedes the onset of hydrogen evolution.

We report here on the employment of the sol-gel technique to entrap and stabilize PSI complexes and produce a stable photo-dependent hydrogen evolution catalyst. The spectrophotometric, photochemical and photocatalytic characteristics of the immobilized enzyme were examined to evaluate the properties of the reaction centers as the sol-gels were dehydrated. The effect of the solvent removal process on the properties of the entrapped reaction centers, particularly on their ability to carry out electron transfer reactions, was investigated.

Experimental

Isolation of Proteins. PSI and plastocyanin were isolated from market baby spinach leaves as previously described.[6]

Preparation of silica-gels. A mixture of tetramethylorthosilicate (TMOS; 6 g), H_2O (2.05 g) and 40 mM HCl (0.08g) was sonicated at 4°C until a homogeneous solution was obtained. The sample was then placed under vacuum (100 kPa) at 20°C for 30 min. The resulting viscous liquid was diluted with 1.4 g H_2O. This sol solution was stable for several hours at 4°C. In a typical immobilization reaction 0.1 ml PSI, 0.3 ml 10 mM sodium phosphate buffer pH 7.2, and 0.5 g glycerol were mixed with 1 ml of sol solution in a 4 ml plastic cuvette. Gelation occurred within a 5 min period. The samples were stored at room temperature in the dark and dessicated under silica-gel. For photo-dependent hydrogen production reactions, PSI and plastocyanin were co-immobilized in a covered cylindrical glass vessel [1.1 × 9.1cm (I.D.)] equipped with gas inlet and outlet ports. The contents covered the bottom of the vessel to a depth of approximately 1 mm. Aging and dehydration were carried out as described for the analytical samples.

Photochemical activity of PSI. The photochemical activity of PSI was determined from the light induced P700 absorption changes at 810 nm using the Dual Wavelength Emitter Detector Unit ED-P700DW-E connected to a PAM 101 Fluorimeter (Walz, Effeltrich, Germany).

Photocatalyzed Hydrogen Evolution. The experimental apparatus used for the continuous measurement of hydrogen was described previously.[5] The immobilized proteins were washed with several changes of 10 mM Na phosphate for 4 hours at room temperature in the dark to allow the diffusion of glycerol from the gels. This buffer was removed and replaced with a solution comprised of 5.0 mM Na-ascorbate, 0.5 mM sodium hexachloroplatinate in 10 mM Na-phosphate pH 7.1. The reaction vessel was assembled into the experimental apparatus and the contents were allowed to equilibrate with the humidified carrier gas. After a baseline had been achieved the 2 hour light on/1 hour light off cycle was commenced and the photocatalyzed production of H_2 was recorded as described previously. The same conditions were employed with the native enzymes except that the reaction was stirred.

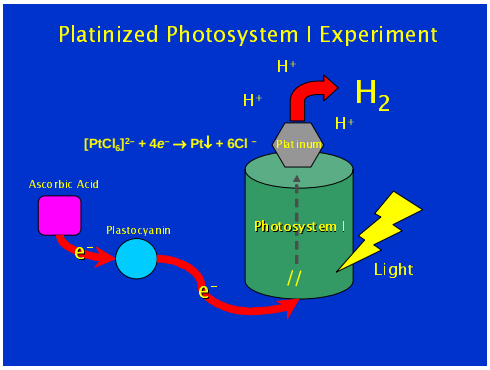

Figure 1. Photodependent platinization of Photosystem I

Results and Discussion

Sol-gel chemistry is an ambient temperature process for the synthesis of inorganic glasses. The utility of this technique for the immobilization of a range of biomolecules in silica glasses has been described.[7] As a prerequisite for this study it was essential to develop a strategy to stabilize PSI during the immobilization process and to preserve the optical properties of the silica glasses throughout the solvent removal process. Two modifications to a previously described method[8] were found to be necessary to achieve this goal. The methanol released during the hydrolysis of the alkoxide precursor was removed by evaporation and glycerol was used as a non-surfactant templating agent. Previous reports[9, 10] have employed these modifications separately. In this study the combination of both were required to attain a stable active PSI complex in an optically clear glass.

Photochemical activity. The photochemical activity of PSI was monitored by near infra-red absorption spectroscopy as described previously. The P700 photo-oxidation and $P700^+$ reduction curves of PSI in solution were compared to PSI entrapped in sol-gel at various time intervals after immobilization (Fig. 2). The P700 reaction centers were able to be photooxidized and recovered indicating that the samples were active directly after immobilization in the sol-gel and also after the solvent removal process was completed. The magnitude

of the photochemical response of the immobilized samples was slightly greater than the native sample after immobilization and when the majority of the water had been removed (91.4%) after 29 days. However the photochemical response decreased by approximately 50%, compared to the native sample, during storage for 8 months over desiccant in the dark. Although this indicates that the reaction centers lost some activity during long-term storage, a significant amount of activity did remain. These data demonstrate that the intra-molecular electron-transfer characteristics of PSI remain intact even after virtually all the solvent is removed.

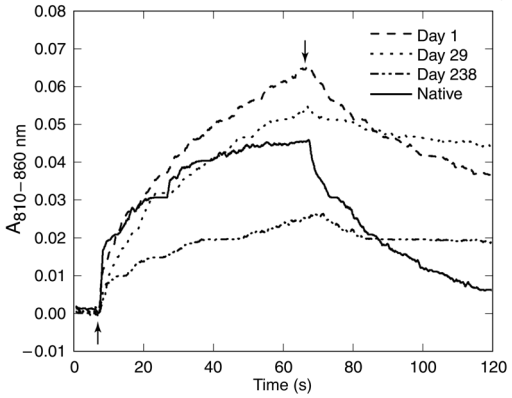

Figure 2. The P700 photooxidation and $P700^+$ reduction profiles of PSI at intervals after entrapment in sol-gels compared to the profile of the native preparation in solution. The up and down arrows indicate the start and finish of actinic light illumination (1400 µmol/m^2/sec, Schott KL 1500 light source)

Photocatalyzed Hydrogen Production. In this biomimetic reaction pathway the source of electrons was Na ascorbate with the electron relay protein plastocyanin serving as the mediator between Na ascorbate and the oxidizing side of PSI. Sol-gels that contained PSI co-immobilized with plastocyanin were prepared and aged as described in Materials and Methods. A characteristic light dependent evolution of hydrogen was observed (Figure 3A). The rates and yield of H_2 observed were similar for an experiment carried out with the native enzymes in solution (Figure 3B). This confirms that the PSI preparation was active after immobilization and able to facilitate intermolecular electron transfer from Na ascorbate via plastocyanin to platinum. This gives good confidence with respect to the structural and catalytic integrity of the PSI complexes.

Conclusions

PSI is a molecular photovoltaic structure that is capable of generating a 1 V potential over a 6 nm distance after absorption of a photon. It can carry out efficient e^- transfer directly from its active site to a metal surface in the absence of a mediator. Its protein architecture is such that two hydrophilic ends are separated by a hydrophobic middle region and therefore it has a natural disposition to orient itself. In this study we report on the entrapment and stabilization of PSI in an organo-hybrid sol-gel glass. The intra- and inter-molecular electron transfer properties of the protein complexes were preserved during immobilization and even after complete dehydration to a glass. The ability to manipulate PSI in a solid-state environment is essential for the exploitation of its unique optoelectronic properties for photo-fuel cells, photovoltaics and other bio-electronics applications. Although Na ascorbate was used as a sacrificial electron donor in this study to demonstrate photo-dependent hydrogen evolution we are currently exploring strategies to obtain reducing equivalents directly from photo-oxidation of water.

Acknowledgement. This work was supported by the Office of Basic Energy Sciences, U.S. Department of Energy, under contract number DE-AC05-00OR22725 with Oak Ridge National Laboratory, managed and operated by UT-Battelle, LLC.

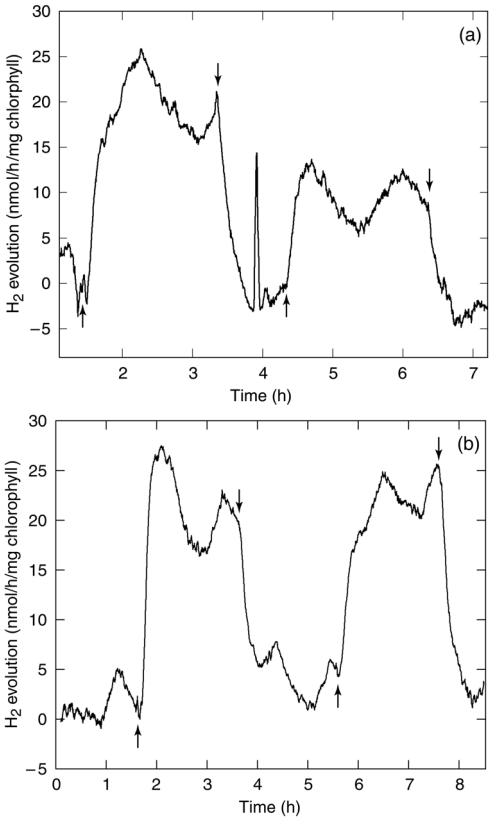

Figure 3. Light Dependent Evolution of Hydrogen by Platinized Photosystem I Reaction Centers. A: Photosystem I and plastocyanin co-immobilized in sol-gel. B: Native enzymes in solution. The reactions were carried out with 0.294 nmol Photosystem I (220 µmol chlorophyll), 20.2 nmol plastocyanin, 0.5 mM Na_2PtCl_6, and 5.0 mM Na ascorbate in 10 mM Na phosphate pH 7.11 at 20°C. Light cycles of 2 h on (↑) and 1 h off (↓) were used at a constant light intensity of 260 µmol/m^2/sec.

References

1. Owens, T.; Webb, S.; Mets, L.; Alberte, R.; Fleming, G. *Proc. Natl. Aca. Sci. USA* **1987,** 84, 1532-1536.
2. Brettel, K. *Biochim. et Bbiophys. Acta* **1997,** 1318, 322-373.
3. Zankel, K. L.; Reed, D. W.; Clayton, R. K. *Proc Natl Acad Sci U S A* **1968,** 61, 1243-1249.
4. Greenbaum, E. *J Phys. Chem.* **1988,** 92, 4571-4574.
5. Millsaps, J. F.; Bruce, B. D.; Lee, J. W.; Greenbaum, E. *Photochem Photobiol* **2001,** 73, 630-635.
6. Evans, B.; O'Neill, H.; Hutchens, S.; Bruce, B.; Greenbaum, E. *Nano Lett.* **2004,** 4, 1815-1819.
7. Livage, J.; Coradin, T.; Roux, C. *J. Phys- Condens Matt* **2001,** 13, R673-R691.
8. Ellerby, L.; Nishida, C.; Nishida, F.; Yamanka, S.; Dunn, B.; Valentine, J.; Zink, J. *Science* **1992,** 255, 1113-1115.
9. Gill, I.; Ballesteros, A. *J. Am. Chem. Soc.* **1998,** 120, 8587-8598.
10. Ferrer, M.; del Monte, F.; Levy, D. *Chem. Mat.* **2002,** 14, (9), 3619-3621.

PHOTOCATALYZED ELECTRON TRANSFER FROM SPINACH PSI TO METAL NANOPARTICLES

Barbara R. Evans[1], Hugh M. O'Neill[1], Jane Y. Howe[2] and Elias Greenbaum[1]

[1]Chemical Sciences Division, [2]Metals and Ceramics Division, Oak Ridge National Laboratory, Oak Ridge, TN 37831-6194

Introduction

Photosynthetic organisms such as plants and green algae convert solar energy to chemical energy by oxidizing water and reducing CO_2. A solar-powered biofuel cell that mimics photosynthesis is thus a very attractive concept for energy production. An essential step towards eventual assembly of such photocatalytic biofuel cells is the establishment of stable electron transfer between biocatalysts and metals.

The chloroplast photosystem I (PSI) protein complex transfers electrons across the chloroplast membrane following light activation of the two chlorophyll molecules in its P700 reaction center. PSI then accepts an electron from the small copper protein plastocyanin (PC). The biological electron acceptor is the iron-sulfur protein ferredoxin. PSI acts as a molecular diode with a potential of 1 V and a size of 6 nm, a property, together with its relative stability following isolation, that makes it a suitable photobiocatalyst for nanotechnology studies.[1,2] A mixture of spinach PC and PSI has been demonstrated to photocatalytically reduce hexachloroplatinate to metallic platinum at the reducing end of PSI to form a PSIPt catalyst that subsequently evolves H_2.[3] Covalent attachment of PC to PSI increased both the rate of both platinum deposition and H_2 production.[4] Decrease in H_2 evolution during successive light cycles was observed for both free and cross-linked PC and PSI, possibly due to growth of the platinum particle beyond the optimal size range of 50-500 atoms.[5]

The studies described here were carried out to investigate the stability of the cross-linked PCPSIPt catalyst and the effect of metal particle size on efficient electron transfer, the effect of limiting platinum particle size and the ability of PSI to transfer electrons to preformed metallic particles. Palladium-cellulose membranes containing catalytically active palladium nanoparticles deposited in hydrated bacterial cellulose pellicules[6] provided a convenient matrix for examination of interaction of PSI with dispersed metal particles. The porous microstructure of bacterial cellulose is composed of cellulose macrofibrils 40 to 60 nm wide that form a gel-like pellicule containing one-hundred times its weight in water. This hydrophilic form of cellulose has successfully been employed for immobilization of several types of cells and enzymes.[7,8]

Experimental

Isolation and cross-linking of proteins. PSI and PC were purified from spinach obtained from local markets and cross-linked by formation of peptide bonds with the reagent 1-ethyl-3(3-dimethylaminopropyl) carbodiimide hydrochloride (EDC) as described previously.[4] Recombinant spinach PC that was used in the platinization experiments was produced from a plasmid construct in a pET vector (Novagen, Inc.) with azurin signal peptide using a procedure adapted from a published method.[9]

Hydrogen evolution assays. The photoreactions were carried out at 23ºC with exclusion of incidental light in continuous flow systems using helium as the carrier gas. Hydrogen production was monitored by an in-line Figaro tin oxide hydrogen sensor as described.[3,4] The light source was a Fiber-Lite A3200 fiber optic illuminator (Dolan-Jenner Industries, Lawrence, MA 01843-1060) fitted with dual fiber optic cables and an OSRAM 150W quartz halogen lamp (OSRAM Corporation, Winchester, KY 40391) and a red filter transmitting light above 600 nm. Illumination was carried out with 2 h on/2 h off cycles with a light intensity of 531 µE m^{-2} s^{-1} at the reaction vessel.

Platinization of cross-linked PCPSI. Platinization was carried out by illumination of incubation mixtures containing 8 mM sodium ascorbate, 0.5 mM Na_2PtCl_6, cross-linked PCPSI (266 µg chl) in 50 mM sodium phosphate pH 7.1 at 23ºC for 2-h cycles in the continuous flow system with helium carrier gas. Excess hexachloroplatinate was removed by dialysis at 4ºC against 50 mM sodium phosphate pH 7.1. The dialyzed PCPSIPt (254 µg chl) solution was injected into the reaction vessel and sodium ascorbate added to a final concentration of 8 mM.

Preparation of palladium-cellulose. Bacterial cellulose membranes were prepared by cultivation of *Gluconacetobacter hansenii* (ATCC 10821) and cleaned before deposition of palladium from hexachloropalladate.[6] Palladium content was estimated by spectrophotometric determination of hexachloropalladate remaining in solution as 0.0483 mg cm^{-2}. Size and composition of the palladium particles was determined by transmission electron microscopy carried out at the Oak Ridge National Laboratory High Temperature Materials facility.

Loading of PC and PSI on palladium-cellulose. Plastocyanin and PS I were loaded into palladium cellulose membranes (diameter 3.8 cm, 5.13 µmol Pd) by filtration on disposable filter sterilization units. For experiments with proteins that were not cross-linked, plastocyanin (8 nmol) was preincubated with PS I (70 µg chl) in 50 mM sodium phosphate buffer, pH 7.1, for 20 min at 23ºC before loading onto a palladium cellulose circle of diameter 4.5 cm. The molar ratio was calculated from the P700 assay of the PS I prep to be 30 plastocyanin: 1 P700. A separate bacterial cellulose membrane containing 8 mM sodium ascorbate in 50 mM sodium phosphate buffer, pH 7.1 was placed under the palladium cellulose to provide a supply of ascorbate by diffusion into the palladium-cellulose layer.

Results and Discussion

Removal of excess hexachloroplatinate from the cross-linked PCPSIPt biocatalyst resulted in stabilization of the H_2 evolution rate at the level of the last platinization light cycle (Fig. 1), presumably by restriction of the platinum particle size. The dialyzed PCPSIPt catalyst evolved H_2 at a steady rate for 23 light cycles (Fig. 1).

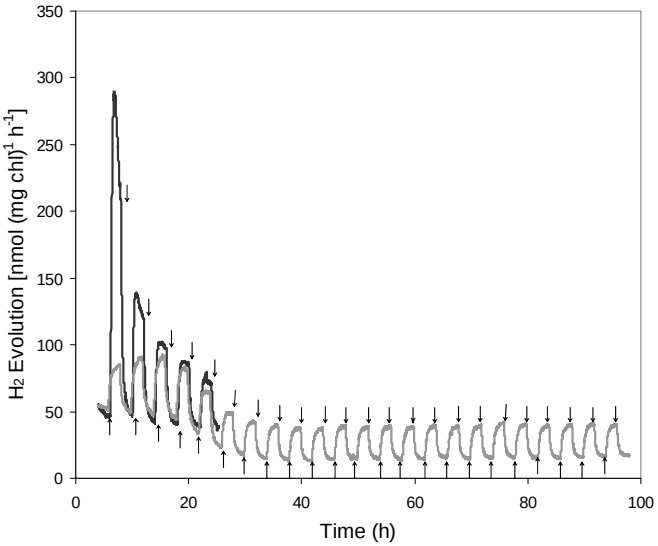

Figure 1. Photocatalyzed evolution of H_2 during platinization of cross-linked PCPSI (black), and following removal of excess hexachloroplatinate from the platinized PCPSI by dialysis (gray) were compared for light cycles of 2 h on (↑)/ 2 h off (↓).

To further investigate electron transfer to catalytic metal particles, PSI with free or covalently attached PC was loaded on hydrated bacterial cellulose membranes containing catalytically active palladium particles. The size of the particles was determined by TEM to range in size from 2 to 20 nm (Fig. 2). Preliminary studies demonstrated the suitability of bacterial cellulose for immobilization of PSI based on optical transmission in the visible range and stability of PSI photocatalytic activity in reduction of $NADP^+$ in the biological assay[4] with ferredoxin and ferredoxin:$NADP^+$ reductase (data not shown). Surface coverage of membrane surfaces based on the amount and size of PSI loaded was estimated to be nearly 100%. Illumination of these membranes resulted in stable photocatalyzed H_2 production during successive light cycles. In the palladium-cellulose membranes, cross-linked PCPSI evolved higher levels of H_2 that the free PC and PSI, similar to the previous results for the platinization reaction.[4]

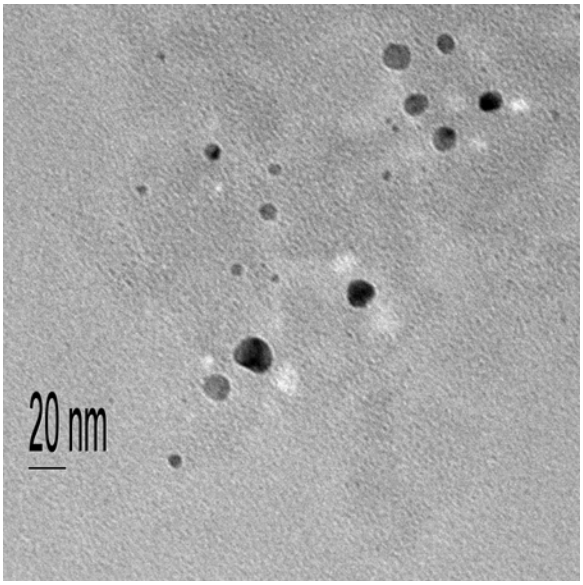

Figure 2. The size of the palladium particles deposited in the bacterial cellulose membranes was determined by imaging with TEM to range from 2 to 20 nm.

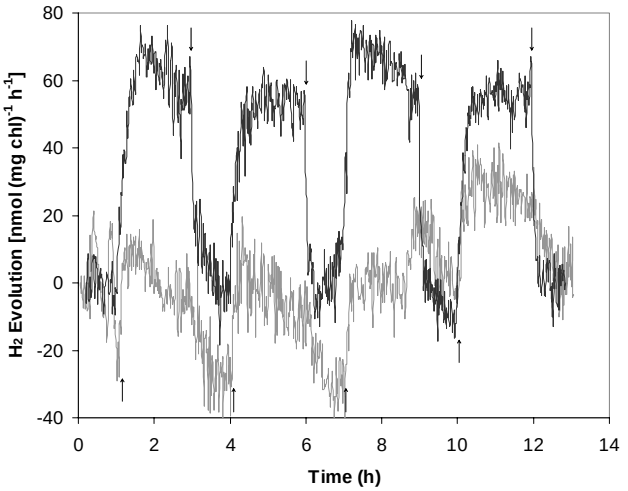

Figure 3. Following loading onto the surface of the palladium-cellulose membranes, cross-linked PCPSI (black) evolved H_2 at higher rate than free PC and PSI (gray).

Conclusions

The importance of particle size in the photocatalyzed electron transfer from PSI to metals was confirmed. Limiting particle size of platinum formed during photocatalytic platinization of cross-linked PCPSI resulted in formation of a stable metallized biocatalyst. Palladium-cellulose membranes contain palladium nanoparticles maintained in dispersion throughout the membrane matrix by the cellulose fibers. Free PSI and cross-linked PCPSI were able to transfer electrons to these palladium particles as evidenced by photocatalytic H_2 evolution. These results indicate that maintaining the correct metallic particle size range is essential for electron transfer from photosystems and other redox active biomolecules.

Acknowledgement. This research was supported by funding from the Office of Basic Energy Sciences, U. S. Department of Energy, and from the Bioflips/Symbiosys Program of the Defense Applied Research Program Agency, U. S. Department of Defense. Research at the Oak Ridge National Laboratory (ORNL) High Temperature Materials Laboratory (HTML) was sponsored by the Assistant Secretary for Energy-Efficiency and Renewable Energy, Office of FreedomCAR and Vehicle Technologies, U.S. Department of Energy under contract DE-AC05-00OR22725 with UT-Battelle, LLC. Oak Ridge National Laboratory is managed by UT-Battelle, LLC for the U.S. Department of Energy under contract DE-AC05-00OR22725. This work was sponsored by a contractor of the U.S. Government under contract DE-AC05-00OR22725. Accordingly, the U.S. Government retains a nonexclusive, royalty-free license to publish or reproduce this document, or to allow others to do so, for U.S. Government purposes.

References

(1) Brettel, K. *Biochim. et Bbiophys. Acta* **1997,** *1318*, 322-373.
(2) Lee, I.; Lee, J. W.; Stubna, A.; Greenbaum, E. *J. Phys. Chem. B* **2000**, *104*, 2439-2443.
(3) Millsaps, J. F., Bruce, B. D.; Lee J. W.; Greenbaum E. *Photochem. Photobiol.* **2001,** *73(6)*, 630-635.
(4) Evans, B. R.; O'Neill, H. M.; Hutchens, S. A., Bruce, B. D., Greenbaum, E. *NanoLett*. **2004**, *4(10)*, 1815-1819.
(5) Greenbaum, E. *J Phys. Chem.* **1988,** *92*, 4571-4574.
(6) Evans, B. R., O'Neill, H. M., Malyvanh, V. P., Lee, I. Woodward, J. *Biosens. Bioelectron*. **2003**, *18(7)*, 917-923.
(7) Iguchi, M.; Yamanaka, S.; Budhiono, A. *J. Materials Science* **2000,** *35(2)*, 261-270.
(8) Cannon, R. E.; Anderson, S. M. *Crit. Reviews in Microbiol.* **1991**, *17(6)*, 435-447.
(9) Chang, T. K.; Iverson, S. A.; Rodrigues, C. G.; Kiser, C. N.; Lew, A. Y. C.; Germanas, J. P.; Richards, J. H. *Proc. Natl. Acad. Sci. USA* **1990**, *88*, 1325-1329.

BIOFUEL CELL BASED ON THE BACTERIA *GLUCONOBACTER OXYDANS* AND THE MEDIATOR OF ELECTRON TRANSPORT 2,6-DICHLOROPHENOL INDOPHENOL

A.N.Reshetilov[1], S.V.Alferov[2], L.G.Tomashevskaya[1], O.N.Ponamoreva[3]

[1]G.K.Skriabin Institute of biochemistry and physiology of microorganisms, RAS, Prospekt Nauki 5, Pushchino, Moscow region, 142290, Russia
[2]Pushchino State University, Pushchino, Moscow region, Russia
[3]Tula State University, Tula, Russia

Introduction

Studies in the field of biofuel cells (BFC) are important for many reasons among which a search for the alternative and the possibility of creating ecologically safety sources of electrical energy are the most weighty.[1] One of the trends in this field of investigation is represented by the development of microbial BFC, which differ in constructions, type of microbial cultures, mediators and substrates [2-6]. The analysis of literature data shows that a search for efficient composition "the type of a microbial culture – the type of a mediator – the type of fuel" is one of the significant and unresolved tasks on construction of BFC. In this connection, studies, orientated to clarification of a relationship between BFC characteristics and the composition alluded above, are in great demand. The use of acetic-acid bacteria of the genus *Gluconobacter* as BFC biocatalyst appears to be promising. These bacteria have a number of unique characteristics, in particular, membrane localization of basic enzymes of cell metabolism. Due to this property substrates [7] and probably mediators may easily reach active centers of the enzyme. Microbial cultures of this genus are widely used for designing a range of mediator microbial biosensors [8-10]. At the same time literature provides no data on the use of bacteria of the genus *Gluconobacter* in BFC construction.

This work was focused on the study of the possibility of electromotive force (EMF) generation by biofuel cell when the strain *Gluconobacter oxydans* sbsp *industrius* B-1280 and the mediator of electron transport, 2,6-dichlorophenol indophenol, was used as a biocatalyst. Glucose was an oxidizable substrate.

Experimental

BFC model was represented as two-chamber cell analogous to that one described in [3]. Volumes of cathode and anode compartments were equal and added up to 1.0 ml. Compartments were separated with nonionselective acetate cellulose membrane (Vladipor MFA-MA № 5, pore diameter, 0,2μm, Russia). Membrane was used to keep the cells in the anode compartment and partially prevented the diffusion of the mediator and glucose to the cathode compartment. The obtained results show (data are not given) that glucose and mediator flowing through the membrane to the cathode compartment was not higher than 4% and 1%, respectively. Since steady-state value of voltage and current achieved for 20-30 min, changes in glucose and mediator concentrations were not taken into account. The measurements were taken at temperature 22^{o}C. Solutions in cathode and anode compartments were mixed by magnetic stirrer. Graphite electrodes, diameter, 6 mm, were used as anode and cathode. The working surface of each electrode was 2,0 cm^2. 2,6-dichlorophenol indophenol was used as the mediator (Sigma); glucose and chemicals for buffer solutions were pure for analysis grade. 30 mM sodium-phosphate buffer solution, pH 7.6, was basic electrolyte for both compartments. Bacterial culture *Gluconobacter oxydans* sbsp. *idustrius* B-1280 was taken from Russian microbial cultures collection, G.K.Skriabin IBPM, RAS. Fresh grown and once frozen and defrozen cells were used in the experiments. Voltage and current were measured with a galvanopotentiostat IPC-2 (Kronas, Russia), the input resistance of which was $10^{13}\Omega$ in the mode of potential measurement.

Results and Discussion

Addition of the composition "bacteria + the mediator + glucose" to the anode compartment was accompanied by generation of a potential difference equal to 55 mV (the mean value with the variation coefficient 6% for ten measurements).

The observed potential difference was interpreted as generation of EMF due to bacterial oxidation of glucose and electron transfer by reduced molecules of the mediator to the anode. The process of EMF generation proceeds in accordance with the mechanism given in [3, 4].

At switching-on of external ohmic load of 10 kΩ the steady-state difference of potentials was 5.6 mV at the current of 0.56 μA and the current density of 0.28 μA*cm^{-2}. The calculated value of the cell internal resistance was 88 kΩ. The power of BFC was $3*10^{-3}$ μW.

For comparison, in [3] one will find the description of BFC in which E.coli bacteria were used as a biocatalyst. As mediators, Neutral Red and potassium ferricyanide were employed in the anode and cathode compartments, respectively. Glucose was a substrate used for oxidation. At the external load of 120 Ω the generated potential was 460 mV at the current of 0.5 mA, which corresponds to the power of 0.23 mW. For that regime, the current density was $8.9*10^{-3}$ μA*cm^{-2}, as the surface of graphite felt electrodes was 0.5 m^2. Hence, the developed BFC exceeds by several times the one based on *E. coli* cells by current density, which characterizes the composition of *G. oxydans* with DCPIP as more effective than the one of *E. coli* with Neutral Red. It should also be noted that the used composition allows to carry out the measurements without additional deoxygenation of the anode compartment. The parameters of the developed BFC can be further improved by optimization of the biomass and mediator contents, use of electron transport mediators in the cathode compartment by analogy with described in [2,3], application of a cathode modified by some enzyme, for example, by laccase [11], use of a cation-selective membrane that separates the anode and cathode compartments).

Conclusions

The obtained data indicate the possibility of using a bacterial strain belonging to the genus *Gluconobacter* as a biocatalyst in the BFC. It seems advisable to continue investigations for possible optimization of the parameters of the proposed BFC model.

Acknowledgment. This work was supported by the Ministry of Industry and Science of the Moscow region and Russian foundation of fundamental research, project No. 04-04-97253.

References

1. Shukla A.K., Suresh P., Berchmans S., Rajendran A., Current Science, 2004, 87(4), 455.
2. Wilkinson S., Autonomous Robots, **2000**, 9, 99.
3. Park D. H. and Zeikus G., *Applied and environmental microbiology*, **2000**, 66, 1292.

4. Daniel R. Bond, Dawn E. Holmes, Leonard M. Tender, Derek R. Lovley., Science, **2002**, 295, 483.
5. Willner I., Arad G., Katz E., *Biochem. Bioenerg.*, **1998**, 44, 209.
6. Satoshi Sasaki and Isao Karube., *TIBTECH*, **1999**, 17, 50.
7. Lusta K.A. and Reshetilov A.N., *Appl. Biochem. Microbiol.*, **1998**, 34(4), 339, (Moscow, Interperiodica Publishing).
8. Ikeda T., Kurosaki T., Takayama K., Matsushita F., *Anal.Chem.***, 1996**, 68, 192.
9. Alferov V.A., *Ponamoreva O.N., Babkina E.E.,* Alferov S.V., Reshetilov A.N., (In Russian) *Izvestiya, Tula State University*, **2004**, 4, 126.
10. Gorton L., *Electroanalysis*, **1995**, 7, 23.
11. Tarasevich M.R., Bogdanovskaya V.A., Zagudaeva N.M., Kapustin A.V., *Electrical chemistry*, **2002**, 38(3), 378, (Moscow, Interperiodica Publishing).

A MINIATURE MEMBRANE-LESS BIOFUEL CELL OPERATING AT +0.60 V UNDER PHYSIOLOGICAL CONDITIONS

Nicolas Mano and Adam Heller

Department of Chemical Engineering and Texas Material Institute-
The University of Texas at Austin-Austin-78712- USA

Introduction

Our work is aimed at engineering a power source enabling further miniaturization of autonomous implanted electronic devices, the size of which is now limited by their battery. As the size of microelectronic circuits and of sensors shrinks, the sizes of low-power sensor-transmitter packages (of potential relevance to physiological research and medicine) becomes increasingly dependent on the size of their power source. If stabilized for operation *in-vivo,* a miniature glucose/O_2 biofuel cell could power an implanted sensor-transmitter that would broadcast, for a few weeks, the local glucose concentration, relevant to diabetes management; or the local temperature, indicative of infection after surgery; or a pressure difference, indicating blockage of the flow of fluid in the central nervous system. [1]

Contrary to conventional cells which contain at least 9 components (anode, cathode, case, case seal, membrane, membrane seal, ion conducting electrolyte, plumbing to the anode compartment and plumbing to the cathode compartment), the miniature biofuel cell that we are developing contains only two, an anode and a cathode. [1-3] These consist of "wired" enzyme bioelectrocatalyst-coated 7 μm diameter carbon fibers.

By eliminating the membrane, the case and the seal, we were able to build a 0.88 mm^2 biofuel cell, the smallest ever, which we implanted and operated in a grape. The in-vivo power output of the cell, made of a pair of 0.44 mm^2 area smooth, non porous carbon fibers, was 2.4 μW at +0.52 V/AgAgCl, translating to a power density of ~ 5.5 μW.mm-2 and ~ 4.4 μW.mm-2 at +0.6V/AgAgCl.[2] Because this potential exceeded half the band gap of silicon, it could be converted, by a conventional silicon voltage converter circuit, to the standard 3V operating voltage of ICs

Here we show that the tailoring of a redox polymer, electrically connecting the reaction centers of glucose oxidase to the carbon fiber anode, led to an efficient biofuel cell, operating at a higher voltage and current density.

.

Experimental

Chemicals. Bilirubin oxidase (BOD) (EC 1.3.3.5, 1.3 $U.mg^{-1}$) from Trachyderma tsunodae was purchased from Amano (Lombard, IL) and purified as previously decribed.[4] Glucose oxidase (GOx) from Aspergillus niger from Fluka, Milwaukee, WI. Poly(ethylene glycol) (400) diglycidyl ether (PEGDGE) from Polysciences, Inc. (Warrington, PA); $NaIO_4$ and NaCl (Sigma, St. Louis, MO) were used as received. A fresh solution of BOD in pH 7.4, 20 mM phosphate buffer (PB) was prepared daily. All solutions were made with deionized water passed through a purification train (Sybron Chemicals Inc, Pittsburgh, PA). The synthesis of the BOD-wiring redox polymer **I** PAA-PVI-$[Os(4,4'\text{-dichloro-}2,2'\text{-bipyridine})_2Cl]^{+/2+}$ and GOx-wiring redox polymer **II** PVP-$[Os(N,N'\text{-alkylanated-}2,2'\text{ bi-imidazole})_3]^{2+/3+}$ were previously reported. [5-8]

Instrumentation and electrodes. The measurements were performed using a bipotentiostat (CH-Instruments, Austin, TX, Model #CHI832) and a dedicated computer. The 2-cm long, 7-μm diameter carbon fibers (Goodfellow, Cambridge, UK) were made by reported procedures.[5, 7-10] One end of the fibers was cemented to a copper wire using conductive carbon paint (SPI, West Chest, PA). The carbon paint was allowed to dry, then insulated with an epoxy cement. The active area of each fiber was 0.44 mm^2. Prior to their coating the 7μm diameter fibers (0.0044 cm^2) were made hydrophilic by exposure to a 1 torr O_2 plasma for 3 minutes.[11] The cathodic catalyst was made of 44.6 wt% of bilirubin oxidase, 48.5 wt % of polymer ***I*** and 6.9 wt% of the crosslinker PEDGE. [5, 7]. The anodic catalyst solution was made as follows : 100 μL of 40 mg/mL GOx in 0.1 M $NaHCO_3$ was oxidized by 50 μL of 7mg/mL of $NaIO_4$ in dark for 1 hour, and then 2 μL of the periodate-oxidized GOx was mixed with 8 μL of 10mg/mL of polymer ***II*** and a 0.5 μL droplet of 2.5 mg/mL of PEGDGE. 5 μL of the anodic catalytic solution was applied to the carbon fiber. The resulting anodic catalyst consisted of the cross-linked adduct of 39.6 wt % GOx, 59.5 wt % polymer ***II*** and 0.9 wt % PEDGE.

Results and Discussion

We described earlier a glucose electrooxidizing anode made by "wiring" glucose oxidase (GOx) with poly(4-vinylpyridine)-$[Os(N,N'\text{-dimethyl-}2,2'\text{-biimidazole})_3]^{2+/3+}$, comprising 10.7 wt % of osmium.[12] The unique features of this "wire" were its 13-atom long flexible tethers, binding the redox centers to the backbone, and the reducing redox potential of the dialkylated biimidazole complex of $Os^{2+/3+}$, -0.2 V vs. Ag/AgCl. The long tethers increased the frequency of effective electron transferring collisions between reduced and oxidized osmium centers and thereby the apparent electron diffusion coefficient, D_{app}, which reached in the crosslinked redox hydrogel 5.8 x 10^{-6} cm^2 s^{-1}, an order of magnitude higher than in earlier redox hydrogels.[13, 14] The effective collection of the electrons from the glucose-reduced GOx allowed poising of the anode at a potential as reducing as - 0.10 V vs. Ag/AgCl (only 0.26 V positive to the redox potential of the $FAD/FADH_2$ cofactor in GOx at pH 7.2) while glucose was electro-oxidized at a current density of 1.15 $mA.cm^{-2}$.

To build a faster glucose anode and to decrease the overpotential for glucose electrooxidation, we synthesized a new redox polymer with 12.8 wt % of osmium. The synthetic strategy for the polymer resembled that reported for the 10.7 wt % of osmium polymer.[12] The NH_2-spacer modified tris (N, N′-dialkylated 2,2′-biimidazole) $Os^{2+/3+}$ was condensed with 6-bromohexanoic acid-quaternized of poly(4-vinylpyridine) to form the amide. The (tethered complex/pyridine/carboxyl-pentylpyridinium) ratios for the 12.8 wt%-Os-polymer were 12.8/85/2.2.

Figure 1 represents the optimal composition (polymer/ enzyme/crosslinker) obtained for the bioelectrocatalysts made with the polymer containing 10.7 wt % osmium (solid circles) and the polymer containing 12.8 wt % osmium (open circles).

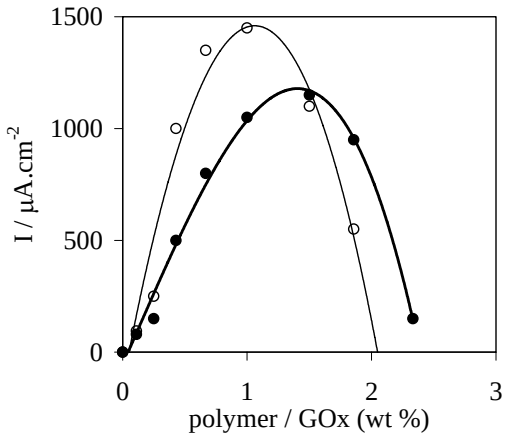

Figure 1. Dependence of the glucose electrooxidation current density on the polymer/GOx weight percentage ratio when the bioelectrocatlyst is made with a polymer containing 10.7 wt % of osmium (black circles), or 12.8 wt% of osmium (open circles). Electrode poised at + 0 V/AgAgCl in a 20 mM phopshate buffer, 37 °C, 1 mV.s^{-1} scan rate, 200 rpm, under 1 atm N_2, 15 mM glucose.

Increasing the osmium content to 12.8 wt. % allowed a lesser polymer/enzyme weight ratio, 1.0 vs. the earlier reported 1.5 for the polymer loaded with 10.7 wt.% Os, and increased the limiting current density by 20 % to 1.5 mA.cm^{-2}.

Using the novel anode, we built a miniature compartment-less biofuel cell, consisting of two 7 µm diameter, 2 cm long carbon fibers. The bioelectrocatalyst of the anode consists of glucose oxidase from *Aspergillus niger* (GOx) electrically "wired" by polymer II, having a redox potential of -0.19V vs. Ag/AgCl. The bioelectrocatalyst of the cathode, which was superior to platinum, was reported earlier. [4] It consisted of purified bilirubin oxidase from *Trachyderma tsunodae* (BOD) "wired" by PAA-PVI-[Os(4,4´-dichloro-2,2´-bipyridine)$_2$Cl]$^{+/2+}$ and had a redox potential of + 0.36 V vs. Ag/AgCl.

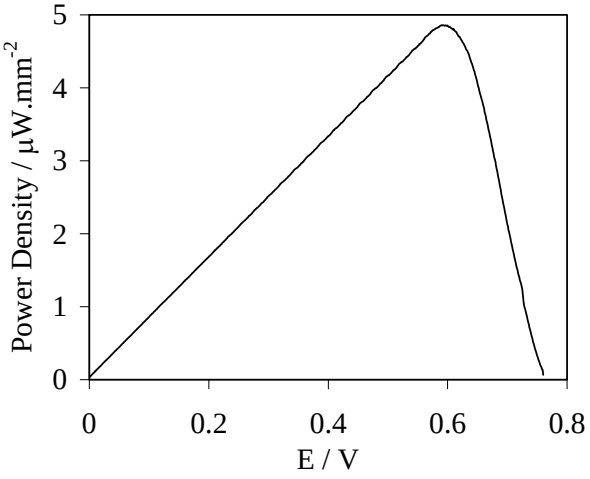

Figure 2. Dependence of the power density on the cell voltage for the cell made with a 7 µm diameter, 2 cm long carbon fiber anode coated with "wired" glucose oxidase and with the novel polymer containing 12.8 wt % of osmium . 15 mM glucose.

As illustrated in Figure 2, the power of the cell made of the two carbon fibers, peaked at ~ + 0.60 V/AgAgCl, where it reached 2.1 µW. The power density was 4.8 µW.mm^{-2}, above the 4.4 µW.mm^{-2} power density of the previously described +0.52 V cell.[2, 6] This value represents the highest operating voltage in a miniature membrane-less biofuel cell in a pH 7.2 physiological buffer solution. Because the redox potential of *A. niger* GOx at pH 7.2 is -0.35 vs. Ag/AgCl [15] and that of bilirubin oxidase from *Trachyderma tsunodae* is about +0.36 vs. Ag/AgCl.[16], the operating potential is just 0.11 V less than the difference between the redox potentials of the two enzymes. The cell lost ~ 8% of its power per day when operating at +0.6V/AgAgCl and at 37 °C in a physiological buffer solution.

Conclusions

Increasing the density of the polymer-bound redox sites, which electrically connect the reaction centers of GOx to the anode, increased the glucose flux limited current density by 20%, and decreased by 50 mV the overpotential for glucose electro-oxidation. A miniature, membrane-less glucose-O_2 biofuel cell built with the novel anode operated in a physiological buffer at 37.5ºC at the highest voltage to date, +0.60V, while producing 4.8µW.mm^{-2}.

Acknowledgement. The study was supported by the Office of Naval Research (N00014-02-1-0144) and by the Welch Foundation. N.M thanks The Oronzio de Nora Industrial Electrochemistry Fellowship of The Electrochemical Society

References

(1) Heller, A.,*Phys. Chem. Chem. Phys.* **2004,** 6, 209-216.
(2) Mano, N.; Mao, F.; Heller, A.,*J.Am. Chem. Soc.* **2003,** 125, 6588-6594.
(3) Soukharev, V. S.; Mano, N.; Heller, A.,*J. Am. Chem. Soc.* **2004,** 126, (27), 8368-8369.
(4) Mano, N.; Fernandez, J. L.; Kim, Y.; Shin, W.; Bard, A. J.; Heller, A.,*J. Am. Chem. Soc.* **2003,** 125, 15290-15291.
(5) Mano, N.; Kim, H.-H.; Zhang, Y.; Heller, A.,*J. Am. Chem. Soc.* **2002,** 124, 6480-6486.
(6) Mano, N.; Mao, F.; Heller, A.,*J. Am. Chem. Soc.* **2002,** 124, 12962-12963.
(7) Mano, N.; Kim, H.-H.; Heller, A.,*J. Phys. Chem. B* **2002,** 106, 8842-8848.
(8) Kim, H.-H.; Mano, N.; Zhang, Y.; Heller, A.,*J. Electrochem. Soc.* **2003,** 150, (2), A209-A213.
(9) Chen, T.; Barton, S. C.; Binyamin, G.; Gao, Z.; Zhang, Y.; Kim, H.-H.; Heller, A.,*J. Am. Chem. Soc.* **2001,** 123, 8630-8631.
(10) Mano, N.; Heller, A. In *A Miniature Membrane-less Biofuel Cell Operating Under Physiological Conditions*, ECS, Salt Lake City, 2002; 'Ed.'^'Eds.' Salt Lake City, 2002; p^pp.
(11) Sayka, A.; Eberhart, J. G.,*Solid State Technol* **1989,** 32, 69-70.
(12) Mao, F.; Mano, N.; Heller, A.,*J.Am. Chem. Soc.* **2002,** 125, (16), 4951-4957.
(13) Heller, A.,*J Phys. Chem.B* **1992,** 96, 3579-3587.
(14) Heller, A.,*Acc. Chem. Res.* **1990,** 23, 128-134.
(15) Stankovich, M. T.; Schopfer, L. M.; Massey, V.,*J. Biol. Chem* **1978,** 253, 4971-4979.
(16) Hirose, J.; Inoue, T.; Sakuragi, H.; Kikkawa, M.; Minakami, M.; Morikawa, T.; Iwamoto, H.; Hiromi, K.,*Inorganica. Chim. Acta* **1998,** 273, 204-212.

ELECTRON/ION MIXED CONDUCTIVE MATRIX FOR ELECTROCHEMICAL REGENERATION OF COFACTORS

Linda de la Garza, Yupo J. Lin, Michelle B. Arora , Marion C. Thurnauer, and Seth W. Snyder

Chemistry Division and Energy Systems Division
Argonne National Laboratory
9700 South Cass Ave.
Argonne, IL 60439

Introduction

Bioprocessing takes advantage of biocatalysts (enzymes or microorganisms) in a bioreactor. Biocatalysts have distinct advantages over chemical catalysts including higher selectivity and milder reaction conditions. Enzyme biocatalysts are preferred because they can be tailored or engineered to perform highly specific reactions. Microorganism biocatalysts are used in most cases because they do not require cofactor replacement, a critical barrier in most enzyme applications. Cofactor within the active site of the enzyme act as electron sinks donating/accepting electrons and protons to/from the substrate in order to convert it to the chemical product. For example, glucose fructose oxido-reductase converts glucose to gluconolactone by donating two electrons and two protons from glucose to the cofactor $NADP^+$ (nicotinamide adenine dinucleotide phosphate) converting it to NADPH and H^+. In a living cell, after the cofactor is consumed, it is replaced by fresh cofactor from the available cellular cofactor pool, allowing the enzyme to retain enzymatic activity. In a bioreactor, cofactors are depleted because the isolated enzyme has no fresh cofactor pool to draw from. Costly cofactors must be continuously added to the bioreactor for the conversion to continue. Most applications use inefficient methods to regenerate cofactor such as the addition of a second enzyme/substrate to catalyze a reaction that regenerates cofactor. The drawbacks are that additional substrate must be added for the second enzymatic reaction and the second reaction leads to unwanted byproducts that must be separated from the desired product. Therefore, a method to directly regenerate cofactor in a bioreactor without addition of a second enzyme/substrate reaction could address a significant barrier to enzymatic-based chemicals production.

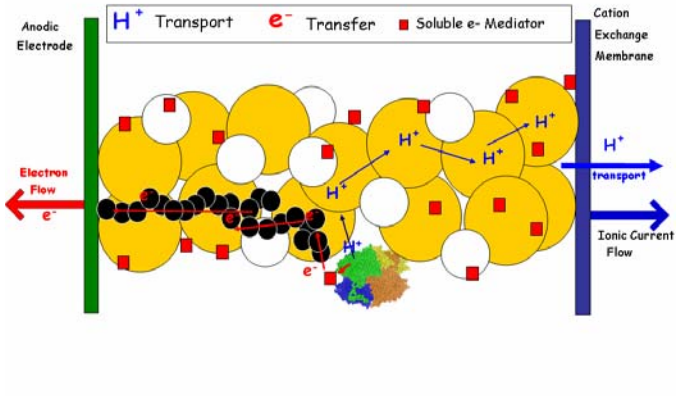

Figure 1. Scheme of the components of electron/ion mixed conductive matrix. A space fill model of GFOR enzyme is displayed. Yellow circles represent ionic resins, white circles represent enzyme capture resins, and the black circles represent carbon nanoparticles.

Direct cofactor regeneration can be achieved by controlling the transfer of electrons and protons to/from the cofactor or to an acceptor/donor provided by electrodes in an electrochemical cell.

To directly regenerate cofactor we constructed a novel porous composite conductive matrix to act as both an electron and proton bridge between the enzyme active site and electrode. As shown in **Figure 1**, three elements are required to form a conductive matrix that can effectively create an electron/proton bridge, (1) a network for proton transport, (2) a network for electron transfer, and (3) enzymes immobilized within the matrix.

Results and Discussion

Fabrication and conductivity tests of electron/ion mixed conductive matrix. Two methods, wet and dry processes, were developed to incorporate the carbon-black nanoparticles with ion-exchange and enzyme capture resin beads. In the wet process, a latex emulsion liquid with curing agent was used to form an elastomer polymer that binds the particles mixture. The porosity of the wafers made by the wet process is around 10-15%. To better control the wafer properties, a dry process to make the wafer was also developed. Thermoplatics were used to bind the particles mixture by hot-pressing all the particles in a mold under high pressure. The porosity of the wafer can be controlled by using removable additives such as sugar or passing air through the mold. Without the carbon particles in the matrix, the regular resin wafer is found to be electrically insulated.

In order to predict the optimal ratio of cation and anion resins in the matrix for effective transport of proton a porous-plug model of ion conductivities in the composite wafer was developed. Using the results of the experimental measurements of ionic conductivity of each tested composite wafer, this model can determine the pathways of ion transport inside the wafer structure. As shown in **Figure 2**, the ionic conductivity of the composite wafer is influenced by the pathways of ion transport. The better the ion-exchange resin network for ion transport (i.e., more ion transport via the pathway of resin network) the higher the ion conductivity of the composite wafer. The highest resin conductivity obtained from different samples is measured to be 0.03 S/cm which is better than the originally anticipated value of 0.01 S/cm for a composite wafer.

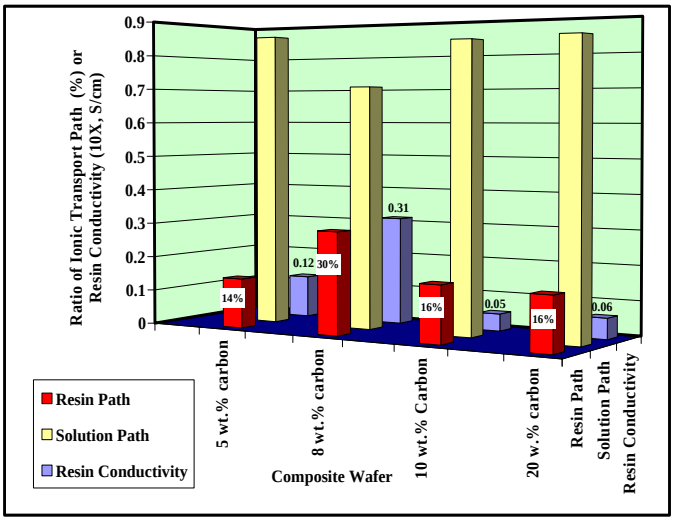

Figure 2. Results from semi-empirical model test for ion transport in the electron/ion conductive matrix in HCl solution.

A standard four-point electric impedance meter was used to measure the conductivity (electric or ionic) of the composite wafer.

The wafer porosity was determined using an organic dye. **Figure 3** shows the electric conductivities and porosities of the tested samples. A too high loading of carbon nanoparticles reduces the ionic conductivity of the wafer. Around 7-8 wt.% of carbon black is found to be the optimal condition. The electrical conductivities of the samples are in the range of 1.5 to 11 mS/cm. The hot-pressed composite wafer shows an increase of electrical conductivity by 5-fold (from 2 mS/cm to 11 mS/cm) and an increase in porosity by 3-fold (10-15% to 30-40%) compared with the wafer made by the wet method.

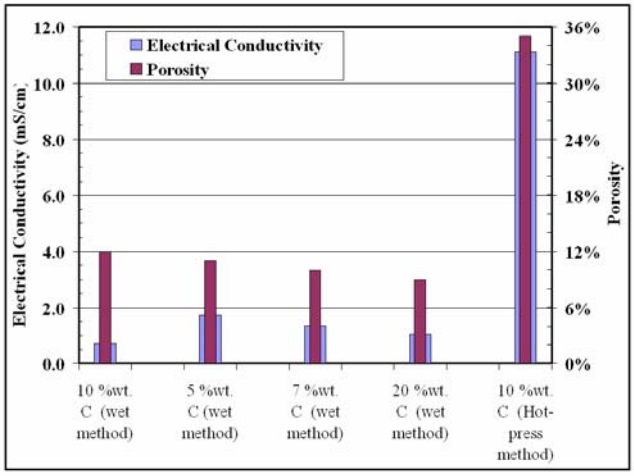

Figure 3. Electrical conductivity of different matrix compositions.

Electrochemical behavior of cofactor in the conductive matrix. Electrochemical behavior of a standard redox couple ferrocene methanol ($FcOH/FcOH^+$, water soluble standard) was undertaken to compare the composite matrix performance vs. a flat GC electrode. We found that the carbon black network in the composite matrix is effective enough to conduct the electron transfer reaction redox potentials for the $FcOH/FcOH^+$ couple. For the $NADH/NAD^+$ couple the composite matrix improved the oxidation potential more than 100 mV (i.e., more negative potential) than the GC electrode. This is very likely due to the simultaneous enhancement of both the electron and proton transfer in the cofactor oxidation/reduction. Several NADH oxidation mediators were evaluated as electron acceptors that potentially shift the oxidation potential to the negative direction. As shown in **Figure 4**, phenazine methosulfate gave larger catalytic currents due to NADH oxidation. The effects of phenazine methosulfate on NADH redox potential in the composite wafer are being carried out.

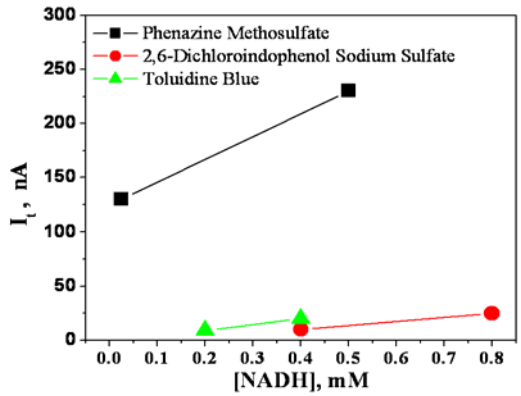

Figure 4. NADH electrocatalytic currents from several mediators.

Evaluation of the conductive matrix with immobilized enzyme. No significant change of ionic and electrical conductivities occurred with the inclusion of enzyme capture resin in the composite wafer matrix. Near 100% of GFOR enzyme was directly immobilized into the new prototype composite wafer with simple injection of the protein solution. The mechanism of capturing the electron from the reduced cofactor (NADPH) inside the GFOR enzyme dissolved in solution has been studied. The preliminary result shown in **Figure 5** indicates that the electron from the reduced cofactor of GFOR can be captured. This is evident by the lower concentration of the oxidized form of a blue indicating dye, 2,6-dichlorophenol indophenol, that turns colorless when it is reduced by an electron accepting mediator which captures the electron from the reduced cofactor (NADPH) inside GFOR. The re-oxidized (regenerated) cofactor ($NADP^+$) can continue to perform bioconversion of the substrate (e.g., glucose).

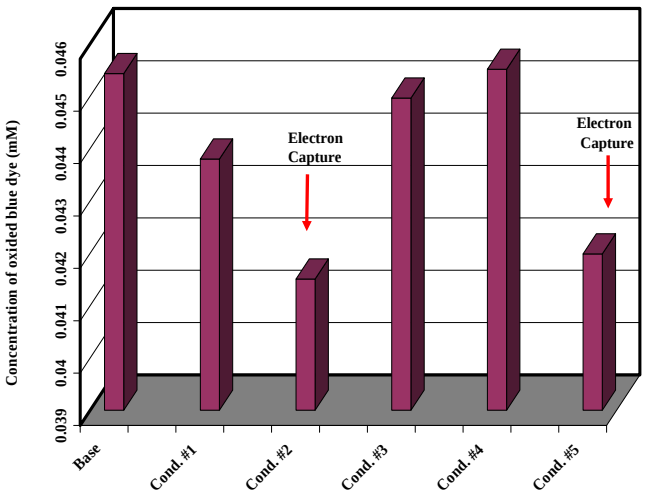

Figure 5. Electron capture from the cofactor in the GFOR enzyme.

Conclusions

We have successfully produced a composite matrix comprised of electronic/ionic mixed conductive wafer (carbon black particles with ion-exchange resin beads). The composite matrix reduces the oxidation potential of the $NADPH/NADP^+$ compared with a flat glassy carbon (GC) electrode. The matrix immobilized almost all of the introduced GFOR. A soluble mediator was used successfully as the electron acceptor to evaluate the capture mechanism of electron transfer from the cofactor inside GFOR.

Acknowledgments. The submitted manuscript has been created by the University of Chicago as Operator of Argonne National Laboratory ("Argonne") under Contract No. W-31-109-ENG-38 with the U.S. Department of Energy. The U.S. Government retains for itself, and others acting on its behalf, a paid-up, nonexclusive, irrevocable worldwide license in said article to reproduce, prepare derivative works, distribute copies to the public, and perform publicly and display publicly, by or on behalf of the Government.

ENZYME-CATALYZED OXYGEN REDUCTION: pH-DEPENDENT ELECTROSTATICS OF LACCASES

Alexander Kantarjiev, Boris Atanasov

Institute of Organic Chemistry, Bulgarian Academy of Sciences, Sofia-1113, Bulgaria

Plamen Atanassov

Department Chemical & Nuclear Engineering, University of New Mexico, Albuquerque, NM 87131

Introduction

Enzymatic bio-fuel cells employ enzymes to catalyze the corresponding anode fuel oxidation and cathode oxygen reduction reaction. Electron transfer between the enzyme and the electrode surface is usually facilitated by low-molecular weight mediators or via Direct Electron Transfer (DET) between the enzyme active site and electrode surface.[1] In the case of DET the structural and kinetic properties of the active site are of critical importance to the process effectiveness and impact cell design and performance.

Electrostatics of laccase (EC 1.10.3.2) is studied to reveal the pH-dependent mechanism of oxygen reduction by this enzyme. Laccases and other four-cooper oxidases (such as Bilirubin oxidase, for example) are being widely employed as cathode catalysts in bio-fuel cells demonstrating in many cases 4e$^-$ direct electron transfer mechanism at neutral or slightly acidic pH. It is universally accepted that copper sites play the key role in the catalytic process of coupled oxygen reduction and organic substrate oxidation. It is understood that this two-substrate, dual site enzymatic process follows formal "ping-pong" kinetics mechanism.

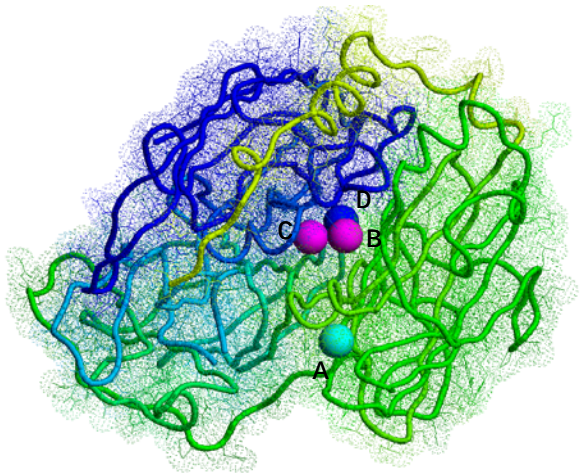

Figure 1. Structure of fungal laccases indicating the protein domains and its active site composed of four copper atoms grouped in two sub-sites: Cu (A) and the tri-copper site Cu (C-B-D)

Laccase is a member of four-cooper oxidases widely distributed in the living world. The presence of 4 Cu^{n+}, some of which change charges during redox action is coupled with transfer of four electrons (e^-) and four protons (H^+) to O_2. These enzymes demonstrate at quite limited pH-optimum of catalysis.[2] All of those features are indicators for quite substantial role of protein electrostatics for understanding principles of enzyme structure-function relationships and design of more effective electro-catalysis.

Main aim of this work is to analyze pH-dependent electrostatic free energy term, ΔG_{el}(pH) ("charge stability") of the protein (pdb1gw0.ent) at variable charges on 4Cu and 2O viewed in this study as reaction intermediates. To achieve this goal many other characteristics were calculated such as pH-dependent proton binding, pI and dipole moment(s) changes, influence of Cl^- as inhibitor. All the calculations are being carried out in terms of given crystal structure of laccases available from the Protein Data Bank. For comparison analogous but limited calculation were made with laccases from other sources, ascorbate oxidase (AscO) and other members of the protein family.

Results and Discussion

More than 140 charge configurations at fixed protein structure were calculated simulating from completely Cu-depleted (APO) to all ligands targeted protein (HOLO). These configurations included all full combinatorial set of Cu-"valence hybrids" and possible O-intermediates. The pH-dependent "charge stability", ΔG_{el}(pH) is highly found to be sensitive to Cu^{n+} valence state and the position of Cu-ions. It was established that increasing the total charge in the copper centers ***n*** leads to an overall decrease in the protein stability. It was also shown that there is a very specific ranking of different copper sites in charge-dependent protein destabilization. The system is least sensitive for ***n*** changes is Cu type I (aCu-site), than followed by Cu type II (dCu-site) and most sensitive for charge accumulation in the Cu type III (b,cCu-site).

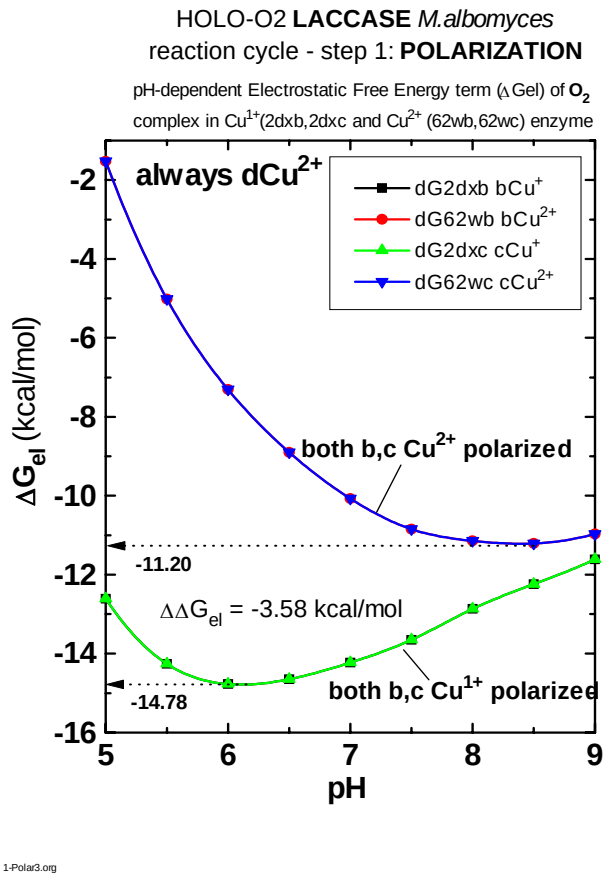

Figure 2. Electrostatic free energy calculation as a function of pH for laccase with fully oxidized copper B and C sites compared with the case of the same sites reduced.

New evidence was found that despite formal structural equivalence of bCu and cCu sub-sites (usually commonly described as undistinguishable type III copper centers) they behave energetically different. This difference is structurally expressed in the way that the bCu site is more close to the [2]O-atom from the residing oxygen undergoing reduction while the second [1]O-atom is more close to cCu and dCu ions. These configurations are found to be most sensitive to charge distribution variations. The proposed bCu…cCu sites non-equivalence for this structure was at first shown in this study and explained as intrinsic property of O_2 activation and it is hypothesized that it plays significant role in the O-O splitting stage or the overall oxygen reduction reaction catalyzed by copper-containing oxidases.

Protein electrostatics allows us to unambiguously confirm the general assumption that the protein globule plays most significant role in "directing" the electron transfer process. It is of even more expressed in catalysis of such irreversible processes as oxygen reduction reaction. This effect is can be illustrated by charge-charge interactions visualized as a big "spring" the protein "shell", which favors reduced Cu+ making difference between sites (a<c<d<b) and thus correspond to directional electron transfer from aCu → bCu more than from aCu → cCu. Many indirect evidences shows fixed charge system on dCu^{2+}.

Inhibition of laccases by chloride ions has always been an impeding factor to their wider technological introduction in redox process catalysis. This inhibition mechanism was not well understood and thus there was no rational basis for decision-making in bio-fuel cell design solutions. This study attempted to address chloride inhibition, which is demonstrated quite unevenly among the copper-containing oxidase enzyme family. The fact that some copper-containing enzymes are inhibited by Cl^- and some are not was taken as an indication that the process is heavily influenced by the structure and accessibility of the oxygen-reduction active site (the tri-copper site). In this study, direct Cl^- binding to dCu was considered as inhibition of oxidase action. The calculation had shown, however, that the including Cl^- into the system do not change qualitatively its ET properties and it only slightly (c.a.0.3-0.4 kcal/mol) destabilizes the protein. In the case of ascorbate oxidase (AscO), an enzyme with quite similar 4Cu configuration in the active site, the azide ion (N_3^-) inhibitor is bond to corresponding bCu and not to dCu site. It is hypothesized in this study that in the case of laccase Cl^- obstrucs the water entrance "micro-channel" to the tri-copper oxygen reduction site. By this steric effect it prevents the conjugated proton transport to the reduced O-intermediates, thus preventing the completion of the oxygen reduction reaction. The paths of incoming molecular oxygen and expulsion of water molecules remain structurally unclear at this point. It should be noted, however that the overall redox process is highly "energy productive" and the protein is separated into 3 structural domains (even SS-linked). Given this structural features one can suggest that the protein globule dynamics during catalysis is very likely to ensure mass-transfer of reactant and the product in a concerted manner. Calculations of such transport, however, were outside of the scope of this work, which was limited to the electrostatics of the crystalline structure of laccases.

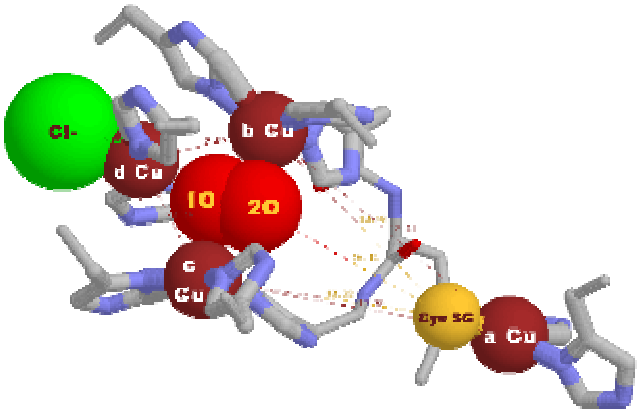

Figure 3. Structural representation of the active site of laccese inhibited by a chloride ion.

Conclusions

It has been established in this study that in 4Cu-enzymes oxidized Cu^{2+} destabilizes the overall protein and thus the structure energetically prefers the reduced Cu+ state. Such energetics supports electron transfer to the enzyme and thus facilitates the catalysis of the highly irreversible oxygen reduction reaction. The active site forms a true catalytic triad (b,c,dCu) resulting in highly asymmetric environment incorporating molecular oxygen. This environment is characterized by high electrostatic gradients between O-O and facilitates in consequence its hydrolytic breaking and "saturation" with H^+ completing by this an effective oxygen reduction as "concerted" process.

References

(1) Clabrese Barton, S; Gallaway, J.; and Atanassov, P.: Bio-Fuel Cells for Implantable and Micro-Scale Devices. *Chem. Rev.* **2004**, *104*, 4867-4886

(2) Solomon, E.I.; Sundaram, U.M.; and Machonkin, T.E:. Multicopper oxidase and Oxygenases. *Chem. Rev.* **1996**, *96*, 2563-2605.

ENZYME BASED HYDROGEN-OXYGEN FUEL CELL

Arkady Karyakin, Sergey Morozov, Mikhail Vagin, Elena Karyakina, Sergey Varfolomeyev

Faculty of Chemistry, M.V. Lomonosov Moscow State University, 119992, Moscow, Russia.

Introduction

Molecular hydrogen is considered nowadays as the most promising chemical fuel, in particular for fuel cells. Fuel electrodes use platinum (or platinum metals) as electrocatalysts. There are, however, crucial problems, which make impossible wide applications of fuel cells in future.

First, it is the problem with the *cost* and *availability*. Platinum-based fuel cells producing one kilowatt of energy will cost from $ 200 to $ 2000. Thus, the 100 kW engine will cost from $ 20 000 to $ 200 000, exceeding the cost of the whole car. Moreover, to equip 57.5 millions of cars available already in 2000 with the 100 kW fuel cells 11500 tons of Pt are required. It is much higher than the annual production (180 tons) and even comparative with the assured Pt resources (100000 tons).

Second, it is the *poisoning problem*. The cheapest hydrogen produced as reforming gas usually contains 1 ÷ 2.5 % of carbon monoxide (CO). However, even in the presence of 0.1 % CO the activity of platinum electrodes decreases irreversibly 100 times in 10 minutes. The only possibility to recover catalytic activity of platinum is to oxidize the absorbed CO at high electrode potential. However, in conventional fuel cell this requires the regime, which is closed to the short circuit. The latter obviously destroys the electrodes after a few cycles.

We propose biocatalysis as a valuable alternative to the catalysis by noble metals in respect to development of fuel electrodes. Certain enzymes being immobilized on electrode materials are able to deliver electrons between their active site and the electrode material, the phenomenon is called direct bioelectrocatalysis.

Bioelectrocatalysis of hydrogen oxidation and oxygen reduction. Hydrogen combustion reaction consists of the two redox half-reactions: hydrogen oxidation and oxygen reduction. The highest possible energy output of the fuel cell will be provided is oxygen is reduced into water without intermediate generation of hydrogen peroxide.

In nature there are enzymes *hydrogenases* responsible for activation and oxidation of molecular hydrogen feeding microorganisms with energy. Direct bioelectrocatalysis by hydrogenases has been reported more than 20 years ago by our group [1]. The most important feature of hydrogen enzyme electrode was a possibility to achieve hydrogen equilibrium potential pointing to possibility for 100% efficiency of energy conversion.

The most important feature of hydrogen enzyme electrodes is that they are practically insensitive to fuel impurities [2], and, thus, solve this crucial problem, which limits development of platinum-based fuel cells.

Considering oxygen reduction to water, there is a number of enzymes able to catalyze this reaction. First oxygen enzyme electrode was shown by Russian bioelectrochemical school more than quarter a century ago [3]. A certain disadvantage of enzyme electrocatalysis in this respect is that the enzymes do not catalyze oxidation of water into oxygen. An absence of the backward reaction does not allow achievement of O_2/H_2O equilibrium potential.

Enzyme based hydrogen-oxygen fuel cell. Both hydrogen and oxygen enzyme electrodes were combined in one system to elaborate the enzyme based hydrogen-oxygen fuel cell. We used as two kind of systems: fuel cell with liquid electrolyte, and fuel cell with solid electrolyte Nafion-type membrane separating anode and cathode [4].

Open circuit voltage of the membrane-containing fuel cell as a function of time is presented in figure 1. As seen, under flow of H_2 through compartment of hydrogen enzyme electrode an open circuit potential reaches the value of 1.15 V, which is at the record level for known hydrogen-oxygen fuel cells. In the absence of fuel cell voltage decreases, however, after restore of H_2 flow it again exceeds 1.1 V. A slow decrease of cell voltage with time is due to drying of this model system.

Conclusions

We have shown a possibility for construction of enzyme based hydrogen-oxygen fuel cell. Use of the enzymes instead of platinum metals solves the most crucial problem connected with the latter. In contrast to noble metals the enzymes are products of biotechnology and, thus, have a completely renewable source. Moreover, the cost of enzymes dramatically decreases upon their mass usage.

Enzymes as electrocatalysts of electrode reactions in fuel cells are highly specific to their reactions. This solves the third problem with platinum based fuel cells: decrease of energy conversion efficiency because of low selectivity. Indeed, as was shown, the enzyme based hydrogen-oxygen fuel cell displays the zero-current voltage at the record value.

Acknowledgement. Authors thank for financial support Program of RAS #26 on Hydrogen Energetics, INTAS Innovation grant 03-56-102, and Russian Science Support Foundation.

References

(1) Yaropolov, A.I.; Karyakin, A.A.; Varfolomeyev, S.D.; Berezin, I.V.; *Bioelectrochem. & Bioenergetics*, **1984** *12* 267-277.
(2) Karyakin, A.A.; Morozov, S.V.; Karyakina, E.E.; Zorin, N.A.; Perelygin, V.V.; Cosnier, S. *Biochemical Society Transactions*, **2005**, *33*, 73-75.
(3) Berezin, I. V.; Bogdanovskaya, V. A.; Varfolomeev, S.D.; Tarasevich, M.R.; Yaropolov, A.I. *Proc.Rus. Acad. Sci.*, **1978**, *240*, 615-618.
(4) Karyakin, A.A.; Morozov, S.V.; Karyakina, E.E.; Vagin, M.Yu.; Varfolomeyev S.D. *Patent of Russian Federation #* 2229515, **2004**.

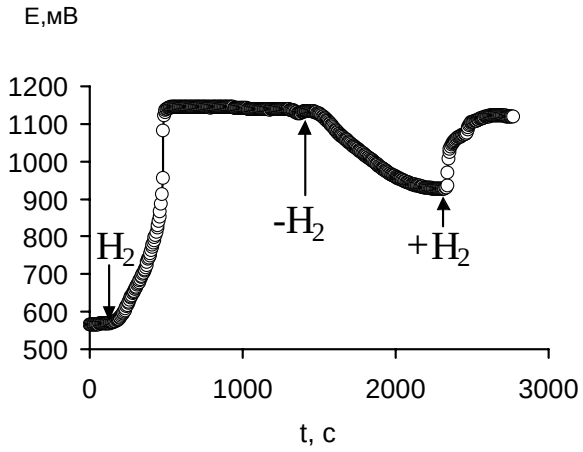

Figure 1. Zero current voltage of hydrogen-oxygen fuel cell with solid electrolyte membrane.

NANOBIOCATALYSTS FOR BIOFUEL CELLS

Ping Wang[1], Jungbae Kim[2], Hongfei Jia[1], and Xueyan Zhao[1].

(1) Department of Chemical Engineering, The University of Akron, Akron, OH 44325-3906, Fax: 330-972-5856, wangp@uakron.edu,
(2) Pacific Northwest National Laboratory

Abstract

Recent advances in nanobiocatalysis are promising for the development of high performance biofuel cells. Glucose oxidase electrodes were prepared via formation of composites with various nanostructured carbon materials such carbon fibers, carbon nanotubes, and nanoporous carbons. Significant enhancement on electrochemical reaction kinetics was observed on the composite-modified glassy carbon electrode. When these electrodes were applied in a model glucose/O2 biofuel cell, a power density of up to 960 μW/cm2 could be achieved. According to the quantitative analysis of the processes involved in the anode, the mass-transfer of mediator appeared to be the limiting factor to the power and current densities of biofuel cell. It is expected that the power density can be greatly improved by the improvement of electron transfer and optimization of the electrode structure.

ELECTRIC "CONTACTS" BETWEEN CONDUCTORS AND PROTEIN ACTIVE SITES – THE BASIS FOR BIOCHEMICAL FUEL CELLS. HYDROGEN-OXYGEN FUEL CELL.

S.D. Varfolomeyev, A.A. Karyakin[#], S.V. Morozov[#]

Institute of Biochemical Physics,
Russian Academy of Science, 119991, Moscow, Russia
[#]Moscow State University, 119992, Moscow, Russia

Introduction

The problems related to the mechanisms of electron transfer between electron-conducting structures (metals, semiconductors or organic conductors) and biopolymer molecules are central and most important in biofuel cells construction. Our interest in this area was to study the enzyme behavior at the interface "ionic conductor (electrolyte solution or solid electrolyte) - electron conductor (metal, carbon or semiconductor)". In the experiments with various enzymes, we have shown that the direct electron transport between a conductor and the active site of redox enzyme is feasible. The rates of electron transfer, which may well proceed by the tunneling mechanism, can exceed the rates of subsequent enzymatic steps. In this case, we can think of an electric "contact" between semiconductor and enzyme active site. The enzyme can act as electrocatalyst "pumping out" the electrons from conductor or donoring them into the conductor. This phenomenon was first revealed for blue copper-containing oxidase (laccase) reducing molecular oxygen to water; the source of electrons was the conductor matrix[1]. The phenomenon of bioelectrocatalysis is the basis for development of biological fuel cells. Different prototypes of hydrogen-oxygen fuel cells were constructed based on direct bioelectrocatalysis by hydrogenases and oxidases immobilized onto different carbon materials.

The phenomenon of direct electron transfer from protein active site to conductor (or reverse process) can be determined as DET-effect. Below are analyzed the DET-effect on an example of some enzymatic reactions.

Blue copper oxidase (laccase): The enzymatic electrochemical reduction of oxygen

Laccase is a copper-containing enzyme performing the four-electron reduction of oxygen, with different aromatic amines and phenols used as donors. The active site of the enzyme consists of four copper ions involved in a coordinated oxygen reduction. It was found that laccase in minor quantities (10^{-9} M) strongly shifts the stationary potential towards the zone of positive values and accelerates oxygen electroreduction[2]. The enzymatic nature of electrocatalysis in this case was proved by a specific inhibition of electrocatalytic effects by fluoride and azide ions, heat inactivation, and by comparing the pH dependence of the electrocatalytic effects and the catalytic activity in the oxidation of ferricyanide ion by oxygen. Experiments showed that the stationary potential of the electrode depends on oxygen partial pressure and the solution pH in accordance with the Nernst equation for the O_2/H_2O system. Rotating disc-electrode experiments did not detect intermediate hydrogen peroxide in the solution. The observed electrochemical process on the electrode with immobilized laccase is governed by the reaction of oxygen four- electron reduction to water:

$$O_2 + 4e^- + 4H^+ \rightarrow 2H_2O \qquad (1)$$

That was the first observation of DET-effect. This phenomenon was investigated experimentally in details[2].

Hydrogenase

As the carbon black electrode with immobilized hydrogenase from *Thiocapsa roseopersicina* was introduced into the buffer phosphate solution saturated with hydrogen, a potential equal to 0.000±0.001 V was set at the electrode (Fig.1).

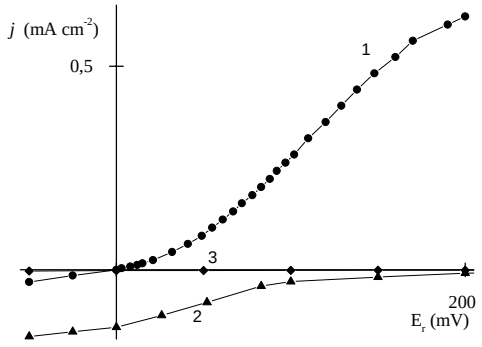

Figure 1. Carbon tissue electrode with directly adsorbed hydrogenase from *T. roseopersicina* in H_2 (1), Ar (2) and blank electrode (3). Phosphate buffer pH=7.0, 30°C. Potential vs. H_2/Pt electrode in same buffer.

Logarithm of current as a function of pH and logarithm of hydrogen partial pressure at different values of overvoltage was studied. The zero order of the electrocatalytic reaction rate with respect to substrate and product concentrations was observed. It was concluded that the hydrogen molecule addition and proton ejection out of the active enzyme center take place faster than the oxidation-reduction stages (electrochemical ones in the given case). To find the kinetics of electron exchange between the enzyme active center and the electrode, the dependence of current on overvoltage was considered. The absence of single slope of the polarization curve in semilogarithmic coordinates attests that, firstly, there is more than one stage (two by the number of transferred electrons) during the catalytic process, and, second, both these stages are dependent on potential and occur at relatively comparable rates. Thus, the formula for the description of the polarization curve should be complicated. The consideration of the process as a consequent two electrons transfer results in equation[3]:

$$j = \frac{\exp\left(2\frac{\alpha nFE}{RT}\right) - \exp\left(-2\frac{(1-\alpha)nFE}{RT}\right)}{K_1 \exp\left(\frac{\alpha nFE}{RT}\right) + K_2 \exp\left(-\frac{(1-\alpha)nFE}{RT}\right)} \qquad (2),$$

where K_1 and K_2 are the constants including the surface concentration of active enzyme and definite combinations of elementary constants. At $K_1 \neq K_2$ the branches of a polarization curve in positive and negative regions will be asymmetrical about the origin of the coordinates, as distinct from the case of single stage ionization reaction. Eq.2 describes the current-potential relationship well. The only kinetic scheme was found to obey the experimental data for hydrogenase catalysis, include the stages of electrochemical or one-electron redox steps. (Hydrogen - proton - electron -transfer, - electron - proton mechanism H_2peltelp mechanism). It was concluded that the kinetic properties of hydrogenase action obtained from electrochemical and homogeneous kinetics describe the same mechanism. The hydrogenase adsorbed on conductor possesses electrocatalytic activity in both the reaction of hydrogen oxidation and evolution. It is possible to describe quantitatively the observed electrocatalytic reactions. The data on the mechanism of hydrogenase action in electrocatalytic process coincide with those obtained in studying the homogeneous kinetics of this enzyme. In bioelectrocatalysis (according to the mechanism of direct electron exchange between the electrode and enzyme active site) it operated

in the same way as in the solution using the electrode as one of the substrates.

One of the most important problem of platinum-based hydrogen fuel electrodes is their poisoning by carbon monoxide. Despite CO is also an inhibitor of hydrogenase activity, the inhibition is completely reversible and characterized by a high inhibition constant. Thus, the use of biological catalysts is expected to avoid this crucial problem of modern fuel cells. Indeed, when the hydrogenase enzyme electrode was tested under different H_2 – CO mixtures, no recognizable inhibition was observed up to CO content of 0.1%. Only under 1% of CO the rate of hydrogen oxidation was decreased by approximately 10%[4]. Moreover, inhibition of hydrogen enzyme electrode by carbon monoxide is completely reversible. Even after exposing to pure carbon monoxide the hydrogenase electrode recovers 100% of its initial activity as soon as the atmosphere is changed back to hydrogen. We resume that using the enzymes as electrocatalysts one can solve the most important problem of the modern fuel cell technology: poisoning of the electrodes by fuel impurities.

The tunneling of electrons, a possible way for the explanation of DET-effects

Active sites of enzymes acting as catalysts of electrode processes are localized inside the protein globule. It is evident that under catalytic conditions electrons are transferred to sufficiently long distance by the DET mechanism. The main conclusion of the analysis given below is that the concept of the tunneling mechanism is adequate for the description of the DET effect. The simplest scheme contains a stage of electron transfer from the electrode to the active site of an enzyme and a reaction of a "catalytic" enzymatic transformation of an electron (or a vacancy) into the final product of the enzymatic reaction:

$$e \xrightarrow{k_1} e^{\#} \xrightarrow{k_{cat}} E + P \qquad (3),$$

where e and $e^{\#}$ are the oxidized and the reduced forms of the active site, k_1 is frequency or the rate constant of electron transfer between the electrode and the active site, k_{cat} is the catalytic rate constant of the enzymatic reaction characterizing the limiting stage of the catalytic process. In a stationary state with respect to $e^{\#}$, the intermediate form, with the material balance equation taken into account, the specific current from the electrode is expressed as:

$$j = -\frac{nFk_{cat}k_1}{k_1 + k_{cat}}[e]_0 \qquad (4),$$

where $[e]_o$ is the surface concentration of the enzyme. K_{cat} values for enzymatic reactions do not vary much and are distributed in a rather narrow zone around the average figure of 10^2 s^{-1}. The mechanism of electron tunneling in chemical and biochemical systems is a subject of a detailed analysis in the literature. The rate constant of electron tunneling depends on the height and the width of the barrier:

$$k_1(r) = v\exp(-r/A) \qquad (5),$$

where v is the frequency factor, r is the width of the barriers, A is a parameter whose value depends on the height of the kinetic barrier. Several quantum mechanical models of electron transfer allowing the values of the frequency factor and the parameter A to be calculated have been developed by now. The solution of the problem of tunneling across rectangular, triangular, and parabolic barriers with a continuous energy spectrum of electrons has been discussed in the literature. If to take into account the discrete character of the spectrum and motion of nuclei in molecules in electron tunneling between two molecules a theory of electron transfer in protein systems making it possible to calculate transfer rate constants on the basis of structure properties of the medium. It is to be emphasized that in all models of electron tunneling transition the dependence of transition rate constant on distance is expresses by Eq. 5. The physical sense and numerical values of the parameters v and A can vary depending on the model. According to the common model, the frequency factor v has a physical sense of the frequency of collisions of an electron with the barrier (the velocity of an electron in a molecule or a crystal) and equals ~ 10^{16} s^{-1}. The value of the parameter A having the dimension of distance is defined by the difference of electron energies and the height of the barrier. It is important to note that the magnitude of A only slightly depends on the shape of the barrier, the main factor determining its numerical value being the energetics of the process. It is of interest to evaluate the distances within which the rate of electron transfer to the active site of an enzyme is greatly exceeding the rate of catalysis. In this case the enzymatic reaction is the rate-determining stage. For carbon electrodes, it was found that for a parabolic barrier A = 0.594 Å. It was shown that for $k_{cat} = 10^2$ s^{-1}, r_{cr} = 19.1 Å. This means that if an electron-accepting particle in the active site of an enzyme is located at a distance from the electrode surface shorter than 19 Å, the rate of donation of electrons to the active site will surpass the rate of the catalytic stage and the catalytic enzymatic reaction will be the rate-determining stage. The model of electron transfer in bioelectrocatalysis can be verified by studying the dependence of the measured bioelectrocatalytic currents on the distance between the electrode and the electron-accepting point in the active site of an enzyme. A comparative study of DET-effects was conducted on electrodes obtained by enzyme adsorption directly on carbon and on carbon coated with a lipid monolayer. Electrodes without lipid monolayer and also with a monolayer of cholesterol in two orientations were prepared. Laccase was adsorbed on the surface of the lipid and electrocatalytic properties of the obtained systems were studied in the reaction of electrochemical reduction of molecular oxygen. Electrodes with a monolayer of adsorbed lecithin were also obtained and studied. The currents obtained in a system without cholesterol and with cholesterol in flat orientation are the same. With vertically oriented cholesterol the current is 5 times less. With the electrodes covered by lecithin the electron transfer efficiency is 270 times less. Thus, the concept of the tunneling of electrons accounts for the observed DET-effects. If the site accepting electrons from the electrode is located at a distance shorter than r_{cr} (r_{cr} 20-30 Å; the radii of protein molecules are 10-30 Å), the rate of its "occupation" with electrons will be much higher than the rate of the enzymatic reaction and the experiment will reveal the effects of a drastic acceleration of the electrochemical reaction by a protein catalyst.

Hydrogen-oxygen fuel cell

On the basis of immobilized hydrogenase and laccase was constructed the hydrogen-oxygen fuel cell with proton exchange membrane. The characteristics of the cell are presented in patent[5]. The great advantage of the enzymatic fuel cells is the renewable nature of the used catalysts. We believe that the future development of the enzymatic fuel cells technology will makes the advantage more and more attractive.

Acknowledgement. The financial support from INTAS grant 03-56-102 is greatly acknowledged.

References

(1) Berezin, I.V.; Varfolomeyev, S.D. *Enzym. Eng.* **1980**, *5*, 95.
(2) Bogdanovskaya, V.A.; Varfolomeyev, S.D.; Tarasevich, M.R.; Yaropolov, A.I. *Electrokhimiya*, **1980**, *16*, 763.
(3) Varfolomeyev, S.D.; Yaropolov, A.I.; Karyakin, A.A. *J. Biotechnology*, **1993**, *27*, 331.
(4) Karyakin, A.A.; Morozov, S.V.; Karyakina, E.E.; Varfolomeyev S.D., Zorin, N.A.; Cosnier, S. *Electrochem. Comm.*, **2002**, *4*, 417.
(5) Patent WO2004114494.

MICROFLUIDIC ETHANOL BIOFUEL CELL

Anna Kinsella, R. Scott Martin, and Shelley D. Minteer

Department of Chemistry, Saint Louis University, St. Louis, MO

Introduction

Recent research has focused on microfluidic batteries and fuel cells (1-4), but the same microfluidic technology has not been thoroughly investigated for biofuel cells. This research focuses on the development of stackable, microchip- based biofuel cells. Microchip-based biofuel cells are compact and lightweight, making them viable portable power sources. In theory, they are also stackable, enabling multiple cells to be linked in series to increase power output. Microchip-based biofuel cells employ hydrodynamic flow of fuel through micron-sized channels containing microelectrodes. In this research, the enzyme pyrroloquinoline quinone (PQQ)-dependent alcohol dehydrogenase (ADH) is used as the catalyst in the biofuel cell to convert chemical energy to electrical energy. The cell is powered by the addition of ethanol through a micron-sized flow channel containing a bioanode, which is fabricated by micromolding carbon inks. This microelectrode is modified with a membrane containing the immobilized enzyme. We have successfully immobilized the enzyme on the electrode and electrochemical characterization has shown that the system is kinetically limited rather than transport limited.

Experimental

A 40 micron wide and 27.5 micron high micromolded carbon electrode is formed on a clean glass substrate using procedures described in Reference 5 and 6. A 100 micron PDMS channel is reversibly sealed over the micromolded carbon electrode. The carbon electrode is coated with a 2:1 ratio of PQQ-dependent alcohol dehydrogenase (ADH) to tetrabutylammonium bromide (TBAB)-modified Nafion membranes (prepared using the procedures described in Reference 7 and 8) by introducing the coating mixture to the 100 micron PDMS channel by hydrodynamic flow from a syringe at 1.0 microliters/min. The coating is allowed to dry overnight in the PDMS channel. Then, the PDMS channel is removed, leaving the immobilized enzyme coating on the carbon electrode. A 200 micron PDMS channel is reversibly sealed over a micromolded arbon electrode coated with immobilized enzyme. A 1.0mM ethanol fuel solution in pH 7.15 phosphate buffer is pumped over the coated electrode at flow rates ranging from 1.0 to 15.0 microliters/min. Cyclic voltammetry is performed to electrochemically characterize the coated carbon electrode. Fuel cell testing is performed by placing an external platinum cathode in the output reservoir of the 200 micron PDMS channel.

Results and Discussion

Figure 1 is schematic of the chemistry occurring at the bioanode. A micromolded carbon electrode is coated with a TBAB-modified Nafion membrane with PQQ-dependent ADH immobilized within. The ethanol fuel diffuses into the membrane and is oxidized by the PQQ-dependent ADH. The PQQ acts as the electron mediator to shuttle electrons from the enzyme to the electrode. Cyclic voltammograms of the bioanode in a fuel solution show sigmoidal voltammograms that are consistent with microelectrodes.

Power curves were generated with the bioanode in conjunction with an external platinum cathode at different flow rates. Figure 2 depicts the effect of flow rate on the maximum current density at the bioanode. The data depicts the average of three different fuel cells and the error bars correspond to one standard deviation. There is no statistical difference between current densities at flow rates ranging from 1mL/min to 15mL/min. This indicates that the system may have kinetic limitations as well as transport limitation.

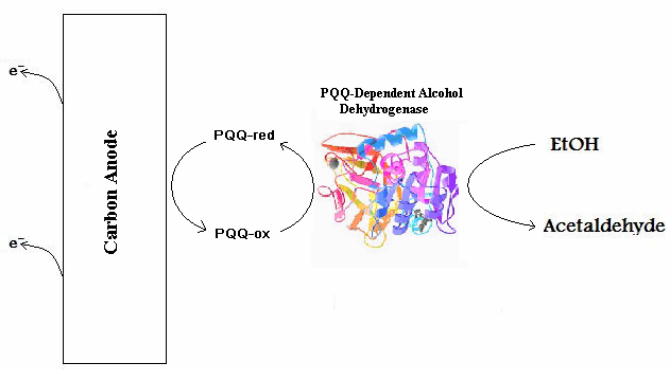

Figure 1. Schematic of the chemistry occurring at the PQQ-dependent bioanode.

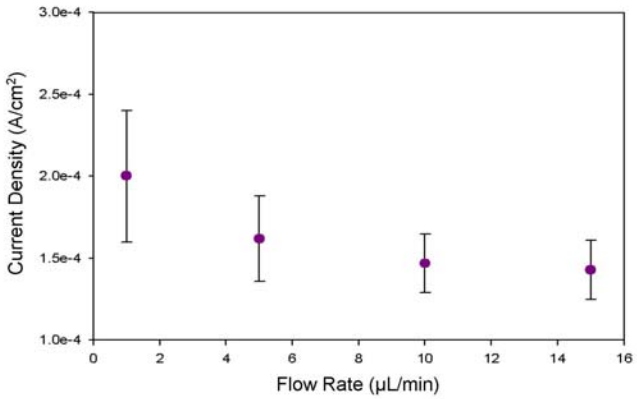

Figure 2. Plot of current density of an ethanol bioanode versus volumetric flow rate of 1.0 mM ethanol in pH 7.15 phosphate buffer (n=3).

Conclusions

Microfabrication and microchip-based systems can be used to form bioanodes. There is no statistical difference in the current densities for the various flow rates of fuel, which is evident that the system is kinetically limited. Future work will focus on integrating the cathode onto the microchip.

Acknowledgement. The authors acknowledge the Office of Naval Research for funding.

References

(1) Ferrigno, R.; Stroock, A.D.; Clark, T.D.; Mayer, M.; Whitesides, G.M. *JACS*, **2002**, *124*, 12930.
(2) Cohen, J.L.; Volpe, D.J.; Westly, D.A.; Pechenik, A.; Abruna, H.D. *Langmuir* **2005**, *21*, 3544.
(3) Choban, E.R.; Markoski, L.J.; Wieckowski, A.; Kenis, P.J. *J. Power Sources*, **2004**, 128, 54.
(4) Choban, E.R.; Markowski, L.J.; Stoltzfus, J.; Moore, J.S.; Kenis, P.J. *Proc. Power Sources Conference*, **2002**, 40, 317.
(5) Moore, C.M.; Minteer, S.D..; and Martin R.S. *Lab-on-a-chip.*, **2005**, *5*, 218.
(6) Kovarik, M.L.; Torrence, N.J.; Spence D.M.; and Martin, R.S. *Analyst* **2004**, *129*, 400.
(7) Schrenk, M.; Villigram, R.; Torrence, N.J.; Brancato, S.; and Minteer, S.D. *J. Mem. Sci.*, **2002**, 205, 3.
(8) Moore, C.M.; Johnson, V.; Hill, A.; Akers, N.L.; and Minteer S.D. *Biomacromolecules*, **2004**, 5, 1241.

ENZYME-BASED BIOFUEL CELLS WITH SWITCHABLE AND TUNABLE POWER OUTPUT

Eugenii Katz and Itamar Willner

Institute of Chemistry
The Hebrew University of Jerusalem
Givat Ram, Jerusalem 91904, Israel

Introduction

Electrical contacting of redox enzymes with electrode supports attracts substantial research efforts directed to the development of biosensors[1] and biofuel cell elements.[2] Recently, we reported on the effective electrical contacting of redox enzymes on electrodes by their structural alignment on electrodes through the surface reconstitution of flavoenzymes or pyrroloquinoline quinone (PQQ)-dependent enzymes on a relay-FAD monolayer assembly[3,4] or redox polymer-PQQ thin film,[5] respectively. This concept was further generalized by tailoring integrated, electrically contacted, cofactor-dependent enzyme electrodes by the cross-linking of affinity complexes between NAD^+-dependent enzymes and an electrocatalyst-NAD^+ monolayer[6] or thin film[7] associated with electrodes. Efficient electron transfer between redox enzymes and conductive electrode supports as a result of structural alignment and optimal positioning of the electron mediators allowed the development of noncompartmentalized biofuel cells.[8] Crossreactions of the anolyte fuel and catholyte oxidizer with the opposite electrodes were prevented due to the high specificity of the bioelectrocatalytic reactions at the electrodes, and thus the use of a membrane separating the catholyte and anolyte solutions could be eliminated. This kind of biofuel cell was suggested as an implantable device that uses physiological fluids, for example, blood, for the generation of electrical power that activates machinery units such as pacemakers or insulin pumps. Also, a noncompartmentalized biofuel cell can be used as a self-powered biosensor for glucose or lactate, because the output voltage and current signals are dependent on the substrate concentration.[9]

In the present paper, we wish to report on novel configurations of biofuel cells, in which the output power (voltage and current) can be reversibly switched between "ON" and "OFF" states and the magnitude of the voltage-current output can be precisely tuned by electrochemical or magnetic input signals.

Experimental

Electrical Switching and Tuning. The electrical switching and tuning of the biofuel cell output was accomplished by the integration of the biocatalysts active in the biofuel cell with a copper-poly(acrylic acid) matrix.[10] The electrodes were modified with a poly-(acrylic acid) thin film using the electropolymerization technique.[11] The polymer-modified electrodes were soaked in 0.1 M $CuSO_4$ solution for 1 h to saturate the polyacrylic film with Cu^{2+} ions and then biocatalytic anodic or cathodic enzyme-based systems were bound to the polymer-modified interfaces.[12] The system consists of two enzyme-functionalized electrodes (ca. 0.19 cm^2 active area) separated by a rubber O-ring (ca. 2 mm thickness). The first electrode functionalized with the reconstituted glucose oxidase (GOx) and the second electrode functionalized with cytochrome c/cytochrome oxidase (Cyt *c*/COx) assembly are acting as the anode and cathode, respectively. Two metallic needles (inlet and outlet) implanted into the rubber ring convert the unit into a flow cell. These needles were also used as external electrodes to apply electrical signals controlling conductivity of the polymer-modified electrodes. A peristaltic pump was applied to control the flow rate. Glucose solutions in 0.1 M TRIS-buffer, pH = 7.0, saturated with air were applied to power the biofuel cell.

Magnetic Control of Biofuel Cells. Biofuel cells composed of biocatalytic anode and cathode based on the enzyme-reconstituted systems[13] were inserted between the poles (diameter of 6 cm, separated by a distance of 1 cm) of an electromagnet (Model DPS-175, Scientific Equipment Roorkee, India) providing a constant magnetic field (±1% homogeneity) of variable strength that was measured with a Digital Gaussmeter (model DGM-102, manufactured by Sestechno, India). The enzyme-modified biocatalytic electrodes were positioned parallel to the direction of the magnetic field. Different magnetic fields applied on the electrochemical cell were generated by a sequential "ON" and "OFF" process. Glucose or lactate solutions saturated with air were applied to power the biofuel cells.

Results and Discussion

The assembly of the biocatalyst/copper-poly(acrylic acid) hybrid system with electrodes allows for the electrical control of the conductivity properties of the matrix, thus enabling the electroswitchable and tunable functions of the biofuel cell, **Figure 1**.

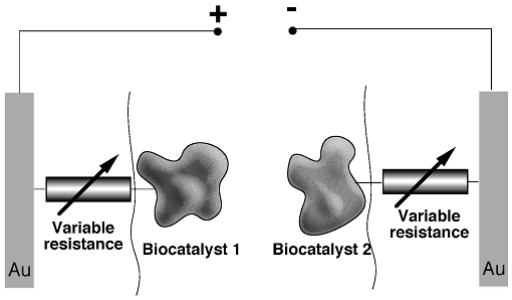

Figure 1. Electrically switchable and tunable enzyme-based biofuel cell with the variable resistances of the biocatalytic electrodes provided by the copper-poly(acrylic acid) thin film.

The anode consists of a Cu^{2+}-poly(acrylic acid) film on which the redox-relay pyrroloquinoline quinone (PQQ) and the flavin adenine dinucleotide (FAD) cofactor are covalently linked. Apo-glucose oxidase is reconstituted on the FAD sites to yield the glucose oxidase (GOx)-functionalized electrode. The cathode consists of a Cu^{2+}-poly(acrylic acid) film that provides the functional interface for the covalent linkage of cytochrome c(Cyt c) that is further linked to cytochrome oxidase (COx). Electrochemical reduction of the Cu^{2+}-poly(acrylic acid) films (applied potential -0.5 V vs SCE) associated with the anode and cathode yields the conductive Cu^0-poly(acrylic acid) matrixes that electrically contact the GOx-electrode and the COx/Cyt c-electrode, respectively. The short-circuit current and open-circuit voltage of the biofuel cell correspond to 105 μA (current density ca. 550 μA cm^{-2}) and 120 mV, respectively, and the maximum extracted power from the cell is 4.3 μW at an external loading resistance of 1 kΩ. The electrochemical oxidation of the polymer films associated with the electrodes (applied potential 0.5 V) yields the nonconductive Cu^{2+}-poly(acrylic acid) films that completely block the biofuel cell operation. By the cyclic electrochemical reduction and oxidation of the polymer films associated with the anode and cathode between the Cu^0-poly(acrylic acid) and Cu^{2+}-poly(acrylic acid) states, the biofuel cell performance is reversibly switched between "ON" and "OFF" states, respectively, **Figure 2**. The electrochemical reduction of the Cu^{2+}-polymer film to

the Cu^0-polymer film is a slow process (ca. 1000 s) because the formation and aggregation of the Cu^0-clusters requires the migration of Cu^{2+} ions in the polymer film and their reduction at conductive sites. The slow reduction of the Cu^{2+} -polymer films allows the controlling of the content of conductive domains in the films and the tuning of the output power of the biofuel cell. The electron-transfer resistances of the cathodic and anodic processes were characterized by impedance spectroscopy. Also, the overall resistances of the biofuel cell generated by the time-dependent electrochemical reduction process were followed by impedance spectroscopy and correlated with the internal resistances of the cell upon its operation.

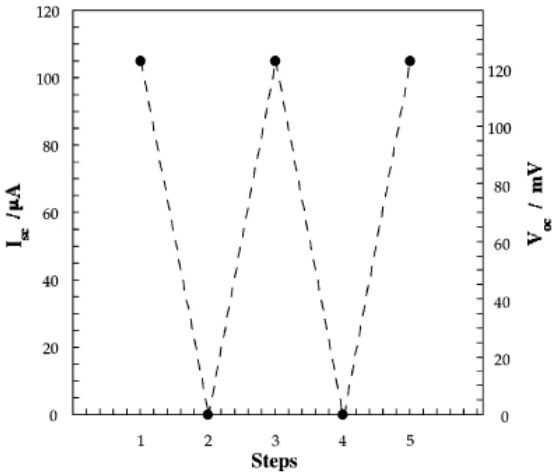

Figure 2. Reversible switching "ON" and "OFF" of the short-circuit current, I_{sc}, and the open-circuit voltage, V_{oc}, generated by the biofuel cell. The cell output is switched "ON" (steps 1, 3, and 5) by the application of the potential of -0.5 V to both biocatalytic electrodes for 1000 s and switched "OFF" (steps 2 and 4) by the application of a potential of 0.5 V to the biocatalytic electrodes for 5 s. The measurements were performed in the presence of 80 mM glucose solution saturated with air.

Magnetohydrodynamic effect recently demonstrated for bioelectrocatalytic systems[14] paves the way to control magnetically the performance of biofuel cells.[13] The effect of a constant magnetic field on bioelectrocatalytic transformations of three different enzyme assemblies linked to electrodes was examined and correlated with a theoretical magnetohydrodynamic mode.[15] The systems consist of surface-reconstituted glucose oxidase (GOx), an integrated lactate dehydrogenase/nicotinamide/pyrroloquinoline quinone assembly (LDH/NAD^+-PQQ), and a cytochrome c/cytochrome oxidase system (Cyt c/COx) linked to the electrodes. Pronounced effects of a constant magnetic field applied parallel to the electrode surface are observed for the bioelectrocatalyzed oxidation of glucose and lactate by the GOx-electrode and LDH/NAD^+-PQQ-electrode, respectively. The enhancement of the bioelectrocatalytic processes correlates nicely with the magnetohydrodynamic model, and the limiting current densities ($\mathbf{i}_L$) relate to $B^{1/3}$ (B = magnetic flux density) and to $C^{*4/3}$ (C* = bulk concentration of the substrate). A small magnetic field effect is observed for the Cyt c/COx-electrode, and its origin is still questionable. The effect of the constant magnetic field on the performance of biofuel cells with different configurations was examined, **Figure 3**. For the biofuel cell consisting of LDH/NAD^+-PQQ anode and Cyt c/COx cathode, a 3-fold increase in the power output was observed at an applied magnetic field of B = 0.92 T and external load of 1.2 kΩ. Besides the general biochemical implications of the results that might shed light on the magnetic field effects on biocatalytic electron-transfer reactions occurring at membrane interfaces, we demonstrated the utility of the magnetohydrodynamic effect for enhancing the power output of biofuel cells. Our results indicate that one has to search for the magnetic field effects on the electrode that controls the power output of the biofuel cells to improve the biofuel cell performance.

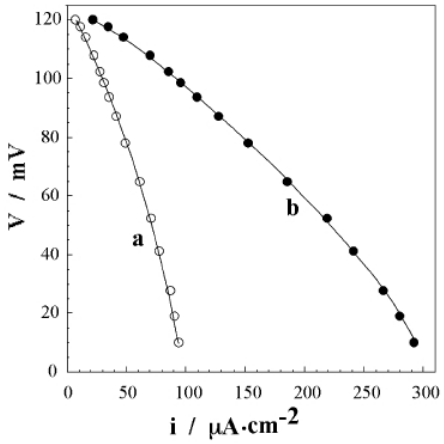

Figure 3. Enhancement of the performance of the biofuel cell composed of the LDH/NAD^+-PQQ-anode and COx/Cyt *c*-cathode: (a) in the absence of magnetic field; (b) in the presence of magnetic field, B = 0.92 T.

References

1. Willner, I.; Katz, E. *Angew. Chem., Int. Ed.,* **2000**, *39*, 1180-1218.
2. Katz, E.; Shipway, A. N.; Willner, I. In *Handbook of Fuel Cells - Fundamentals, Technology, Applications*; Vielstich, W., Gasteiger, H., Lamm, A., Eds.; Wiley: Chichester, 2003; Vol. 1, Part 4, pp 355-381.
3. Willner, I.; Heleg-Shabtai, V.; Blonder, R.; Katz, E.; Tao, G.; Bückmann, A. F.; Heller, A. *J. Am. Chem. Soc.,* **1996**, *118*, 10321-10322.
4. Zayats, M.; Katz, E.; Willner, I. *J. Am. Chem. Soc.,* **2002**, *124*, 2120-2121.
5. Raitman, O. A.; Patolsky, F.; Katz, E.; Willner, I. *Chem. Commun.,* **2002**, 1936-1937.
6. Bardea, A.; Katz, E.; Bückmann, A. F.; Willner, I. *J. Am. Chem. Soc.,* **1997**, *119*, 9114-9119.
7. Raitman, O. A.; Katz, E.; Bückmann, A. F.; Willner, I. *J. Am. Chem. Soc.,* **2002**, *124*, 6487-6496.
8. Katz, E.; Willner, I.; Kotlyar, A. B. *J. Electroanal. Chem.,* **1999**, *479*, 64-68.
9. Katz, E.; Bückmann, A. F.; Willner, I. *J. Am. Chem. Soc.,* **2001**, *123*, 10752-10753.
10. Chegel, V. I.; Raitman, O. A.; Lioubashevski, O.; Shirshov, Y.; Katz, E.; Willner, I. *Adv. Mater.,* **2002**, *14*, 1549-1553.
11. Katz, E.; De Lacey, A. L.; Fernandez, V. M. *J. Electroanal. Chem.,* **1993**, *358*, 261-272.
12. Katz, E.; Willner, I. *J. Am. Chem. Soc.,* **2003**, *125*, 6803-6813.
13. Katz, E.; .Lioubashevski, O.; Willner, I. *J. Am. Chem. Soc.,* **2005**, *127*, 3979-3988.
14. Katz, E.; Lioubashevski, O.; Willner, I. *J. Am. Chem. Soc.,* **2004**, *126*, 11088-11092.
15. Lioubashevski, O.; Katz, E.; Willner, I. *J. Phys. Chem. B,* **2004**, *108*, 5778-5784.

LAMINAR FLOW-BASED BIOFUEL CELLS: INDEPENDENT TAILORING OF THE pH AT THE CATHODE AND ANODE TO ENHANCE THE ACTIVITY AND STABILITY OF BOTH ENZYMES

Eric R. Choban, Lajos Gancs, Ranga S. Jayashree, Michael Mitchell, Jacob S. Spendelow, Seong Kee Yoon, and Paul J.A. Kenis

Chemical & Biomolecular Engineering
University of Illinois at Urbana-Champaign
600 South Mathews Avenue
Urbana, IL 61801

Introduction

Recently, research towards the development of biofuel cells has gained significant momentum. In enzymatic biofuel cells many of these efforts have focused on improving electrical between biocatalysts and electrodes communication by mediated or by direct electron transfer to enhance the performance.[1] Use of a mediator, be it free in solution or immobilized, typically increases the rate of electron transfer between the active site of enzyme biocatalysts and the electrode. For example, dissolved $NAD(P)^+$ and ABTS can function as a mediator for enzymatic anodes and cathodes, respectively. Electropolymerized methylene green for electro-oxidation of NADH is an example of an immobilized mediator. Bio-anodes can be formed from poly(methylene green) modified electrodes with dehydrogenase enzymes immobilized within a Nafion layer.[2] A recently reported bio-cathode is comprised of the enzyme laccase and a redox mediator (Os^{2+}) immobilized within a polymer hydrogel on carbon-fiber paper support.[3] An performance limiting issue in enzymatic biofuel cell systems for which no solution has been reported is that these cells are operated at a certain compromise pH that may be optimal for the activity and stability of one enzyme, but sub optimal for the other.[1] We intend to address this issue here.

Recently, we have developed membraneless microfluidic fuel cells that exploit a characteristic of fluid flow at the microscale, *laminar flow*, to keep two streams containing fuel and oxidant, respectively, separated while still in diffusional contact.[4] The fuel and oxidant containing streams merge in a Y-shaped microfluidic channel and continue to flow in parallel without turbulent mixing as schematically shown in **Figure 1**. Two physicochemical phenomena govern the chemical conversion and accompanied energy and mass transport phenomena in these laminar flow-based fuel cells: depletion of reactants at the electrode walls and diffusion across the mutual liquid-liquid interface. This membraneless fuel cell system eliminates several of the issues encountered in the more common polymer electrolyte membrane (PEM)–based fuel cells including the occurrence of fuel crossover and membrane dry out. Moreover, the membraneless fuel cell design is media flexible: the same fuel cell can be run in acidic or alkaline media. Of relevance to this work, one can even tailor the composition (e.g. pH) of the fuel and oxidant streams independently to optimize the reaction kinetics at the cathode and anode.[5]

This paper will report our preliminary results on tailoring the composition, in particular pH, of the individual cathode and anode streams in a laminar flow-based biofuel cell to maximize the activity and stability of the respective biocatalysts used at the cathode and the anode in a microscale biofuel cell. Being able to operate the individual electrodes at their respective optimum pH will not only increase the overall biofuel cell performance, it will also increase the stability of the enzymes used and thus it will increase the lifetime of the biofuel cell.

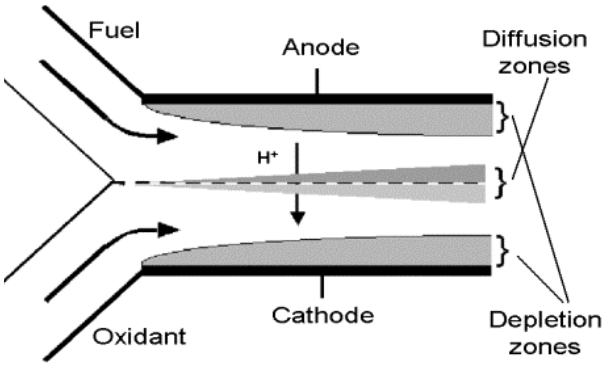

Figure 1. Schematic of a laminar flow-based, membraneless microfuel cell. The diffusion and reaction depletion zones are indicated (not too scale).

Experimental

Fuel Cell Assembly. Two graphite plates are placed side by side separated by 0.5 mm to 1.0 mm, and form the length of the channel where the fuel and oxidant streams flow next to each other. The 0.250 mm-wide inlets are milled out of the graphite plates with a drill bit. Before assembling the fuel cell, catalyst is applied to the sides of the graphite plates. The Y-shaped channel is capped with 1-mm thick polycarbonate slabs, while using polydimethylsiloxane (PDMS) as gasket material. The anode and cathode catalysts were unsupported Pt/Ru 50:50 atomic weight % alloy nanoparticles and unsupported Pt black nanoparticles, respectively, both deposited from a 10%wt Nafion solution to result in a loading of 2 mg/cm^2. An optical micrograph of an assembled cell is shown in **Figure 2**.

Fuel Cell Testing. Polyethylene tubing (I.D. 1.57 mm.) is used to guide the fuel and oxidant into the LF-FC and to guide the waste stream out of the cell. Fluid flow in all fuel cell experiments is pressure driven and regulated using a syringe pump. Operating conditions: flow rate per inlet channel = 0.3 ml/min; channel length = 2.9 cm; channel height = 1 mm and channel width = 0.75 mm. This flow rate and these cell dimensions correspond to a Reynolds number of around 0.1, well within the laminar flow range. To analyze the individual performance of each electrode, an external Ag/AgCl reference electrode in a 3.0 M NaCl solution was placed in a small compartment filled with 1N sulfuric acid and connected to the laminar flow based fuel cell using capillary tubing (ID 1.57 mm) ending in the waste stream collection beaker.[6] Polarization curves were obtained using an in-house fabricated fuel cell testing station equipped with a data acquisition device run with Labview.

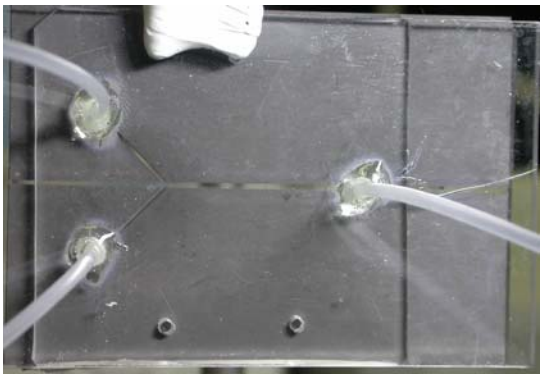

Figure 2. Optical micrograph of a membraneless fuel cell assembled from graphite plates. Main channel: 3 cm long, 1 mm wide and high.

Results and Discussion

In previous work we[5,6,7] and others[7] have reported on various membraneless fuel cells using different fuels (e.g. methanol, formic acid) and appropriate catalysts to obtain current densities as high as 10 mA/cm^2. The lack of a membrane lifts the constraint of only being able to operate in acidic media. Once mass transport issues at the cathode can be resolved, improved performance can be expected by running these fuel cells in alkaline media, as both fuel oxidation and oxygen reduction kinetics are known to be better in alkaline media. Moreover, the lack of a membrane and the ability to inject separate fuel and oxidant streams enables individual tailoring of the composition of these streams. **Figure 3** shows the individual anode and cathode performance of a membraneless fuel cell in which the anode is exposed to methanol in alkaline media (1N KOH) while the cathode is exposed to an oxygen saturated acidic stream (1N sulfuric acid). The difference in pH results in a very large open cell potential of 1.4V. The cathode curve drops fairly rapidly in region I due to the aforementioned mass transfer limitations (low solubility of oxygen in water). In the unusual region 2 the reduction of H^+ becomes the dominating cathode reaction, leading to the cathode curve to flatten. Until a short circuit current density of almost 50 mA/cm^2 is reached.[5]

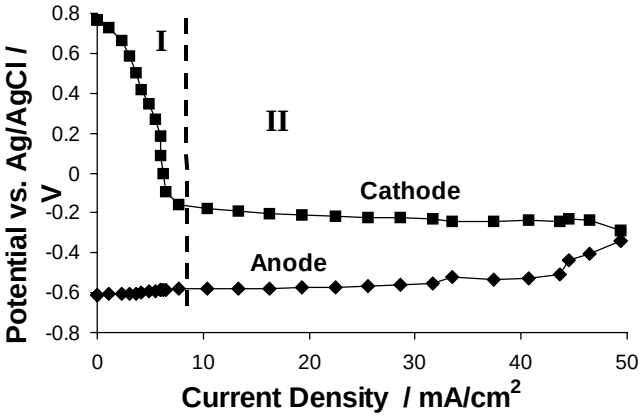

Figure 3. I-V performance curve of a membraneless fuel cell in which the anode and cathode are exposed to media of different pH. Fuel stream for this experiment: 1M formic acid in 1N KOH; Oxidant stream: oxygen saturated 1N sulfuric acid.

The ability to run the cathode and anode at different pH in a single fuel cell can be exploited in the further improvement of enzymatic biofuel cells. Different enzymes typically exhibit the best activity at different pH, yet in most biofuel cell designs a certain compromise pH is used, somewhere between the optimum pH of the respective enzymes used at the anode and cathode.[1] In preliminary experiments we have been able measure an open circuit potential of 0.4V and a maximum current density of ~75 μA/cm^2 in a membraneless fuel cell using methylene green as the mediator and NADH as the oxidizing agent dissolved in a phosphate buffer (pH 7) while using a stream of 1N sulfuric acid at the cathode. The performance of this cell is already similar to the performance of most recently reported biofuel cells.

In this paper we will report proof-of-principle experiments of membraneless fuel cells that enable enzymatic biofuel cells to be operated at conditions so both the anode and cathode enzyme chemistries can reach their full activity, thereby increasing the performance of the overall cell. In addition, operating both biocatalysts in their optimum pH is expected to improve their stability, and thus the longevity of biofuel cells.

Acknowledgment

This work was supported by the University of Illinois and the Beckman Institute.

References

1. Barton, S. C., Gallaway, J., Atanassov, P. *Chem. Rev.* **2004**, *104*, 4867-4886
2. Minteer, S. D., Akers, N. L., Moore, C. M. *Lab Chip* **2005**, *5*, 218-225
3. Hudak, N. S., Barton, S. C. *J. Electrochem. Soc.* **2005**, *152 (5)*, A876-A881
4. Choban, E.R., Markoski, L.J., Stoltzfus, J., Moore, J.S., Kenis, P.J.A., *40th Power Sources Conf., Cherry Hill, NJ, 10-13 June*, **2002**. Choban, E.R. Markoski, L.J. Wieckowski, A. Kenis, P.J.A. *J. Power Sources*, **2004,** *128*, 54-60. U.S. Pat. No. 6713206, **2004**.
5. Choban, E.R., Spendelow, J.S., Gancs, L., Wieckowski, A., Kenis, P.J.A., *Electrochimca Acta*, **2005**, *in press.*
6. Choban, E.R., Waszczuk, P., Kenis, P.J.A., *Electrochemical and Solid-State Letters*, **2005**, *in press.*
7. Cohen, J.L., Westly, D.A., Pechenik, A., Abruna, H.D., *J. Power Sources*, **2005**, in press.

DEVELOPMENT AND TESTING OF AN AIR BREATHING, MEMBRANE SEPARATED, ENZYME ANODE FUEL CELL FOR GLUCOSE FUELS

Christopher Apblett, David Ingersoll, Greg Roberts

Sandia National Laboratories
PO Box 5800
Albuquerque, NM, 87185-0603

Introduction and Background

The development of fuel cells as possible alternatives for portable power has been drawing considerable attention in recent years. Determining the power density of a fuel cell system requires the consideration of the volume of the fuel tank as well as the volume of the fuel cell converter. For long duration applications, such as sensors in remote sites, both batteries and traditional fuel cells (hydrogen and direct methanol) contain insufficient energy to operate for long periods of time while delivering technologically interesting (~mW) levels of continuous power. Environmentally harvestable fuels, such as glucose and sucrose (carbohydrates) from plant saps and animals have the potential to allow for continous fuel replenishment from the local environment. This would allow the volume of the fuel tank to be removed, significantly reducing the volume of the system and increasing the volumetric power density levels of the power system to well above the volumetric power densities of any available battery system or more traditional fuel cells.

In addition to harvesting fuel from the environment, oxygen must also be harvested from the environment, which requires special care in designing the cathode for the fuel cell to maximize the diffusive transport of oxygen to the electrodes in a passive system. This problem is further exacerbated in applications involving biological implantation. In this case, although there exist relatively constant and concentrated fuels in the biological systems, the unbound oxygen concentrations within these systems is quite low, and represents a mass transport limitation for the arrival of oxygen to the cathode of the fuel cell. Traditional cathodes, such as platinum black, are very active, but can quickly become poisoned by the other constituents within the vascular system. To prevent the cathode from being poisoned and inactivated by other contaminants in the vascular fuel stream, some form of membrane separator must be used that limits the cross diffusion of poisons to the cathode.

Catalysis of the fuel stream, as mentioned previously, can result in the poisoning of the anode catalyst by byproducts of the fuel oxidation when attempting to use carbohydrate based fuels. Several workers[1] [2] have investigated the oxidation of glucose on platinum and platinum alloy catalysts, and have demonstrated the poisoning of these catalysts. Enzymatic catalysis have much higher specificity to specific oxidation reactions, and are much less susceptible to contaminants in the fuel stream, i.e., less poisoning. Other researchers[3] [4] [5] [6] have developed and presented performance data on carbohydrate fuels (notably glucose). The current density of these fuel cells remains low and also have relatively short lifetimes, presumably due to the denaturing of the enzymes, or due to the loss of enzymes and/or mediators from the electrode into solution. This problem is exacerbated in a flow through system, as mediator or enzyme lost to solution is pumped away, severely restricting the amount of material that can redeposit onto the electrodes.

In light of these difficulties in realizing a carbohydrate fuel cell that can run on animal or plant carbohydrates, we have endeavored to fabricate a membrane separated, platinum cathode, enzyme anode fuel cell, and test it under both quiescent and flowthrough conditions.

Experimental

Miniature internally manifolded, closed cell graphite end plates were fabricated and used as the flow field and current collectors for the cells. The cathode electrode was a standard 50μm thick electrode comprised of Pt-Black with Nafion and Teflon binders, and the gas diffusion layer was a standard Toray backing. For the anode side, unteflonized toray paper was used, which had been treated by various methods for attaching glucose oxidase, the enzyme responsible for the first two electron oxidation from glucose. Various mediators were used along with this anode, and the Toray paper anode was placed directly in contact with the Nafion. The Nafion membrane was pH neutralized prior to assembly of the cell by soaking in a pH 7 phosphate buffer solution for 24 hours prior to assembly. The flow plates were attached over the electrodes by an acetate seal and lightly compressed to insure a leak free seal. The assembled cell was then placed into a test rig which allows for heating, flow control, and measurement of the power output of the cell. All experiments, unless otherwise noted, were performed at 25C, 20sccm flow of O_2 at atmospheric pressure, and 120μl/min flow rate of 50mM glucose fuel in a pH 5.4 phosphate buffer.

In the case of quiescent testing, the anode flow plate and test rig were replaced with a modified plate and rig, which was open on the backside of the anode to allow a static reservoir of liquid to rest directly against the anode toray paper. In this case, a fixed volume (0.8cc) of liquid was placed into the reservoir and allowed to equilibrate prior to the collection of the polarization curves.

Results and Discussion

The first experiments on the enzyme anode were half cell experiments with a Ag/AgCl reference electrode and platinum counterelectrode. These experiments used a well understood mediator of ferrocenyltrimethylundecylammonium bromide (FTMAB) along with the glucose oxidase in a co-immobilization onto the toray paper. The solution in this test was not stirred, so transport away from the electrode occurred only through diffusion. The data is shown in Figure 1 for a number of days after the preparation of the electrode. The electrochemical response is quickly lost, but is regained after spiking the electrode with more FTMAB mediator, indicating that the enzyme itself is stably bound to the electrode surface, but that the mediator is quickly being lost to the solution.

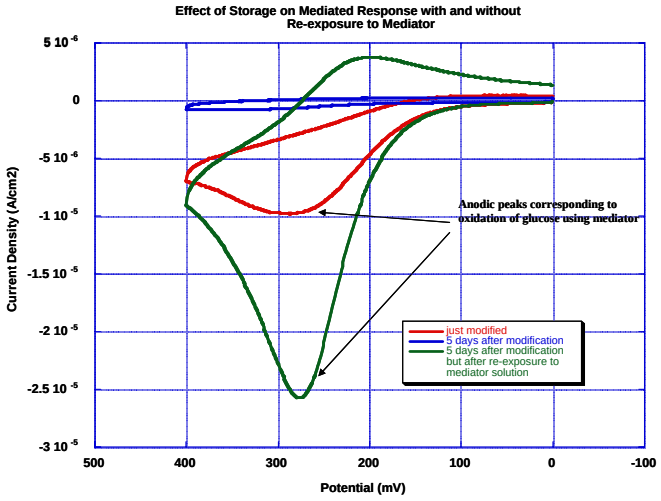

Figure 1. Half Cell CV of glucose oxidase/FTMAB electrode, 50mM glucose, room temperature. The performance is lost after a few days, but can be restored by the addition of more FTMAB.

FTMAB is a stable, reversible mediator molecule with a redox potential near +200mV vs. Ag/AgCl, making it unattractive for use with glucose oxidase. Glucose oxidase oxidizes glucose at roughly -300mV vs. Ag/AgCl, which means that almost 500mV are lost to the oxidation voltage. Against a Pt-O_2 cathode, this would result in, at best, an open cell potential of only 500mV. Better choices for mediators in terms of the potential are available, however, and these fall into several classes. The most promising for our work were phenazine derivatives, which operated in the -80mV to -180mV range vs. Ag/AgCl at neutral pH and room temperature. Using phenazine methosulphate with glucose oxidase in the half cell test previously described resulted in a much improved cyclic voltammetric response, with a redox potential for glucose at roughly -80mV, and having high current density for an enzymatic half cell. The addition of glucose fuel to the electrode only nominally affects the operating potential of this electrode. These results are shown in Figure 2.

These half-cell electrodes can be applied directly into the full fuel cell architecture, and tested against a neutralized seven mil Nafion membrane using a Pt-O_2 cathode. A typical polarization curve for these cells under flow through conditions is shown in Figure 3. As can be seen from the data, although the cell potentials are close to what would be expected from the half cell measurements, the current densities are well below those expected from the half cell. It is not expected that the Pt cathode would be limiting in this case in any form, as the activity of the Pt-O_2 reduction reaction is much

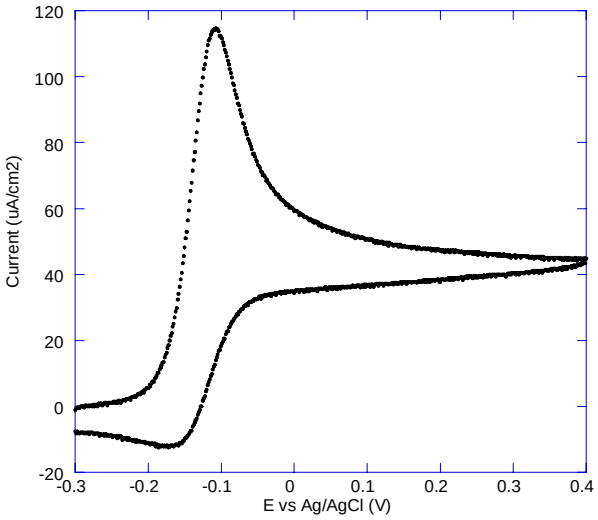

Figure 2. Half Cell performance of phenazine methosulfate and glucose oxidase immobilized on a glassy carbon electrode. The PMS is mediating at -80mV vs. Ag/AgCl, a significant improvement over FTMAB.

higher than the currents that are shown here. These cathodes have been tested against a H_2 cathode and shown to polarize by less than 30mV at a 1mA. Therefore, it can reasonably be expected that the low currents observed in this performance are being caused by poor performance at the anode.

This performance can be somewhat improved by moving from a flowthrough system to a quiescent system. By operating in this mode, current densities under the same conditions are increased above those found for the flow through system, indicating that the stability of the mediator may again be in question. The data for the quiescent case are also plotted in Figure 3. In this case, transport to the anode is through diffusion only, and the loss of the mediator to solution is also controlled by the diffusion of the mediator away from the anode. From this data, it can be seen that the supportable currents from the anode are much higher than in the case of the flow through configuration, and much closer to the values measured in the half cell case.

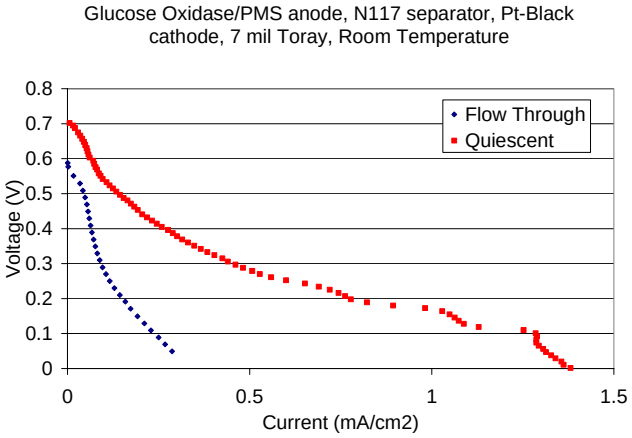

Figure 3. Flow through vs. Quiescent cell. 50mM glucose fuel at 120ml/min or static, 20sccm O2 flow cathode, room temperature, PMS mediated, phosphate buffered to pH 5.4. The loss in performance in flowthrough is due to loss of the mediator to solution.

Conclusions

From the initial experiments using oxygen cathodes and membrane separators in flowthrough fuel cells, it is apparent that mediator loss to the flowing solution is the largest contributor to power loss. Use of the phenazine derivative mediators was demonstrated to offer decent open circuit potentials for half cell and full cell performance, but suffer from quick loss to the solution which hampers long term operation. A means to stabilize the phenazine molecules to the electrode will need to be developed in order to extend the lifetime of the cell beyond its current level of a few hours. Work is underway currently to address this issue.

Acknowledgements

Sandia is a multiprogram laboratory operated by Sandia Corporation, a Lockheed Martin Company, for the United States Department of Energy's National Nuclear Security Administration under contract DE-AC04-94AL85000.

References

1 Beden, B., Largeaud, F., Kokoh, K. B, Lamy, C., *Electrochimicha Acta* **41** 5 (1996) 701-709.

2 Ernst, S., Heitbaum, J., Hamann, C., *Ber. Bunsenges., Phys. Chem.* **84** (1980) 50-55.

3 Willner, I., Katz, E., Patolsky, F., Buckmann, A., *J. Chem. Soc. Perkin Trans.* **2** (1998) 1817-1822.

4 Katz, E., Willner, I., Kotylar, A., *J. Electroanal. Ch*em. **479** (1999) 64-68.

5 Chen., T., Barton, S. C., Binyamin, G.,Gao, Z., Zhang, Y., Kim, H-H., Heller, A., *J. Am. Chem. Soc*. **123** (2001) 8630-8631.

6 Kim, H-H., Mano, N., Zhang, Y., Heller, A., *J. Electrochem. Soc.* **150** 2 (2003) A209-A213.

SYNTHESIS AND CHARACTERIZATION OF BIOELECTROCATALYTIC POLYMER COMPOSITES

G. Tayhas R. Palmore, and Jiangfeng Fei

Division of Engineering, Division of Biology and Medicine, Brown University, 182 Hope Street, Box D, Providence, RI 02912, Fax: 401-863-7677

Abstract

The molecule 2,2'-azinobis-(3-ethylbenzothiazoline-6-sulfonate) (ABTS) is an important redox-active compound with broad chemical, material, and biomedical applications. ABTS and its derivatives have been used as the electrochromic component in smart windows, as a chromogenic substrate in assays for enzymatic activity, and as a mediator for electron transfer in the cathode compartment of a biofuel cell. Interest in the use of ABTS in the bioelectrocatalytic reduction of oxygen to water has increased primarily because its redox potential is near that of oxygen under mildly acidic conditions. I will discuss the synthesis and characterization of polymer composites of ABTS and the performance of these composites in a hydrogen/oxygen biofuel cell operated at room temperature and atmospheric pressure.

DESIGN OF MACROPORE STRUCTURE FOR ENZYME FUEL CELLS OPERATION

Michael Cooney[✉], *Bor Yann Liaw*[✉], *Wayne Johnston, Vojtech Svoboda, Forest Quinlan, and Nathan Maynard*

Hawaii Natural Energy Institute, School of Ocean and Earth Science and Technology, University of Hawaii, Honolulu, HI 96822, USA

[✉]mcooney@hawaii.edu or bliaw@hawaii.edu

Introduction

There has been increasing attention concerning direct alcohol fuel cells (DAFCs) using platinum based catalysts [1]. Both methanol and ethanol have been proposed as reactants although ethanol is increasingly attractive because it exhibits less toxicity than methanol and is readily produced from renewable resources. Direct oxidation of ethanol on platinum, however, is plagued by fouling of the electrode surface by reactive intermediates such as those with CO groups. Despite improvements, however, fouling of the electrode remains problematic because the extra C-C bond in ethanol increases the number of chemical intermediates available to foul the electrode. Enzyme bioelectrocatalysts have been proposed as an alternative to transition metal catalysts for power generation; they oxidize alcohols at relatively low overpotential without producing CO-related intermediates that will foul the electrode, and they operate at lower temperatures [2]. Such reactant specificity has also led to the development of a membrane-less glucose biofuel cell in which glucose is oxidized at the anode by glucose oxidase whilst the reaction of the stripped proton with oxygen to form water at the cathode is catalyzed by the enzyme laccase [3].

Full realization of the membrane-less biofuel cell as a power source requires a 3-D solid-liquid boundary microstructure that balances the overall effective surface area against porosity, thus ensuring the maximum number of catalyst sites are available without suffering the liquid sealing effect, which occurs if the pore size is so small it blocks fuel transport. Without such a delicate engineering practice, the optimization of power density on those reactant specific electrodes cannot be realized. Control over porous microstructure has been addressed via sol gel techniques, and by entrapment in functionalized mesoporous silica, but these materials lack the required electronic conductivity. That said, electronic conducting conjugated polymers (ECP's), or their derivatives, have been proposed to immobilize redox enzymes in biosensors and biofuel cells [4]. While this approach has led to a widespread application in the biosensors, including those for measurement of ethanol [5], they have been only successful in addressing part of the issues important to enzyme fuel cells. The foremost critical one, namely the control over an effective 3-dimensional solid-liquid boundary microstructure for optimal power generation, remains untouched.

In this work we present data comprising *in situ* determination of the effective diffusion coefficient and in situ documentation of film growth using imaging ellipsometry to evaluate the effect of macropore structure on enzyme fuel cell performance. The results suggest that pyrrole films can pose significant mass transfer limitation as compared to direct absorption. Images of pyrrole deposition from imaging ellipsometry suggest that the growth of pyrrole films via electrochemical deposition is affected by monomer concentration, growth rate, and imposed potential. The deposition began with a one-dimensional filament growth on the metallic electrode support surface. As the density of the filaments increases with film thickness to a threshold the growth pattern changed from 1-D to 2-D as the film continues to grow. The density, porosity, and microstructure of the film are therefore varied as the film develops into a thick film. These results suggest new techniques are required to create a sufficient macropore structure and some ideas in this direction are suggested, including computer modeling to understand the effects of transport and reaction kinetics on the electrode behavior.

Experimental

Reagents. Alcohol dehydrogenase was purchased from Sigma, as was Crystalline NAD^+. Stock solutions of BSA (100 mg ml^{-1}) were dissolved in phosphate buffer (0.05 M, pH 8.0). Working solutions of lithium perchlorate were made on a daily basis by dilution with 0.05M phosphate buffer. Pyrrole solutions were made daily from a stock solution that was de-aerated and stored at –4ºC in the dark to avoid degradation over time. Ethanol (17.0 M, 200 proof) was diluted as needed (i.e. 300 mM) with ultra pure water.

Flow cell. The cell is built from a modular stacking design approach, which employs stackable polycarbonate plates that serve defined functionalities. The core stack comprises a 6 cm diameter hole of ¼" height with ports along the sidewalls of the reaction chamber for inlet and exit lines as well as the reference electrode. The working and counter electrodes are located on either side of the reaction chamber. The working electrode was constructed of either a carbon mesh material or 316 stainless steel wire mesh. The counter electrode was nickel sheet. All electrodes were pretreated by soaking in acetone for 5 minutes under mild agitation, rinsed with ultra pure water, and then soaked for an additional 5 minutes in 10% nitric acid. The electrodes were then copiously rinsed with ultra pure water and blot dried with absorbent paper. The electrodes were used immediately after drying. Media was delivered to the cell by peristaltic pumping from an external reservoir maintained at 37°C.

Immobilization. For direct absorption the pretreated carbon mesh was soaked *ex situ* in 20 µl of the ADH stock solution (50 mg ml^{-1}) for 15 minutes at 25°C. The cell was then fully assembled and filled to capacity with phosphate buffer solution, after which buffer solution (20 ml) was slowly pumped through the flow cell (~1.6 ml min^{-1}) to purge the cell of non-adsorbed enzyme (Fig 1). For pyrrole immobilization, the micro cell was assembled using the pretreated stainless steel mesh electrode and then filled to capacity with 0.3 ml of de-aerated immobilization solution (pyrrole monomer (0.1M), electrolyte salt (0.1M), and enzyme (50 mg ml^{-1}) dissolved in phosphate buffer. The working electrode was polarized in potentiostatic mode at +0.8 V vs. Ag/AgCl at 37 °C until a defined charge of 1.27 coulombs had passed. After polarization, immobilization solution was removed by syringe and 20 ml of phosphate buffer at 37°C was slowly pumped (~1.6 ml min^{-1}) to remove non-entrapped enzyme from the system.

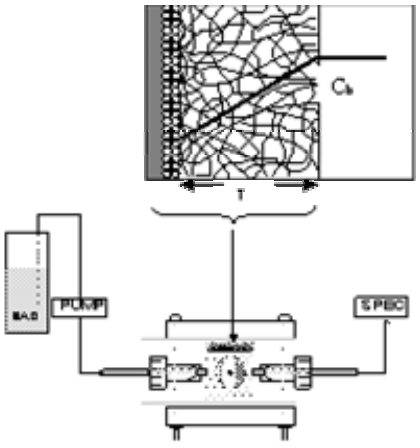

Figure 1. Micro flow cell system

Modeling. If the halo-enzyme complex scenario is used to describe the alcohol dehydrogenase catalyzed oxidation of ethanol in the presence of NAD^+, the following expression can be developed from a mass balance around the enzyme fuel cell.

$$F \bullet NADH_b = \frac{V_{max}^{NAD^+} \bullet (NAD_{res}^+ - NADH_b - \frac{F \bullet NADH_b}{D'_{NAD^+,eff}})}{K_M^{NAD^+} + (NAD_{res}^+ - NADH_b^+ - \frac{F \bullet NADH_b}{D'_{NAD^+,eff}})} \quad (1)$$

The usefulness this equation is that the LHS can be measured experimentally and the RHS can be plotted in the form of a Lineweaver-Burke plot, assuming a value for the effective diffusion coefficient (D'_{eff}) is assumed. Further, if the assumption is made that the value for K_M will not change from that measured for the enzyme in free solution, then a value of effective diffusion coefficient can be derived assuming the Line-Weaver Burke intercept yields the value for K_M determined in free solution. The value of V_{max} can then be taken as the activity of the immobilized enzyme.

An interesting feature of equation 1 is that it permits the data to be plotted in Lineweaver-Burke form using the modeling concentration of enzyme at the enzyme surface. Why this is important can be seen in Figure 2, which uses the bulk concentration of NAD^+ along the x-axis, instead of plotting the concentration of NAD^+ at the enzyme surface. The varying intercepts illustrates that it is difficult to distinguish between mass transfer and kinetic limitation when using bulk concentrations. Thus the model illustrates the important point that the interpretation of real assay data to measured values of K_M and V_{max} from experimental data will not be accurate unless the effects of mass transfer on reaction kinetics are considered.

Figure 2: Lineweaver-Burke plot.

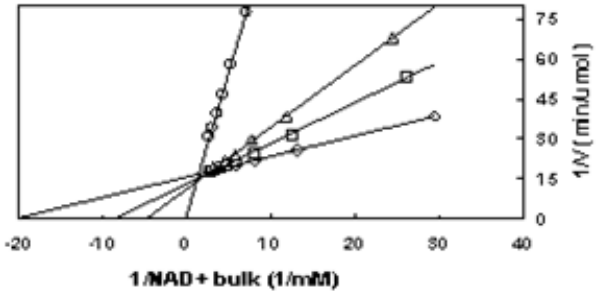

Results and Discussion

Study of Interplay of Reaction Kinetics and Transport via Modeling. Test of this procedure was conducted two types of immobilization techniques: 1) direct adsorption to carbon type electrode and 2) enzyme immobilized to stainless steel mesh by polypyrrole. For each case the solution to Equation 1 was used to estimate both the reaction velocity and the effective diffusion coefficient. The results are presented in Table 1.

Table 1. Summary of estimated model parameters

F (ml/min)	K_M (mM)	V_{max} (µmol/min)	D'_{eff} (cm^3/min)
		Carbon felt	
1.6	0.0501	0.0636	0.91
1.6	0.0500	0.0539	0.97
2.4	0.0490	0.0684	0.68
		Pyrrole immobilized enzyme	
0.27	0.057	0.0025	0.26

Direct adsorption to carbon felt provided 26 times the activity of the immobilized polypyrrole electrode (0.062 versus 00025 µmol min^{-1}). This may have been due to two factors. First the effective surface area of the carbon felt could have been much greater than the stainless mesh electrode. A second possibility is that the enzyme within the pyrrole film lacked the diffusive pathways for NAD^+, and hence did not contribute to the production of NADH. This would suggest that only enzymes immobilized at the surface of the immobilized film were available to catalyze the oxidation of NAD^+ to NADH in the presence of excess ethanol. As such, the fabrication of a polypyrrole film with increased diffusive pathways would increase activity. The modeling technique presented in this work provides a mechanism to test this hypothesis, provided a series of films of different thickness and porosity (as modified through the immobilized technique) are constructed and the effective diffusion coefficient calculated.

Characterization of Microstructure. For SEM images, electrodes with fabricated films were recovered from the micro-cell, dried in air, and transferred to the PBRC Biological Electron Microscopy Facility (PBRE-BEMF) for imaging taking. Figure 3 presents typical SEM images of pyrrole films that have been electropolymerized. One salient feature of the SEM images (A and B) is the cauliflower shape microstructure covering the electrode surface. The thicker the films the more pronounced cauliflower shape microstructure is developed. The cauliflower shape microstructure presents films that surpass a threshold thickness, usually less than 1 µm, and presumably possess a dense membrane structure that would inhibit mass transport. The ellipsometry image (C) revealed an initial open microstructure that might be preferred for fuel cell application, for thin films with a dense film forming at a threshold thickness.

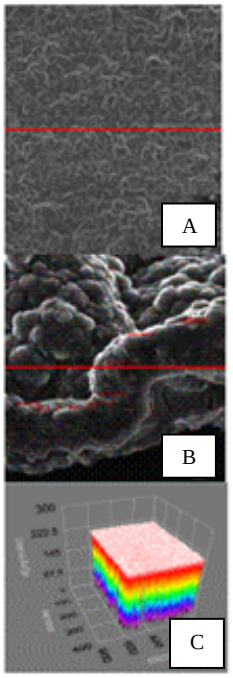

Figure 3. SEM and imaging ellipsometry images of PY films.

Acknowledgements

This work was funded by the Office of Naval Research (N0014-01-1-0928) through the Hawaii Environmental and Energy Technology (HEET) initiative (R. Rocheleau, PI), and by the Director of Central Intelligence Postdoctoral Fellow Research Program (HM1582-01-1-2013).

References

1. Lamy, C., S. Rousseau, E.M. Belgsir, C. Coutanceau and J.M. Leger, (2004). Electrochimica Acta, **49**: p. 3901 - 3908.
2. Palmore, G.T., H. Bertschy, S.H. Bergens and G.M. Whitesides, (1998). Journal of Electroanalytical Chemistry, **443**: p. 155 - 161.
3. Barton, S.C., M. Pickard, R. Vazquez-Duhalt and A. Heller, (2002). Biosensors and Bioelectronics, **17**: p. 1071 - 1074.
4. Bartlett, P.N. and P.R. Birkin, (1993). Synthetic Metals, **61**: p. 15 - 21.
5. Lobo Castanon, M.J., A.J. Miranda Ordieres and P. Tunon Blanco, (1997). Biosensors and Bioelectronics, **12**(6): p. 511 - 520.

EVIDENCE OF A YSZ CONDUCTIVE PHASE NEAR SOFC ANODES

Michael B. Pomfret[a], Oktay Demircan[a], A. Mary Sukeshini[a], Gregory S. Jackson[b], Robert A. Walker[a,c]

[a]Department of Chemistry and Biochemistry, University of Maryland, College Park, MD 20742
[b]Department of Mechanical Engineering, University of Maryland, College Park, MD 20742
[c]Chemical Physics Program, University of Maryland, College Park, MD 207

Introduction

To date, research into fuel oxidation in fuel cells has focused on engineering and electrochemical issues to improve the overall cell efficiency.[1-4] While progress in these areas is important, numerous questions remain about the actual chemical mechanisms by which fuel cells, particularly solid oxide fuel cells (SOFCs), oxidize fuel to produce electricity, CO_2 and water. Identifying these reaction pathways should help improve cell efficiency and help minimize the problem of anode poisoning.

Due to its ability to conduct oxide anions at high temperatures (800 °C), yttria stabilized zirzonia (YSZ) has become the standard electrolyte in a wide variety of SOFCs.[2,5,6] Although several studies have cited a potential chemical role for YSZ related to reaction spillover from the anode onto the electrolyte,[7,8] there has been no consideration for YSZ's role in side reactions that might occur during SOFC operation. Previous work suggests that YSZ reduces in an oxygen-poor atmosphere such as that found on the anode side of a SOFC.[9] Furthermore, even modest currents are known to reduce YSZ so that it becomes electrically conducting. [15-17] Reduced forms of zirconium (Zr^{3+} and Zr^{2+}) have been shown to be very efficient catalysts in organic and polymer synthesis.[10-13] Should reduced YSZ in SOFCs have similar catalytic properties, then many existing models of fuel cell oxidation mechanisms have to be re-examined to consider alternative reaction pathways that are accessible on the electrolyte surface. Published reports already suggest that YSZ-based SOFCs can operate without a metal anode.[14] This condition necessarily requires that YSZ be electrically conductive, a property not considered in traditional SOFC models, but supported by several recent reports.[15-17] Much of our understanding about processes occurring in SOFCs has resulted from studies using classical electrochemical methods such as cyclic voltammetry and impedance spectroscopy. However, most of these studies have neglected to consider oxidation pathways out of those processes occurring at the anode/electrolyte boundary.

This work employs impedance spectroscopy to investigate the electrical conductivity of YSZ in a working fuel cell. Further evidence of a reduced conducting phase of YSZ on the anode side of SOFCs comes from comparing impedance data in the presence and absence of electrochemical operation. These results demonstrate a larger potential role for YSZ – or any reduced species – as a participant in current collection and fuel oxidation. With a complete understanding of the chemical and electrochemical properties of each SOFC component can fuel oxidation mechanism(s) be exhaustively identified. By identifying the conductive and chemical properties of an electrolyte we can begin to evaluate another source of non-anodic SOFC fuel chemistry.

Experimental

Fuel Cell Construction. The SOFCs used in this study consisted of an electrolyte supported, three-layer architecture with a 1.5 mm thick, 8 mole % YSZ electrolyte (ITN Energy Systems, Inc.) sandwiched between a porous LSM ($La_{0.85}Sr_{0.15}MnO_3$) cathode and a Ni/YSZ cermet anode. Both the anode and cathode were prepared by a tape casting method. The 12 mm diameter cathodes were sintered in air by heating to 400 °C at a rate 0.3 °C/min. The temperature was held at 400 °C for one hour before the cathodes were heated to 1300 °C at 3 °C/min. After one hour at 1300 °C, the sample temperature was lowered to 25 °C at 3°C/min. Ni/YSZ cermet anodes were prepared by tape casting a commercially available, 50% post-reduction Ni content NiO/YSZ cermet (NexTech Materials Lot # 112-45) over a 12 mm x 2 mm area in the center of the YSZ electrolyte. These anodes were then sintered at 1300 °C – the careful temperature cycle used for cathode sintering is not necessary for anode preparation. Two gold electrodes were placed on either side of the NiO/YSZ at 2.3 mm and 3.9 mm, respectively. The NiO/YSZ was reduced by an atmosphere of 5% H_2 – 95% Ar to Ni/YSZ while heating the fully assembled fuel cell assembly to operational temperature (800 °C) at 3 °C/min.

The membrane electrode assemblies (MEAs) were attached cathode-side-out to an alumina tube (22.2 mm OD, 15.9 mm ID) with a high temperature, zirconia-based ceramic paste. An alumina fuel-feed tube (4.8 mm OD, 3.2 mm ID) was centered in the larger tube and the entire assembly was placed in a temperature-controlled furnace. A second feeder tube was centered near the cathode to deliver air. Electronic mass flow controllers (Brooks 5850E) regulated the flow rates of the fuel stream. Data from the mass flow controllers were collected by a National Instruments SCXI data acquisition system. The cathode flow was regulated by a rotameter.

Cell Operation and Evaluation. H_2 was used as fuel for this experiment at an operating temperature of 800 °C. A 70 sccm flow of H_2 on the anode side was balanced by a 35 sccm flow of air on the cathode side. All experiments used a fuel flow of 33% fuel, with a balance of Ar.

An Autolab PGSTAT30 (Eco Chemie) was used to monitor fuel cell performance. AC impedance spectra were taken using five electrode configurations as shown in **Figure 1**. The first configuration measured the total cell impedance using the Ni/YSZ anode as the working electrode and the cathode as the counter electrode. The second and third configurations measured the anodic overpotential using the same working and counter electrodes while introducing each gold electrode individually as reference electrodes. The fourth and fifth configurations used the same working electrode, but employed each gold electrode individually as two separate counter electrodes. These last two configurations intended to measure the impedance across the YSZ surface between Ni/YSZ anode and the respective gold electrodes. Impedance spectra were made under open circuit conditions over a frequency range from 100 kHz to 10 mHz. A 6.00 mA current was drawn from the cell when measurements are not being made.

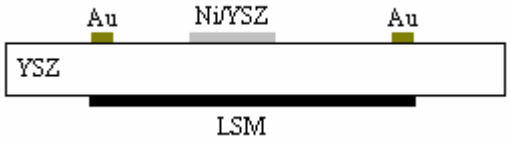

Figure 1. Scheme of the YSZ electrolyte supported fuel cell with a LSM cathode, Ni/YSZ cermet anode and two gold reference electrodes.

Results and Discussion

Once the SOFC is at 800 °C the performance is monitored with IV curves to ascertain system stability and reproducibility. Once cell performance has become stable, impedance measurements begin. **Figure 2** shows the impedance curves of the fuel cell. The data

corresponding to the cell operating without a reference electrode displays a polarization resistance (R_P) of 73.7 Ω that is largely electrolytic, but also contains cathode and anode related processes. When an inert Au reference is employed on the anode side, the data show the impedance associated primarily with the anode overpotential. Cathode impedance data are not represented in the curve, resulting in the smaller R_P. Ideally the two referenced impedance curves would be identical since the same anode is used in each measurement. The 12.1 Ω difference in the impedance curves when using two separate reference electrodes suggest an irregularity in reference electrode contact resistance, likely due to imperfections in the electrodes.

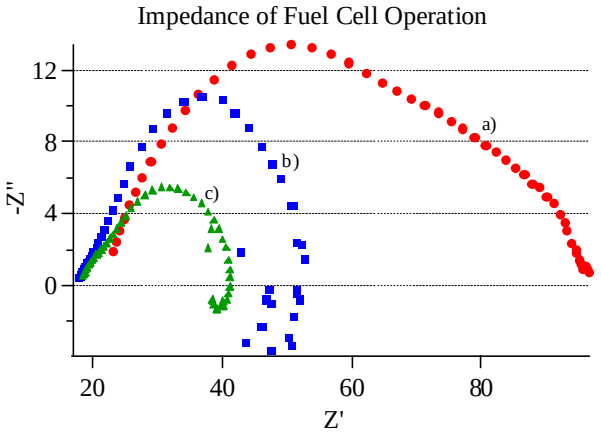

Figure 2. Impedance curves of the operational fuel cell with a) Ni/YSZ anode and LSM cathode, b) a gold reference 3.9 mm from the anode and c) a gold reference 2.3 mm from the anode.

To investigate the interaction between the two Au references and the Ni/YSZ anode, the impedance was measured between the anode and each of the references – now operating as counter electrodes – individually. **Figure 3** shows the impedance curves of the Ni/YSZ – Au systems. Also included is an impedance curve of an Au electrode 1.3 mm from the anode on an inoperable fuel cell without a cathode lead.

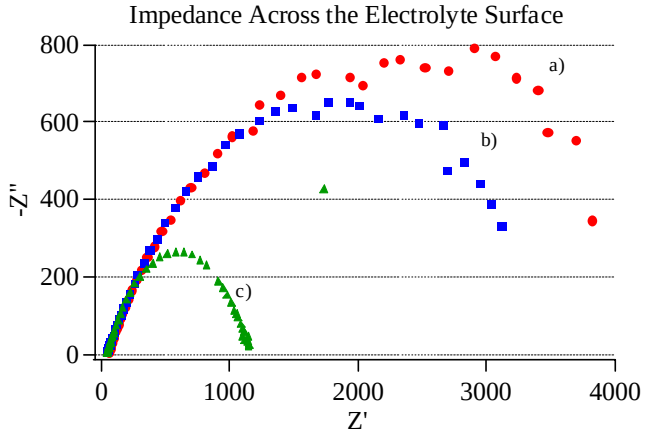

Figure 3. The impedance across the surface a) from a Ni/YSZ anode to a gold cathode 3.9 mm away, b) to a gold cathode 2.3 mm away, and c) to a gold cathode 1.3 mm away in a non-electrochemically active cell.

The oscillation of the 2.3 mm and 3.9 mm Au counter electrode curves at lower frequencies and the incomplete arcs indicate that the YSZ between the Ni/YSZ and Au electrodes never reaches full DC conductance. The arcs are fit as semi-circles and an impedance for the YSZ surface is extrapolated in each case. The resulting values were 3.41 kΩ for the 2.3 mm electrode separation case and 4.03 kΩ when the electrodes are 3.9 mm apart. These values are then normalized to 1mm, resulting in a mean value of 1.26 ± 0.23 kΩ/mm. Assuming uniform resistance across the YSZ surface, the first micrometer away from the anode has a resistance of ~1 Ω, implying that fuel oxidation and current collection can occur at considerable distances from the anode/electrolyte boundary.

The curve of the Ni/YSZ – Au electrode in the absence of electrochemistry gives a surface impedance value of 0.85 kΩ/mm, a drop of 31.4% from the operational fuel cell surface. The arc is also complete and does not oscillate suggesting a DC conductive YSZ surface. Given the extremely small current passed during impedance measurements, the conductivity in this case is thought to result primarily from chemically, not electrically, reduced YSZ as has been reported previously.[15-17] The difference in the conductivity of the cell without electrochemistry is likely due to the lack of O^{2-} flux. When electrochemistry is occurring the O^{2-} flux repopulates the reduced YSZ surface sites.

Conclusion

The present experiment clearly demonstrates the conductive behavior of the YSZ surface in a SOFC. The conductivity of the YSZ surface is enhanced when electrochemistry is halted. These results suggest a degree of YSZ reduction on the anode (fuel) side of SOFCs. This reduced electrolyte may participate in electrochemical fuel oxidation as well as non-electrochemical side reactions. Future experiments will aim to devise a chemical mechanism based on the knowledge of the presence of reduced YSZ on the anode side.

Acknowledgement. This work is supported by the Office of Naval Research through the MURI grant # 0110138816, in association with the Colorado School of Mines and CalTech.

References

(1) Minh, N. Q. *Solid State Ion.* **2004**, *174*, 271-277.
(2) Ormerod, R. M. *Chemical Society Reviews* **2003**, *32*, 17-28.
(3) Srikar, V. T.; Turner, K. T.; Ie, T. Y. A.; Spearing, S. M. *J. Power Sources* **2004**, *125*, 62-69.
(4) Weber, A.; Ivers-Tiffee, E. *J. Power Sources* **2004**, *127*, 273-283.
(5) Song, C. S. *Catal. Today* **2002**, *77*, 17-49.
(6) Zhu, W. Z.; Deevi, S. C. *Materials Science and Engineering* **2003**, *A362*, 228-239.
(7) Bieberle, A.; Swiss Federal Institute of Technology: Zurich, Switzerland, 2000.
(8) Basini, L.; Cavalca, C. A.; Haller, G. L. *J. Phys. Chem.* **1994**, *98*, 10853-10856.
(9) Pomfret, M. B.; Stoltz, C.; Varughese, B.; Walker, R. A. *Anal. Chem.* **2005**, *77*, 1791-1795.
(10) Miller, T. M.; Grassian, V. H. *Journal of the American Chemical Society* **1995**, *117*, 10969-10975.
(11) Miller, T. M.; Grassian, V. H. *Catalysis Letters* **1997**, *46*, 213-221.
(12) Marek, I., Ed. *Titanium and Zirconium in Organic Synthesis*; Wiley-VCH, Inc.: Weinheim, Germany, 2002.
(13) Busca, G. *Catal. Today* **1996**, *27*, 323-352.
(14) Hirabayashi, D.; Tomita, A.; Brito, M. E.; Hibino, T.; Harada, U.; Nagao, M.; Sano, M. *Solid State Ion.* **2004**, *168*, 23-29.
(15) Wright, D. A.; Thorp, J. S.; Aypar, A.; Buckley, H. P. *Journal of Materials Science* **1973**, *8*, 876-882.
(16) Nagle, D.; PaiVerneker, V. R.; Petelin, A. N.; Groff, G. *Mat. Res. Bull.* **1989**, *24*, 619-623.
(17) Levy, M.; Fouletier, J.; Kleitz, M. *J. Electrochem. Soc.* **1988**, *135*, 1584-1589.

PHYSICAL CHEMISTRY STUDIES OF PROTON CONDUCTION IN HETEROPOLY ACIDS

Fanqin Meng,[1] James Horan,[2] Jennifer L. Malers,[1,3] Steven F. Dec,[2] Andrew M. Herring,[1] John A. Turner[3]

Department of Chemical Engineering[1] and Chemistry and Geochemistry[2]
Colorado School of Mines
Golden, CO 80401-1887

Hydrogen and Electricity, Systems and Infrastructure Group[3]
National Renewable Energy Laboratory
Golden, CO 80401-3393

Introduction

The importance of fuel cells has been recognized as the world confronts more and more severe fossil fuel shortage. Among others, proton exchange membrane fuel cell system is seen to be best suitable for vehicle power applications. Although the PEMFC technology has advanced quickly in the past years, a number of issues remain to be resolved, such as to enhance the functionality of these devices under dry gas condition at 80 °C and above. However, the current state-of-art PEMs are based on perfluorinated sulfonic acid polymer such as Nafion®, which decomposes above 100 °C and requires rigorous hydration for continuous operation. HPAs are promising PEM materials because they have exhibited exceptional proton conductivity not only at ambient temperature, but also at elevated temperatures without external humidification.

The most thoroughly studied HPA, 12-tungstophosphoric acid, exhibited proton conductivity of 0.2 S/cm^2 at room temperature,[1] higher than that reported for Nafion®. Meanwhile, a variety of HPAs have shown high water retention and the protons remain mobile at elevated temperatures according to the literature and the work done in our laboratory. These properties are ideal for an electrolyte material in PEM fuel cells to be operated at elevated temperatures and low relative humidity. While this is a huge class of materials, only the few commercially available HPAs have been studied to any great extent. A large number of HPAs are readily available to synthetic chemists. Furthermore the simple salts of the HPA almost always contain residual protons. We therefore synthesized a library of HPA where charge, shape and hydration state were varied, and investigated their proton conduction structures in the solid state using TGA, IR and NMR techniques.

Experimental

HPA sample preparation. The syntheses of many heteropoly acids are well documented.[2] In general, HPAs are made by acidification of solutions containing the requisite simple anions or by introduction of the heteroelement after first acidifying the tungstate. Lacunary HPAs are obtained by removal of one or more tungsten with the terminal oxygen atoms at higher pH. The HPA anions are typically isolated as their potassium salts first, and then free acids are obtained by column exchange or an acid-ether extraction method.

Characterization Methods. TGA-DTA (thermal gravimetric analysis and differential thermal analysis) measurements were performed over a temperature range of 20 to 600 ºC using a Seiko SSC/5200 with a heating rate of 5 ºC min^{-1}. Powder X-ray diffraction patterns were recorded using a Scintag X-ray diffractometer using Cu K_α radiation. All MAS (magic-angle spinning) ^{1}H spectra were recorded on a two-channel Chemagnetics CMX Infinity 400 NMR spectrometer operating at 400.0 MHz, using a Chemagnetics 5mm double-resonance MAS probe equipped with a Pencil spinning module, sample spinning at 10 kHz. Proton diffusion measurements were performed with the use of a 5mm Doty Scientific, Inc. #20-40 z-gradient pulsed-field gradient NMR probe. The stimulated-echo pulse sequence[3] was used and the gradient coil was calibrated using water at 25 ^{o}C. The resulting NMR spectra were integrated and fit to a two-Gaussian decay using Spinsight® software available from Varian, Inc. DRIFTS (diffuse reflectance FTIR spectroscopy) samples were heated *in situ* (ambient temperature to 150 °C) under constant helium flow, the spectra were recorded on a Thermo Nicolet Nexus 670 FT-IR spectrometer using the Omnic®6.0 software package and with a specially designed Harrick Praying Mantis diffuse reflection attachment.

Results and Discussion

TGA results of the HPAs can generally be defined in terms of the following generalities. At ambient conditions a large amount of loosely bound disorganized water is associated with the HPA, many HPAs are hydroscopic so the amount of this low temperature water can be very variable depending on the ambient conditions. At ambient conditions the HPA secondary structure truly is a "pseudo-liquid" phase and explains the high conductivity of these materials at room temperature. Above 100 °C there is usually a significant but smaller amount of more tightly bound water which is held positionally but is free to rotate, it is this tightly bound secondary structure water and its movement that is important to understand so that HPA proton conductors for elevated temperatures can be designed. We have found that if one heats an HPA above 100 °C it will eventually, over a period of months, reach a limiting hydration state where the residual waters do not leave the lattice and are presumably necessary for structural stability. At temperatures above 200 °C a further mass loss is observed, which has been ascribed to a neutralization reaction in which the anhydrous proton associates itself with the HPA as an OH and two such protons leave with a structural oxygen atom as water leaving behind a neutralized HPA. This transition is irreversible and eventually a neutral oxide is formed. At much higher temperatures >400 °C an exotherm is observed which signifies the decomposition of this oxide.

DRIFTS spectra of the free acid HPAs not only show information on the bonding of water and protons but also show changes in the outer anion bands as these bonds become more or less involved in bonding to the secondary structure. The υ(OH) can be fit to a number of OH stretches involved with progressively stronger hydrogen bonding from a free OH at 3640 cm^{-1} to an OH involved in a strong O-H…O at 1100 cm^{-1}or lower. As the strength of the H-bonds increases, the peaks become progressively broader and appear at lower wavenumbers. Using the peak positions and areas under them it is possible to calculate an ΔH_{ave} for the hydrogen bonds in the system.[4] When a hydrogen bond is formed "the IR wavenumber of the OH stretching vibration shifts to a low wavenumber and generates heat ($\Delta H < 0$)."[5] The DRIFTS of 12-phosphotingstic acid from ambient temperature to 350 °C is shown in Figures 1-2.

We expect structures containing OH to be poor proton conductors, as the energy required to break the OH bond would be close to the energy required to neutralize the HPA. Only 21-HAs2W and 39-HB3W show no evidence of OH. For the vehicle mechanism to prevail structures with $H^+(H_2O)_x$ are expected to be favorable and 12-HSiW, 12-HSiV3Mo, 21-HAsW and 39-HB3W all show this phase above 100 °C. Of course we can't distinguish between $H^+(H_2O)_x$ and a mixture of $H_5O_2^+$ and H_3O^+. More favorable for low humidity applications would be proton conduction by a purely

Grotthus mechanism and a number of phases are present that do not contain $H^+(H_2O)_x$ which may exhibit this phenomenon.

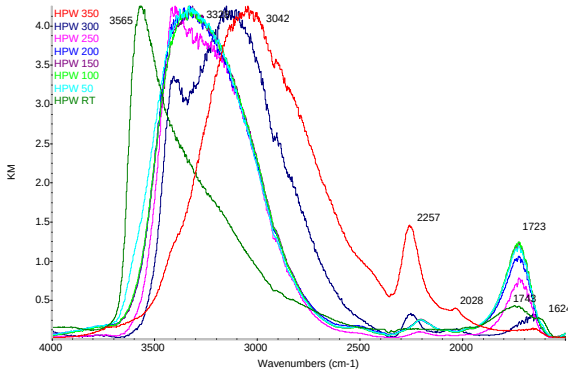

Figure 1. DRIFTS of the OH band region for $H_3PW_{12}O_{40}$ under He at different temperatures.

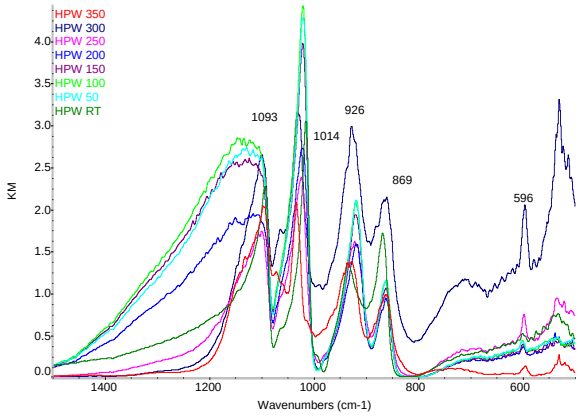

Figure 2. DRIFTS of the anion band region for $H_3PW_{12}O_{40}$ under He at different temperatures.

Table 1 summarizes some of the structural and diffusion data discussed above for the free HPA. Generally for the Keggin HPA, the maximum diffusion coefficients decrease and the activation energies increase as the central heteroatom becomes heavier. This is reflected in the increased observation of OH. The lacunary material, 11-HSiW, has a very low activation energy, but we suspect that not all the protons in the sample are mobile as the IR shows the presence of immobile OH. For this the calculated IR H-bond strength is instructive, where it matches the activation energy we can assume that all observed H_2O and H^+ are involved in H^+ transport, where it is much higher we can infer that some of the H_2O and H^+ are not available for H^+ transport. This is almost certainly the case for the sterically hindered 39-HB3W where presumably proton transport is facile between the sheets of the structure but restricted in other dimensions, note that the IR bond strength is higher than the observed activation energy. The activation energy matches the H-bond strength for 21-HAs2W and so presumably all the secondary structure is involved in proton transport and the same is almost true for 21-HP2W. The channels of the partial Rb salt of 21-diarsenotungstic acid, give a very high diffusion coefficient but this is not applicable at higher temperatures as the channels are easily dehydrated.

Table 1. Summary of Diffusion Coefficients for HPAs

HPA	Max Diffusion Coefficients $\times 10^{-6}$ $cm^2 \cdot s^{-1}$	Temperature of maximum D, °C	Ea before max T $kJ \cdot mol^{-1}$
12-HPW	25	117	13
12-HSiW	30	130	20
12-HZnW	2	108	27
12-HGeW	0.7	90	35
11-HSiW	3	108	6
39-HB3W	7	128	8
18-HP2W	1.2	> 150	20
21-HAs2W	3.7	> 150	20
21-H2Rb4As2W	30	25	-
21-HP2W	2.3	110	24

Conclusions

The HPA act as good model compounds for the study of proton conduction in the solid state, using TGA, NMR, IR, and X-Ray diffraction we were able to probe the proton conducting structures in these materials. This information was correlated with diffusion coefficients measured by pulse field gradient spin echo NMR in order to elucidate the proton conduction mechanisms observed.

Acknowledgment

This work was supported by the US DOE science initiative, DE-FC02-0CH11088.

References

1. Nakamura, O., Kodama, T., Ogino, I., Miyake, Y. *Chem. Lett.*, 17-8, **1979**
2. Early Transition Metal Polyoxoanions. *Inorganic Syntheses.* A. P. Ginsberg, John Wiley and Sons. 1990, **27:** 71.
3. Tanner, J. E. *The Journal of Chemical Physics* **1970**, *52*, 2523. 159
4. Miura, K., Mae, K., Li, W., Kusakawa, T., Morozumi, F. and Kumano, A., "Estimation of Hydrogen Bond Distribution in Coal through the Analysis of OH Stretching Bands in Diffuse Reflectance Infrared Spectrum Measured by in-Situ Technique", *Energy & Fuels*, **15**, 599 (2001).
5. K. Miura, K. M., W. Li, T. Kusakawa, F. Morozumi, A. Kumano, "Estimation of Hydrogen Bond Distribution in Coal through the Analysis of OH Stretching Bands in Diffuse Reflectance Infrared Spectrum measured by in-Situ Technique", *Energy & Fuels*, **15**, 599 (2001).

NOVEL PROTON CONDUCTIVE MEMBRANE BASED ON CLAY

Takuichi Arai, Gen Ikeda and Masatugu Nakanishi

Functional Material Dept.
Material Engineering Div. II
Vehicle Engineering Group.
Toyota Motor Corporation
1, Toyota-Cho, Toyota,
Aichi, 471-8572 JAPAN

Introduction

Perfluorinated proton conducting polymers such as Nafion® have been studied for using in proton exchange membrane fuel cell at low temperature. However, these polymers have several problems such as thermal stability and their costs. To improve above problems, applications of inorganic materials have been investigated as additives in an organic matrix[1] but are still far from essential solution.

In this study, a novel fully inorganic material, a kind of clay, is investigated as a proton conducting membrane. Montmorillonite (MON) which is the clay investigated in this study is layered compound, has high ion exchange capacity and can be expected to show proton conductivity by exchanging cations at interlayer of MON for protons.

Experimental

Membrane preparation MON membrane was prepared by phosphoric acid treatment method.[2] At first, 2.6 wt% of the MON dispersed solution was prepared by addition of sodium MON (Na^+-MON) in deionized water under constant stirring for more than 12 hours. Excess amount of conc. ortho phosphoric acid was added to the MON dispersed solution while stirring. After continuous stirring for 1 hour, the obtained mixture was a slightly turbid dispersion and was cast on polystyrene dishes. The opaque brown membrane was obtained after drying for 2 weeks at room temperature and following hardening process at 70 °C for 12 hours. The membranes were peeled from dishes and washed by deionized water to remove excess phosphoric acid and to obtain protonated MON (H^+-MON). Finally, the membranes were dried in air at 40 °C for 12 hours.

Characterization and measurement To confirm the result of cation exchange, elemental analysis of Na^+-MON and H^+-MON were done with X-ray fluorescence spectroscopy. Layered morphology and crystal structure were investigated by scanning electron microscope (SEM) and X-ray diffraction (XRD), respectively.

The proton conductivity was determined by ac impedance conductivity measurement using an impedance analyzer (NF corp., NF5090) in the frequency range between 1 Hz to 2 MHz. The temperature and humidity were controlled at 80 °C and 30-90 %RH, respectively, in a chamber.

Results and Discussion

Figure 1 shows a photograph and a cross sectional SEM image of the membrane. As shown in **Figure 1** (a) the membrane was self-supporting and showed flexibility in spite of entirely inorganic membrane.

MON is a layered clay containing cations in the interlayer and known to be bridged each other through phosphoric acid at the edge of layers. Layered structure observed in **Figure 1** (b) is thought to reflect the layered structure of bridged H^+-MON.

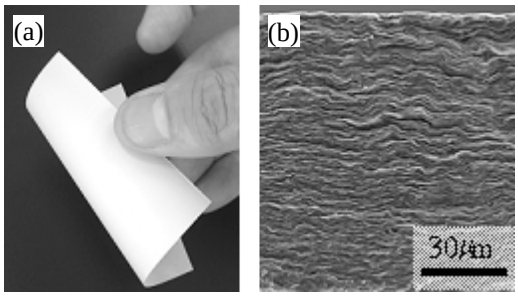

Figure 1. (a) a external view and (b) SEM image of cross section of the H^+-MON membrane.

The result of elemental analysis of H^+-MON showed elimination of sodium cations which is observed Na-MON, *i.e.*, sodium cations in the interlayer of the MON are completely exchanged for protons. The results of XRD measurement show 5 Å of increase in the interlayer distance of H^+-MON compared to Na-MON. The increment of interlayer distance should be a result of cation exchange because proton is expected to form hydronium ion which is larger than sodium ion. However, the difference in diameters of hydronium ion and sodium ion is smaller than 1 Å and it is difficult to explain the difference in interlayer distance by the difference of diameters of cations. Therefore, proton forms cluster larger than hydronium ion or excess amount of water is contained in the interlayer of H^+-MON.

The proton conductivity of H^+-MON membranes at 80 °C is shown in **Figure 2** as a function of relative humidity. The H^+-MON membrane exhibits high conductivity of $1x10^{-2}$ S/cm at 90 %RH. Observed conductivity strongly depending on relative humidity suggest proton conducting mechanism in H+-MON strongly depends on water content of the membrane, *i. e.*, dehydration of the interlayer cause rapid decrement in conductivity.

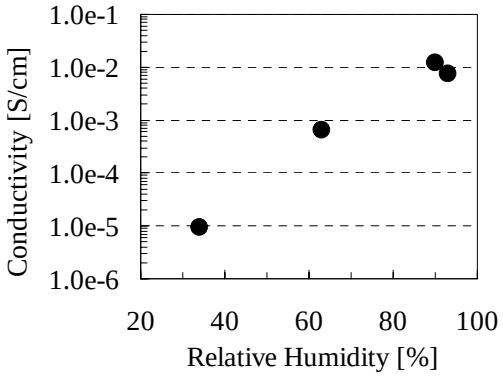

Figure 2. Proton conductivity of H^+-MON as a function of relative humidity at 80°C

Acknowledgment. The authors thank the valuable advices of Dr. Isayama of Fukuoka Industrial Technology Center and express appreciation to Kunimine Kogyo Ind. Ltd. for providing samples.

References

(1) Jones, D. J.; and Roziere, J. In *Handbook of Fuel Cells Fundamentals Technology and Applications*; Vielstich, W.; Gasteiger, H. A.; and Lamm, A. Ed.; John Wiley & Sons Ltd., 2003; (3), pp. 447-455

(2) Isayama, M.; Sakata, K.; and Kunitake, T. *Chem. Lett.*, pp. **1993**, 1283-1286

MESOPOROUS CERAMIC OXIDES AS PROTON EXCHANGE MEMBRANES

Warren H.J. Hogarth[1], João C. Diniz da Costa[1], John Drennan[2], G.Q.(Max) Lu[1]

[1]ARC Centre for Functional Nanomaterials
[2]Centre for Microscopy and Microanalysis
The University of Queensland, Brisbane 4072 AUSTRALIA

Introduction

While Nafion® is currently the benchmark proton exchange membrane (PEM) technology, it has many limitations. For example, many manufactures of PEM fuel cells for vehicle applications would like to operate the cells at high temperatures (>140^{o}C) because of CO poisoning, heat management and cost challenges.[1] At present, state of the art polymer membrane technology cannot operate in this temperature range because it degrades and looses water necessary to conduct protons. Current polymer technology is also limited in its operation lifetime and by mechanical properties.

Moving away from polymer technology has also presented similar problems. Solid acid membranes have been shown to operate well in limited temperature regimes. However they often suffer more significant mechanical shortcomings than their polymer counterparts.

Recently we proposed a new membrane design for high temperature operation based on surface functionalized mesoporous solid acid membranes[1] and demonstrated the first steps of an approach to systematically design the required membranes.[2] These membranes have the ability to be synthesized into robust thin membranes, are highly taylorable and do not suffer the same cost constraints as flourinated polymers.

Our recent work expands on these concepts demonstrating how it is possible to engineer membranes to predetermined requirements. We discuss the process of exploiting self assembly to engineer new PEMs based on current state of the art technology. The discussion is supported by a demonstration of how this process can be applied and demonstrates the flexibility that this easily tunable procedure affords.

Experimental

Samples were prepared using sol-gel synthesis techniques following a route similar to Tian et al.[3] and Soler-Illia et al.[4-6] Tri-block copolymers (Pluronic P123 or F127) were dissolved in a solution of ethanol before adding metal oxide and phosphor precursors. The molar ratio of copolymer:metal precursor:phosphor precursor:water was 70:1:2:20. Samples were either gelled to form xerogels or dip coated to form thin films under controlled temperature and relative humidities. Selected samples were calcined up to either 350^{o}C or 550^{o}C at 1^{o}C.min^{-1}.

Nitrogen Sorption. Surface area and pore size analysis was conducted using a Quantachrome Nova 1200 in a liquid nitrogen dewar. BET analysis was used to determine the surface area and BJH desorption isotherms were used for pore size distributions.

TEM. Transmission electron microscopy (TEM) was undertaken using a Tecnai T20 Field Emission Electron Gun Transmission microscope operating at 200 kV. Thin film samples prepared as described elsewhere[7] were scraped from their glass substrates and coated onto holey carbon film supported by a copper grid. The samples appeared to be stable under the beam.

a.c. impedance spectroscopy. Impedance spectroscopy was conducted using a Solatron 1260 in standalone mode for proton conductivity measurements. The frequency was cycled between 10 and 3.2e07 Hz. Samples were equilibrated at specific relative humidities over saturated salt solutions for a minimum of 7 days prior to testing.

Results and Discussion

Materials Design. The concept of the design of a new proton conductor needs to be considered from a fundamental basis. Detailed consideration must be given to the specific advantages and disadvantages of the current technology that should be retained and the failures of the competing technologies.

The unique properties of Nafion membranes are its stable perflourniated backbone for morphological stability and its highly interconnected, acidic, hydrophilic channel (or cluster) network that extend throughout the membrane. While extensive research on zirconium hydrogen phosphates was able to replicate the conductivity showed by Nafion,[8-11] it cannot be fabricated into a robust membrane. From a fundamental perspective, the key to the high proton conductivity of Nafion is its strong acidity, caused by anchored functional groups which are highly interconnected and able to arrange into the lowest energy configuration giving the highly interconnected pore network which provides the conduction pathways.

Materials Synthesis. Recent advances in mesoporous material synthesis provide an avenue to replicate the fundamental properties of Nafion while providing a robust supporting matrix and overcoming the shortfalls of zirconium hydrogen phosphates. Figures 1 and 2 demonstrate that self assembled, high surface area, ordered, interconnected, mesoporous zirconium phosphates can be synthesized forming the backbone of these new proton conductors. It has also been demonstrated that they can easily be synthesized into thin films, capable of being barrier to feed fuels.

Figure 1 shows a typical type IVb adsorption isotherm which is produced by these materials. The pronounced H2 type hysterisis loop indicates that the samples are mesoporous. The hysterisis is a consequence of the interconnectivity of the real porous network and is caused by pore blocking and network effects.[12] The pores have an average pore size between 2 and 4 nm.

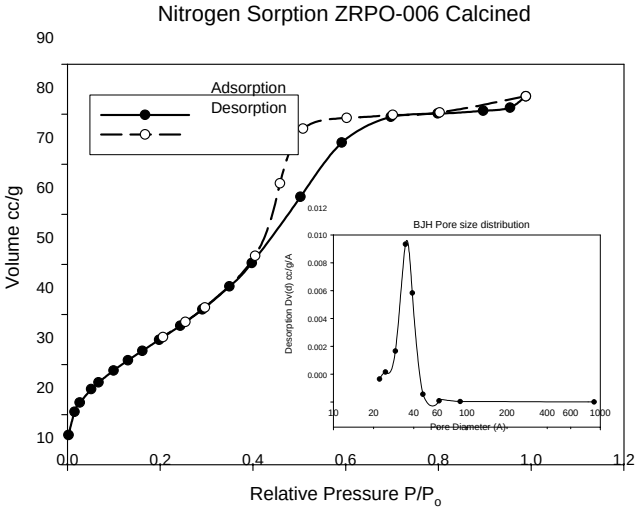

Figure 1. Typical nitrogen sorption isotherm for self assembled mesoporous zirconium phosphate.

Figure 2 shows the TEM image of the zirconium phosphate sample synthesized from trimethyl phosphate and zirconium tetrachloride precursors and Pluronic F127 as the structure directing agent. Long range hexagonal mesostructure is evident with pore diameters of approximately 4 nm confirming the nitrogen sorption results. This structure has also been synthesized using the appropriate alkoxide and phosphorous trichloride precursors. In

addition Figure 2 provides a good pictorial representation of the interconnected pore network and how these may form ion transport channels when functionalized.

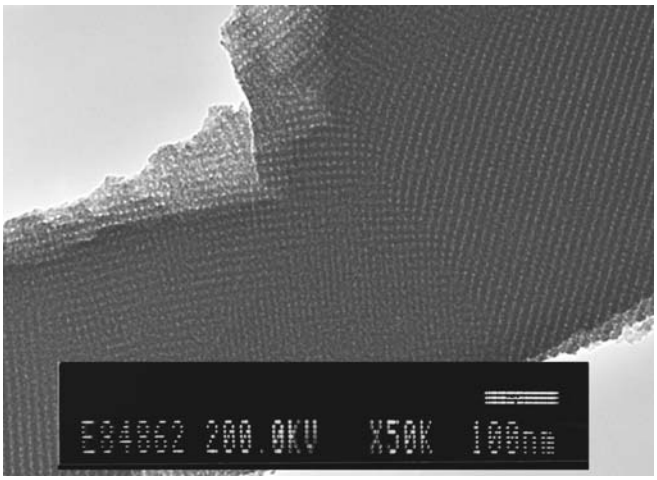

Figure 2. Two dimensional TEM pattern of mesoporous zirconium phosphate from a thin film sample heat treated to 130°C.

Functionalizing for Conductivity. After creating a highly controlled and taylorable functional matrix material, the next challenge is to engineer the conducting pathways. This can be achieved either during the synthesis steps or as a post-fictionalization process.

Figure 3 shows the inherent conductivity of the backbone and demonstrates the applicability of this class of materials as proton conductors. While the conductivity is low compared to Nafion, the conductivities are equal to that of other solid acids prior to functionalization. For example, the highest conductivity achieved was 1.5x10-6 S.cm^{-1} at 22°C and 85% RH. This is an improvement of approximately 2 fold on the results reported elsewhere for sol-gel zirconium phosphates[3, 13] and comparable to α-zirconium hydrogen phosphate.[14]

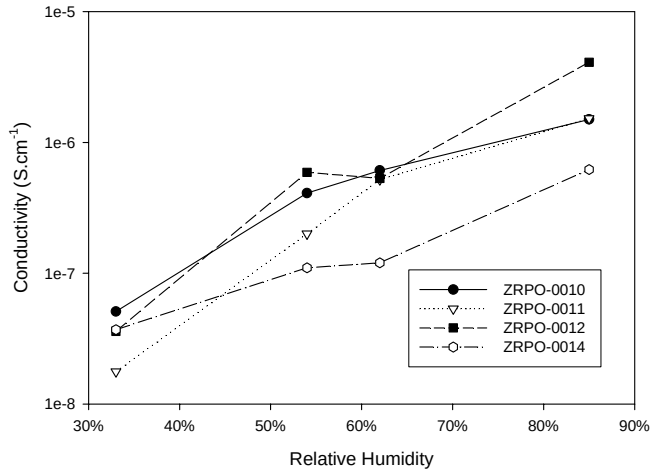

Figure 3. Proton conductivity of mesoporous zirconium phosphates, demonstrating the inherent conductivity of the backbone matrix.[2]

One of the greatest advantages afforded to materials design by the self assembly route is the taylorability of the process. Figure 4 displays the impact of tuning the synthesis of mesoporous zirconium phosphates on the proton conductivity. It demonstrates how significant improvement can be made by understanding the synthesis process.

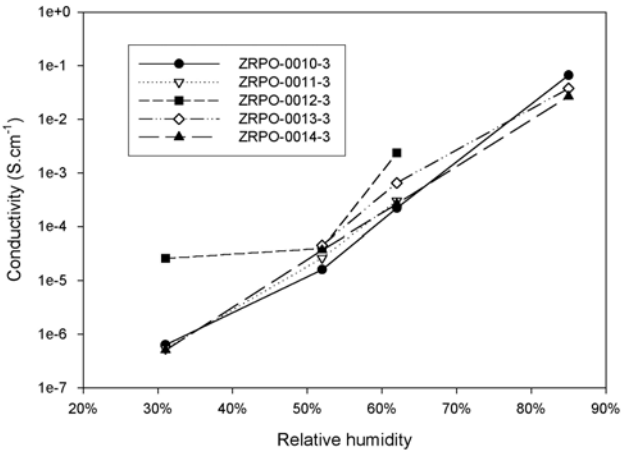

Figure 4. Proton conductivity of mesoporous zirconium phosphates after tuning the synthesis process.

Conclusions

We have demonstrated how the design of new fuel cell membranes can be achieved from a fundamental analysis. By taking the key properties of existing technologies and exploiting the advantages of ethanol-induced self assembly of mesoporous oxides we have been able to engineer designer materials to meet our required goals: a cheap, robust membrane which can be easily synthesized and which displays exceptional proton conduction.

Acknowledgement. The authors wish to thank the Australia Research Council Discovery Program (DP0344931) and the ARC Centre for Functional Nanomaterials for financial support. WH acknowledges the Australian-American Fulbright commission for financial support.

References

(1) Hogarth, W. H. J.; Diniz da Costa, J. C.; Lu, G. Q., *J. Power Sources* **2005,** *142* (1-2), 223.
(2) Hogarth, W. H. J.; Diniz da Costa, J. C.; Drennan, J.; Lu, G. Q. M., *J. Mater. Chem.* **2005,** *15* (7), 754.
(3) Tian, B.; Liu, X.; Tu, B.; Yu, C.; Fan, J.; Wang, L.; Xie, S.; Stucky, G. D.; Zhao, D., *Nat. Mater.* **2003,** *2*, 159.
(4) Soler-Illia, G.; Angelome, P. C.; Bozzano, P., *Chem. Commun.* **2004,** (24), 2854.
(5) Soler-Illia, G. J. D.; Sanchez, C.; Lebeau, B.; Patarin, J., *Chem. Rev.* **2002,** *102* (11), 4093.
(6) Soler-Illia, G.; Louis, A.; Sanchez, C., *Chem. Mater.* **2002,** *14* (2), 750.
(7) Soler-Illia, G.; Crepaldi, E. L.; Grosso, D.; Sanchez, C., *Curr. Opin. Colloid Interface Sci.* **2003,** *8* (1), 109.
(8) Alberti, G.; Boccali, L.; Casciola, M.; Massinelli, L.; Montoneri, E., *Solid State Ionics* **1996,** *84* (1-2), 97.
(9) Alberti, G.; Casciola, M., *Solid State Ionics* **1997,** *97* (1-4), 177.
(10) Clearfield, A., *Curr. Opin. Solid State Mat. Sci.* **1996,** *1*, 268.
(11) Clearfield, A.; Bortun, A. I.; Bortun, L. N.; Garcia, J. R., *Inorg. Chem. Commun.* **1998,** *1* (6), 206.
(12) Thommes, M.; Kohn, R.; Froba, M., *Studies in Surface Science and Catalysis*. 2002; (142), p 1695-1702.
(13) Rodriguez-Castellon, E.; Jimenez-Jimenez, J.; Jimenez-Lopez, A.; Maireles-Torres, P.; Ramos-Barrado, J. R.; Jones, D. J.; Roziere., J., *Solid State Ionics* **1999,** *125* (1-4), 407.
(14) Alberti, G.; Casciola, M. In *Layer Hydrates;* Colomban, P. Eds.; Cambridge University Press: New York, 1992; pp.238-251.

COMPOSITE PROTON EXCHANGE MEMBRANES

*Ping Liu and Gregory L Baker**

Department of Chemistry
Michigan State University
East Lansing, MI 48823

Introduction

The proton exchange membrane is one of the most important components of PEM fuel cells. Nafion® has long been the prototype membrane material, but its widespread application is limited by high cost and poor high temperature performance. One approach to low cost proton conducting membranes is the preparation of bicontinuous composite materials that combine a proton conducting phase with an insulating phase that provides mechanical stability.[1-2] Previous results from our lab (shown schematically below at left) show that mechanically stable Li^+ electrolytes are easily prepared by dispersing hydrophobic fumed silica particles in a hydrophilic polymer electrolyte matrix. The agglomerated silica forms a network structure within the polymer that dramatically improves the mechanical properties of the electrolyte.[3] Our hypothesis is that inverting the polarities and functions of the silica and surrounding polymer (shown at right) will lead to a similar network structure embedded in polymer, but in this case, the silica network will be the conductive phase. The silica networks in these materials might be thought of as a crude analog of the channel structure believed to be

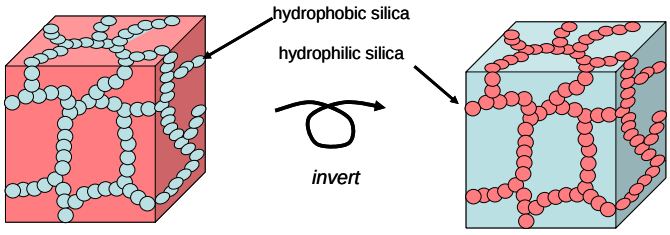

Scheme 1. Schematic diagram showing the structure of composite polymer electrolytes prepared by dispersing silica particles in a polymer matrix. At left, hydrophilic fumed silica is dispersed in a Li^+ conducting matrix to improve mechanical properties; at right, network formation polymer leads to a proton conducting network in a hydrophobic matrix.

important for ion conduction in Nafion®. Unlike Nafion®, however, the properties of these two-component composites can be easily tuned and membranes based on this approach should be available at lower cost.

The case described here is the preparation of silica particles decorated with sulfonic acids followed by their dispersal in a poly(vinylidine fluoride) (PVDF) matrix (Scheme 1). While a variety of organic and inorganic particles could be used, silica particles have good thermal and chemical stability, and are available in a broad range of sizes and surface areas. In addition, the chemistry needed to convert the silica surface to sulfonic acids is well-established and is practiced on a commercial scale. Since the number of sulfonic acid groups that can be placed on the surface is limited by the surface area of the particles (i.e. the number of silanols on the surface) we also can increase the effective concentration of acid groups by tethering polystyrene chains to the particle surface[2,5] followed by sulfonation of the polymer.[4] (Scheme 2).

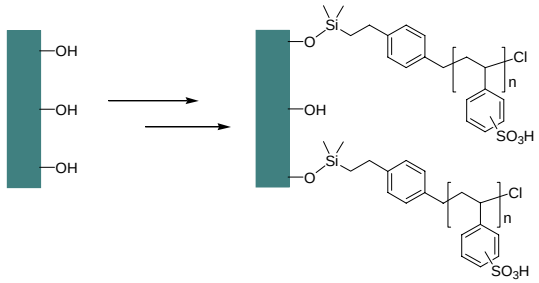

Scheme 2. Structure of the modified silica used in this work.

Experimental

Membranes were prepared by adding 0.01g of the modified silica (ground to a fine powder with a mortar and pestle) to 0.5 mL of DMF. After stirring until the solution was homogeneous, 0.5 mL of a solution of PVDF was added and the resulting solution was stirred until homogeneous (~4 hr). The solution was cast onto a glass slide heated to 50 °C on heating plat. After ~5 min, the glass slide was placed in a vacuum oven at 80 °C overnight. The dried membrane was cut into rectangular shape with a razor blaze, and the thickness of the membrane with measured with a micrometer. Membranes were conditioned by boiling the membrane in 8% HNO_3 for 30 min, rinsing with water, and then boiling the membrane in deionized water for 30 min. After blotting the membrane dry with filter paper, it was soaked in different concentrations of phosphoric acid and heated at 45 °C in a sealed vial for 3 days.

Results and Discussion

Scheme 1 shows the structure of the modified silica used in this work. Figure 1 shows influence of silica content on composite membrane on conductivity. Generally the conductivity rapidly increases with the silica (and sulfonic acid) content to ~30 wt%, followed by minor increases for >40 wt% silica. This behavior may represent a percolation threshold where the large increase in conductivity is related to increasing connectivity of the silica particle agglomerates in the PVDF matrix. The highest conductivity measured was 0.09 S/cm for a membrane with 50% silica, which is

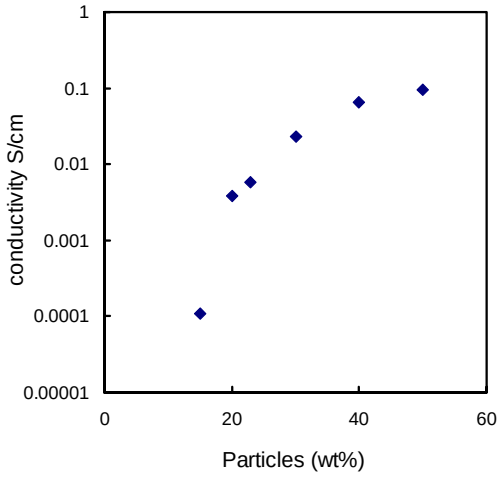

Figure 1. Room temperature proton conductivity of composite electrolytes as a function of silica content. Measurements were run at 100% humidity.

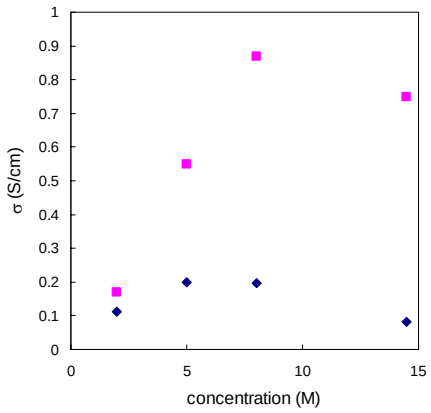

Figure 2. Conductivity of a membrane with 50 wt% silica after soaking in various concentrations of H_3PO_4 (squares). Data for H_3PO_4 solutions (diamonds) are shown for comparison

slightly higher then Nafion 117 measured under the same conditions (0.06 S/cm).

Addition of H_3PO_4 is a common strategy for increasing the protonic conductivity of polymer electrolytes. Figure 2 shows room temperature conductivity data for the membrane with 50% silica after soaking in different concentrations of H_3PO_4. Data for pure H_3PO_4 is shown for comparison. For these membranes, soaking in 8M H_3PO_4 resulted in the highest conductivity, which reflects a trade off between acid concentration and viscosity. Since PEM membranes that show useful conductivities >100 $^{\circ}$C are particularly desirable, we soaked membranes with various silica contents in 8M H_3PO_4 and measured their conductivity as a function of temperature at a water vapor pressure of 0.3 atmosphere. The data of Figure 3 show two effects. First, over the entire temperature range, the membrane conductivity increase almost linearly with the silica content, indicating the contribution of surface SO_3H groups to conductivity. Second, the temperature dependent conductivity of each membrane was similar, initially decreasing and then stabilizing at higher temperatures.

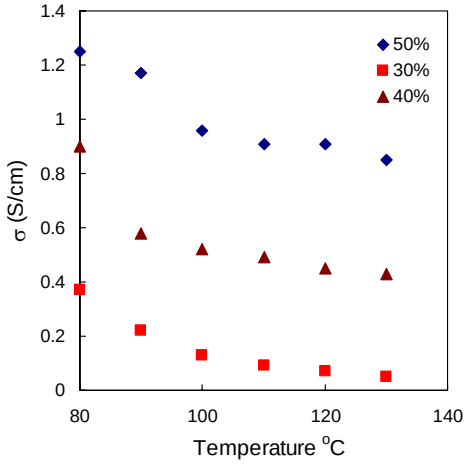

Figure 3. Temperature dependent conductivity for membranes prepared with different particle contents. Each membrane was soaked in 8 M H_3PO_4 prior to measurement.

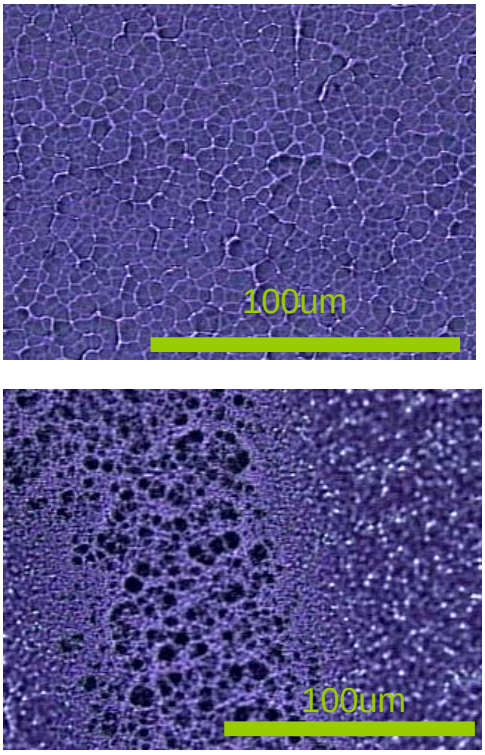

Figure 4. Transmission optical micrographs of PVDF (top) and a 50 wt% PVDF/silica composite (bottom) after soaking in H_3PO_4. The center of the lower micrographs shows the biphasic nature of the membranes.

Figure 4 shows the surface morphology of PVDF and a 50% PVDF/silica composite film. The biphasic structure is increasingly apparent as the silica content increases, in accord with the proposed model for network formation.

Conclusion

This paper provides proof of principle for the preparation of fuel cell membranes based on a "particle in polymer" approach. The composite membrane approach should permit some decoupling of the optimization of the conductivity and physical properties of the membranes. Current membranes have properties comparable to or better than Nafion®, and improvements in membrane properties are likely.

References

(1) G Alberti; M casciola, *Annu Rev Mater Res*, **2003**, *129-54*
(2) Kenji Miyatake; Masahiro Wantanabe, *Electrochem*, **2004**, *12-19*
(3) A S Khan; G L Baker; S Colson, *Chem Mater*, **1994**, *2359-63*
(4) T V Werne; T E Patten, *J Am Chem Soc*, **1997**, *7409-7410*
(5) Hunt, J. E.; Winans, R. E.; Ahrens, M.; and Xu, L. Prepr. Pap. - *Am. Chem. Soc., Div. Fuel Chem.*, **1999**, *44*, 610.

FORMATION OF CARBON DEPOSITS FROM HYDROCARBON FUELS IN SOLID OXIDE FUEL CELLS

Oktay Demircan, Mary Sukeshini, Bindhu Varughese, and Bryan W. Eichhorn

Department of Chemistry and Biochemistry,
University of Maryland,
College Park, MD 20742

Introduction

Fuel cells are currently drawing interest due to their high potential as stationary and portable power sources. Fuel cells are classified according to their electrolytes, which separate the anode compartment from the cathode compartment. High-temperature solid oxide fuel cells (SOFCs) employ solid oxide electrolytes making them distinct from other types of fuel cells. The solid electrolytes are electronic insulators and designed to conduct O^{2-} ions and operate at high temperatures (>500^{o}C).[1] The typical fuels used in fuel cells are either hydrogen or hydrocarbons. These high temperatures help the oxidation of hydrocarbons so that SOFCs can use fossil-derived natural resources such as natural gas, petroleum distillates, liquid propane and gasified coal, as well as renewable sources such as hydrogen, methanol, and ethanol. Logistic fuels (diesel fuel, gasoline, and jet fuel (JP-8)) are likely to be transition energy sources for fuel cells before hydrogen takes the place of fossil fuels.

Typical SOFC anodes are composed of a catalyst to oxidize the fuel, a conductive material to collect current, and an interface material between catalyst and electrolyte (8 mole % yttria stabilized zirconia, YSZ, in this study). Many research groups have focused on Ni based SOFC anodes due to its low cost compared to other metals. Ni is a well-studied catalyst for the oxidation of hydrogen. However, Ni also catalyzes coke formation[2] on the anode surface with hydrocarbon fuels which inhibits cell performance and causes anode degradation. Several research groups have considered different anode materials to avoid coke formation. Cu/CeO_2/YSZ anodes have been investigated for the electrochemical oxidation of longer chain hydrocarbons. Ceria (CeO_2) has been well established as a catalyst for methane oxidation and for hydrocarbon activation.[3] However, there is a distinction between Ni/YSZ and Cu/CeO_2/YSZ anodes. Gorte and co-workers[4] have observed that Cu/CeO_2/YSZ anode cell performance is enhanced by a factor of 2-3 after the formation of carbon deposits, which is in sharp contrast to Ni/YSZ behavior. They claimed that this improvement is caused by the increase in the anode conductivity due to the carbon deposit formation. The structure and composition of the carbon deposits and the formation mechanism have not been fully characterized.

In this study, the carbon deposits, produced on the SOFC anode surface with butane as a hydrocarbon fuel, were studied. The compositional and structural characterization of the carbon deposits were studied by using X-ray Diffraction (XRD), X-ray Photoelectron Spectroscopy (XPS), and Scanning Electron Microscopy (SEM). The effects of these carbon deposits on SOFC anode performance were investigated by using Linear Scan Voltammetry (LSV).

Experimental

Preparation of the membrane electrode assembly (MEA): The MEA for the single SOFC cell was prepared on a polycrystalline YSZ disk (8 mole % yttria stabilized zirconia disk) with a 25.4mm diameter and a 1.5mm thickness. The porous, LSM-YSZ (50% $La_{0.85}Sr_{0.15}MnO_3$-50% YSZ) cathode was prepared as a thin layer by tape casting methods. The porous YSZ layer (mixture of 60% YSZ powder-40% glycerin) for the anode was painted on the opposite side of the disk and then sintered at 1300^{o}C. 10% ceria and 5% copper, where needed, were deposited to the porous YSZ layer by using aqueous solutions of cerium and copper nitrates. The MEA was then sintered at 800^{o}C under reducing atmosphere. Pt and Au wires were placed on the cathode and anode sides, respectively, as current collectors. The MEA was then attached to an alumina tube by using zirconia-based ceramic paste.

To monitor the effects of carbon deposition on anode performance, a MEA with two different anodes (semicircle-design) was prepared. Both semicircle anodes were evaluated simultaneously by flowing first 5 hours H_2, and then followed by 100 hours butane, and lastly 5 hours H_2.

SOFC Operation Conditions: The complete SOFC was placed in a furnace and heated to 785^{o}C at a rate of 5^{o}C/min under Ar/H_2 flow. The diluent (Ar)/fuel (H_2 or butane) ratio is 2:1. The adjustment according number electrons per minute between H_2 and butane flows is accomplished by using the number of electrons produced by total oxidation of fuels so that the number of electrons per unit time is same for both fuel flows. Flow rates of fuel mixtures were controlled by using electronic mass flow controllers. A National Instruments SCIX data acquisition system was employed to accumulate all mass flow controller data.

Characterization Methods: For electrochemical measurements, an Autolab PGSTAT30 was used. XRD data were recorded by using a Bruker C2 Discover X-Ray Powder Diffractometer with a CuK_α radiation and a HiStar area detector. XPS data were acquired by using a Kratos Axis 165 spectrometer at a vacuum $4x10^{-10}$ Torr with a non-monochromatic MgK_α radiation. The X-ray power used for the measurements is 150W. SEM analyses were performed with an AMRAY 1820K Scanning Electron Microscope with an acceleration potential of 25kV.

Results and Discussion

The power density values, which are shown in **Figure 1**, were calculated by using simultaneous LSV measurements on both semicircular anodes,. As illustrated, the SOFC anode power densities with H_2 fuel after 100 hours of butane exposure increase by a factor of approximately 2 with respect to the initial H_2 fuel power density values. Similar enhancement values between 100 hours in our experiment and half an hour butane exposure in Gorte and co-workers[4] reveal that the longer butane exposure time has the same effect on the SOFC anode performance as the shorter time although the anode surface is completely covered with carbon deposits after a long butane exposure.

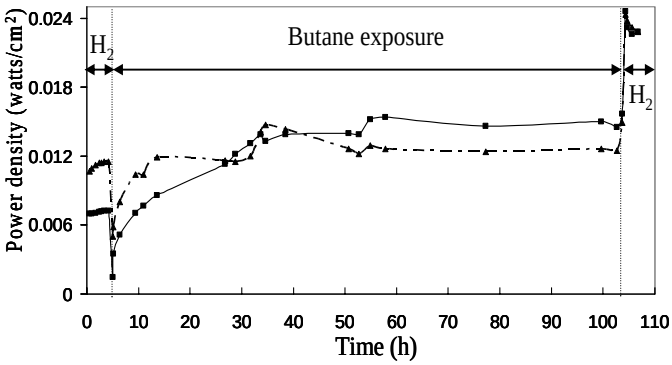

Figure 1. The SOFC power density vs. time plots for H_2-Butane-H_2 cycle representing 100 hours of butane exposure (━CeO_2/YSZ, and -- Cu/CeO_2/YSZ anodes)

SEM images of carbon deposits on anode surface and isolated from YSZ disk surface are shown in **Figure 2**. These carbon deposit spheres on the anode surface have diameters of approximately 5 μm and the thickness of carbon deposits isolated from YSZ disk surface is also 5 μm.

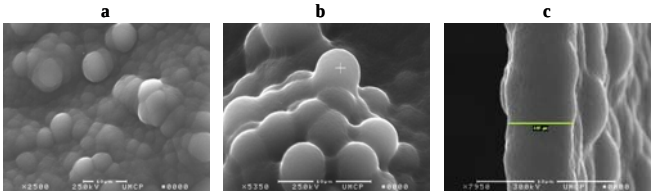

Figure 2. SEM pictures of a) Carbon deposits on anode surface b) enlargement of sample (a), c) the carbon film on YSZ disk. (White bars are 10 μm in all images, the green bar in (c) is 5 μm)

XRD patterns of 325-mesh graphite (average particle size of 44 μm), as well as the carbon deposits isolated from the electrolyte surface and both anode surfaces are illustrated in **Figure 3**. The two sharp peaks at 30^o, and 31.4^o are due to YSZ and the relatively sharp reflection at 28.5^o is due to CeO_2. The peak at 27^o is caused by SiO_2 in ceramic paste. The 325-mesh graphite XRD profile is shown as a standard to compare to the rest of the samples. The sharp graphite (002) reflection is observed at 26.5^o. All of the other samples have one broad peak shifted to 25.5^o, which is attributed to the graphite-like crystal structure discussed below.

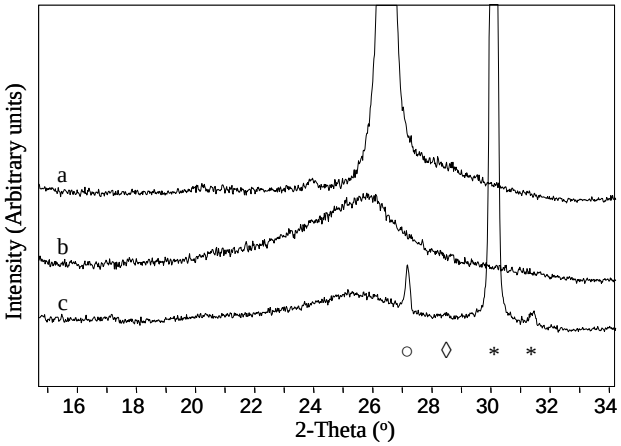

Figure 3. XRD Patterns a) 325-mesh graphite, b) carbon deposit isolated from anode surface, **c**) CeO_2/YSZ surface exposed to butane for 100 hours, (o: SiO_2 from ceramic paste, *: YSZ, ◊: CeO_2)

The shift to a lower angle and the broadness of the peak has been observed in many similar cases[5] and can be explained by the thickness (L_c) and the grain size (L_a) of the graphene layers of graphite-like structure. Due to a decrease in L_c, the d-spacing between graphene layers increases and fluctuates. As a result, this peak appears at a lower angle (2-Theta) with respect to the standard graphite (002) peak. The fluctuation in d-spacing causes the broadness. When the grain size, L_a, gets smaller (L_a<50 nm)[6], the possibility of diffraction diminishes, thus the intensity of the peak also decreases. These observations suggest that the carbon deposits on these anode surfaces have graphite-like crystal structures with small grain sizes, L_a, and small thicknesses, L_c.

The detailed C1s region XPS profiles of different semicircular anode surfaces (after linear inelastic scattering background subtraction) are demonstrated in **Figure 4** showing how the C1s regions can be fitted to a number of component peaks.

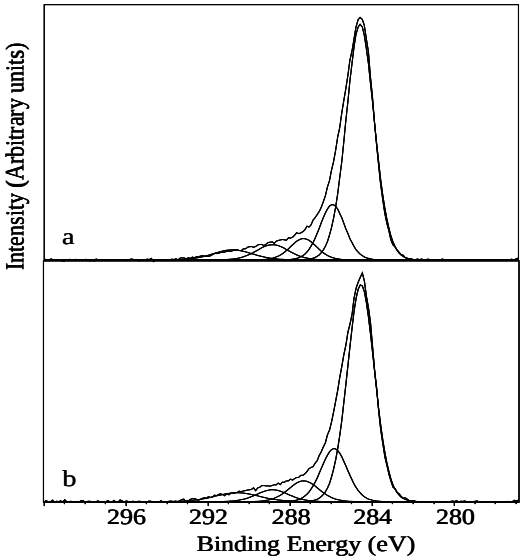

Figure 4. XPS C1s region of (a) CeO_2/YSZ anode surface, (b) Cu/CeO_2/YSZ anode surface.

The two spectra in **Figure 4** have a similar fitting features suggesting that the same type of carbon exists in both samples. The lowest binding energy peak at 284.3-284.6 eV is assigned to the sp^2 hybridized (graphitic) carbon atoms and is in agreement with binding energies reported for single crystal graphite.[7] The second lowest binding energy peak at 285.1-285.6 eV is attributed to sp^3 carbon atoms (C-H), which have also been reported elsewhere.[7] The higher binding energy peaks are consecutively assigned with respect to their chemical environments and oxidation levels. XPS results show that carbon deposits on the SOFC anode surfaces have graphitic carbon properties.

Acknowledgement

This work was supported by the Office of Naval Research thorough the Multiple University Research Initiative grant # 0110138816, in association with the Colorado School of Mines and the California Institute of Technology.

References

(1) Will, J.; Mitterdorfer, A.; Kleinlogel, C.; Perednis, D.; Gaukler, L. J. *Solid State Ionics* **2000**, *131*, 79.
(2) Gorte, R. J.; Kim, H.; Vohs, J. M. *J. Power. Sources* **2002**, *106*, 10.
(3) Minachev, K. M.; Kondratev, D. A.; Antoshin, G. V. *Kinet. Catal.* **1967**, *8*, 108.
(4) McIntosh, S.; Vohs, J. M.; Gorte, R. J. *J. Electrochem. Soc.* **2003**, *151*, A470.
(5) Tsai, .H. C.; Bogy, D. B. *J. Vac. Sci. & Tech. A-Vac. Sur. & Films* **1987**, *5*, 3287.
(6) Ergun, S. in *Chemistry and Physics of Carbon Vol.3.*, Walker, P. L., Ed. Marcel Dekker: New York, 1968, pp 289.
(7) Sherwood, P. M. A. *J. Electron Spectrosc. Relat. Phenom.*, **1996**, *81*, 319.

BENDABLE, SPLICEABLE, TUBULAR BIOFUEL CELL CABLE

Shawn Applegarth & Stuart Wilkinson

Mechanical Engineering Department
University of South Florida
Tampa, FL 33620

Introduction

With recent advances in the bioelectrochemical aspects of biofuel cells (BFC), a demand for novel mechanical configurations has begun to emerge. Early biofuel cell research was carried out with bench top apparatus involving glassware. This was eventually superseded by stacked flat-plate designs, borrowed ostensively from H_2/O_2 fuel cells used in NASA's space program. Now the emphasis has shifted to microfluidic concepts for small-scale applications[1], and flow-through designs for macro-scale installations such as with wastewater flows[2].

This paper describes a new type of biofuel cell configuration dubbed "BFC cable". This prefabricated tubular biofuel cell can be produced in long lengths and shipped in a coiled state. The current design has an outside diameter of ¾ inch, and is totally flexible, with a minimum bend radius of 6 inches. In addition, the "BFC cable" can be easily spliced together or interfaced with plumbing fixtures (manifolds, valves, etc.) using just a pair of cutters and a screwdriver. To make a connection the "BFC cable" is simply cut to length and then pushed onto a standard hose fitting. A complex biofuel cell system can thereby be assembled quickly and easily.

Design Details

The anatomy of the "BFC cable" is shown in Figure 1. At the center is a fine stainless steel wire wrapped in a helical form (weak spring). This wire acts as the anode current collector, prevents tube collapse during bending and provides an unrestricted central passageway that permits fluid permeation into the next layer. The anode spring is also crucial in the splicing process, which will be

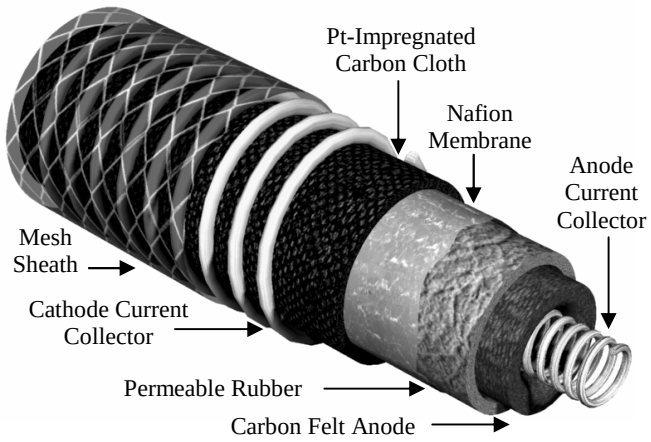

Figure 1. Anatomical configuration of the "BFC cable"

discussed later. Around the central spring is wrapped an annular anode layer made from electrically conductive carbon (graphite) felt. This felt provides a flexible, inert and non-toxic anodic scaffold structure with a high surface area capable of supporting a biofilm. The biofilm is formed *in-situ* once the system has been fully assembled, by circulating an inoculated liquid substrate through the central passageway. The inoculum must include direct-exchange microbes for successful operation since no mediation is provided. Over time the biofilm will naturally develop on the fibers of the carbon felt and act as a biocatalyst. The carbon felt anode is placed within the bore of a highly liquid-permeable rubber tube. The elastic nature of this tube allows it to expand around and tightly grip barbed-style hose connectors. The permeability creates a multitude of fluid passageways capable of transporting ions through the rubber. The outer surface of the rubber tube is surrounded by a Nafion ion-exchange membrane, which is itself bonded to one side of a platinum impregnated conductive woven carbon cloth. This latter integrated assembly (Nafion-Carbon Cloth-Pt) fulfills the role of an oxygen (air) cathode. The cathodic cloth assembly, which begins as a flat sheet, is wrapped around the rubber tube and sealed along a longitudinal overlap seam. The seal is accomplished using a rubber adhesive, which allows for expansion when a hose connector is inserted during splicing. This latter property is important since the woven carbon cloth can be readily flexed but not significantly stretched. The cathodic cloth is not itself bonded to the rubber tube, but held firmly in place by a wire wrapped around the outside. This wire also serves as the cathode current collector. The cathodic cloth becomes moist during normal operation and therefore requires pretreatment with water repellant. The "BFC cable" is completed by an external sheath of nylon mesh fabric, which provides some protection to the delicate cathodic cloth while allowing the air cathode to "breathe" and shed water.

Cable Connections

Splicing and interfacing are achieved using standard off-the-shelf metal barbed-style hose connectors. Plastic fittings are precluded, as they do not conduct electricity, while brass fittings must be avoided due to their biocidal properties. Stainless steel hose barbs are ideal, and widely available in a variety of configurations. As shown in Figure 2., the hose barb is simply pushed into the end of the "BFC cable". In so doing the anodic felt is readily squashed or crushed to accommodate the fitting, while the rubber expands and provides a positive grip. The anode current collector spring is

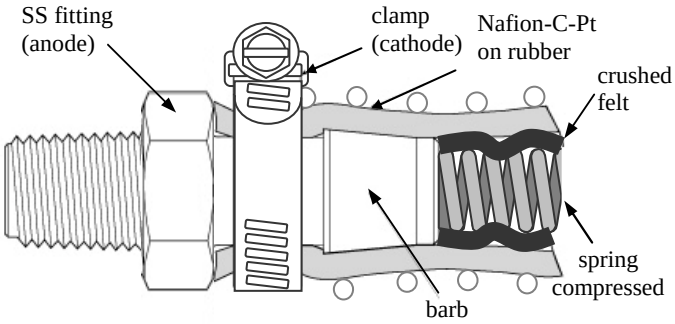

Figure 2. Typical "BFC cable" plumbing & electrical connections

compressed by the advancing hose barb and thereby creates a sprung-loaded electrical contact with the tip. The entire stainless steel connector therefore becomes the anode electrical terminal. A standard off-the-shelf stainless steel hose clamp (band and screw type) is used to ensure a liquid-tight joint, while the clamp screw serves as the cathode electrical terminal provided that some portion of the cathode current collector wire is clamped beneath the band.

References

(1) Palmore, G. T. R. in *Small Fuel Cells for Portable Applications*, Knowledge Press, Brookline, MA, **2002**, *5*, 79-98.

(2) Liu, H.; Ramnarayanan, R.; Logan, B. E. *Environ. Sci. Technol*. **2004**, *38*, 2281-2285.

AEROBIC POWER GENERATION BY A MINIATURIZED MICROBIAL FUEL CELL

Bradley R. Ringeisen,[*] Emily Henderson,[+] Jeremy Pietron,[*] Brenda Little,[§] Ricky Ray,[§] Joanne Jones-Meehan[*]

[*] Naval Research Laboratory/Code 6113, 4555 Overlook Ave. SW, Washington, D.C. 20375

[+] Wright State University/Mechanical and Materials Engineering Department, Dayton, OH 45435

[§] Naval Research Laboratory/Code 7303 and 7330, Stennis Space Center, MS 39529

Introduction

Within the next five to twenty years, networks with small, unattended sensors should be able to deliver a range of sensing capabilities (i.e., temperature, sentry, acoustic, magnetic, audio, etc.) for defense, intelligence, commercial and homeland security applications.[1] Current state-of-the-art networked sensors are relatively large (~200 cm^3 to >10^4 cm^3) and the size is often limited by the power source and the antenna. Recent advances and predicted improvements in low-power electronics, MEMs and RF communication technology will both shrink these devices and reduce power requirements to less than 100 μW, opening the possibility for non-traditional power sources to be utilized.[2-4]

For applications requiring long-time surveillance, sensing in corrosive environments (seawater, etc.) or function *in vivo*, power sources that can harvest energy from their environment are an attractive alternative to batteries and fuel cells that require replacement, recharging or fuel re-supply.[5] One example is a 1 m^2 footprint microbial fuel cell (MFC) that operates in an anaerobic environment on the seafloor by utilizing naturally occurring nutrients in the sediment.[6] Recently, we have shown that power can be continuously generated by a miniaturized microbial fuel cell functioning under aerobic conditions, opening the possibility for microbial-based power generation in more diverse environments. The miniaturized design creates shorter diffusion paths, the possibility for efficient series and parallel stacking, as well as, generating uniform nutrient flow over the electrodes. In this study, we used *Shewanella oneindensis* strain DSP10, a Gram-negative bacterium capable of respiring aerobically and anaerobically using a variety of compounds as terminal electron acceptors. DSP10 cells are used in the anode chamber, enabling power generation in both aerobic and anaerobic environments. The carbon and energy source fed to the bacteria is lactate, which can be found in marine, estuarine and freshwater environments. Therefore, a MFC operating aerobically could generate power throughout the ocean column instead of being confined to the seafloor.

Experimental

Miniaturized Microbial Fuel Cell. Figure 1 shows the miniaturized MFC used in this study. The MFC housed two 4X compressed 40 pore per cm reticulated vitreous carbon (RVC) electrodes. The anode and cathode were positioned to maximize proton diffusion across a 2.8 cm^2 Nafion™ membrane (125 μm thick) separating the two chambers, each with 1.5 cm^3 volumes. Attached 1/8" O.D. Teflon™ tubing enabled uniformly distributed flow of the anolyte and catholyte across the electrodes at rates of 1 to 50 mL/min.

Anode and Cathode Parameters. The anode and cathode used during in this study were 4X compressed 40 pore per cm RVC with equal 0.5 cm^3 volumes with macroscopic geometrical surface areas of 3.84 cm^2. The microscopic surface area of uncompressed 40 pore per cm RVC is reported by the manufacturer to be 65.6 cm^2/cm^3, but no surface areas are reported for the 4X-compressed material. We used environmental scanning electron microscopy to obtain images of the foam that indicate an increased density but fractured pore structure for the 4X compressed material (data not shown). From these micrographs we conclude that portions of the 4X compressed RVC will most likely not be available for electron transport due to broken pathways and reduced pore size. Based on cyclic voltammetry, the RVC appears to be an excellent electrode material with good electrochemical behavior.

Figure 1. NRL miniaturized MFC shown with 3D reticulated vitreous carbon (RVC) electrodes. Also, other electrode materials are shown including carbon and titanium.

The anolyte was an aerobic culture of *S. oneindensis* in 50 mL of Luria-Bertani (LB) broth with subsequent addition of lactate and anthraquinone 2,6-disulfonate (AQDS) after 48 h (final concentration was 30 mM lactate and 100 μM AQDS). Voltage data was taken in open circuit, short circuit and closed circuit (1200 Ω load) configurations when cell concentrations reached 10^8/mL. The catholyte was a 50 mM $K_3Fe(CN)_6$ prepared in 5X phosphate buffer saline (PBS).

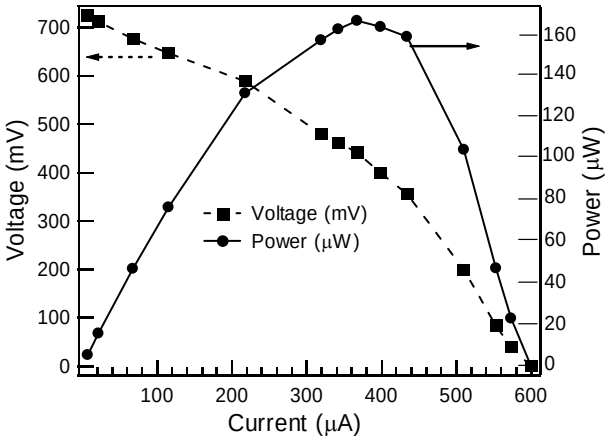

Figure 2. Voltage and power versus current for an aerobic miniaturized microbial fuel cell running on lactate fuel.

Results and Discussion

Voltage (V) was measured across variable resistance (R) to calculate current (I) generated from the miniaturized MFC (V = IR). Figure 2 shows the variance in voltage and power over the entire

range of current for the miniaturized MFC for the conditions described above. The peak power was 162 μW ($P = I^2R$) and was generated with 368 μA at 0.44 V. The open circuit voltage (V_{oc}) and short circuit current (I_{sc}) were measured at 0.725 V and 600 μA, respectively. These measurements were taken with 2 mL/min flow rates for both the anolyte and catholyte.

The current and power densities are maximized at 96 $\mu A/cm^2$ and 42 $\mu W/cm^2$ by using the geometric surface area of the electrodes in the calculation. In an attempt to make fair comparisons with other literature current densities, we will estimate of the actual microscopic surface area by using the following assumptions. Because the compressed carbon was roughly four times more dense than the uncompressed (65.6 cm^2/cm^3), one could assume that the microscopic surface area is 262 cm^2/cm^3. However, we observed only a moderate increase in current (20%) and power (15%) when using 4X compressed RVC rather than uncompressed RVC. Based on estimated surface area alone, one would expect up to a four-fold increase in output current. It is possible that portions of the compressed carbon were unavailable for electron transport (non-conductive due to fractures, compressed areas block mediators, etc.) and present only 20% more usable surface area per volume rather than four times. If this 20% increase in surface area is used (78.7 cm^2/cm^3), current and power per area are 9.3 $\mu A/cm^2$ and 4.1 $\mu W/cm^2$, respectively. By using the entire calculated microscopic surface area of 131 cm^2, current and power per area are 2.8 $\mu A/cm^2$ and 1.2 $\mu W/cm^2$.

This range in current and power density is in the same order of magnitude as those found in experiments using various *anaerobic* cultures with or without soluble electron mediators and higher than most studies when using anaerobic cultures without soluble electron mediators.[7-10] One would expect that by using *S. oneindensis* in an aerobic environment the current and power density of our MFC would be substantially lower than comparable literature cells utilizing various *Geobacter* spp. (i.e., *G. sulfurreducens*, *G. metallireducens*, etc.), which are capable of more complete oxidation of electron donors.[10] It is possible that the miniaturized scale of our MFC enhances efficiency and increases the current output above what would be expected for a macroscopic device in an aerobic environment.

One advantage of using a miniaturized MFC is the current and power output generated per volume. The anode and cathode chambers (1.5 cm^3) are at least an order of magnitude smaller than most microbial fuel cells and several orders of magnitude smaller than some MFCs. Using the maximum power data and the volume of the anode chamber, we calculated the current and power densities for our miniaturized MFC to be 245 $\mu A/cm^3$ and 108 $\mu W/cm^3$. These densities are nearly the same as the highest current per volume reported for any MFC in the literature where microbial H_2 evolution and direct microbe-to-electrode electron transport were both utilized for power generation (estimated at 400 $\mu W/cm^3$).[11] There is one example of a microfabricated MFC described by Chiao, *et. al*, but the calculated power per volume (0.5 $\mu W/cm^3$) is 200 times less than that calculated for our MFC.[12] In addition, our power per volume is 170 times larger than the best MFC using *S. oneindensis* (0.625 $\mu W/cm^3$).[13] By utilizing a high surface area electrode that resides over a third of the total chamber volume, our device most likely harnesses electrons from a greater percentage of the bacterial cells than most MFCs.

It needs to be pointed out that the power and current per volume for our device is obtained with continuous nutrient flow, a small working volume inside the fuel cell and a larger bath of anolyte and catholyte solution (50 mL) that resides external to the anode and cathode chambers. We have observed a moderate drop-off in current over time (50% over 24 h) when the flow was stopped and a slight increase in power with higher fluid flow rates (up to 10% for two times faster flow). Due to the small chamber size, a miniaturized MFC will need to be refreshed more often than larger devices, but we envision an environmental system that uses available nutrients and an oxygen cathode, either eliminating or minimizing the need for a fluidic pumping network.

Conclusions

This paper describes power generation by an aerobic, miniaturized microbial fuel cell. The current and power output of our device is similar to other MFCs described in the literature even though it is run in sub-optimal, aerobic conditions with microorganisms that are unable to oxidize electron donors as completely as other bacteria. This data suggests that there may be advantages to running MFCs in miniaturized reaction vessels rather than macroscopic chambers. If larger currents are required, then the smaller cells could be stacked in parallel rather than building a single device with a large electrode. On their own, we believe miniaturized devices may best serve as power sources for small, networked sensors or for *in vivo* applications.

Acknowledgement. This research was funded by the Office of Naval Research through Naval Research Laboratory Block Program (WU#61-6009).

References

(1) Warneke, B.; Last, M.; Liebowitz, B; Pister, K.S.J. *Computer* **2001**, *34*, 44.
(2) Roundy, S.; Leland, E.S.; Baker, J.; Carleton, E.; Reilly, E.; Lai, E.; Otis, B.; Rabaey, J.M.; Wright, P.; Sundararajan, V. *IEEE Pervasive Computing* **2005**, *4*, 28.
(3) Otis, B.P.; Rabaey, J.M. *IEEE J. Solid State Circuits* **2003** *38*, 1271.
(4) Scott, M.D.; Boser, B.E.; Pister, K.S.J. *IEEE J. Solid State Circuits* **2003**, *38*, 1123.
(5) Roundy, S.; Wright, P.K.; Rabaey, J. *Computer Comm.* **2003**, 26, 1131.
(6) Tender, L.M.; Reimers, C.E.; Stecher, H.A.; Holmes, D.E.; Bond, D.R.; Lowy, D.A.; Pilobello, K.; Fertig, S.J.; Lovley, D.R. *Nat. Biotechnol.* **2002**, *20*, 821.
(7) Skukla, A.K.; Suresh, P.; Berchmans, S.; Rajendran, A. *Current Science* **2004**, *87*, 455.
(8) Holmes, D.E.; Bond, D.R.; Lovley, D.R. *App. Envir. Microbio.* **2004**, *70*, 1234.
(9) Jang, J.K.; Pham, T.H.; Chang, I.S.; Kang, K.H.; Moon, H.; Cho, K.S.; Kim, B.H. *Process Biochem.* **2004**, *39*, 1007.
(10) Bond, D.R.; Lovley, D.R. *App. Envir. Microbio.* **2003**, *69*, 1548.
(11) Schroder, U.; Nieben, J.; Scholz, F. *Angew. Chem. Int. Ed.* **2003**, *42*, 2880.
(12) Chiao, M.; Lam, K.B.;Lin, L. *Proc. IEEE MEMS Conf.*, **2003**, Kyoto, Japan, 383.
(13) Park, D.H.; Zeikus, J.G. *Appl. Microbiol. Biotechnol.* **2002**, *59*, 58.

POLYANILINE-COATED HIGH−SURFACE-AREA CARBON FOAMS AS ANODE MATERIALS IN REAGENTLESS, AEROBIC, SMALL-SCALE MICROBIAL FUEL CELLS

Jeremy J. Pietron[†] *Joanne Jones-Meehan*[††], *Brenda Little*[†††], *Richard Ray*[†††], *Bradley R. Ringeisen*[††]

[†]Surface Chemistry Branch, Code 6170 and [††]Chemical Dynamics and Diagnostics Branch, Code 6110
Naval Research Laboratory
Washington, DC 20375
[†††]Ocean Science Branch, Code 7330
Naval Research Laboratory
John C. Stennis Space Center, MS 39529

Introduction

Small-scale microbial fuel cells (MFC) offer the possibility of low-cost, long-lived, low power-level (high-μW to low-mW) applications such as unattended sensor grids for ship and threat detection, self-sufficient water-borne chemical and biosensors, and temperature, vibration, acoustic, audio, magnetic and accelerometer surveillance via networked sensors. Appropriate bacteria can use biological fuels such as sugars and products of plant and animal decomposition likely to be found in biologically rich environments, particularly the littoral environment. Optimally, microbial fuel cells deployed in the littoral environment would be small, reagentless and operate in aerobic conditions.

We have recently developed MFCs using high-surface-area reticulated vitreous carbon (RVC) foams as both anode and cathode materials that feature surface area-to-volume ratios of roughly 65 cm^2/cm^3. This design parameter maximizes the current output per unit volume achievable with MFCs. *Shewanella oneindensis* was chosen to serve as the source of catabolic activity on the anode side as it works under both aerobic and anaerobic conditions, oxidatively breaking down lactate flowing through the cell and transferring electrons to freely diffusing anthraquinone 2,6-disulfonate (AQDS), which in turn transfers electrons to the 0.5 cm^3 (~3.8 cm^2 geometric area and 33 cm^2 microscopic surface area) current-collecting carbon foam. The catholyte consists of a ferricyanide solution as is common in laboratory microbial fuel cells. Configured as such, the microbial fuel cell generates 368 μA and 162 μW across a 1.2 kΩ resistor. Practical application will require both optimization of the cathode for utilization of ambient aqueous oxygen as the electron acceptor and *elimination of the diffusing electron-transfer mediator.* Park and Zeikus achieved current densities of 16 $\mu A/cm^2$ using *S. oneindensis*-based MFCs with carbon cloth anodes modified with Mn^{4+} ions or neutral red dyes.[1] Schröder and coworkers demonstrated MFC current densities of 90 $\mu A/cm^2$ using *E. coli* and conducting polymer (polyaniline)-modified platinum electrodes under anaerobic condtions.[2] In our study, we applied polyaniline to the RVC foam electrodes by direct electrochemical polymerization to act as a bound anodic electrochemical mediator between *S. oneindensis* and the graphite electrode, eliminating the need for a diffusing mediator

Experimental

Coating of Anodes with Polyaniline by Electropolymerization of Aniline. Polyaniline was deposited on 4X compressed 40-pore-per-cm RVC anodes by electrochemical polymerization of aniline using cyclic voltammetry, as described by Zotti *et al.*[3] Approximately 0.5 cm^3 of RVC foam was used as a working electrode in a three-electrode electrochemical cell with a gold foil counter electrode and a Ag/AgCl reference electrode. Sixty cycles between -0.05 V and 0.85 V versus Ag/AgCl at 50 mV/s in 0.1 M aniline/0.25 M H_2SO_4 (aq) were applied to the working electrode. Anodes were subsequently cycled in 0.25 M H_2SO_4 at 100 mV/s and showed oxidation and reduction waves characteristic of deposited polyaniline.[3]

Microbial fuel cell apparatus. The NRL miniaturized MFC comprises two 4X-compressed 40-pore-per-cm reticulated vitreous carbon (RVC) electrodes contained within in-house designed molded plastic housing. The anode and cathode are positioned to maximize proton diffusion across a 2.8 cm^2 Nafion™ membrane (125 μm-thick) separating the two chambers, each with 1.5 cm^3 volumes. The RVC was typically cut to ~0.5 cm^3. Attached 1/8"-O.D. Teflon™ tubing enables uniformly distributed flow of anolyte and catholyte across the electrodes at rates of 1 to 50 mL/min.

Anode and Cathode Parameters. The anode and cathode used for these experiments were 4X compressed 40 pore-per-cm RVC with equal 0.5−cm^3 volumes. The anolyte was an aerobic culture of *S. oneindensis* in 50 mL of luria burtani (LB) broth, with subsequent addition of lactate after 48 h to create a solution with 30 mM lactate. Voltage data were taken in open circuit, short circuit, and closed circuit (2200-Ω load) configurations when cell concentrations reached 10^8/mL. The catholyte was 50 mM $K_3Fe(CN)_6$ prepared in 5X phosphate buffer saline (PBS).

Results and Discussion

Figure 1 is a voltage−time plot for the polyaniline-modified MFC in closed-circuit configuration over several days, with lactate periodically added to the anode solution as fuel.

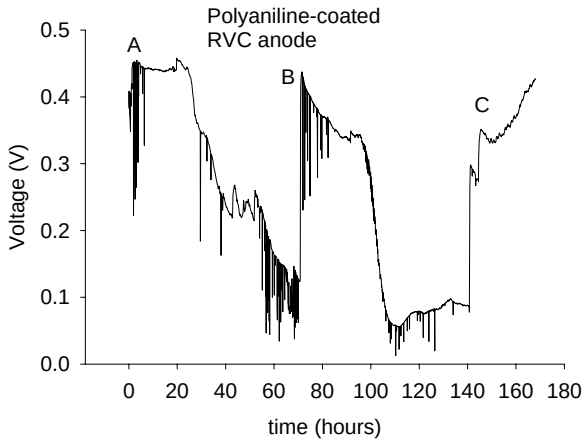

Figure 1. Voltage−time plot for the MFC with polyaniline-modified anode.

Initially data were gathered from the voltage plateau achieved after the first feeding with lactate, beginning at time "A". The MFC steadily produces 450 mV across the 2200 Ω resistor, yielding 205 μA and 92 μW for ~30 h, after which the voltage drops to about 140 mV over about 40 h. Fresh lactate was added at about 70 h (time "B") and the voltage rises to about 420 mV before decaying to a somewhat lower plateau of roughly 350 mV. The total time of useful power generation for this feeding is again roughly 30 h. Addition of fresh *S. oneindensis* to the anode reservoir with the next lactate feeding at "C" resulted in an initial rise to 350 mV and a steady rise nearly to the previous plateau of ~450 mV. Subsequent cycles of lactate depletion and re-feeding (not shown) again yielded declines in power output to ~350 mV. After this voltage decline, the anolyte was replaced, and the old solution was diluted and plated to LB agar to determine the extent of contamination. We found equal numbers of

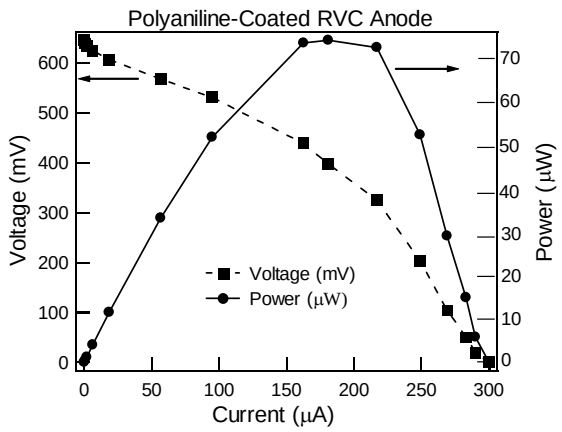

Figure 2. Voltage−Power−Current data for the MFC with polyaniline-coated anode.

S. oneindensis and *Bacillus* sp. (common environmental bacteria) in the contaminated anolyte (10^8/mL). Corresponding experiments with only environmental contaminants in the anolyte resulted in an output voltage of 0.2 mV with all other conditions the same. This result implies that environmental bacteria eventually start competing with *S. oneindensis*, resulting in a decrease in cell voltage. Future experiments will attempt to more thoroughly sterilize the electrodes and MFC housing.

Figure 2 shows both voltage and power versus current for a microbial fuel cell with a polyaniline-modified anode. Optimum power output occurs at ~400 mV with a 2.2 kΩ load, yielding ~70 μW. This power spectrum was measured shortly after time "B" shown in Figure 1, when the MFC was beginning to show signs of environmental contamination. However, the plot still shows the power and voltage spectrum characteristic of the mini-MFC operating with a polyaniline-coated RVC anode and no soluble electron mediator. The open circuit voltage (V_{oc}) is 650 mV and a short circuit-current (I_{sc}) is 300 μA.

The current and power densities estimated for our MFCs with polyaniline-modified anodes are in the 1.5−6.2 μA/cm^2 and 0.7−2.8 μW/cm^2 range, depending on the exact specific surface area of the compressed foams. Uncompressed foams feature surface areas of 65 cm^2/cm^3. The 4X-compressed foams, with which we were experimenting in our "unmodified" MFCs (no polyaniline, with AQDS) to try to improve our current per unit volume, have uncertain specific surface areas. In unmodified MFCs, the 4X-compressed foams improved currents, but only by about 20% (data not shown). The specific surface areas are certainly higher than with the uncompressed foams, but likely less than a full factor of four. Additionally, much of the diminished electrochemical utility of surface area, both in the polyaniline-modified anodes and in the unmodified anodes of compressed RVC, may be due to smaller pores that are less accessible to *S. oneindensis*. In the polymer-modified RVC, the problem of access to pores may be compounded by the thickness of the polymer film. *Alternately, if one calculates current and power density in terms of the geometric surface area of the approximately 0.5-cm^3 electrodes, each electrode is approximately a cube with 0.8 cm per edge and 0.64 cm^2 per side. Six sides yield a total geometric surface area of 3.84 cm^2, and thus current and power densities of 52 μA/cm^2 and 24 μW/cm^2.*

We find that in the absence of both a polyaniline-coated anode and a soluble electron mediator, our MFCs with bare RVC electrodes typically generate optimum power at 275 mV and 125 μA for a total power output of ~ 35 μW. This performance corresponds to current and power densities of 0.95−3.8 μA/cm^2 and 0.27−1.1 μW/cm^2 for the estimated specific surface areas, and 32.5 μA/cm^2 and 9.1 μW/cm^2 when using geometric surface areas. This in itself is an important result that demonstrates the potential advantages of using a miniaturized MFC versus a macroscopic device. The literature power density for *S. oneindensis* functioning in a mediatorless MFC is 0.03 μW/cm^2, a factor of 9 to 35 times lower than the value reported here using the much more conservative estimates from estimated specific surface areas.[1,4] The advantage of the MFC is even greater when using a polyaniline-coated anode, increasing the current density by 60% and the power density by over 150% from the bare RVC.

Future experiments will include electron microscopy of the polymer-modified electrodes to elucidate polymer film thickness, deposition of polymer films on uncompressed RVC, experimentation with polymer film thickness, polymer charge state (to optimize electron-transfer characteristics) as well as trying other electrochemically active polymers. Ideally, correct choice or modification of polymer film will allow growth *S. oneindensis* directly on the polymer, improving electron transfer characteristics and rendering the MFC completely self-contained.

Conclusions

A small, aerobic, mediatorless MFC using polyaniline-modified RVC has been described. Current and power densities are modest when considering microscopic specific surface areas, but quite promising when considering geometric surface areas. Much improvement is likely possible through optimization of electrode porosity, polymer thickness, polymer charge state and selection of polymer.

Acknowledgement. Research supported by the Office of Naval Research through Laboratory block WU#61-6009.

References

(1) Park, D. H.; Zeikus, J. G. *Appl. Microbio. Biotechnol.* **2002**, *59*, 58.
(2) Schröder, U.; Nießen, J.; Scholz, F. *Angew. Chem. Int. Ed.* **2003**, *42*, 2880.
(3) Zotti, G.; Cattarin, S.; Comisso, N. *J. Electroanal. Chem.* **1987**, *235*, 259.
(4) Kim, H.J.; Park, H.S.; Hyun, M.S.; Chang, I.S.; Kim, M.; Kim, B.H. *Enzyme Microbial Technol.* **2002**, *30*, 145.

ELECTRICITY AND HYDROGEN PRODUCTION USING DIFFERENT TYPES OF MICROBIAL FUEL CELL TECHNOLOGIES

Bruce Logan[1,2], Hong Liu[1], Jenna Heilmann[1], SangEun Oh[1], Shaoan Cheng[1], and Stephen Grot[3]

[1]Department of Civil and Environmental Engineering,
[2]The Penn State Hydrogen Energy (H_2E) Center, Penn State University, University Park, PA, 16802, U.S.A.
[3]Ion Power Inc., Bear, DE, U.S.A.

Introduction

Virtually any form of biodegradable organic matter can be used to produce electricity in a microbial fuel cell (MFC), including carbohydrates such as glucose, starch, fatty acids, amino acids and proteins (*1-4*). The process can also be used with animal and human wastewaters, resulting in both electricity generation and wastewater treatment method (*5*).

Further improvements in MFC performance are needed. Factors that affect MFC performance include: the rate of substrate degradation, the rate of electron transfer from bacteria to anode, circuit resistance, proton mass transfer in the liquid, oxygen diffusion from the cathode into the anode chamber, and the performance of the cathode. Most MFCs are operated at neutral pH in order to optimize bacterial growth conditions. However, the low concentration of protons at this pH makes the internal resistance of the cell relatively high compared to chemical fuel cells that use acid or alkaline electrolytes. There are two ways to decrease the internal resistance without changing the bulk solution pH. One is to increase the solution conductivity by increasing the ionic strength (IS); the other is to decrease the electrode spacing. Up to now, these two factors have not been systemically examined in MFCs for their effect on power generation. MFC performance can also be affected by temperature as a result of its effect on: bacterial kinetics, oxygen reaction rates catalyzed by Pt on the cathode, and the rate of mass transfer of protons through the liquid. MFC studies are normally conducted at elevated temperatures of 30-37^{o}C. However, operating the reactor at lower temperatures may reduce operational costs, especially if the reactor is used for wastewater treatment. Thus more information is needed on the performance of MFCs as a function of temperature.

The cathode electrode materials and methods of construction can also affect MFC performance. Oh *et al.* (*6*) have shown that the relative size of the anode and cathode electrodes affects power output. High Pt loading rates (0.5 mg cm^{-2}) are usually used in MFCs in order to ensure that a lack of sufficient catalyst does not limit power generation. However, Cheng et al. (*7*) found that Pt loadings on a carbon cloth electrode as low as 0.1 mg cm^{-2} did not affect performance. They also found that the cathodes prepared with Nafion® as the bonding agent achieved higher power densities than those using PTFE. Both carbon paper and cloth have been used in MFC systems, but the effect of these carbon materials on power generation in air-cathode MFCs has not been examined.

In this study, we examined the effect of solution ionic strength, electrode spacing, and temperature on electricity generation using a single chamber, membrane-free MFC. Two different cathode materials were evaluated in order to ascertain the effect of these materials on power generation.

Electricity is not the only possible product using MFC technologies. It is shown here by using a completely anaerobic system (no oxygen at the cathode), hydrogen can be produced from fermentation end products if the electrochemical potential achieved by bacteria is augmented using an external power source. This makes it possible to produce hydrogen directly from the oxidized organic matter. We call this MFC adapted process a bio-electrochemically assisted microbial reactor (BEAMR).

Methods

MFC construction. The single chamber MFC consisted of an anode and cathode placed in a plastic cylindrical chamber 4 cm long by 3 cm in diameter (empty volume 28 ml) as previously reported (*8*). The anode electrode was made of plain toray carbon paper (without wet proofing; E-Tek, USA), and was pierced in several places, forming holes ~1 mm in diameter) so that water motion in the chamber was not blocked when the anode was placed at the far end of the chamber or moved to within 2 cm of the cathode. The cathode was made of carbon paper containing 0.5 mg/cm^2 of Pt (10% of Pt/C catalyst, 30% wet-proofing; E-TEK, USA).

All MFCs were inoculated with domestic wastewater and a nutrient medium amended with sodium acetate (1 g/l). Maximum power density was determined by changing the circuit resistor and measuring power output over a complete batch cycle of operation. Each cycle was re-started by refilling the medium in the reactor when the voltage dropped below ~30 mV. The conductivity of the solution was increased by adding NaCl. Electrode spacings were 4 cm or 2 cm, and temperature was 32 or 20^{o}C as indicated.

BEAMR process. A two chamber, glass bottle reactor was composed of anode and cathode chambers separated by a proton exchange membrane (NAFION™ 117) constructed as previously described except the cathode was not aerated (*6*). The anode was plain carbon cloth and the cathode was made of carbon paper containing 0.5 mg-Pt/cm^2. The reactor was inoculated as described above, and fed a phosphate buffer (50 mM, pH=7.0) and nutrient medium containing acetate. The anode potential was set by the potential of the respiratory enzymes used to make energy for the cell from the oxidation of organic matter. A voltage in the range of 250-850 mV was applied to the circuit by connecting the positive pole of a programmable power supply.

Calculations and analysis. Voltage (V) produced by the MFC was measured using a multimeter with a data acquisition system with power ($P=IV$) normalized by the cross sectional area (projected) of the anode. Electrode potentials were measured by using a multimeter. The Coulombic efficiency was calculated as: $E=C_p/C_T \times 100\%$, where $C_{p,}$ is the total coulombs calculated by integrating the current over time. C_T is the theoretical amount of coulombs that can be produced from acetate. Gas composition was measured by gas chromatography (*22*).

Results and Discussion

MFC experiments. Increasing the solution ionic strength from 100 to 400 mM by adding NaCl increased power output from 720 mW/m^2 to 1330 mW/m^2. Power generation was also increased from 720 mW/m^2 to 1210 mW/m^2 by decreasing the distance between the anode and cathode from 4 cm to 2 cm (Figure 1). This increase in power density corresponded to a decrease of internal resistance from 161 Ω to 77 Ω when the electrode spacing was reduced from 4 cm to 2 cm. No further improvement in power generation was observed if the medium IS was increased to 400 mM because there was little change in internal resistance. The internal resistance was 71 Ω for an electrode spacing of 2 cm (Is=400 mM), which is only 10% lower than that obtained under the same conditions but with a 4 cm electrode spacing (79 Ω). Improvements on both the cathode and anode potentials were seen with a decrease in the electrode spacing with the low IS solution (IS=100 mM), while no improvement was observed when the solution IS was increased to 400 mM. Power output was also increased by 68% by replacing the cathode

(purchased from a manufacturer) with our own carbon cloth cathode containing the same Pt loading.

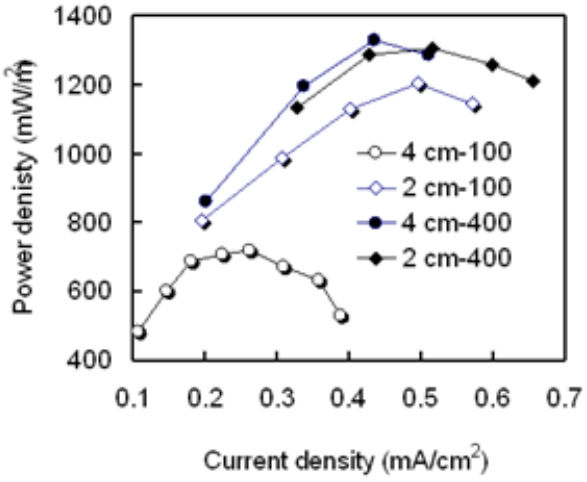

Figure 1. Effect of electrode spacing (2 and 4cm) on power generation at different current density using medium with different ionic strengths (100 and 400 mM) at 32°C.

Coulombic efficiency and energy recovery were both improved by decreasing the electrode spacing when the low IS solution was used (IS=100 mM). However, the Coulombic efficiency and energy recovery were not affected when using the higher IS solution (IS=400 mM).

The performance of conventional anaerobic treatment processes, such as anaerobic digestion, are adversely affected by temperatures below 30°C. However, decreasing the temperature from 32°C to 20°C reduced power output by only 9%, primarily as a result of the reduction of the cathode potential.

BEAMR experiments. Hydrogen production via bacterial fermentation can produce only a maximum of 4 moles of hydrogen per mole of glucose, but typically only 2 mol are produced. Acetate that is produced (2 mol/mol) cannot be further converted to hydrogen by bacteria. Using the BEAMR process, acetate was converted to hydrogen by augmenting the electrochemical potential achieved by bacteria to produce hydrogen directly from the oxidized organic matter. A small voltage (a minimum of 0.25 V) was applied to the circuit of a completely anaerobic microbial fuel cell resulting in the recovery of more than 90% of the protons and electrons produced by the bacteria from the oxidation of acetate (Coulombic efficiency range of 60-78%). This is equivalent to an overall yield of 2.9 mol-H_2/mol-acetate (assuming 78% Coulombic efficiency and 92% recovery of electrons as hydrogen).

This bio-electrochemically assisted process, if combined with hydrogen fermentation, has the potential to produce 8-9 mol-H_2/mol-glucose at an energy cost equivalent of 1.2 mol-H_2/mol-glucose. This assumes 2-3 mol-H_2/mol-glucose from bacterial fermentation, and ~3 mol-H_2/mol acetate (two moles of acetate produced per mole of glucose from the fermentation process). Production of hydrogen by this process is not limited to carbohydrates, as in a fermentation process, as any biodegradable dissolved organic matter can be used in this process to generate hydrogen from the complete oxidation of organic matter.

Acknowledgement. The Penn State researchers were supported by National Science Foundation Grants BES-0331824 and BES-0124674, a seed grant from The Huck Institutes of the Life Sciences at Penn State, and the Stan and Flora Kappe endowment.

References

(1) Park, H.S.; Kim, B.H.; Kim, H.S.; Kim H.J, Kim, G.T.; Kim, M.; Chang, I.S.; Park, Y.K.; Chang, H.I. *Anaerobe* **2001**, *7*, 297-306.
(2) Kim, H.J.; Park, H.S.; Hyun, M.S.; Chang, I.S.; Kim, M.; Kim, B.H. *Enzyme Microbiol. Technol.* **2002,** *30*, 145-152.
(3) Bond, D.R.; Lovely, D.R. *Appl. Environ. Microbiol*. **2003,** *69*, 1548-1555.
(4) Rabaey, K.; Boon, N.; Siciliano, S.D.; Verhaege, M.; Verstraete, W. *Appl. Environ. Microbial*. **2004**, *70*, 5373-5382.
(5) Liu, H.; Ramnarayanan, R.; Logan, B.E. *Environ. Sci. Technol.* **2004**, *38*, 2281-2285.
(6) Oh, S. E.; Min, B.; Logan, B. E. *Environ. Sci. Technol.* **2004**, 38, 4900-4904.
(7) Cheng, S.-A., H. Liu and B.E. Logan. 2004. Extended Abstract, Proc. 228th American Chemical Society Annual Meeting. CD ROM.
(8) Liu, H.; Logan, B.E. *Environ. Sci. Technol.* **2004**, *38*, 4040-4046.

MEDIATOR-LESS MICROBIAL FUEL CELL

Byung Hong Kim, In Seop Chang, Jae Kyung Jang and Jiyoung Lee

Korea Institute of Science & Technology,
39-1 Hawolgok-dong, Sungpook-ku, Seoul 136-791, Korea

Introduction

Cyclic voltammetry showed that some anaerobic bacteria are electrochemically active. They oxidize electron donor in the anode compartment of a fuel cell-type device without an electron acceptor, transferring electron to the electrode [1-7]. Electrochemically active bacterial consortia can be enriched in fuel cell-type electrochemical cell under various nutritional conditions. They were studied as a novel wastewater treatment process with energy recovery and as a novel biochemical oxygen demand sensor.

Electron transfer to the electrode

There are conflicting reports on the electron transfer from bacterial cells to the anode in a microbial fuel cell (MFC). Though an electron shuttle is involved in the electron transfer [7], the effluents from enriched MFCs were devoid of electrochemically active soluble compounds. A cell surface cytochromes mutant (*mtrA*) of *Shewanella oneidensis* was not electrochemically active whilst the wild strain showed the activity in cyclic voltammetry and generated electricity in an MFC (Figure 1). These results show that the electron transfer is a process through direct contact between bacterial cell and the electrode.

Microbial diversity in the enriched MFCs

Electrodes were retrieved from MFCs enriched with different nutritional conditions to analyze microbial diversity through the conventional culture method and 16S rDNA analysis. Less than 0.1% of the population could be cultured on solids media with various combinations of electron donors and acceptors. Small ribosomal RNA gene analyses showed that the fuel (electron donor) determines the dominating bacterial group in MFCs during the enrichment process. *Deltaproteobacteria* comprise around 70% in an acetate enriched MFC [8], whilst they were devoid in an MFC enriched with wastewater from a starch processing factory [9]. Fluorescent in-situ hybridization (FISH) confirmed these results.

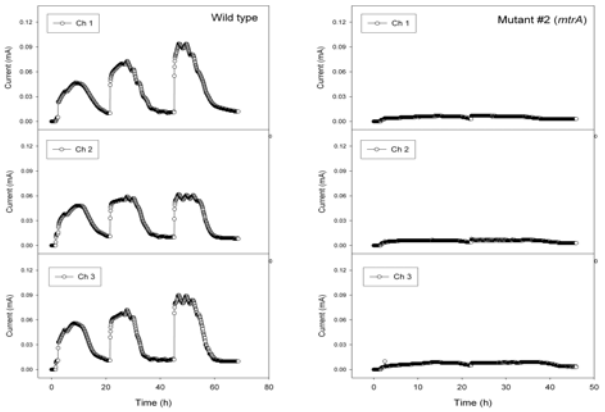

Figure 1. Current generation catalyzed by wild and *mtrA* mutant strains of *Shewanella oneidensis* with the addition of lactate as fuel. Each strain was tested using 3 separate fuel cells.

Optimization

Various rate-limiting factors were identified in electricity generation using an MFC [8]. They are (1) fuel oxidation, (2) electron transfer to the anode, (3) circuit resistance, (4) proton transfer from the anode compartment to the cathode compartment, (5) oxygen supply to the cathode, (6) oxygen diffusion into the anode compartment, (7) uneven fuel flow in the anode compartment, and others. Different factors limit the performance of MFCs under specific nutrient conditions. Oxygen diffusion into the anode compartment was most serious in an oligotrophic MFC reducing the coulomb yield, whist proton diffusion is the bottle-neck in a large scale MFC. Based on these findings, studies were made to test various MFC designs including a membrane-less MFC [11] and reduced membrane size for oligotrophic MFCs [12].

MFC as a biochemical oxygen demand (BOD) sensor

Since the current or the coulomb is directly proportional to the concentration of the fuel used in the MFC, it could be used as a BOD sensor. Since the fuel used in MFCs determines the bacterial population, enrichment was made using samples to be analyzed. When low BOD values such as river water was determined, oxygen diffused in the anode compartment was more than needed for the complete oxidation of degradable organic concentration in the samples. Nitrate is the electron acceptor preferentially used over the electrode. The terminal oxidase inhibitors such as azide and cyanide could be used to reduce the effects of the electron acceptors of higher redox potential inhibiting the aerobic respiration and denitrification (Figure 2) [13].

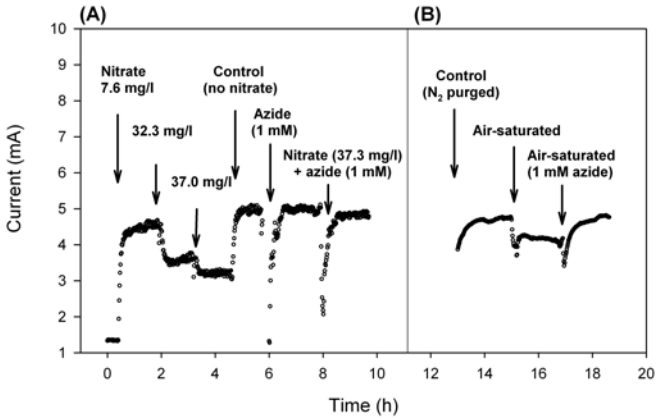

Figure 2. The current generation from MFCs fed with artificial wastewater (AW) containing nitrate and azide (A) and with aerated AW containing azide (B). AW with the BOD concentration of 113.5 mg/l was fed to MFCs at a feeding rate of 0.35 ml min^{-1}. Different nitrate concentrations and gas treatments (N_2 and air) are indicated in the figure.

Membrane-less MFC

The cation specific membrane used in a 2-compartment fuel cell is expensive, and can be suffered from fouling in the use with wastewater. A reactor was designed with the anode at the bottom and the cathode on the top without membrane. The fuel was fed through the bottom, and the cathode at the top was aerated. The performance of the membrane-less MFC was much lower than those with membrane in terms of power density. This was analyzed due to the slow proton diffusion with the increase distance between the anode and cathode. Another problem was the uneven fuel flow through the

electrode section. This could be improved using perforated electrode [14].

Stabilization of sediment

Sediment was collected from a local river to fill the bottom 1/3 of a 20 L reactor with anode buried in the sediment and cathode in the overlaying water. A set of 3 reactors was operated under the closed circuit conditions connecting the 2 electrodes, whilst the second set of 3 reactors under open circuit conditions. The closed circuit reactors generated a current of 7.6 mA/m^2 over a year. The anode redox potential was measured as 0.3 volt in the closed rectors and -0.5 volt in the open circuit reactors. More gas production was observed from the open circuit reactors than the closed ones, but more reduction in organic contents was achieved in the closed circuit reactors. The organic content reduction from the open circuit reactors seems due to methanogensis at the redox potential of –0.5 volt. Methane generation is not expected from the closed circuit reactors with the redox potential of 0.3 volt. These results show that this system can be used to accelerate sediment stabilization with reduced green-house effect gas, methane.

The current density of the closed circuit reactors is relatively low in comparison with small size MFCs. When the cathode was supplied with acid or increased aeration the current increased, showing that the reactor performance is limited by cathode reaction. This could be improved in an open system with bigger water body.

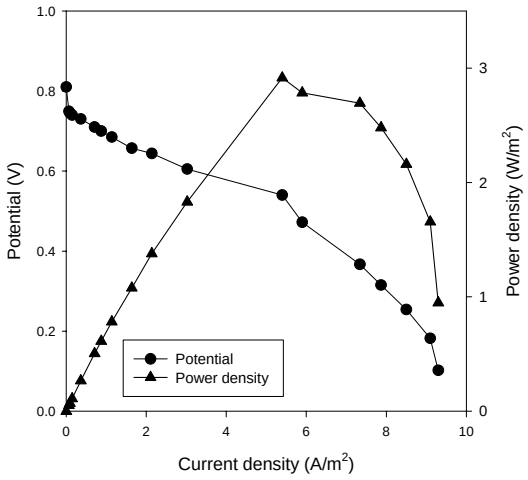

Figure 3. Polarization curve of a microbial fuel cell. The MFC was operated continuously with artificial wastewater of biochemical oxygen demand of 300 mg l^{-1} BOD, at the retention time of 8 hr.

Performance of MFSc

When an MFC is applied to treat wastewater, reduced generation of excess sludge is expected considering that a major proportion of energy carried by the organic contaminants is transformed into electricity. When an MFC with a capacity of 100 ml was operated in a continuous mode with artificial wastewater containing glucose and glutamate (300 mg l^{-1} BOD), a maximum power density of 2.9W/m^2 was achieved with a BOD removal rate of 41.7kg/m^3 day (Figure 3). The sludge generation ratio was 0.1g dry weight/g BOD removed.

The power density of a membrane-less MFC with the capacity of 2 L was one order of magnitude lower than the smaller MFCs with membrane. The performance was improved with decreasing the distance between the anode and cathode, and with acidification of the cathode area. These results clearly show that the proton mass transfer is the rate-limiting factor.

Conclusions

Electrochemically active microbial consortia can be easily enriched with wastewater as the electron donor (fuel). In most cases the effluent from MFCs fed with wastewater contained BOD less than 10 mg L^{-1} with the sludge production less than 1/4 of the conventional activated sludge process. MFC as a novel wastewater treatment process is promising not only because of the energy recovery in the form of electricity but also because of energy saving to treat sludge generated. But there are many bottle-necks to be solved before commercialization including proton mass transfer, cathode materials with better affinity for oxygen among others.

MFC can be used as a BOD sensor as well as stabilizing sediment to improve water quality in lakes.

Acknowledgement. This study was supported partly by the Ministry of Science & Technology through the National Laboratory Programme.

References

(1) Kim, B. H.; Kim, H. J.; Hyun, M. S.; and Park, D. H. *J. Microbiol. Biotechnol.* 1999, *9*, 127.
(2) Kim, B. H.; Kim, H. S.; Kim, H. J.; Kim, G. T.; Kim, M.; Chang, I. S.; Park, Y. K.; and Chang, H. I. *Anaerobe*. 2001, *7*, 297.
(3) Kim, H. J.; Park, H. S.; Hyun, M. S.; Chang, I. S.; Kim, M.; and Kim, B. H. *Enzyme Microb. Technol.* 2002, *30*, 145.
(4) Pham, C. A.; Jung, S. J.; Phung, N. T.; Lee, J.; Chang, I. S.; Kim, B. H.; Yi, H.; and Chun, J. *FEMS Microbiol. Lett.* 2003, *223*, 129.
(5) Bond, D. R.; and Lovley, D. R. *Appl. Environ. Microbiol.* 2003, *69*, 1548.
(6) Holmes, D. E., D. R. Bond, and D. R. Lovley. *Appl. Environ. Microbiol.* 2004, *70*, 1234.
(7) Bond, D. R.; and Lovley, D. R. *Appl. Environ. Microbiol.* 2005, *71*, 2186.
(8) Lee, J.; Phung, T. N.; Chang, I. S.; Kim, B. H.; and Sung, H. C. *FEMS Microbiol. Lett.* 2003, *223*, 185.
(9) Kim, B. H.; Park, H. S.; Kim, H. J.; Kim, G. T.; Chang, I. S. Lee, J.; and Phung, N. T. *Appl. Microbiol. Biotechnol.* 2004, *63*, 672.
(10) Gil, G. C.; Chang, I. SKim, .; B. H.; Kim, M.; Jang, J. K.; Park, H. S.; and Kim, H. J. *Biosen. Bioelectron.* 2003, *18*, 327.
(11) Jang, J. K.; Pham, T. H.; Chang, I. S.; Kang, K. H., Moon, H.; Cho, K. S.; and Kim, B.H. *Process Biochem.* 2004, *39*, 1011.
(12) Kang, K. H.; Jang, J. K.; Pham, T. H.; Moon, H.; Chang, I. S.; and Kim, B. H. *Biotechnol. Lett.* 2003, *23*, 1357.
(13) Chang, I. S.; Moon, H.; Jang, J. K.; and Kim, B. H. *Biosen. Bioelectron.* 2005, *20*, 1856.
(14) Moon, H.; Chang, I. S.; Jang, J. K.; Kim, B. H. *Biochem. Eng. J.* 2005, *in press*

MICROBIAL FUEL CELLS: A BIOTECHNOLOGICAL APPROACH TO POWER GENERATION

James J. Sumner and Scott R. Crittenden

US Army Research Laboratory
AMSRD-ARL-SE-EO
2800 Powder Mill Road
Adelphi, MD 20783

Introduction

In the mid-1980's a new class of anaerobic microbes was found in the Potomac River by D. Lovely then of the USGS. (Ref. 1) These organisms were found to directly oxidize organic material in the aquatic sediment and reduce solubilized iron chelates. This type of organism was found to be very prevalent in marine sediments and freshwater aquifers. They are typically anaerobic but some are facultative (grow in both aerobic and anaerobic environments). One of the unique characteristics exhibited by these microbes is the ability to directly oxidize organics and produce free electrons as part of their metabolic cycle. Specific mechanisms of this process are still being investigated. (Ref. 2)

In nature, these anaerobic microbes metabolize organic matter in the sediments of aquifers including organic acids, sugars and anhydrides. The electrons produced are normally donated to moieties such as Fe (III), Mn (IV), oxygen, nitrates, or sulfates. Engineers rapidly found the microbes were ideal candidates for bioremediation of aquatic environments, including removal of hydrocarbons, PCBs and fuel oils from marine and freshwater environments especially in the groundwater table. (Ref. 3) The ability to reduce metals and precipitate them has also been used to remove soluble uranium from aqueous solution in order to dramatically reduce the volume of radioactive wastes. Although much has been discovered about these organisms the actual electron donation mechanism is still being explored. (Ref. 2)

Recent reports describe power harvested from marine sediments containing these microbes. (Ref. 4) A fuel cell was constructed by implanting a carbon electrode into the anaerobic region of seabed sediments. A platinum electrode was placed in the saltwater above the seabed. The fuel cell produced power in the tens of milliWatt range. After weeks of operation the electrodes were removed and the carbon anode scraped of microbes that had cultured on it. The recovered bacteria were very similar to those found in the Potomac.

Power production from these organisms in the laboratory was first described in 2003 and 2004. D. Lovely and B. Logan authored these articles and are also active in bioremediation using these organisms. Power production of up to 0.5W/m^2 of electrode area has been achieved along with electron transfer efficiencies of 86%. Final power efficiency is as yet unreported and the only fuels utilized so far have been simple organics such as acetate and sugars as well as waste water. (Ref. 5)

Our goal is to increase the efficiency and power density of the microbial fuel cell by replacing the semi-permeable membrane used to separate the anodic and cathodic compartments of the cell. Current systems use Nafion 117 which is ideal for PEM fuel cells as it is capable of preventing hydrogen gas from passing but protons move relatively freely when properly hydrated. In this application Nafion 117 is "overkill". There is no need for this level of selection. The only need is to keep cells from moving from the anodic to the cathodic compartment and shorting out the system. The Nafion was replaced with a dialysis membrane which has a much lower resistance yet still easily stops the cells. This should increase both power output and efficiency.

Experimental

Microbes and Media. We used the facultative bacterium *Shewanella putrefaciens* (ATCC#49138, Raven Biologicals, Omaha, NE). The media for culture maintenance and fuel cell operation was trypticase soy broth (TSB) (BD, Franklin Lakes, NJ) *S. putrefaciens* was resuspended from a lyophilized pellet form and then incubated aerobically in TSB for 24 to 48 hours at 30 C. Many other fuels (e.g. sugars, acetate, hydrocarbons, etc.) could be used, especially if *S. putrefaciens* is replaced with one of the other metal reducing anaerobes, however, it is necessary to make sure that neither the growth media nor the electrolyte contains any electron acceptors except for the carbon electrode. Otherwise the microbes can donate their electrons to these acceptors and not the electrode, thus reducing or eliminating power production.

Fuel Cell and Electrodes. A microbial fuel cell has been constructed and power production has been demonstrated from organic fuels directly, without a reformation process. The fuel cell is a modified design from that described in reference 5B. Pictured in **Figure 1,** it consists of an H-shaped glass vessel assembled from process pipes (Ace Glass, Vineland, NJ) with the halves separated by a semi-permeable membrane. The membranes used in these experiments are either Nafion 117 (DuPont, Wilmington, DE) or dialysis membrane (Benoylated, Sigma, St. Louis, MO).

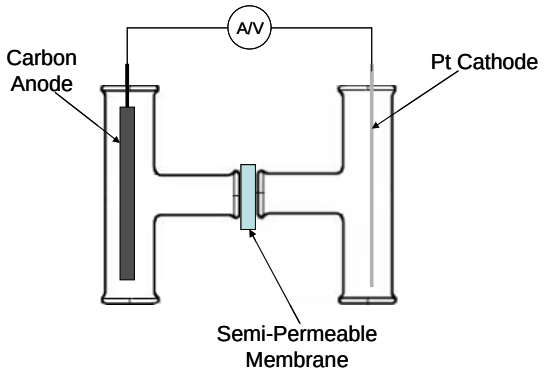

Figure 1. Microbial Fuel Cell.

The anode was constructed of a 0.25 in. by 4 in. graphite rod connected to a copper lead with silver epoxy. The joint was sealed with a non-conductive epoxy. Platinum wire (0.5mm by 25cm, Alfa Aesar, Ward Hill, MA) served as the cathode. The anodic compartment was first bubbled with nitrogen to displace all oxygen and subsequently continually flushed with nitrogen to prevent introduction of oxygen after inoculation.

The voltage was measured across an adjustable (1 Ohm to 10,000 Ohms) resistor. Data was collected using an electrochemical workstation (CHI, Austin, TX) set to monitor potential versus time.

Results and Discussion

Two identical fuel cells were constructed with the anodic chamber continuously purged with nitrogen and the cathodic compartment open to atmosphere. The anodic chamber was filled with TBS and the cathodic with Trizma at pH 7. The cells were allowed to equilibrate for several hours before the anode was inoculated with approximately 100 uL of *S. putrefaciens* culture stock. The data was collected as a voltage drop across a 10,000 Ohm resistor verses time for several days. The only difference between the two fuel cells was that one had a dialysis membrane separating the compartments and the other had Nafion 117. Typical results are shown in **Figure 2**.

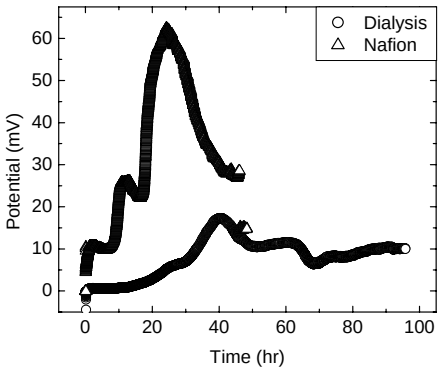

Figure 2. Voltage verses time for identical fuel cells with either Nafion (higher trace) or dialysis membrane (lower trace) separators. Note the power reduction and slowed kinetics of the dialysis membrane.

The results are opposite of the initial expectations. The fuel cell with the dialysis membrane was not only lower power but also slower to respond than the Nafion separated cell. This is probably due to the fact that oxygen can easily cross the dialysis membrane. *S. putrefaciens* is a facultative so it can survive the oxygen environment but the oxygen can act as an electron acceptor thus reducing the number of electrons donated to the electrode.

Conclusions

Leaving the cathodic compartment open to atmosphere could introduce small amounts of oxygen to the anodic compartment compromising the performance of the fuel cell utilizing the dialysis membrane. The convention for this type of device is to leave the cathode open to allow oxygen to react with generated protons to yield water. However with the platinum surface and electrons provided from the completed circuit the protons should be able to form hydrogen gas. This can be tested by purging both halves with nitrogen.

Much more than just the membrane affects the power output of a microbial fuel cell. The low power production in this system could be from the relatively low surface area anode or the growth media could have electron acceptors present. These issues will be addressed in the near future. Many other characteristics need to be met for a successful technology. The maximum power output and efficiency are only the beginning. Other characteristics include fuel tolerance, temperature range, storage conditions and resistance to chemical contaminants.

Recent work has shown that the whole organism may not be necessary as it has been reported that ruptured cell membranes can produce free electrons from nicotinamide adenine dinucleotide (NADH) which opens another realm of opportunities. (Ref. 6)

Acknowledgements. The authors would like to acknowledge Dr. Doran D. Smith and Dr. Deryn Chu of the US Army Research Laboratory for helpful discussions concerning this work.

References

(1) A) Lovely, D.R.; Phillips, E.J.P. *Applied and Environmental Microbiology*, **1986**, 51(4), 683-689. B) Lovely, D.R.; Phillips, E.J.P. *Applied and Environmental Microbiology*, **1986**, 52(4), 751-757.

(2) For Example: A) Lovely, D.R.; Phillips, E.J.P. *Applied and Environmental Microbiology*, **1988**, 54(6), 1472-1480. B) Leang, C.; Coppi, M.V.; Lovely, D.R. *Journal of Bacteriology*, **2003**, 185(7), 2096-2103. C) Holmes, D.E.; Bond, D.R.; Lovely, D.R. *Applied and Environmental Microbiology*, **2004**, 70(2), 1234-1237.

(3) For Example: A) Anderson R.T.: Vrionis H.A.; Ortiz-Bernad I.; Resch C.T.; Long P.E.; Dayvault R.; Karp K.; Marutzky S.; Metzler D.R.; Peacock A.; White D.C.; Lowe M.; Lovley D.R. *Applied and Environmental Microbiology*, **2003**, 69(10), 5884–5891. B) Lovley D.R. *Nature Reviews|Microbiology*, **2003**, 1, 36-44. C) Lovley D.R.; Anderson R.T. *Journal of Hydrology*, **2002**, 8, 77–88. D) Lovley D.R. *Science*, **2001**, 293, 1444-1446.

(4) A) Bond, D.R.; Holmes, D.E.; Tender, L.M.; Lovely, D.R. *Science*, **2002**, 295, 483-485. B) Tender, L.M.; Reimers, C.E.; Stecher, H.A.; Holmes, D.E.; Bond, D.R.; Lowry, D.A.; Pilobello, K.; Fertig, S.J.; Lovely, D.R. *Nature Biotechnology*, **2002**, 20, 821-825.

(5) A) Bond, D.R.; Lovely, D.R. *Applied and Environmental Microbiology*, **2003**, 69(3), 1548-1555. B) Finneran, K.T.; Johnsen, C.V.; Lovely, D.R. *International Journal of Systematic and Evolutionary Microbiology*, **2003**, 53, 669-673. C) Chaudhuri, S.K.; Lovely, D.R. *Nature Biotechnology*, **2003**, 21(10), 1229-1232. D) Liu, H.; Logan, B.E. *Environmental Science and Technology*, **2004**, 38(14), 4040-4046. E) Liu, H.; Ramnarayanan, R.; Logan, B.E. *Environmental Science and Technology*, **2004**, 38(7), 2281-2285.

(6) Magnuson, T.S.; Hodges-Myerson, A.L.; Lovely, D.R. FEMS Microbiology Letters, **2000**, 185, 205-211.

EFFECT OF METHANOL FEED CONCENTRATION ON DIRECT METHANOL FUEL CELL PERFORMACNE

Jun Lin, Jeong K. Lee, Ryszard Wycisk and Peter N. Pintauro

Department of Chemical Engineering
Case Western Reserve University
10900 Euclid Avenue
Cleveland, OH 44106

Introduction

Fuel cell technology is a viable option for, at least partial, satisfaction of the future energy needs. It is predicted that hydrogen fuel cells will dominate the automotive applications while direct methanol fuel cells (DMFC) are to take over the demanding portable electronics market.

The advantage of DMFC comes from the fact that both, the volumetric energy density and gravimetric energy density of fuel and containment are greater for methanol than for hydrogen.

Commercialization of DMFC is impeded mainly by high methanol crossover of the current state of the art membranes (especially Nafion materials used in PEM systems). Un-oxidized methanol permeating through the membrane to the cathode causes several deleterious effects contributing to serious power loss. The effect can be, to a certain extent, minimized by using diluted aqueous methanol solution as the feed. It was found that for Nafion 117, MeOH concentration around 1-2 M is optimal. However, the requirement to use diluted feed translates into serious complications with accommodation of either large fuel tanks or specialized dilution subsystems.

Taking into account methanol oxidation stochiometry (i.e., one mole of H_2O is required for each mole of MeOH) the optimal feed concentration should be 64 wt. % (ca. 18 M MeOH). Use of feed of such a high concentration with a Nafion-based MEA leads to serious degradation of the DMFC power due to: (i) chemical oxidation of MeOH with O_2 at the cathode bringing about electrode depolarization, (ii) surface poisoning of the cathode by methanol oxidation intermediates, (iii) lowering of O_2 concentration for cathodic reduction, and (iv) excessive flooding. The energy conversion efficiency is further lowered by the irreversible loss of a significant fraction of the fuel.

Our group has been investigating blended polymeric membranes and composites for DMFC applications (1-3) with the aim of developing materials with reduced methanol crossover. Among the systems studied are: sulfonated polyphosphazene/polyacrylonitrile (SPOP/PAN), sulfonated polyphosphazene/poly(vinylidenefluoride-co-hexafluoropropylene) (SPOP/PVDF-HFP), sulfonated polyphosphazene/polybenzimidazole (SPOP/PBI) and various Nafion blends.

The general question that we ask is whether it may be possible to not only diminish the DMFC loss of performance, but ultimately, achieve an increase in power density at higher feed concentration when using membranes with reduced methanol crossover fabricated from Nafion or polyphosphazene blends.

In this paper, we will discuss the properties and fuel cell performance of membranes prepared from Nafion/FEP, Nafion/PVDF, SPEEK/PBI and SPOP/PBI blends. Fuel cell data collected at 60°C with 1-10 M methanol feed and ambient air shows that the blended membranes outperformed Nafion 117, especially at the higher methanol concentration where the power output was higher and methanol crossover lower than that of Nafion 117. Specific examples of DMFC operation with blended membranes will be given in this talk, along with our understanding of the relationship between membrane characteristics and DMFC performance.

Experimental

Materials. The sulfonated polyphosphazene blends were prepared according to references 1-3. Nafion-PVDF blends were prepared by spin-coating a clear solution of Nafion (dried from 5 wt% solution) and PVDF in dimethyl acetamide (DMAc) solution on silicon wafer. After evaporation of DMAc at 120°C and final annealing at 145°C for 1 hour, the membranes were boiled in 1.0M H_2SO_4 and rinsed with deionized water. Nafion-FEP blends was prepared in the following way: Nafion precursor (R1100, Ion-power) and FEP (FEP 100, DuPont) pellets were mixed and extruded using DACA microcompounder at 300°C. The blends were hot pressed at 300°C and 5000 psi into films, which were then immersed in 15% NaOH aqueous solution at 80°C for 24-72 hours to hydrolyze sulfonyl fluoride groups of the precursor. The membranes were then boilded in 1.0M H_2SO_4 and rinsed with deionized water.

Characterization. Conductivity measurements were performed by an AC impedance technique using an open-frame, two-electrode cell.[1-3] Methanol permeability was measured in a custom-built two-compartment diffusion cell.[3] The morphology of the membranes were determined using a scanning electron microscope (SEM, Hitachi S4500).

Preparation of Membrane Electrode Assembly (MEA). A two layer catalyst system was used for both the anode and cathode. The first anode layer was composed of platinum-ruthenium alloy (1:1, Alfa Aesar) with 7 wt % Nafion ionomer (5 wt % solution, Aldrich) that was deposited onto A-6 ELAT/SS/NC/V2 carbon cloth, where the catalyst loading was 3.0 mg/cm^2. The second layer, which was painted directly on the first, composed of platinum-ruthenium alloy and 30 wt % Nafion ionomer (5 wt % solution, Aldrich) with a loading of 1.0 mg/cm^2. Additionally, Nafion solution (5 wt % solution, Aldrich) was painted onto the surface of the second layer at a loading of 2 mg/cm^2. Similarly, the two layer cathode was made using platinum black catalyst ink and A-6 ELAT/SS/NC/V2 carbon cloth, where the first layer (3.0 mg/cm^2) composed of 7 wt % Nafion ionomer and the second layer (1.0 mg/cm^2) contained 40 wt % Nafion. As in the case of the anode, the second Pt-black layer was painted with Nafion solution (5 wt % solution, Aldrich). Both the anode and cathode were dried at 80 ^{o}C for 30 minutes, cured at 140 ^{o}C for 5 minutes and finally hot pressed onto the membrane. The prepared MEA was soaked in 1.0M H_2SO_4 for overnight, washed thoroughly with distilled water prior to fuel cell test.

Direct Methanol Fuel Cell Tests. Steady-state current density/voltage data were collected using a single cell test station (Scribner Series 890B) with mass flow and temperature control. The fuel cell (5.0 cm^2 geometric area) operated at 60^{o}C, with 1.0-10.0 M methanol (at a flow rate of 2 ml/min) and humidified air (70^{o}C and atmospheric pressure, at a flow rate of 500 sccm). The methanol crossover flux was determined by measuring the carbon dioxide concentration in the cathode air exhaust at open circuit, using a Vaisala GMM12B or GMM220A CO_2 detector. Prior to measurements, the sensor was calibrated with reference CO_2/N_2 gas mixtures containing 400-5000 ppm of CO_2.

Results and Discussion

Figure 1 shows the morphology of a Nafion/FEP blend containing 50 wt.% of FEP (50/50) and a Nafion/PVDF blend containing 50 wt% of PVDF (50/50). It can be clearly seen that Nafion/FEP membranes show strong orientation of the blended components, while Nafion/PVDF system doesn't show any orientation. This morphological difference could be related to the processing condition during the preparation of the two blends. For

Nafion/FEP blends, both melt extrusion and hot-pressing cause strong orientation of the dispersed phase. On the other hand, solution casting seems to result in a very homogeneous, fine morphology.

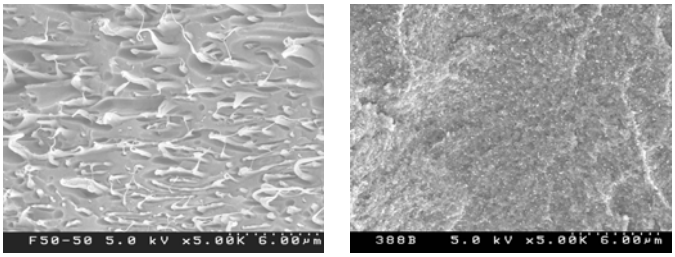

Figure 1. The SEM pictures of Nafion/FFP 50/50 (left) and Nafion/PVDF 50/50 (right).

The resulting membranes were characterized in terms of proton conductivity (in-plane and through-plane AC impedance) and methanol permeability. A comparison of fuel cell performance for a Nafion/FEP 50/50 blend is shown in the Figure 2. It can be seen that the blended membrane showed better performance than Nafion 117, especially at the higher methanol concentration of 5.0 M (where the power output was higher and methanol crossover lower than Nafion 117). Similarly, Nafion/PVDF blends and SPOP/PBI blends also showed better fuel cell performance than Nafion 117 at methanol concentration higher than 1.0 M.

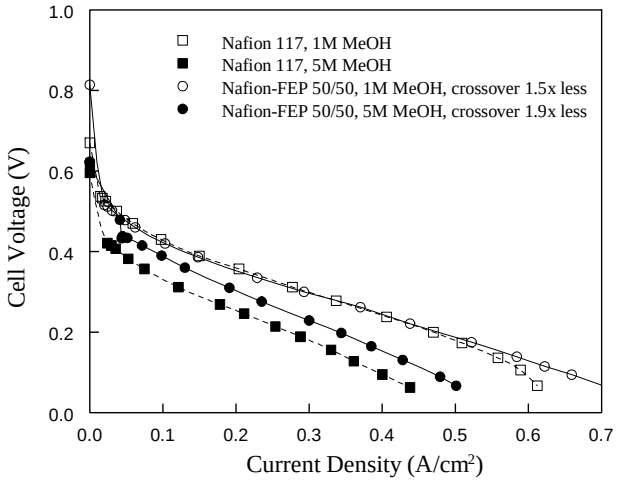

Figure 2. Direct methanol fuel cell performance with Nafion 117 and a Nafion-FEP blended membrane at 60°C, atmospheric pressure and 500 sccm.

In Figure 3, the maximum power densities of Nafion 117 and an SPOP/PBI membrane were plotted as a function of methanol concentration in the range of 1.0 to 10.0 M. The SPOP/PBI blend contained 3 wt% PBI and the IEC of SPOP was 1.2 mmol/g. It can be seen that maximum power density of Nafion 117 drastically decreased from 96 mW/cm^2 down to 9 mW/cm^2 as methanol concentration increased to 10 M. This Nafion 117 performance deterioration is attributed to the combined effects of the higher methanol crossover that resulted in a decrease of cathode potential and increased ohmic resistance of membrane with an increase of methanol concentration. Although at 1.0 M MeOH, the maximum power density of the SPOP/PBI-based MEA was lower than that of Nafion 117, the situation changed dramatically when methanol feed concentration greater than 2.0 M was used. Upon operation on 10.0 M methanol solution, the maximum power density of SPOP/PBI was 6.67 times higher than that of Nafion 117. Consequently, it could be stated that the decrease of fuel cell performance of SPOP/PBI was due to merely diminished cathode potential resulting from higher methanol crossover flux since the resistance of SPOP/PBI was almost constant in the whole range of methanol concentration.

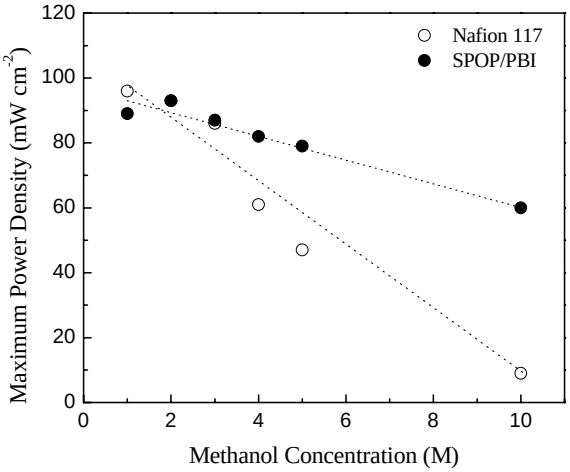

Figure 3. Maximum power density dependence on methanol concentration for SPOP/PBI blends compared with Nafion 117.

Acknowledgment

This work was funded by the Army Research Office, Grant No. DAAD19-00-1-0517. The authors would also like to thank DuPont, Atofina Chemicals and Unitel Technologies, Inc., for providing samples.

References

1. Carter, R., Wycisk, R., Yoo, H., Pintauro, P.N., "Blended Polyphosphazene/Polyacrylonitrile Membranes for Direct Methanol Fuel Cells", *Electrochem. and Solid-State Lett.*, **2002**, 5**,** A195.
2. Wycisk, R., Carter, R., Pintauro, P.N., Byrne, C., "Ion-Exchange Membranes from Blends of Sulfonated Polyphosphazene and Kynar Flex PVDF", in: *Advanced Materials for Membrane Separations*, I.Pinnau and B.D.Freeman (Eds.), ACS Symposium Series 876, ACS, Washington, DC, 2004, 335-351.
3. Wycisk, R., Lee J.K., Pintauro, P.N., "Sulfonated Polyphosphazene-Polybenzimidazole Membranes for Direct Methanol Fuel Cells", *J. Electrochem. Soc.*, **2005**, *in press.*

CATALYST LAYER NETWORK FORMATION AND ITS EFFECT ON FUEL CELL PERFORMANCE

Christine Hronec[1], Charles W. Walker[2] and Yossef A. Elabd[1]

[1]Department of Chemical Engineering
Drexel University
Philadelphia, PA 19104

[2]U. S. Army Research Laboratory
Sensors and Electron Devices Directorate
Adelphi, MD 20783

Introduction

Polymer electrolyte membrane (PEM) fuel cells are intensely being investigated as an alternative to current power sources because of their potential to achieve higher efficiencies with renewable fuels at a lower environmental cost.[1] Despite the numerous advantages of PEM fuel cells, there are several shortcomings with current PEMs, catalysts, and the catalyst layer (CL) structure that hinder fuel cell efficiencies. This study focuses on the morphology of the CL and its subsequent effect on fuel cell performance. Currently, membrane electrode assemblies (MEAs) or CL/PEM/CL composites are most often fabricated by hand painting the catalyst ink unto a decal followed by a decal/hot press ink transfer step.[2] Additional deposition techniques to form the CL in the MEA have been investigated, such as spraying, screen-printing, and rolling.[3] These studies reveal differences in fuel cell performance, which can be related to the morphology of the CL. A number of investigators have suggested that the structure of the CL, or more specifically the reactant gas/Pt/Nafion triple phase boundary (TPB), must be optimized to allow for the appropriate balance of hydrogen gas diffusion, catalytic activity, and proton conductivity.[4]

In this study, a new CL deposition technique was investigated: *in situ* sonication. The CL morphology and fuel cell performance of the new technique was compared to the standard hand painting ink transfer method. In addition, the microstructure of the CL was characterized before and after fuel cell testing to determine the effects that fuel cell tests may have on altering the CL morphology and subsequently fuel cell performance.

Experimental

Materials. Catalyst ink consisted of de-ionized water, 2-propanol (Aldrich, 99.5%), 5 wt% Nafion® in solution (Fluka), and Vulcan XC-72R (ElectroChem, 20wt% Pt/C). Teflon®-coated Fiberglass supports (5 cm^2, C.S. Hyde Co.) or decals were used for the decal/hot press MEA fabrication technique. In addition to the CL, MEAs consisted of a Nafion® 117 perfluorinated membrane (Aldrich) and carbon cloth diffusion layers (ETEK, Inc.).

CL Preparation. Catalyst ink was prepared by ultrasonically mixing Pt/C catalyst in a solution of 2-propanol/water (3:1 volume ratio) for 15 minutes. 10 wt% Nafion® binder was then added and the resulting suspension was ultrasonically mixed for an additional 15 minutes at 30°C.

In this study, four different CL/MEA preparation techniques were investigated (**Table 1**). Method A represents the most commonly used MEA fabrication technique, a decal/hot press transfer. For this method, the catalyst ink was hand painted unto a Teflon®/Fiberglass decal, allowed to dry, and subsequently applied in multiple painting/drying steps to obtain a desired Pt loading of approximately 0.5mg/cm^2 (multilayer hand painting). A dry Nafion® 117 membrane (> 5 cm^2) was sandwiched between two of these catalyst covered decals, with the catalyst side of each decal facing the membrane, and hot pressed at 150°C and 440 kg/cm^2 for 10 s (decal/hot press). The Teflon®/Fiberglass decals were then removed with the catalyst layers remaining on both sides of the membrane. Method B is similar to Method A, however, the decal/hot press step was replaced with a direct deposition of catalyst ink unto the Nafion® 117 membrane *via* multilayer hand painting. This method was explored to determine if direct deposition can replace the decal/hot press step to simplify the fabrication process.

In this study a new deposition technique, *in situ* sonication (ISS), was developed (Methods C and D in **Table 1**). For this technique, a Teflon® Petri dish was suspended in a sonicating bath with the CL substrate (Teflon®/Fiberglass decal or Nafion® 117) adhered to the bottom of the dish. The catalyst ink was applied directly onto the substrate and allowed to dry at 25˚C under sonication for 3 hrs.

Table 1. CL and MEA Preparation Techniques

Method	CL substrate	CL deposition technique	MEA Fabrication Technique
A	Teflon®/Fiberglass decal	Multilayer hand painting	Decal/hot press
B	Nafion® 117	Multilayer hand painting	Direct deposition
C	Teflon®/Fiberglass decal	*in situ* sonication	Decal/hot press
D	Nafion® 117	*in situ* sonication	Direct deposition

Instrumentation. A FEI/Phillips XL30 Field Emission Environmental Scanning Electron Microscope (SEM) was used for CL and MEA characterization. All samples were sputter coated with Pt for 20 seconds using a Denton Desk II sputter coater. Fuel cell testing was performed with a fuel cell test station (Fuel Cell Technologies, Inc.), where the MEA was sandwiched between carbon cloth diffusion layers (double sided at the anode and single sided at the cathode), flow-channel graphite blocks, and bolted between stainless steel heated endplates (fuel cell test fixture) with a testing cross sectional area of 5 cm^2. Fuel cell tests were performed at a hydrogen flow rate of 50 cm^3/min, an oxygen flow rate of 100 cm^3/min, a backpressure at the anode and cathode of 30 psi, and a cell temperature of 80˚C. Cells had an open circuit potential of approximately 0.9 V, and tests were conducted by sweeping potential from 0.9 to 0.2 V by increments of 0.02 V every 10 s and recording current.

Results and Discussion

The SEM images in **Figure 1** show clear structural differences in the CL prior to MEA fabrication when comparing two different deposition techniques, multilayer hand panting and ISS. Multilayer hand-painted samples reveal catalyst ink agglomeration and cracks on the order of 10 to 100 microns in size generating a non-uniform surface (**Figures 1 (a)** and **(b)**). CLs prepared by ISS forms a more uniform, well-packed layer as shown in **Figure 1 (c)**. Simultaneous sonication and solvent evaporation during CL preparation deters catalyst particle agglomeration. This suggest that prolonged sonication during deposition hinders the van der Waals attractive forces between catalyst particles that promote agglomeration.[5] For

Methods A and C, similar CL structures were evident after transferring from the decal to the Nafion® 117 membrane.

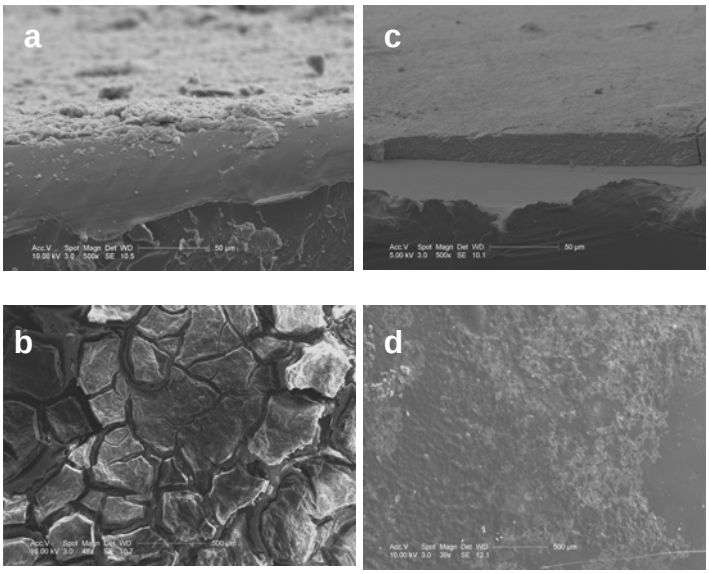

Figure 1. SEM images of the **(a)** cross section of hand painted CL **(b)** top view of hand painted CL **(c)** cross section of ISS CL and **(d)** top view of ISS CL. All samples shown here were deposited on a Teflon®/Fiberglass decal.

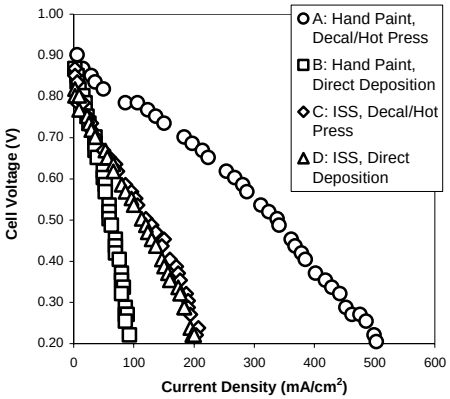

Figure 2. Fuel cell performance data for different CL preparation techniques.

Figure 2 shows the fuel cell performance of the four different CL fabrication techniques listed in **Table 1**. The MEA prepared by multilayer hand painting of the catalyst ink directly onto Nafion® 117 (Method B) displayed the lowest performance. CLs made by ISS, regardless of whether the decal/hot press transfer or direct deposition technique was used (Method C and D), had a similar fuel cell performance, while the standard multilayer hand painting and decal/hot press transfer method (Method A) demonstrated the highest performance. Based on the CL morphology shown in **Figure 1**, it appears that less catalyst surface area is available in Method A, where less pores are available for gas diffusion in Method C. However, based on **Figure 1**, it is unclear which CL possesses a more favorable TPB.

Figure 3 displays an MEA after a fuel cell test. The MEA prepared by Method A reveals catalyst particle agglomeration and cracks within the CL before and after fuel cell tests. These cracks allow for reactant gas flow to catalyst sites on the exterior of densely packed catalyst particle agglomerates. A noteworthy result is evident in a higher magnification image of the CL shown in **Figure 3 (b)**, where a network of Nafion® fibers and smaller catalyst particle agglomerates was formed. These networks were not present in the CL prior to fuel cell tests. These networks were present in post fuel cell MEAs prepared by the other techniques (Methods B-D); however more of these networks were evident in the MEAs prepared by Method A when compared to the other techniques. The morphology after or during fuel cell testing as opposed to before may contribute to the differences in fuel cell performance shown in **Figure 2**. A network of Nafion® fibers connecting catalyst particles dispersed throughout seems to provide a more favorable TPB, where high porosity allows for reactant gas diffusion, smaller catalyst agglomerates possess a higher available surface area for reaction, and the Nafion® fibers provide a pathway for proton diffusion to the PEM. This network was found within the CL microstructure in areas of high porosity. The mechanism for the formation of this network has not yet been determined; however it appears that CLs with higher initial porosity (e.g., Method A) allow for more network formation during fuel cell testing.

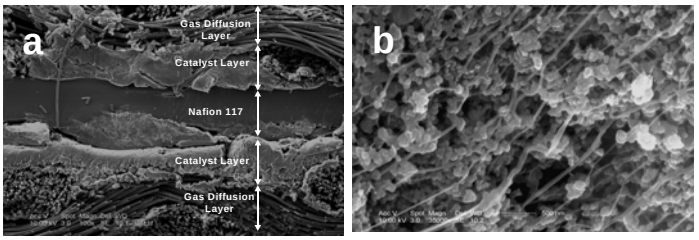

Figure 3 SEM image of **(a)** an MEA (Method A) after a fuel cell test and **(b)** the CL (magnified image) displaying a network of Nafion® fibers connecting catalyst particles.

Conclusions

In this study, a new deposition technique was explored, *in situ* sonication, which produced a more uniform and less porous CL. The fuel cell performance of this new technique was considerably lower than the standard fabrication technique. However, SEM images of the CL after fuel cell testing displayed different CL structures, a network of Nafion® fibers connecting catalyst particles. This network microstructure, and not the CL microstructure prior to fuel cell testing, may be responsible for the differences in fuel cell performance. Current investigations are focused on determining the causes leading to the formation of this favorable CL network.

Acknowledgement. Dee Breger (Drexel University, Department of Materials Science and Engineering) for SEM imaging assistance and NSF-BES-0216343 for SEM equipment.

References

(1) U.S. Department of Energy. Fuel Cell Handbook, 6th ed. B/T Books: Orinda, CA, 2002.
(2) Ahn, S.Y.; Lee Y.C.; Ha, H.Y.; Hong, S.A.; Oh, I.H. *Electrochimica Acta* **2004**, *50*, 673.
(3) Abaoud, H.A.; M. Ghouse, K.V.; Lovell, K.V.; Al-Motairy G.N. *International Journal of Hydrogren Energy* **2005**, *30*, 385.
(4) O'Hayre, R.; Prinz, F.B. *J. Electrochem. Soc.* **2004**, *151*, A756.
(5) Schueler, R.; Petermann, J.; Schulte, K.; Wentzel, H.P. *J. Appl. Polym. Sci.* **1997**, *63*, 1741.

THERMAL STABILITY IN AIR OF Pt/C CATALYSTS AND PEM FUEL CELL CATALYST LAYERS

Olga A. Baturina[1], *Steven R. Aubuchon*[2], *and Kenneth J. Wynne*[1]

[1] Department of Chemical and Life Science Engineering
Virginia Commonwealth University
Richmond, VA 23284-3028
[2] TA Instruments-Waters, LLC
109 Lukens Drive, New Castle, DE 19720

Introduction

Development of carbon-supported platinum catalysts was one of the major steps to commercialization of PEM fuel cells. The main advantages of these catalysts are high surface area, sufficient electronic conductivity of carbon and sluggish catalyst agglomeration under fuel cell operation conditions. Due to increased surface area of Pt/C catalysts, Pt loading in fuel cell cathodes can be reduced 20-40 times (compared to Pt black catalysts) to obtain a similar cell performance.

Unfortunately, using carbon support in Pt/C catalysts also has shortcomings. It is well known that carbon corrodes in a fuel cell environment[2]. As a result, a fuel cell might lose performance during long-life operation. Moreover, it has been found recently that Pt facilitates carbon oxidation in PEM fuel cell simulated conditions[3, 4]. In addition, Pt accelerates the thermal decomposition of Nafion®, (another component of PEM fuel cell catalyst layer) at high temperatures[5].

Due to increased interest to high temperatures PEM fuel cells (operating at temperatures 100-200^{0}C), it is important to explore the limits of thermal stability of carbon supported Pt catalysts and PEM fuel cell catalyst layers.

Experimental

20% and 40% Pt/Vulcan XC72 from E-TEK and 50% Pt/Vulcan XC72 (Tanaka KK, Japan) were used in these studies. Nafion 112 membrane was purchased from Ion Power, Inc. Catalyst layer was prepared by electrospraying Pt ink[1] consisting of ~40% of Nafion ionomer (equivalent weight of 1100, Aldrich) and ~60% of 50% Pt/Vulcan XC72 (dry base) on Nafion 112 membrane. Catalyst layer was sampled for TGA by scraping from the Nafion 112 substrate. Thermogravimetric analyses (TGA) were collected on a Q500 TGA (TA Instruments-Waters, LLC.). Heating rates of 2.5, 5, 10 and 20°/min were employed under an atmosphere of flowing air (100 mL/min).

Results and Discussion

Fig.1 contains the TGA (weight loss vs. temperature) curves for carbon supported Pt catalysts with different platinum loading in air. This data suggest that Pt accelerates decomposition of carbon in carbon supported catalysts; a shift between TGA plots for base carbon and Pt/C is ~200^{0}C. Decomposition of carbon supported catalysts occurs gradually in the beginning and ends with abrupt weight loss at ~ 400^{0}C. The residue above 400^{0}C is stoichiometrically consistent with elemental platinum as the decomposition product. In addition, further analyses of TGA curves for catalysts with different Pt loadings suggests that the amount of carbon loss during the TGA experiment increases with increasing Pt loading.

TGA and DTG (derivative weight loss) plots for catalyst layer, consisting of 50% Pt/C and Nafion® ionomer, Nafion 112 and 50% Pt/C and are presented in Fig.2 and 3, respectively. The TGA curve for the catalyst layer shows three distinct regions corresponding to three peaks on the DTG curve. The sample loses ~4% between 50°C

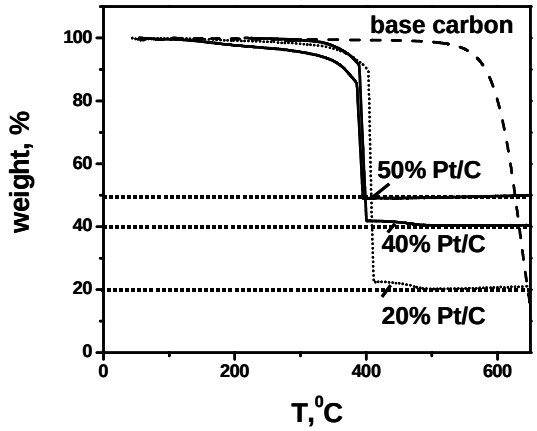

Figure 1. TGA (20^0/min) plots of 20%, 40% and 50% Pt/C in air.

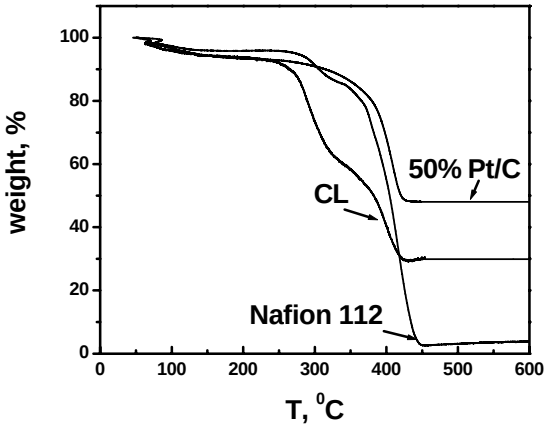

Figure 2. TGA (2.5^0/min) plots of 50% Pt/C, Nafion 112 and catalyst layer (CL) in air.

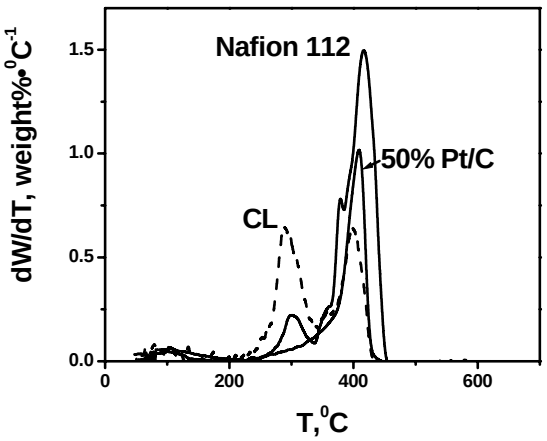

Figure 3. DTG (2.5^0/min) plots of 50% Pt/C, Nafion 112 and catalyst layer (CL) in air.

and 200°C, ~36% between 200°C and 350°C, and ~31% between 350°C and 425°C.

As the amounts of Nafion and carbon in the catalyst layer are 38% and 28% respectively, we assumed that the second region of the weight loss curve of the catalyst layer is related to Nafion decomposition and the third is due to carbon decomposition. This assumption was confirmed by the results of TGA-MS measurements.

Thus, presence of Pt in the carbon-supported catalyst layer lowers the temperature of Nafion decomposition by about 100^0C to 300^0C. Similar observation was made when thermal decomposition of Nafion in the presence of Pt catalysts was studied[5].

TGA-MS data will also be discussed as well as the potential application of TGA as an analytical tool to determine Pt concentration in catalyst coated membranes.

Conclusions

TGA was employed to characterize the thermal stability of Pt/C catalysts and PEM fuel cell catalyst layer in air. It was found that Pt/C catalysts decompose quantitatively in air to Pt at ~400°C. It was further determined that Pt/C catalyst decomposition is affected by Pt loading, as 50% Pt/C weight loss due to carbon oxidation becomes noticeable at 200 °C.

Pt facilitates decomposition of Nafion in PEM fuel cell catalyst layers; the thermal decomposition temperature of Nafion is lowered by about 100°C to 300°C in the presence of 50% Pt/C.

TGA may be useful as an analytical tool to determine Pt concentration in catalyst coated membranes.

Acknowledgement.. This work was supported by NASA's Space Science Office (Grant Numbers NAG5-12560 and NNC04GB13G) and the VCU School of Engineering Foundation.

References

(1) Baturina, O.A. and Wnek, G.E. *Electrochem. Solid-State Let.*, **2005**, *8 (6)*, 1.
(2) Kinoshita, K. and Bett, J.A.S. Carbon, **1973**, *11(4)*, 403.
(3) Roen, L.M.; Paik, C.H.; Jarvi, T.D. *Electrochem. Solid-State Let.*, **2004**, *7 (1)*, A19.
(4) Stevens, D.A.; Dahn, J.R. *Carbon*, **2005**, *43(1)*, 179
(5) Samms, S.R.; Wasmus, S.; Savinell R.F. *J. Electrochem.Soc.*, **1996**, *143(5)*, 1498.

PALLADIUM DEPOSITION ON PROTON EXCHANGE MEMBRANES FOR DIRECT METHANOL FUEL CELLS

H. Xu, H. R. Kunz*, J. M. Fenton***

*Department of Chemical Engineering
University of Connecticut
Storrs, CT 06269, USA

** Florida Solar Energy Center
University of Central Florida
Cocoa, FL 32922, USA

Introduction

Direct methanol fuel cells (DMFCs) have received attention for portable applications due to their high energy density and easy use of methanol. Unfortunately, the performance of DMFCs is still not satisfactory due to high methanol crossover despite considerable efforts to develop new membranes that are impermeable to methanol. The methanol that crosses over poisons the cathode catalyst and leads to a large loss in performance. One approach in developing new membranes is to introduce additives into Nafion® membranes to block the methanol. However, although these additives reduced the methanol crossover, they also decreased the conductivity of the membrane. Recently, Kim *et al* reported a palladized Nafion® membrane where palladium particles were deposited into the membrane via an ion-exchange and chemical reduction method[1]. The palladium significantly decreased the methanol crossover. Fortunately, since palladium is a pseudo-proton conductor[2], the conductivity of the membrane was not changed. This concept of making a barrier-layer membrane for DMFCs is very promising. However, the production of the membrane via ion-exchange and chemical reduction is quite complicated.

Experimental

Palladium (Alfa Aesar) was deposited onto Nafion® 117 and 112 membranes using a spraying technique. First, methanol and palladium were mixed; the mixture was then processed using an Omni® TH-115 homogenizer; the obtained palladium ink was then sprayed onto the membrane under nitrogen pressure. Composite membranes with different Pd thickness were prepared. The palladium-containing membranes were then characterized using Atomic Force Microscopy (AFM), X-ray Diffraction (XRD) and Scanning Electron Microscopy (SEM). Complete MEAs made by screen-printing ere tested for methanol crossover, membrane resistance and performance.

Results and Discussions

Figure 1 shows an AFM image of a Pd-deposited Nafion® 117 membrane. The thickness of the Pd films is 0.1μm at both the anode and the cathode. The image is of one side of the composite membrane from which numerous palladium particle protuberances stretch out of the Nafion® membrane plane. Palladium particles were successfully deposited onto the Nafion® membrane without any cracks.

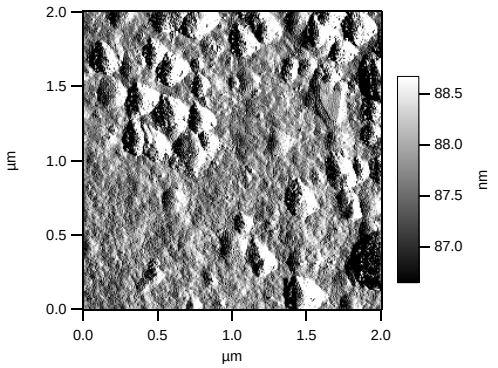

Figure 1. AFM Image of Pd-deposited Nafion® 117 Membrane

Figure 2 shows the methanol crossover current density for Nafion® 117 and Pd-deposited Nafion® 117 at two temperatures. The methanol concentration was 2M at the anode and nitrogen gas was supplied to the cathode. At 30°C, the methanol crossover was 70mA/cm^2 for the Nafion® 117 membrane; however, the crossover was reduced to 40mA/cm^2 for the Pd-deposited Nafion® 117 membrane at the same temperature. The effect of the Pd-deposited membrane on methanol crossover reduction is even more apparent at higher temperature. At 75°C, the crossover for the Pd-deposited membrane at 0.8V is 110mA/cm^2, which is much less than the 180 mA/cm^2 of Nafion® 117.

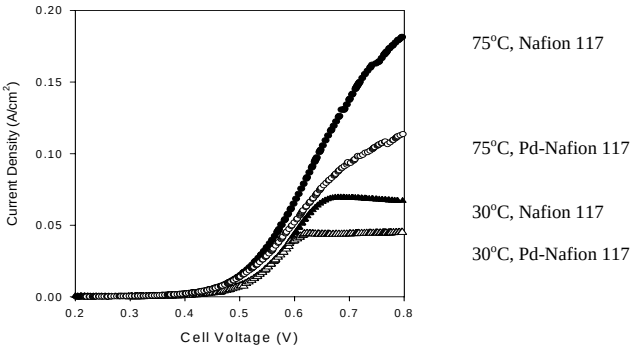

Figure 2. Methanol crossover for Nafion® 117 and Pd-deposited Nafion® 117 Membrane. Anode: 2 M meOH, flow rate: 5cc/min; cathode: N_2, 200cc/min, scan rate: 1mv/sec.

Figure 3 shows cell performance and resistance curves of two DMFCs, one based on the Nafion® 117 membrane, the other using Pd-deposited Nafion® 117. The resistances of the two cells are very close, around 0.25 Ohm-cm^2. This indicates that the deposition of Pd onto the Nafion® membrane does not change its resistance and therefore conductivity. However, the cell performance improved significantly by using the Pd-deposited Nafion® 117 membrane; the whole curve of Pd-deposited Nafion® 117 shifts up compared to the Nafion® 117 curve.

Obviously, the voltage gain with Pd-deposited Nafion® 117 membrane is due to reduced methanol crossover.

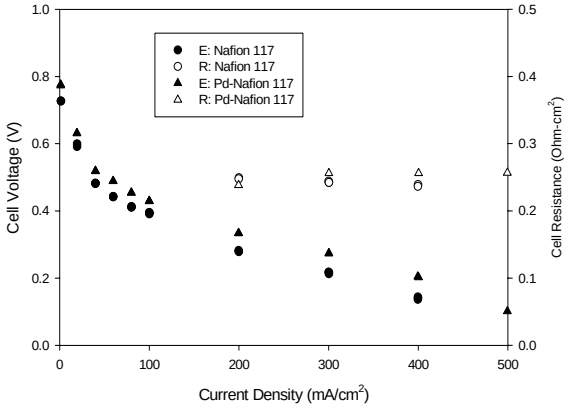

Figure 3. Cell performance and resistance for Nafion 117 and Pd-deposited Nafion 117 Membrane. Anode: 1 M meOH, flow rate: 5cc/min; cathode: air, 200cc/min.

Conclusions

Compared to un-coated membranes, palladium-coated Nafion® 117 membranes have reduced methanol crossover, but unchanged membrane conductivity, which results in an increase in cell performance. This work shows that there are promising applications of Pd-deposited proton exchange membranes for DMFCs. For further improvement of cell performance, the thickness of the palladium film needs to be optimized.

Acknowledgement. the financial support from the U. S. Army through the Connecticut Global Fuel Cell Center at the University of Connecticut is greatly appreciated.

References

1. Kim, Y. Jin, Choi, W. C., Woo, S. I, and Hong, W. H., *Electrochimica Acta*, **2004**, 49, 3227
2. E. S. Smotkin, WO02/11226 A2
3. Ye, X. R., Lin, Y. L., Wang, C., Engelhard, M. H., Wang, Y., and Wai, C. M., *J. of Mater. Chem*., **2004**, 14, 908

IN-SITU ELECTRON SPIN RESONANCE STUDY OF FUEL CELL POLYMER MEMBRANE DEGRADATION

Alexander Panchenko, Emil Roduner

University of Stuttgart, Germany

Introduction

The long term stability of the membrane is an important factor limiting the fuel cell lifetime. During extended use the membrane degrades, probably via reaction with hydroxyl and superoxide radicals which are regular intermediates of the oxygen reduction at the cathode. Only extremely stable membranes can withstand the aggressive chemical and physical environment in an operating fuel cell. Within a given set of operating conditions, intrinsic chemical and mechanical properties of the membrane as well as its water content impact its durability dramatically.

Here we present a novel method for monitoring radical formation and membrane degradation *in-situ* in a working fuel cell which is placed in the microwave resonator of an electron spin resonance (ESR) spectrometer. By introduction of a spin trap molecule at the cathode the formation of immobilized organic radicals on the membrane surface is observed, revealing the onset of oxidative degradation which is more pronounced for F-free membranes than for Nafion. At the anode, free radical intermediates of the fuel oxidation process are observed. No traces of degradation are detected at this side of the fuel cell.

Experimental

The *in-situ* fuel cell consists of two Teflon half-cylinders. Gas feeding channels inside each half-cylinder admit oxygen and hydrogen. The active part includes a Pt mesh as a spacer that allows gas distribution and at the same time provides electrical contact, and a Catalyst Coated Membrane (CCM, that is a membrane with Pt electrodes deposited on both sides) without any Nafion binder. The Pt loading corresponds to 0.77 mg*cm^{-2}. Nafion 115 and a F-free polyaryl-blend covalently cross-linked membrane were employed.

Results and Discussion

The concentration of *free* radicals produced in a fuel cell is extremely low and their lifetime is relatively short, so that it is not possible with conventional methods to observe them directly. We therefore employed the spin-trapping technique, using the spin trap molecules alpha-(4-pyridyl-1-oxide)-N-tert-butylnitrone (POBN) and 5,5-dimethyl-1-pyrroline 1-oxide (DMPO). It allows the trapping of short-lived radicals under formation of relatively stable nitroxide radicals (the spin adducts) which are detectable by ESR The spin trap solution is applied separately at the anode or the cathode side, permitting selective investigation of radical formation and of degradation reactions.

After five minutes of operation with 10 µL of 1 M aqueous solution of POBN at the anode side the POBN-•H adduct is detected (Fig. 1a). The spectrum is characterized by a g-factor that is typical for POBN radical adducts, and it consists of a triplet of triplets due to 1:1:1 and 1:2:1 splittings by one ^{14}N and by two equivalent ^{1}H nuclei, respectively. The result does not depend on the nature of the membrane.

The mechanism of formal H atom addition to the spin trap molecule is studied further in the following set of experiments: the fuel cell is fed with H_2 or D_2, and the POBN solution is applied. Both results in the spectrum shown in Fig. 1a. No influence of D_2 was observed. Then, the two experiments are repeated, but now using a heavy water solution of the spin trap. As a result the formal D adduct to POBN was observed, as revealed by the additional splitting (Fig. 1b). This is evidence of a mechanism involving reduction of POBN at the electrode surface followed by protonation by solvent molecules, H_2O or D_2O:

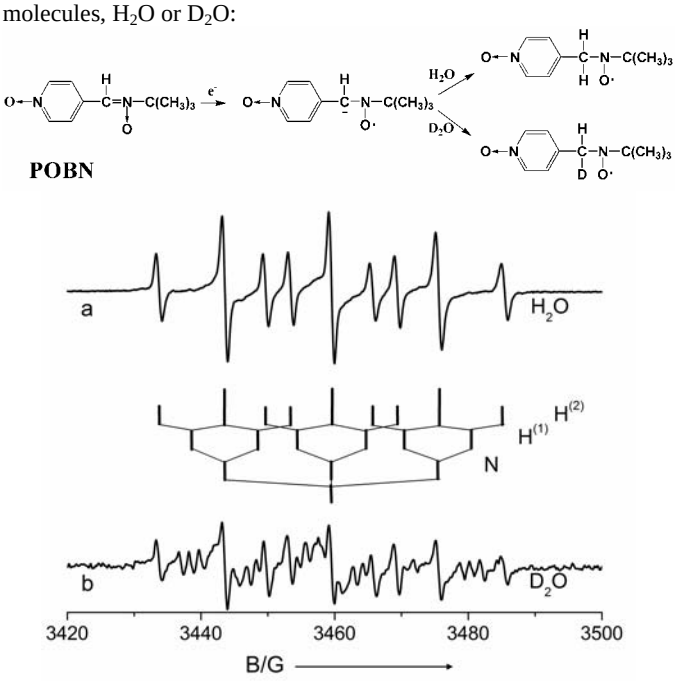

Figure 1. ESR spectrum obtained with an aqueous POBN solution at the anode side of the in-situ fuel cell. **a)** H_2O as solvent for the spin trap. **b)** D_2O as solvent for the spin trap. This spectrum represents a superposition of the D adduct and, from residual protons, the H adduct.

An analogous experiment was also performed with an aqueous DMPO solution at the cathode of the CCM based on a Nafion membrane. Fig. 2, recorded after five minutes of closed circuit operation, depicts the characteristic spectrum corresponding to the DMPO•OH adduct where the single proton coupling happens to be of the the same magnitude as the nitrogen coupling. Observation of this spectrum is quite remarkable, as it proves that •OH radicals are indeed formed at the cathode.

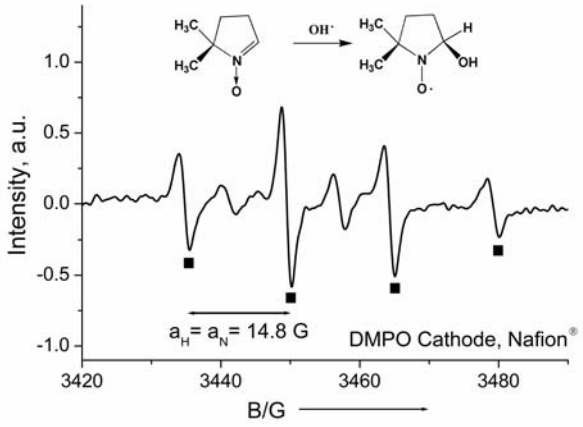

Figure 2. ESR spectrum obtained with DMPO water solution at the cathode side of the in-situ fuel cell. Lines marked with squares belong to the DMPO-•OH adduct. a_N and in particular a_H are quite different for adducts of organic radicals.

When the same experiment is performed with a F-free polyaryl-blend membrane •OH is not normally observed. Instead, a different signal with much broader lines builds up (not shown). The large line width is indicative of incomplete averaging of hyperfine anisotropy, and we conclude that the reduced mobility of the spin trap adduct must be due to the fact that the species is bound to the membrane. This means that we have trapped a radical defect on the membrane, originating from the reaction of •OH with the aromatic constituents, whereas Nafion because of its higher inertness leaves the spin trap sufficient time to trap •OH.

Conclusions

In summary, we have developed a method for the direct investigation of radical processes in a running fuel cell. We observed intermediates of the anode reaction when hydrogen was used as a fuel. Furthermore, evidence is provided for radical centers produced at the cathode side of the polymer membrane as a likely intermediate of oxidative degradation via free radical processes. The method opens numerous possibilities for more quantitative studies of membrane degradation, mechanisms of oxygen reduction, and fuel oxidation. Systematic studies as a function of current and voltage, temperature, gas pressure, and membrane humidity are expected to reveal what the critical operating parameters are which lead to membrane degradation in a fuel cell.

Acknowledgement. We thank J. Kerres and his group from the University of Stuttgart and T. Kaz from the German Aerospace Center for providing us with CCMs. Financial support by the Federal Ministry of Education and Research (BMBF), Germany, and the Graduate College “Advanced Magnetic Resonance Type Methods in Materials Science” is gratefully acknowledged.

References

(1) Panchenko, A.; Dilger, H.; Kerres, J.; Hein, M.; Ullrich, A.; Kaz, T.; and Roduner, E. *Phys. Chem. Chem. Phys.* **2004**, *6*, 2891.

MAGNETIC RESONANCE IMAGING (MRI): A NEW TOOL FOR FUEL CELL RESEARCH

Su Ha, Zachary Dunbar, and Rich Masel

School of Chemical Sciences
University of Illinois at Urbana-Champaign
600 S Mathews, Urbana Il, 61801

Introduction

The Direct Formic Acid Fuel Cell (DFAFC) is a promising candidate for portable power applications owing to its high energy efficiency and high power density.[1-3] During the DFAFC operation, formic acid is oxidized at the anode electrode producing electrons, protons, and carbon dioxide (CO_2). These protons are transported from the anode to the cathode through the polymer electrolyte membrane (PEM), and then combine with oxygen and the electrons to produce water at the cathode electrode. Additional water is moved from the anode to the cathode by both a molecular diffusion and an electro-osmotic drag processes. The excess water in the cathode is either evaporated or diffused back to the anode.

The proton conductivity of PEM and thus performance of the DFAFC decreases dramatically when the water content of the membrane decreases.[4-6] Therefore, to operate the cell with a high performance, a proper water management to maintain the membrane hydrated is so important. On the other hand, too much water in the cathode would cause the water flooding and limit the oxygen transport to the cathode electrode.[4-6]

Having a proper fuel (formic acid) distribution at the DFAFC's anode is another important aspect for achieving a good cell performance. CO_2 bubbles are generated as formic acid is oxidized at the anode electrode. This CO_2 evolution in the liquid feed anode of the DFAFC results in strongly two-phase flow, making the transport processes of fuel supply and product removal more complicated. If the CO_2 bubbles are not properly removed from the anode, they will block the catalyst sites from oxidizing formic acid and create a large pressure drop across the flow channels.[7,8]

Understanding both the water and fuel transport processes in DFAFC under the operating conditions is essential for developing its advanced fuel cell materials and designs. In this paper, we describe a novel method of using MRI technology for measuring both the water and fuel distributions at the cathode and anode of the operating DFAFC respectively. Additionally, we correlate the time dependant performance of the DFAFC with time-resolved MRI measurements of the water content in the cathode electrode.

Experimental

Construction of Test Fuel Cell. The MRI system generates strong magnetic fields. To prevent any distortions of these strong magnetic fields, we built a test fuel cell from nonmagnetic materials as it is shown in Figure 1. Both the anode and cathode current collectors were constructed out of titanium foil. In order to protect the titanium from being corroded by the formic acid solutions, they were electrochemically coated with 5 microns of gold. Both the anode and cathode flowfields have serpentine flow channels. The membrane electrode assembly (MEA) was fabricated in house using a 'direct paint' technique with the active area of 1 cm^2. The 'catalyst inks' were prepared by dispersing the catalyst powders into appropriate amounts of Millipore water and 5% recast Nafion® solution (1100EW, Solution Technology, Inc.). Then both the anode and cathode 'catalyst inks' were directly painted onto either side of the Nafion® 115 membrane. A commercially available platinum black (HiSPEC™ 1000 from Johnson Matthey) was used for the cathode catalyst layer at a loading of 8 mg/cm^2.

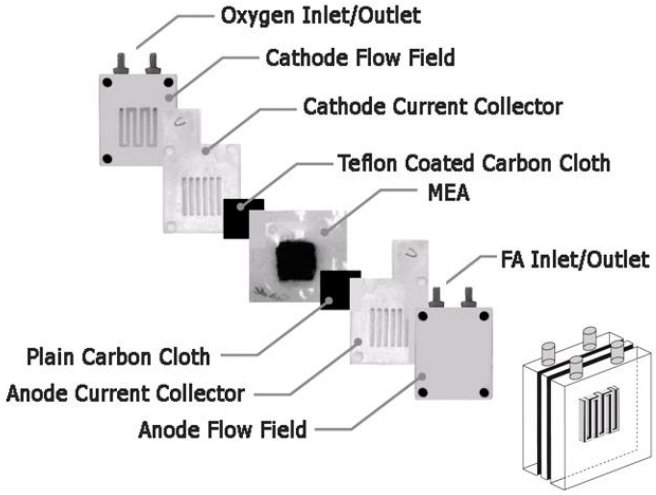

Figure 1. The Direct Formic Acid Fuel Cell Diagram

Palladium black from Sigma Aldrich was used for the anode catalyst layer at a loading of 6 mg/cm^2. The final catalyst layers contained 15% Nafion® by weight.

MRI Test System. To acquire MRI images of water and fuel contents in the operating DFAFC, we placed the cell in the cylindrical test section of our MRI system (14.7 T). The experimental setup is shown in Figure 2. Oxygen was supplied to the cathode of the DFAFC from a compressed gas tank. 5M Formic acid was supplied to the anode using a syringe pump. The experiments were performed using a Varian Unity/Inova NMR spectrometer with a 600MHz wide-bore (89mm) magnet (Oxford Instruments). The system is equipped with gradients with a maximum strength of 90 Gauss/cm. The nucleus observed in our MRI experiment was hydrogen atom (^1H). The experiments were performed at room temperature. The cell current was controlled by adjusting the external load resistance connected to the cell. The data was acquired and processed using VNMRJ 1.1C software.

A pulse sequence with a conventional spin-echo method was used to obtain images of water and fuel contents at the cathode and anode of the DFAFC respectively. For our experiments, a 128 x 128 point matrix was formed to image the field of view (FOV) of 1.4 cm x 1.2 cm. A slice thickness was 0.5 mm.

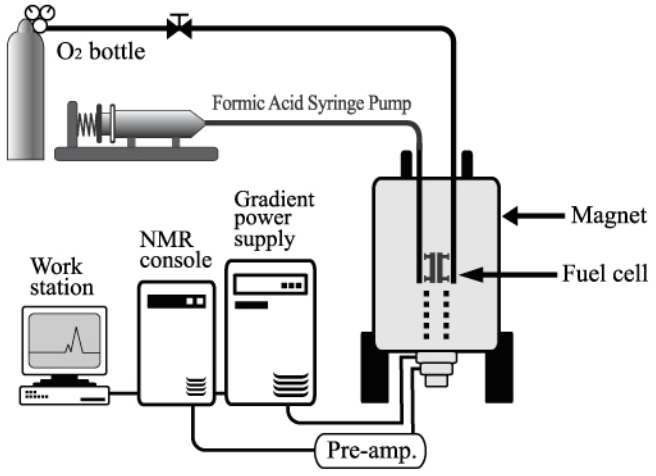

Figure 2. The MRI experimental Setup for Active Direct Formic Acid Fuel Cell Testing

Results and Discussion

In Figure 3, a constant voltage test of the DFAFC is reported at 0.70 V. According to Figure 3, the DFAFC initially generates the current density of 53 mA/cm^2 at 0.70 V. However, its current density gradually decreases as its operation time increases. After operating the cell for 135 minutes, its current density drops from 53 to 36 mA/cm^2.

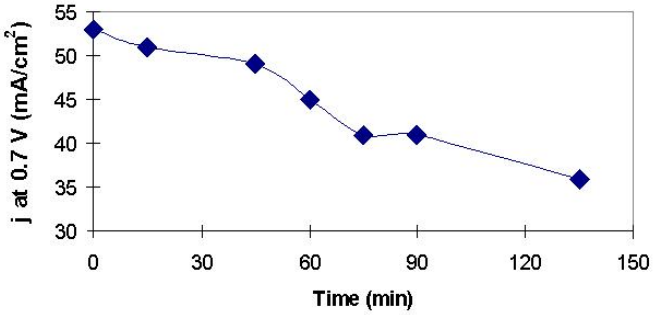

Figure 3. Plot of constant cell potential test at 0.70 V. The DFAFC was operated using 5M formic acid and oxygen with the applied magnetic field inside the MRI system.

Figure 4 shows the MRI image of the anode flowfield after operating the DFAFC with 5M formic acid for 135 minutes. In Figure 4, the bright image represents the 5M formic acid, which is flowing through the anode flow channels at a flow rate of 50 micro liter per minute. These anode flow channels are oriented vertically (up and down). According to Figure 4, the bottom part of the anode flow channels has more fuel (higher NMR signal which gives brighter image), while the upper part of the flowfield has less fuel (lower NMR signal which gives darker image). This would be explained in terms of CO_2 formation and orientation of the anode flow channels. As the formic acid is oxidized at the anode, CO_2 bubbles are formed which would rise up through the flow channels. Consequently, these CO_2 bubbles are accumulated in the upper part of the anode flow channels and occupy most of its volume. Since CO_2 has no hydrogen atom, there would be a weaker NMR signal to image from the flowfield area with partially filled CO_2.

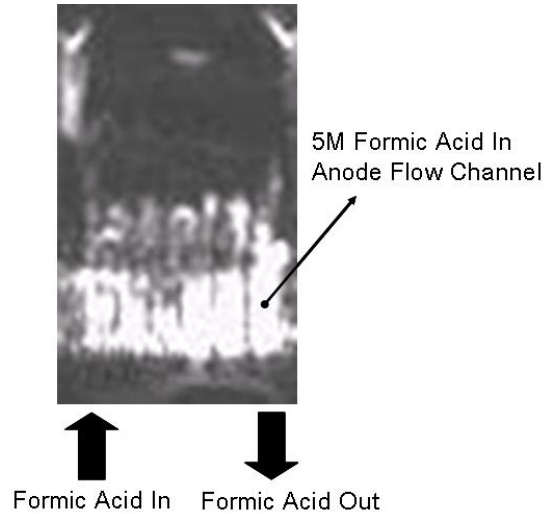

Figure 4. The MRI image of 5M formic acid flowing through the anode flow channels after operating the cell for 135 min.

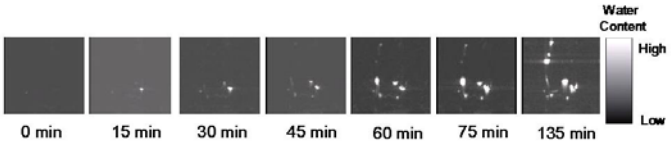

Figure 5. The MRI images of the water distribution in the cathode electrode after the DFAFC starts to operate at 0 min.

To investigate if there is any water flooding in the cathode of the operating DFAFC, we measured the MRI images of the water content in the cathode electrode of the operating cell in every 15 minutes (Figure 5). From Figure 5, at zero minute, no water is observed at the cathode electrode. According to Figure 5, as the cell operation time increases, the number of the water flooded spot also increases at the cathode electrode. Figure 5 shows that sizes of these water flooded spots also grow and shrink as the cell operation time increases. According to Figure 5, the cathode electrode of the DFAFC is severally flooded by water after operating it for 135 minutes. Comparing Figures 3, 4, and 5, we speculate that both CO_2 bubble accumulation at the anode and the water flooding at the cathode are two main causes of the current density drop of the DFAFC that we observe in Figure 4.

Acknowledgement

This material is based upon work supported by the Defense Advanced Research Projects Agency under U.S. Air Force grant F33615-01-C-2172.

References

(1) Ha, S.; Adams, B.; Masel, R. Journal of Power Sources, **2004**, 128 (2), 119.
(2) Zhu, Yimin; Ha, Su Y.; Masel, Richard I. Journal of Power Sources, **2004**, 130 (1-2), 8.
(3) Rice, C.; Ha, S.; Masel, R. I.; Wieckowski, A. Journal of Power Sources (2003), 115(2), 229-235.
(4) Berg, P.; Promislow, K.; St. Pierre, J.; Stumper, J.; Wetton, B. Journal of the Electrochemical Society, **2004**, 151 (3), A341.
(5) Larminie, J.; Dicks, A. Fuel Cell Systems Explained, John Wiley & Sons, Ltd., 2000.
(6) Rice, C.; Ha, S.; Masel, R. I.; Waszczuk, P.; Wieckowski, A.; Barnard, Tom, Journal of Power Sources, **2002**, 111 (1), 83.
(7) Barragan, V.M. Ruiz-Bauza, C.; Villauenga, J.P.G.; Seoane, B. Journal of Power Sources, **2004**, 130 (1-2), 22.
(8) Yang, H.; Zhao, T.S. Journal of Power Sources, **2005**, 139 (1-2), 79.

FUEL CELL DESIGN: THE IMPACT OF FUEL CELL DYNAMICS ON OPERATION

Warren H. J. Hogarth[1, 2] James P. Nehlsen[1], and Jay B. Benziger[1]

[1]Department of Chemical Engineering, Princeton University, Princeton, NJ 08544, USA
[2]ARC Centre for Functional Nanomaterials, The University of Queensland, Brisbane 4072, Australia

Introduction

Proton exchange membrane fuel cells are a very promising clean energy technology with the potential to help reduce harmful environmental and health pollution emissions. The main reasons that they show so much potential is that they have higher energy densities than batteries and can operate more efficiently than combustion engines which are limited by Carnot efficiency. It is therefore important, at least in the short term where energy will most likely still be derived from hydrocarbon sources, to ensure that the cells are capable of operating as close as possible to their highest efficiency to realize these benefits.

However, there are few reports in the literature which consider what is the optimal operating regime for a fuel cell.[1-3] While there is presently a significant focus on the design on new materials for fuel cells,[4,5] it is important to understand what is the optimal operation range in terms of power to be delivered, load being driven, current, voltage and efficiency, to best determine the benchmarks to be used.[6,7]

Experimental

Short term current-voltage data was obtained on both a fuel cell and a battery. The battery was a single cell, size AAA, nickel-metal hydride rechargeable battery (Radio Shack) rated at 1.2 V and 700 mAh. I-V data on the battery was obtained using an Arbin Instruments MSTAT4+ battery test station.

The fuel cell was a 5 cm^2 cell using Nafion 115 (Ion Power, Inc.) with two Pt catalyzed ELAT-style electrodes from E-tek (E-tek division of DeNora, Somerset, NJ). The fuel cell was operated with H_2 and O_2, 1 atm of pressure, at 80ºC, with both gas streams humidified to saturation at the cell temperature. The fuel cell I-V data was obtained on a Globetech fuel cell test station.

Results

Current-voltage data for both types of cells is shown in Figure 1. The data for the fuel cell is plotted versus total current rather than the more traditional current density in order to compare it to the battery data. The cell area is 5 cm^2. The internal resistance, R_{int}, of each cell is given by the slope of the voltage versus current line. R_{int} represents the overall cell resistance and is the value that would be used for the resistor when representing the fuel cell or battery as a battery and a resistor in series in a circuit diagram (Figure 2).[6,7] For the fuel cell, the linear "ohmic region" is used for this determination. The internal resistance of the battery is 0.096 Ω, and the fuel cell is 0.085 Ω.

When considering a battery and resistor in series as part of an electrical circuit, the internal resistance, R_{int}, of the fuel cell varies with the area of the cell. The value of $R_{int} \cdot A_{cell}$ is constant with area, but varies with the state of hydration of the membrane and the quality of the electrode-membrane interfaces. Reducing R_{int} by increasing the fuel cell area is equivalent to reducing the internal resistance of the battery by placing several batteries in parallel. The resistance values add for either fuel cells or batteries in series. Using the above values of R_{int} shows that 4.8 cm^2 of fuel cell area has the same internal resistance as the AAA sized battery used in this study.

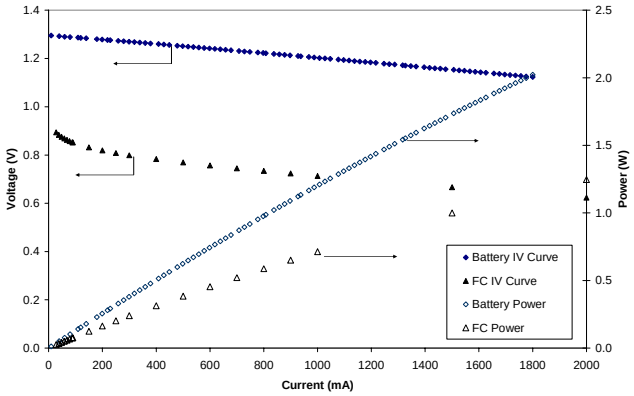

Figure 1. Current-Voltage data for both a standard H_2/O_2 PEMFC with humidified feeds, at 80ºC and 5 cm^2 area and a standard AAA nickel-metal hydride rechargeable battery.

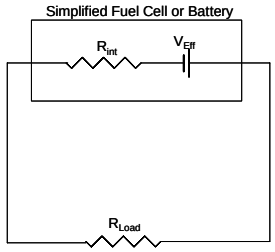

Figure 2. Equivalent circuit diagrams for a PEMFC or battery directly connected to an external load.

Figure 3 shows the same data plotted as a power performance curve (PPC), or power output as a function of load resistance. The load resistance, R_{load}, is equal to V_{load}/I. The efficiency shown on the secondary axis is the discharge efficiency, defined as V_{load}/V_{oc}, where V_{oc} is the open circuit potential of the cell. This efficiency value shows the power obtained from the cell divided by the power that could be obtained if there were no internal voltage losses. The efficiency of the fuel cell will always be less than a battery with identical internal resistance due to the initial voltage drop in the activation region.

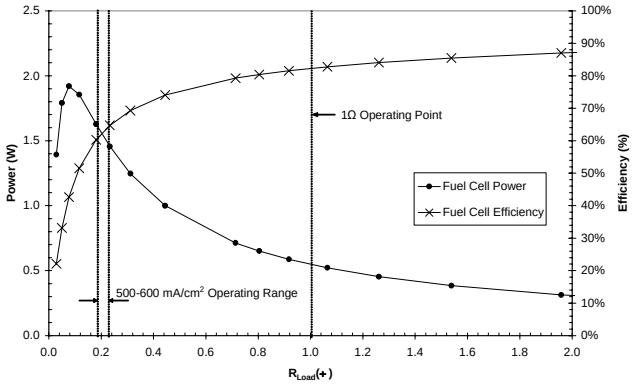

Figure 3. Detail of the PEMFC power performance curve (PPC) and efficiency curve. Highlighted are the 500 and 600 mA cm^{-2} and 1Ω operating points.

Discussion

A fuel cell is typically controlled by altering the load impedance. The load impedance can be manipulated in order to hold one of the dependent variables (current, voltage, or power) constant at a set point. In many laboratory situations, either current or voltage output from a fuel cell is controlled. Controlling one of these variables is not desirable in real applications however. By controlling either voltage or current, all of the degrees of freedom in the system are used, and the third variable, power, cannot then be controlled independently. Since the power output by the fuel cell and the power consumed by the load must balance exactly at all times (conservation of energy), the ability to regulate power output is vital. Therefore, both current and voltage must not be specified, leaving load resistance as the independent variable and power as the dependent variable. Controlling the load resistance and power in this way creates issues not normally observed under potentiostatic or galvanostatic control.

The main control problem is created because there is a peak in the PPC. If the peak is crossed while the cell is controlled, the necessary control action reverses. For a controller to be direct acting, it must operate to the left of the power peak in Figure 3. This will allow for more power to be provided as the load resistance increases (e.g. accelerating a motor). If the peak is crossed however, the controller will continue to increase the load resistance in response to the demand for more power but the cell is not capable of providing more power.

To operate at maximum efficiency, a fuel cell must be operated to the right of the power peak (Figure 3). In this case care must be taken not to cross back over the power peak when operating the cell near maximum power.

Fuel cell dynamics compound control problems. The peak in the power performance curve occurs when the load resistance equals the internal resistance of the cell. Unlike batteries, the internal resistance of fuel cells varies with the state of hydration of the membrane. As the load conditions change, more or less water is generated as the current increases or decreases. The state of hydration of the membrane can vary as the rate of water generation changes, and so the internal resistance of the fuel cell can vary during operation, particularly in less-than-saturated humidity conditions (Figure 4).

The minimum allowable load resistance therefore will change during operation. Using a current limiter to prevent the controller from crossing the peak would require the limit to be placed a safe distance from the peak to account for any drying of the membrane during operation, significantly reducing the maximum power output of the fuel cell.

Conventional fuel cell operating specifications do not seem to consider the need to control the power output from a fuel cell. Figures 3 and 4 show the relevant portions of the fuel cell data from Figures 1. A common design specification calls for operation at 500-600 $mA.cm^{-2}$, placing the operating point in the center of the linear ohmic region of the I-V curve. This operating point appears to be an obvious choice, providing the widest range of linear I-V behavior. However, conservation of energy requires that we instead consider the power output as the primary variable when designing a fuel cell to drive a load, and the power output is highly non-linear and non-monotonic in this region of the curve. The load resistance on this cell (or, equivalently, the internal resistance of the cell) needs only to change by 0.15 Ω to reach the peak.

Adding cells in series increases the necessary change in the load resistance to reach the peak, but increasing the area of the cells decreases it. Based on the single cell performance obtained here, a stack of 200 cells, with each cell of area 500 cm^2 and operating at 500 $mA.cm^{-2}$ could drive a load of 29 kW but would only require a load change of 0.31 Ω to cross the peak.

A better approach is to operate the stack at a much lower current density, away from the peak. Although this technique limits the power output from the stack, control is much simpler and efficiency is higher. The power output is also more linear at lower current densities (higher load resistances). This approach is often used for batteries, where the current drawn from each battery is kept relatively low compared to the location of the peak in the power performance curve for the battery. Perhaps a better option still is to use a hybrid system in which the fuel cell is used at a constant operating condition to charge a battery pack.

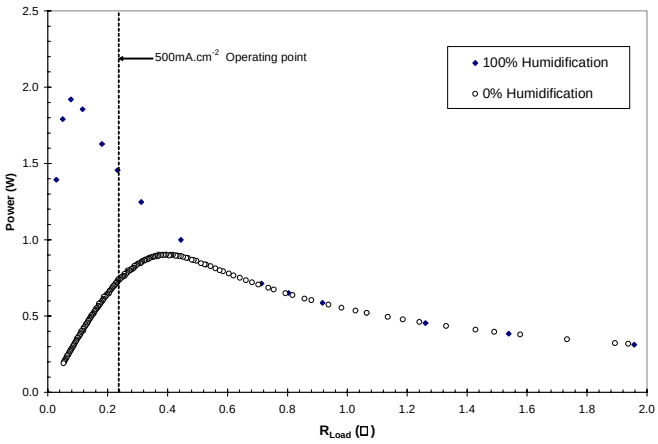

Figure 4. Basic power performance curve of PEMFCs operating under full humidification and no external humidification at 80°C.

Conclusions

Fuel cells are sensitive dynamic systems. Their dynamics and performance characteristics must be considered when designing cells, stacks, and control systems. Design specifications offered as guidelines do not reflect the operating regimes necessary to create stable, controllable fuel cell systems. Typical specifications select an operating point with linear current-voltage characteristics, but highly non-linear power output. When driving a load, power output must be regulated tightly. Current and voltage can be adjusted with transformers. Operating at lower current densities, perhaps closer to 100-200 $mA.cm^{-2}$, provides higher efficiency and more linear power output from fuel cells.

Acknowledgement. The authors would like to thank Jonathan Mann for conducting the fuel cell testing experiment. WH acknowledges funding from the Australian-American Fulbright Commission and the ARC Centre for Functional Nanomaterials. This work was supported in part by the Air Force Office of Scientific Research (Dynamics and Control).

References

(1) Arita, M., *Fuel Cells* **2002,** *2* (1), 10.
(2) Masten, D. A.; Bosco, A. D. In *Handbook of Fuel Cells;* Vielstich, W.; Lamb, A.; Gasteiger, H. Eds.; Wiley: Indianapolis, 2003; pp.714-724.
(3) Konrad, G.; Sommer, M.; Loschko, B.; Schell, A.; Docter, A. In *Handbook of Fuel Cells;* Vielstich, W.; Lamb, A.; Gasteiger, H. Eds.; Wiley: Indianapolis, 2003; pp.693-713.
(4) Hogarth, W. H. J.; Diniz da Costa, J. C.; Lu, G. Q., *Journal of Power Sources* **2005,** *142* (1-2), 223.
(5) Hogarth, W. H. J.; Diniz da Costa, J. C.; Drennan, J.; Lu, G. Q. M., *J. Mater. Chem.* **2005,** *15* (7), 754.
(6) Benziger, J. B.; Satterfield, M. B.; Hogarth, W. H. J.; Nehlsen, J. P.; Kevrekidis, I., *Submitted to Journal of Power Sources* **2005**.
(7) Hogarth, W. H. J.; Nehlsen, J. P.; Benziger, J. B., *Submitted to AIChE Journal* **2005**.

HIGH PERFORMANCE DRY FEED HYDROGEN PEMFCS: UNDERSTANDING THE WATER BALANCE AS A DESIGN TOOL FOR NOVEL POLYMER MEMBRANES

Warren H.J. Hogarth[1,2], Jay B. Benziger[1]

[1] Department of Chemical Engineering, Princeton University, Princeton, NJ 08544, USA
[2]ARC Centre for Functional Nanomaterials, University of Queensland, Brisbane 4072, AUSTRALIA

Introduction

Designing and operating an efficient fuel cell which has very tight control over the water inventory of the cell, is a very powerful tool for designing new fuel cell membranes and fuel cell modeling. In addition it is a simpler, commercially viable alternative to current fuel cell technology.

The water balance in PEMs is the most influential factor on proton conduction and hence on optimizing the operation of PEM fuel cells.[1] The proton conductivity of PEM membranes varies by orders of magnitudes as the water activity (relative humidity) varies at the cathode and anode (as the hydration level of the membrane varies). For this reason PEMFCs are almost always operated with close to 100% relative humidity feeds, restricting their operating regions and preventing a clear delineation of water migration within the cell.

Adding extra water to a fuel cell creates problems with flooding. Both commercial and laboratory operated fuel cells have significant performance limitations at high currents caused by an inability to remove all the water added and created within the fuel cell. This flooding phenomenon prevents oxygen and hydrogen reaching the catalyst and hence the fuel cell is starved of fuel. This excess water also prevents scientists from understanding how new membranes are affected by and affect the water balance in the fuel cell and provides great challenges for modeling fuel cells.

By stripping away the complexity of having multiple water sources in a fuel cell, it is possible to get a significantly more detailed understanding of how a PEMFC is working from a fundamental level. This can be done by operating a fuel cell with dry feeds and monitoring the exit concentrations or water (relative humidity) of the effluent streams. This creates what is termed an Autohumidified fuel cell. The design used in this analysis is a continuous stirred tank reactor (CSTR) design which ensures uniform concentration of the reactants at anode and cathode.[2-4] Based on this simple analysis, it is possible to observe the effects of flow rates, temperature and pressure on the membrane, electrode and gas diffusion coefficients and the general operation of the fuel cell. This not only provides valuable information for the design of a fuel cell, but also, important information which can be used for evaluating key properties of new fuel cell membranes.

While traditionally people have hesitated with the autohumidified approach because of issues associated with drying the membrane, we demonstrate the power of this technique by designing a new fuel cell which runs on completely dry feeds and is capable of operating as well as commercial fuel cell test cells with fully humidified streams at the same operating conditions. Concurrently we have significantly reduced the onset of flooding. Furthermore the new fuel cell is used for fundamental analysis and design of new fuel cell membranes.

Experimental

CSTR fuel cell experiments were conducted on a custom designed in-house cell to ensure that the gas composition was uniform within the cell and that the liquid water produced within the cell would drain from the cell preventing flooding (Figure 1). The cell temperature and pressure were tightly controlled and monitored. Relative humidity sensors with temperature probes were placed in the exit gas streams of both the anode and cathode. The cell area was 1.9cm^2. Control experiments were run on a commercial Globetech fuel cell test station with 5cm^2 area and serpentine flow channels.

Commercial Extruded Nafion® 1100 weight membranes and 5wt% Nafion solution were obtained from Ion Power, Inc. (Bear, DE). Composite membranes were cast with 3wt% composite TiO_2 with an average particle size of 20nm from Degussa-Hüls. All membranes were cleaned with a peroxide, water and sulfuric acid procedure prior to pressing into an MEA. A6 ELAT electrodes with 5wt% platinum on carbon were used for electrodes (E-tek division of DeNora, Somerset, NJ). MEAs were pressed at 140^{0}C for 90 seconds with 1 metric tonne over a constant area.

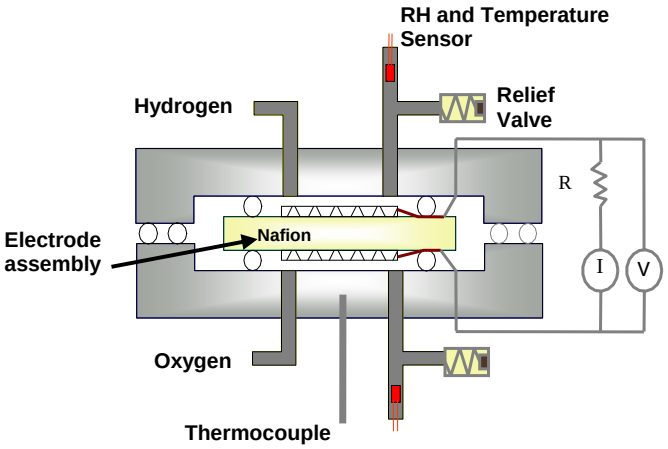

Figure 1. Schematic of custom autohumidified CSTR fuel cell setup which allows tight control of the water balance within the fuel cell and excellent performance with dry feed streams.[2]

Results and Discussion

Performance of Autohumidified CSTR Fuel Cell. If a fuel cell is limited by flooding then it would appear counter intuitive to be continually adding excess water in the feed streams. Figure 2 and 3 show that, through clever design, it is possible to operate a fuel cell equally as well as commercially available fully humidified cells under the same operating conditions by controlling the water balance in the fuel cell.

Figure 2 demonstrates that the polarization curves for the autohumidified CSTR fuel cell overlay those of the same membrane in a commercial Globetech fuel cell with serpentine flow channels. In addition, as can be seen by the CSTR 95^{0}C curve there are fewer limitations caused by mass transport at high current which is attributed to flooding of the fuel cell. Figure 3 displays the power performance curves for the same tests as Figure 2.[5, 6] This demonstrates that the internal resistances of the fuel cells are all equal as the internal resistance occurs at peak power which is essentially the same for all cells.

CSTR FC for fundamental fuel cell understanding. The autohumidified CSTR fuel cell is a powerful tool for design and assessment of new fuel cell membranes and for fuel cell modeling.[4, 7] By limiting the water generation in the fuel cell to the reaction and having uniform concentrations of both reactants and products in the cell it is possible to evaluate the performance of and hence design new membranes.

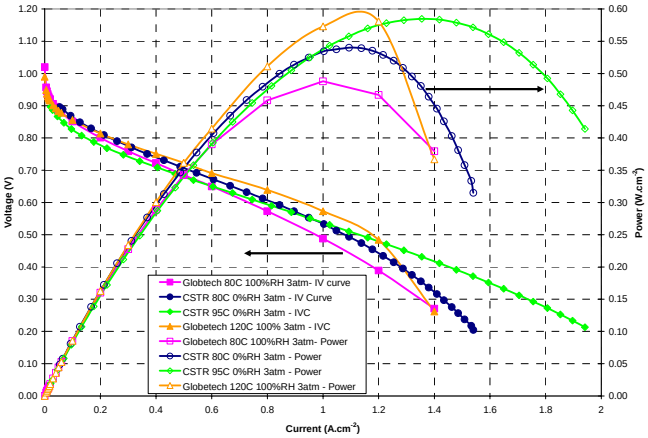

Figure 2. Polarization curves of the autohumidified CSTR and commercial Globetech fuel cells using standard operating conditions (shown) and Nafion 115.

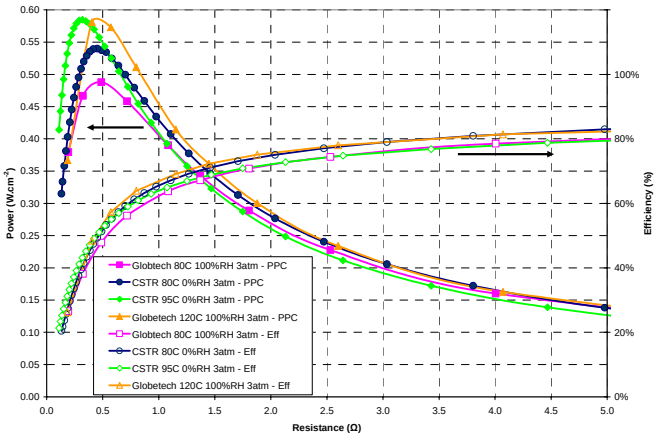

Figure 3. Power performance curves (PPC) of the autohumidified CSTR and commercial Globetech fuel cells using standard operating conditions (shown) and Nafion 115.

For example, by monitoring the relative humidities of the effluent streams it is possible to observe changes in the water content in the membrane and make inferences regarding the back diffusion of water. This can then be directly correlated to changes in the level of hydration within the membrane and hence conductivity. Careful monitoring of the relative humidity when the cell is subject to step changes in load and reactant flow rates also allows for comparison of the diffusion rates through the membrane. Additional data regarding the membrane hydration can be gather simultaneously be using a current interrupt method to monitor the internal resistance of the membrane.

As an example of how this approach can be used consider Figure 4. A recast composite 3 wt% TiO_2 Nafion 115 membrane was at 80^0C was subject to a series of step changes in the external load and the dynamic response of the system was measured as it returned to steady state. The recorded variables were: current, voltage, internal resistance of the membrane (as measured using a current interrupt technique), RH anode and RH cathode. Figure 4 shows that the response of the system and that the hydration of the membrane is not constant reinforcing the complex role that system dynamics play and membrane properties have on fuel cell performance.

This dynamic information can then be taken and used to compare different membranes, membrane materials and MEA setups to optimize material and fuel cell design. In addition it provides valuable information, necessary for the control and dynamic operation of fuel cells.

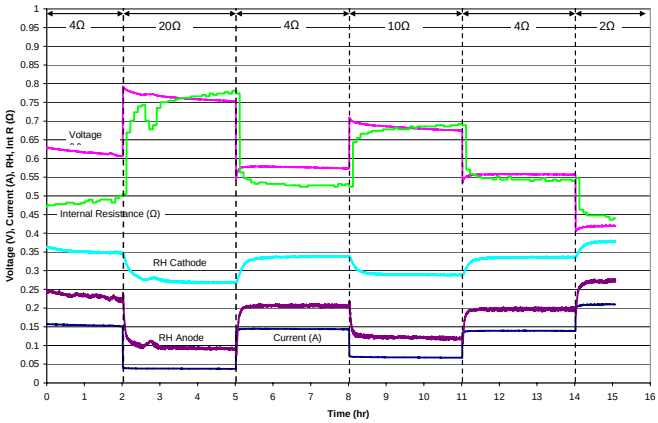

Figure 4. Steady state response of a composite polymer membrane in an autohumidified CSTR fuel cell to step changes in external load, displaying the response time of the fuel cell under dynamic operation.

Conclusions

The CSTR membrane fuel cell is capable of operating equally as well as commercially available fully humidified cells. Removing the complexity of adding water into a fuel cell and using simple fuel cell design significantly reduces issues associated with fuel cell flooding and allows for full accounting of the water balance within the cell. This allows important properties such as membrane diffusion coefficient to be derived which are not only important in the assessment of new membrane technology, but also are also important in developing robust fuel cell models.

Acknowledgement. The authors thank the National Science Foundation (CTS– 0354279 and DMR-0213707 through the Materials Research and Science Engineering Center at Princeton) and Tao Zhang for assistance with fuel cell testing. WH acknowledges funding from the Australian-American Fulbright Commission and the ARC Centre for Functional Nanomaterials.

References

(1) Yang, C.; Srinivasan, S.; Bocarsly, A. B.; Tulyani, S.; Benziger, J. B., *J. Membr. Sci.* **2004,** *237* (1-2), 145.
(2) Benziger, J.; Chia, E.; Karnas, E.; Moxley, J.; Teuscher, C.; Kevrekidis, I. G., *AIChE J.* **2004,** *50* (8), 1889.
(3) Benziger, J.; Chia, E.; Moxley, J. F.; Kevrekidis, I. G., *Chem. Eng. Sci.* **2005,** *60* (6), 1743.
(4) Moxley, J. F.; Tulyani, S.; Benziger, J. B., *Chem. Eng. Sci.* **2003,** *58* (20), 4705.
(5) Hogarth, W. H. J.; Nehlsen, J. P.; Benziger, J. B., *Submitted to AIChE Journal* **2005**.
(6) Benziger, J. B.; Satterfield, M. B.; Hogarth, W. H. J.; Nehlsen, J. P.; Kevrekidis, I., *Submitted to Journal of Power Sources* **2005**.
(7) Chia, E.; Benziger, J.; Kevrekidis, I. G., *AIChE J.* **2004,** *50* (9), 2320.

CHEMICAL DURABILITY STUDIES OF PFSA POLYMERS AND MODEL COMPOUNDS UNDER MIMIC FUEL CELL CONDITION

David A. Schiraldi,[1*] *Chun Zhou*[1], *Thomas A. Zawodzinski Jr.*[2]

1. Case Western Reserve University, Department of Macromolecular Science and Engineering Cleveland, OH 44106, 2. Case Western Reserve University,Case Applied Power Institute & Department of Chemical Engineering,Cleveland, OH 44106

Introduction

Fuel cell technology has emerged as a promising platform from which to deliver future energy needs, directly converting the chemical oxidation of hydrogen or methanol to electricity. In the case of hydrogen fuel cells, Perfluorosulfonic acid (PFSA) polymers currently represent the leading candidates for use in proton exchange membranes, because of their high ionic conductivity and good mechanical, thermal and chemical stabilities. The chemical durability of these polymers is a critical issue for successful fuel cell applications and therefore has received a great deal of attention. Previous studies of membrane durability are both confusing and contradictory, suggesting radical attack at main chain carboxylate groups, tertiary C-F bonds in the main chain, and at side chain sulfonate groups. A systematic investigation of fuel cell membrane degradation mechanisms under operating conditions, using carefully selected model compounds as well as polymers, will be presented. This study shows that both carboxylic acid chain ends and ionomer side chains are kinetically-competent sites for peroxide radical attack. Degradation kinetics, reaction products, and radical trapping evidence will be presented in support of the conclusions.

Experimental

Key Materials. Nafion® film (structure shown in Figure 1) was purchased from Aldrich and used after transformation to its acid form. A developmental fluoropolymer ionomer was provided by 3M, and activated in a similar manner. Various model compounds (structures shown in Figure 2) were supplied from Synquest, 3M, and Lancaster.

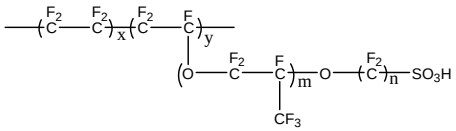

Figure 1. Chemical structure of Nafion ionomer

Methods

Durability Test Settings and Procedures. Aging experiments were carried out using Fenton's reagent[2]; the mechanism of the resulting radical generation using this treatment is shown in Figure 3. Two sets of Fe^{2+} and H_2O_2 reactant concentrations were employed – designated as "harsh" and "milder" – these are listed in Figure 3.

Nafion ionomer film samples were immersed in a flask containing Fenton's regaents as discussed above, and during the course of the aging experiment three additional follow-up additions of H_2O_2 were added in the flask to maintain the concentration of radical-generating species. Fluoride generation was measured (as will be discussed below) about every 24 hours. For Model Compound studies, the Model Compound was thoroughly mixed and stirred with the aqueous solution, and the H_2O_2 was added in the flask through an addition funnel. The reaction was allowed to sit for about 24 hours followed by fluoride concentration measurement, then the MC was separated and underwent subsequent aging and measurement. All the systems were continuously bubbled with nitrogen and maintained to be 70°C, which closely approximates polymer fuel cell operating temperatures. In an effort to separate the effects of model compound degradation from radical intermediates and any participation from the iron ions used in Fenton's reagent, selected model compounds were also subjected to hydrogen peroxide aging under UV irradiation (medium pressure mercury lamp). Samples were also UV aged in the absence of hydrogen peroxide to eliminate direct photolysis reactions as possible degradation pathways.

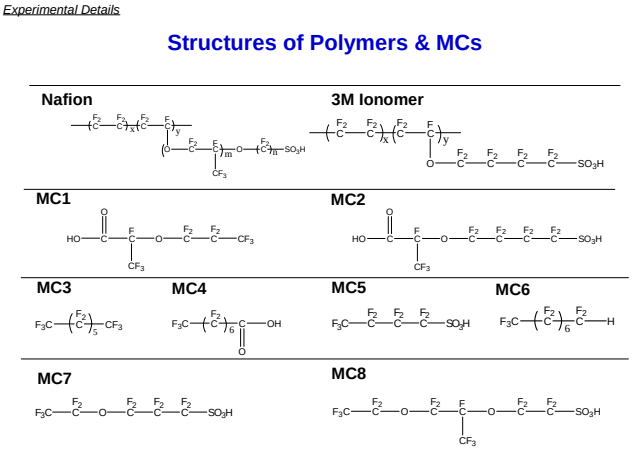

Figure 2. Chemical structures of Model Compounds

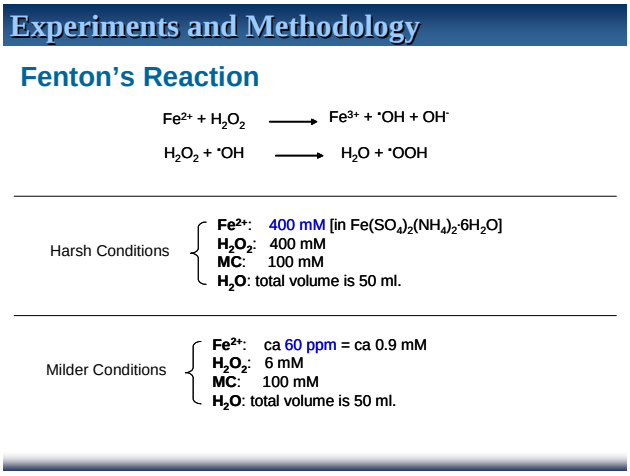

Figure 3. Fenton's reactions to create radicals (PH < 3)

Fluoride Concentration Measurement and Product Determination. The concentration of fluoride ions was measured by an ion selective electrode (ISE) (Mettler-Toledo), which was calibrated over the range 0.01 – 1000 ppm fluoride using NaF aqueous solutions. The interference from Fe^{2+} and Fe^{3+} as well as OH^- was eliminated by the dilution of tested sample (the sample was diluted for 100 folds), the validity of which was experimentally proven. Products of Fenton's reagent aging of model compounds were determined using ^{19}F nmr (Varian, 600 MHz).

Results and discussion

It is widely reported that fluoride ion is evolved in actual fuel cell effluent and during laboratory accelerated life studies[3-4]. The specific polymers sites from which fluoride is generated and mechanism of fluoride loss from the fluoropolymer membranes has not been unambiguously established, hence the motivation for this current work. We find that fluoropolymers, such as Nafion ionomer and the developmental alternative material from 3M, both generate fluoride ions at a linear rate when exposed to Fenton's Reagent. In our testing, the 3M material lost fluoride at approximately one third of the rate of the Nafion polymer. These polymers did not lose detectable levels of fluoride in the absence of hydrogen peroxide (i.e. neither hydrolysis, nor iron-catalyzed degradation are important in fluoride generation under our conditions).

Treatment of the model compounds with Fenton's Reagent also resulted in fluoride ion generation. The levels of fluoride ion generated from the most reactive model compounds closely matched those obtained with fluoropolymers. As can be seen in Figures 4 and 5, both the "harsh" and "milder" sets of Fenton's Reagent aging conditions resulted in largely linear fluoride release rates, and significant discrimination between specific model compounds. These results, when combined with 19F nmr analysis of the degraded model compounds, and with radical trapping of reaction intermediates, provide important insights into the mechanism of both model compound and PEM fluoropolymer membrane material degradation. Specific findings include: (1) confirmation that carboxylic end groups do indeed lead to rapid degradation of sulfonated fluorocarbon materials (supporting some literature reports); (2) the presence of alpha ether linkages enhance degradation rates; (3) the presence of tertiary C-F links significantly enhance radical degradation; (4) no evidence for degradation at the sulfonic acid moieties were observed, contradicting some literature reports; and (5) while carboxylic acid end groups are highly activated for degradation, side-chain fluoroether chain groups can also degrade at such a rate that they would be expected to contribute to the overall degradation of PEM membrane materials.

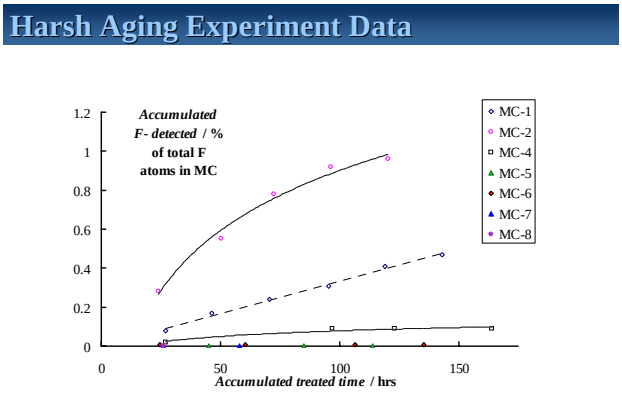

Figure 4. F^- concentration of Model Compound system as a function of aging time, Harsh Conditions

Table 1. Comparison initial rates of F^- generation

	F- Generated/Total Fluorine content, %
Nafion Ionomer	0.03 (0.26*)
MC-1	0.08
MC-2	0.28
MC-4	0.02
MC-5	0.008
MC-6	0.007
MC-7	< 0.001
MC-8	< 0.001

* Ratio % is Fluoride generated over the approximated total fluorine atoms on the side chains of Nafion.

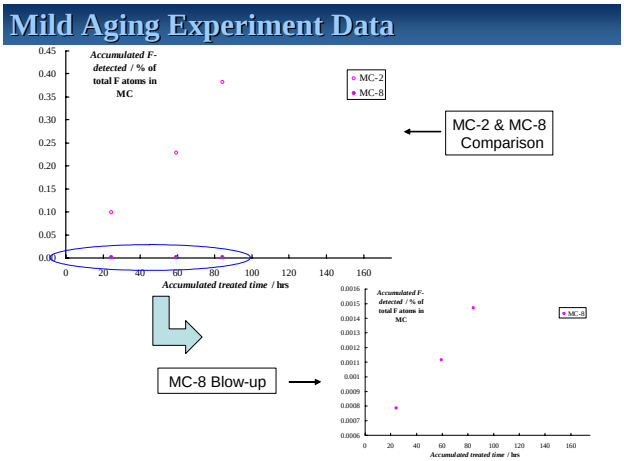

Figure 5. F^- Concentration of Model Compound system as a function of aging time, Milder Conditions

Conclusions

Operating under accelerated lifetime conditions, a systematic study of chemical decomposition products resulting from fluoropoplymer and model compound decomposition under Fenton's Reagent aging was performed. These data show that generation of fluoride is largely linear with treatment time, and is highly structure-dependent. Results to date strongly suggest that both carboxylic acid end group and side chain degradations can play kinetically-competent roles under simulated fuel cell operating conditions.

References

1. Gottesfeld, S.; Zawodzinski, T. *Advances in Electrochemical Science and Engineering*, Volume 5, Wiley, **1997**, edited by Alkire, R.C. et al..
2. Walling, C. *Acc. Chem. Res.* **1975**, *8*, 125.
3. Pozio, A.; Silva, R.F.; Francesco, M. De; Giorgi, L. *Electrochimica Acta* **2003**, *48*, 1543.
4. Baldwin, R.; Pham, M.; Leonida, A.; McElroy, J.; Nalette, T. *J. Power Sources* **1990**, *29*, 399.

Nafion® is a trademark of DuPont.

This research was supported in part by the Department of Energy, Cooperative Agreement No. DE-FC36-03GO13098. DOE support does not constitute an endorsement by DOE of the views expressed in this talk.

SHORT-SIDE-CHAIN PERFLUORINATED PROTON EXCHANGE MEMBRANES FOR PEMFC'S

Alessandro Ghielmi, Vincent Meunier, Luca Merlo, and Vincenzo Arcella

Solvay Solexis
viale Lombardia 20
20021 Bollate
(Milano) Italy

Introduction

Perfluorinated membranes known as 'short-side-chain' (SSC) are obtained by copolymerization of tetrafluoroethylene (TFE) and the sulfonyl vinyl ether monomer $CF_2CF\text{-}O\text{-}CF_2CF_2SO_2F$. Membranes with this chemistry were originally developed by Dow in the 80's, but relevant data in the literature are very scarce, due to the fact that these membranes were never widely available. The paper containing the most complete characterization is that by Tant et al.[1] The SSC perfluorinated membranes are presently becoming available again under the tradename Hyflon Ion. In the present paper more data are reported regarding the physical and electrochemical properties of the SSC membranes. From an applicative point of view, it is especially interesting to compare these properties with those of the long-side-chain (LSC) perfluorinated ionomer (Nafion), which is the current reference ionomer material for fuel cell (FC) membranes. While it is known that a higher glass transition temperature of Hyflon Ion (vs. Nafion) makes it more promising for high temperature PEMFC operation (T>100°C), favourable properties in terms of conductivity and FC performance are demonstrated also at lower temperatures, ranging from ambient temperature to temperatures in the order of 80°C currently used for the stationary application.

Experimental

Sample preparation. Membranes of different equivalent weight (EW) were obtained by melt extrusion of the polymer in the precursor (sulfonyl fluoride) form, and subsequent hydrolysis in a strong base at 80°C and acid exchange in a strong inorganic acid at ambient temperature. EW was determined by base titration of the sulfonic groups of a pre-weighed dry piece of membrane.

Tensile properties. Tensile properties were measured according to ASTM D1708. Measurements were carried out both on dry and wet membranes. Here, 'dry' stands for the membrane at laboratory conditions, i.e., 23°C and 50% relative humidity, while 'wet' refers to the membrane soaked in water at 100°C. In all cases the tensile test was carried out at laboratory conditions (23°C and 50% RH). In the case of wet membranes, these were extracted from the water and the measurement was carried out immediately.

Water uptake. Water uptake from liquid water at 100°C was measured by weighing the samples dry and after soaking in boiling pure water for 30 min. Weighing after water soaking was performed by blotting the samples dry on the surface and rapidly weighing.

Water uptake from water vapour at different relative humidities was measured by weighing the samples dry and after exposure to water vapour in a closed vessel containing water saturated with different salt systems, corresponding to different vapour activities.

Dry weight was determined on the samples kept for 1h at 105°C under vacuum.

Conductivity. Membrane conductivity as a function of relative humidity was measured by impedance spectroscopy analysis inside a thermostatted cell where relative humidity was controlled by injection of measured quantities of water vapor.

Fuel cell performance. Fuel cell performance was measured using a Fuel Cell Technologies test station with 25cm^2 active area single cells. Commercial Elat (E-Tek) gas diffusion electrodes with 0.5 mgPt/cm^2 catalyst loading (30% Pt/C) were used. Before taking the polarization curve measurement, the membrane-electrode-assembly was conditioned in the cell at the temperature, pressure and relative humidity conditions of the measurement and at a fixed voltage (0.4V) until the current was constant for at least three hours.

Results and Discussion

Tensile properties are shown in Figure 1 as a function of EW both for wet and dry membranes. It can be seen that stress at break is significantly growing with increasing EW's, which can be related to increasing crystallinities and molecular weights of the polymer.

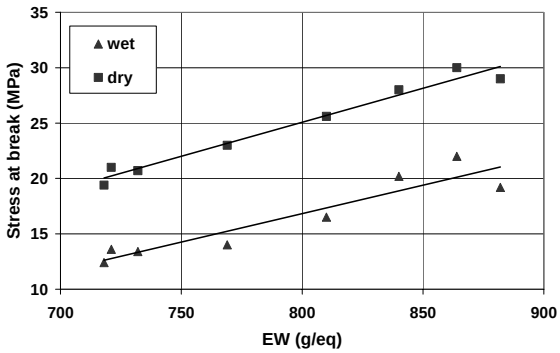

Figure 1. Tensile stress as a function of EW.

It was shown by Arcella et al.[2], that SSC membranes with EW around 850-900 g/eq have similar tensile properties compared to Nafion with EW=1100. This is true both in the dry and wet state, and can be likely related to similar levels of crystallinity.

Figure 2 shows the water uptake behavior from vapor at different relative humidities measured at 30°C on a membrane of EW=850. The curve measured on Nafion 1100 EW is also reported. A sigmoidal shape curve results, in agreement with previous data reported in the literature for Nafion. It can be seen that water uptake is similar for Hyflon Ion (850 EW) and Nafion (EW 1100) up to over 80% RH. At saturation, Hyflon Ion absorbs more water than Nafion, which is in agreement with higher water uptake values measured on Hyflon Ion in pure liquid water (about 45% water uptake for Hyflon 850 EW vs 35% water uptake for Nafion 1100 EW at 100°C).

Figure 3 shows the conducitivity of Hyflon Ion 850 EW vs. Nafion 1100 EW as a function of relative humidity at 35°C. It can be seen that the conductivity of Hyflon Ion is higher. Since this happens throughout the whole RH range, this can be related mainly to the lower EW of the Hyflon Ion (higher concentration of the ion-exchange groups), since the water uptake has been shown to be practically the same in a wide range of RH (Figure 2). This higher conductivity of an 850 EW Hyflon Ion clearly represents an advantage for fuel cell operation. It is noteworthy that higher conductivity levels are obtained with similar mechanical properties.

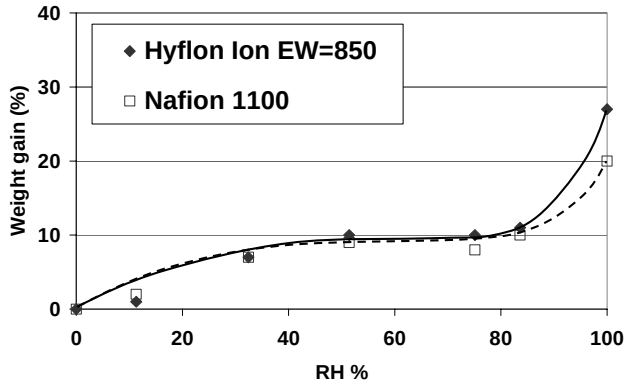

Figure 2. Water uptake from the vapor phase at different relative humidities.

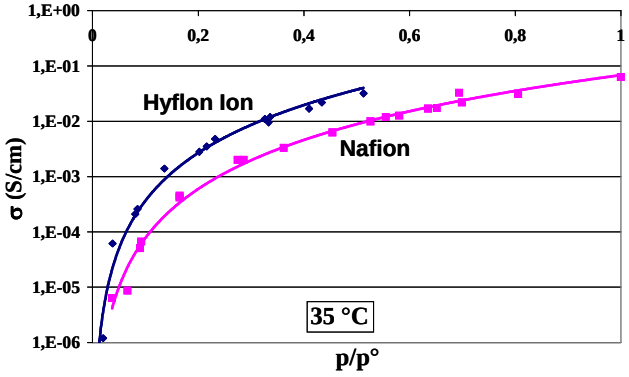

Figure 3. Conductivity data of ionomers at increasing RH (p/p^0)

Fuel cell performance of Hyflon Ion membranes 850 EW was measured at temperatures ranging from 30°C to 80°C and above. In all cases, it was found that the higher conductivity of the membrane delivers higher fuel cell performance in terms of polarization behavior. Figure 4 shows as an example the FC performances measured at 30°C in H_2 and air under complete reactant humidification. The gain given by the use of the lower EW SSC ionomer is apparent. Similar results are obtained at different temperatures, the gain in polarization behavior being more or less marked according to FC operating conditions. In no operating condition among those examined was the performance of Hyflon Ion found to be worse.

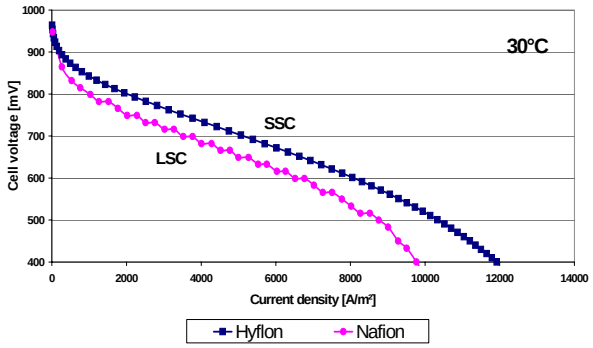

Figure 4. Fuel cell performance at 30°C.

Conclusions

Favorable mechanical, thermal and conductivity properties measured on short-side-chain (SSC) membranes make them ideal candidates to be employed in PEMFC's, both in high temperature systems (e.g. automotive, >100°C), in medium temperature systems (e.g. stationary, 70-80°C) and ambient temperature micro-FC's (portable application). SSC ionomer membranes are currently under development at Solvay Solexis with the tradename Hyflon Ion.

References

(1) Tant, M.R.; Darst, K.P. ; Lee, K.D. ; Martin, C.W.; Multiphase polymers: blends and ionomers, L.A. Utracki, R.A. Weiss (Eds.), ACS Symp. Ser. 395, ACS: Washington, 1989.

(2) Arcella, V.; Ghielmi, A.; Tommasi, G.; *Ann. N.Y. Acad. Sci.*, **2003**, *984*, 226.

IMPORTANCE OF SULPHONIC ACID DISTRIBUTION PATTERN FOR LOW EQUIVALENT WEIGHT POLYAROMATIC MEMBRANES

N. Walsby[1], M. Hogarth[1], D. Thompsett[1], H. M. Colquhoun[2], W, Mortimore[2], Z. Zhu[2]

[1]Johnson Matthey Technology Centre,
Blounts Court, Sonning Common, RG4 9NH, UK
[2]School of Chemistry, University of Reading,
Whiteknights, Reading RG6 6AD, UK

Introduction

There is a need for fuel cell membranes capable of operating at low relative humidities, either at 80°C or at higher temperatures. Polyaromatic membranes are the main rivals to commercial perfluorinated membranes. They are attractive because of their good thermo-mechanical characteristics and chemical stability, and because a vast range of different ionomers is possible.[1] Thus, we can systematically vary the ionomer structure and assess the significance of specific structural changes. Our general aim is to maximise the conductivity of polyaromatic membranes and to determine the ultimate performance limits of this class of membrane. The simplest way to increase proton conductivity is clearly to increase the concentration of sulphonic acid groups on the polymer chain. However, the maximum achievable concentration before the polyaromatic polymer becomes water-soluble has always been lower than in commercial perfluorinated membranes such as Nafion. We now report that controlling the sequence-distribution of sulphonic acid groups along the polymer chain can extend the concentration range possible with polyaromatics. Three aromatic polymers of very similar equivalent weight but different structure were prepared. The first (A) was a standard statistical polyethersulphone copolymer, the second (B) a statistical copolymer with more extended (3- and 4-ring) comonomers, and the third (C) a homopolymer with a highly extended (9-ring) repeat unit. The structures are shown in Figure 1.

Experimental

Polymer Synthesis[2] *Polymer A* was synthesized as described in US 5,693,740. The ratio of m:n was m=0.5n.

*Polymer B.*The dihalide monomers were made by conventional Friedel-Crafts reactions, and comonomers 4,4'-biphenol, 4,4'-dihydroxydiphenylsulphone, 4,4'-bis(4-chloro-benzenesulphonyl)biphenyl and 1,3-bis(4-fluorobenzoyl)benzene were polymerised in diphenylsulphone in the presence of K_2CO_3 at 290 °C.

Polymer C. Monomer synthesis: Isophthaloyl dichloride, 4-(4'-chlorobenzenesulphonyl)-biphenyl and aluminium chloride were heated with stirring in trichlorobenzene at 150 °C until HCl evolution virtually ceased. After cooling, the viscous solution was poured into a mixture of water and concentrated HCl. The aqueous phase was separated and the yellow viscous product was treated with hexane and then stirred in methanol. The white–yellow powder was dried under vacuum overnight and then recrystallized twice from DMF to give the monomer as a white powder. Polymerisation: the monomer underwent polycondensation with 4,4'-biphenol in diphenylsulphone in the presence of K_2CO_3 at 290 °C. The solid product was extracted with methanol and with water before drying under vacuum.

All polymers were sulphonated in concentrated sulphuric acid. Membranes were cast from ionomer solutions in NMP.

Fuel Cell Evaluation. Membranes were sandwiched between two electrodes in an electrochemical cell. The 3cm² active area electrodes were prepared using Toray TGP-H-60 carbon fibre current collecting substrate that was coated with a combination of carbon black, polytetrafluoroethylene polymer, platinum black electrocatalyst and Nafion® ionomer. The fabricated electrodes and membranes were pre-wetted in pure water prior to testing to ensure full hydration. The Membrane Electrode Assemblies (MEAs) were characterised using steady state electrochemical polarisation experiments. The fuel cell operated at 80°C with fully humidified hydrogen and oxygen, both at a pressure of 30 psig. Current-interrupt experiments were carried out to determine the ionic resistance of the membranes.

The long-term performance of membrane C was determined by fuel cell testing over an extended period until the MEA failed e.g. through the formation of pin-holes. Fully humidified hydrogen and air were supplied to the MEA, which contained 35µm thick membrane. Testing was carried out at 80 °C at a pressure of 30 psig at a constant current density of 500 mA/cm² with the same electrodes detailed previously, but with an active area of 49 cm^2.

Results and Discussion

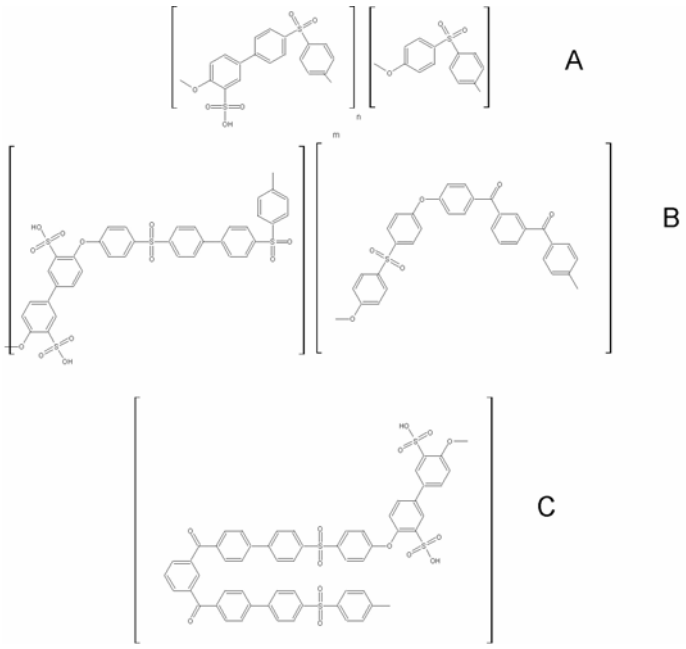

Figure 1. Structures of the polymers studied in this work.

Table 1 shows some of the characteristics of the polymers. Viscosity measurements on the unsulphonated polymers show A, B and C to be of high molecular weight (inherent viscosities > 1.0).

Table 1. Properties of polymers A, B and C.

	IV dL/g	Tg °C	IEC meq/g	$[SO_3H]$ mol/L
A	1.28	261	1.98	2.41
B	1.16	234	1.98	2.56
C	1.35	247	2	2.48

Acid-base titrations confirmed that the three polymers had very similar ion-exchange capacities. At around 2 meq/g, these ion-exchange capacities are very high (corresponding to an equivalent weight of ca. 500). The concentrations of sulphonic acid groups (calculated for dry membranes) are also similar and around 2.5

mol/dm³. In comparison, the measured ion-exchange capacity and concentration of sulphonic acid groups for the Nafion 1100 series membranes were 0.91 meq/g and 1.74 mol/dm^2 of dry membrane. For Flemion SH30 (Asahi Glass) the values were 1.02 meq/g and 1.86 mol/dm^2 of dry membrane.

The water uptake characteristics of membranes A, B and C as a function of temperature are shown in Figure 2. The water uptake values follow a general pattern common to ionomers: there is a gradual increase followed by a rapid swelling as the membrane becomes gel-like and finally dissolves. Kreuer[3] reported that, for sulphonated polyetheretherketoneketone of ion-exchange capacity 1.78 meq/g, the dramatic swelling that preceded dissolution began at ca 65 °C. For Nafion this temperature was reported to be 140 °C. Figure 2 shows that, despite similar concentrations of sulphonic acid groups, the water uptake behaviour is very different for membranes A, B and C. Membrane A has a higher water uptake at low temperatures and begins to swell dramatically at ca 60°C. For membrane B, excessive swelling is not encountered until 80 °C, while membrane C did not begin to swell excessively below 100 °C. It is clear that concentrating the sulphonic acid units in groups along the polymer chain and increasing the average separation between them, i.e. going from structure A to structure B, reduces the tendency of the membrane to swell in water. Taking this further and imposing a fully-defined "spacer" between sulphonic acid groups suppresses water uptake further. For fuel cell membranes this is highly advantageous as it allows the concentration of sulphonic acid groups to be increased beyond what was previously possible in polyaromatic membranes.

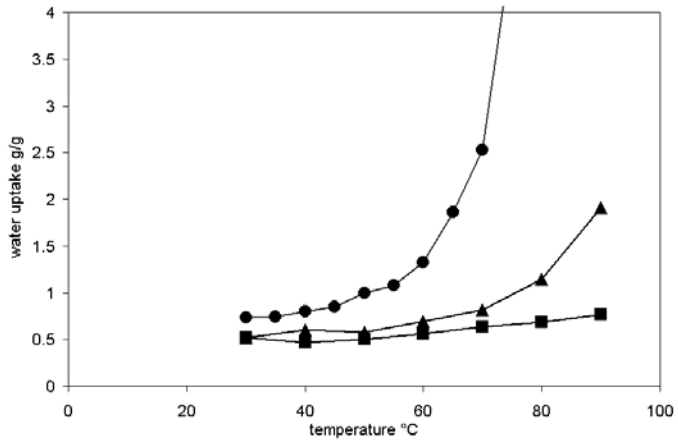

Figure 2. Water uptake as a function of temperature for membranes A (●), B(▲) and C (■)

The fuel cell data obtained with membranes A, B and C are shown in Figure 3, along with data for a commercial "state-of-the-art" membrane, Flemion SH30. All three aromatic membranes show excellent performance, comparable to that of Flemion SH30. The similarity in performance for membranes A, B and C indicates that, at these high concentrations of sulphonic acid groups and when compressed in a cell, differences in morphology resulting from the different structures give no clear advantage in terms of performance. A very clear difference, however, was seen in lifetime: membrane A barely survived long enough for the data to be collected. Membrane B was more robust but failed rapidly when tested in 50 cm^2 hardware. A lifetime test at a constant current density of 500 mA/cm^2 with membrane C is shown in Figure 4. The performance was stable for 500 hours. These differences reflect the difference in mechanical properties between the polymers in a fully humidified environment. The highly swollen polymer A, and to a lesser extent polymer B, are susceptible to partial dissolution and also liable to bursting under very small pressure differences.

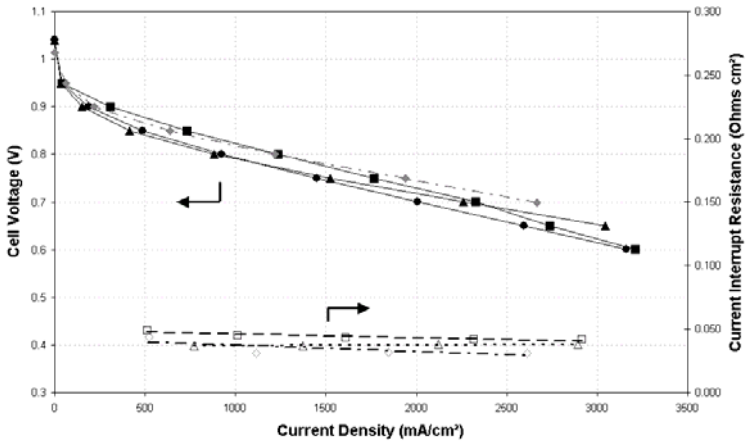

Figure 3. Oxygen polarisation data for membranes A (●), B(▲) and C (■) and Flemion SH30 (♦).80°C, 30 psig. Fully humidified H_2/O_2

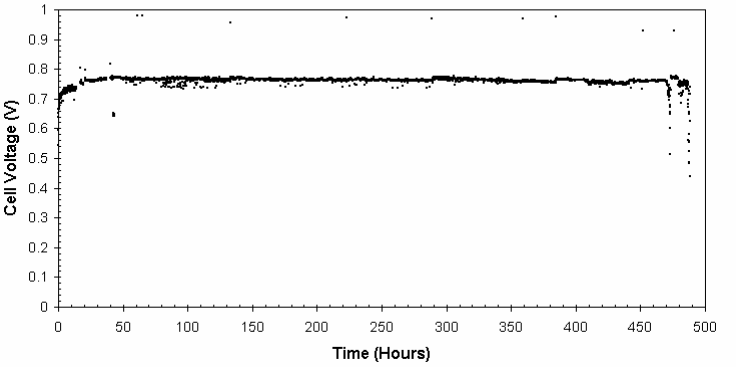

Figure 4. Lifetime test for membrane C in 49 cm^2 cell at a current density of 500mA/cm^2, 80°C, 30 psig. Fully humidified H_2/Air, stoichiometries of 1.5 and 2 respectively.

Conclusions

Imposing a fully-defined hydrophobic spacer between pairs of sulphonic acid groups along the polymer chain has a dramatic effect on the macroscopic swelling of polyaromatic membranes. The reduction in swelling enables membranes of lower equivalent weight to be used. This in turn improves conductivity and should enable the membrane to be used at lower relative humidities. Studies are underway to probe the differences in micro/nanostructure between the statistical copolymers and the homopolymer.

References

(1) Hickner, M. A.; Ghassemi, H.; Kim, Y. S.; Einsla, B. R.; and McGrath, J. E. Chem. Rev. **2004**, *104*, 4587

(2) Johnson Matthey, PCT/GB2005/000077

(3) Kreuer, K. D. *J. Memb. Sci.* **2001**, *185*, 29

THE USE OF HETEROPOLY ACIDS IN HIGH PERFORMANCE COMPONENTS FOR PROTON EXCHANGE MEMBRANE FUEL CELLS

Andrew M. Herring,[1] John A. Turner,[2] Steven F. Dec,[3] Fanqin Meng,[1] Jennifer L. Malers,[1,2] Ronald J. Stanis,[1,2] Niccolo Aieta,[1,2] and James Horan[3]

Department of Chemical Engineering[1] and Department of Chemistry and Geochemistry,[3] Colorado School of Mines,
Golden, CO 80401.
Hydrogen and Electricity, Systems and Infrastructure Group,[2]
National Renewable Energy Laboratory,
Golden, CO 80401.
Email:aherring@mines.edu

Introduction

There is increasing interest in using the heteropoly acids, HPA, as proton conducting components or additives in proton exchange membrane (PEM) fuel cells for elevated temperature operation, 120 – 200 °C, or to decrease the humidification requirements of PEMs.[1-6] Operation of a PEM fuel cell at these elevated temperatures will allow the integration of the stack into existing vehicular cooling systems, as well as stationary CHP, and use of hydrogen with an elevated CO content, simplifying the overall design of the reformer needed to generate hydrogen from hydrocarbons. The ultimate goal of a PEM requiring no external humidification will lead to further system simplification. The heteropoly acids (HPA) are a large and structurally diverse class of inorganic proton conducting materials[7] with extremely high room temperature proton conductivities, as high as 0.2 S cm^{-1} for 12-phopshotungstic acid.[8] importantly, for elevated temperature PEM fuel cell operation, the HPA are structurally stable to temperatures in excess of 600 °C and incorporate water molecules and protons to temperatures in excess of 300 °C depending on the system.

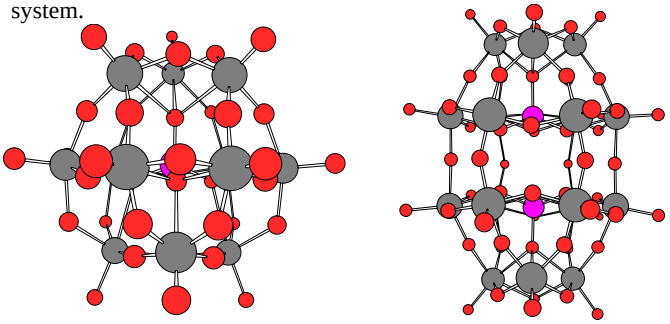

Figure 1. Structures of the Keggin anion, $H_3PW_{12}O_{40}$, 12-HPW , left and Dawson anion, $H_6P_2W_{18}O_{62}$, 18-HP2W, right.

Most studies to date have only considered the commercially available Keggin structures, consisting of a tetrahedral arrangement of three tungsten or molybdenum oxygen octahedral surrounding a central heteroatom, Figure 1. Many other structures are possible including the more thermally Dawson structure, Figure 1 and structures of increasing complexity. Importantly Lacunary structures may be derived from the parent Keggin or Dawson by the removal of 1,2 or 3 metal oxygen octahedral leaving a vacant site that may be used as a covalent attachment point for the synthesis of hybrid materials or a coordination site for another metal center.

Because of their structural diversity these materials are particularly suitable for incorporation into a wide variety of membrane materials. In addition, the HPA have interesting redox and catalytic properties that can be exploited for PEM fuel cell applications and must also be fully understood before a practical system incorporating HPA can be developed. We have continued to study HPA in perfluorinanted sulfonic acid, PFSA, polymers such as Nafion®. As the HPA are not immobilized in these systems they can migrate towards one or other of the electrodes leading to improvements in performance that may have more to do with the electrode/membrane interface than to intrinsic changes to the properties of the membranes alone.

Experimental

The HPA were either purchased from Aldrich (12-phosphotungstic acid (HPW) and 12-silicotungstic acid (HSiW)) or synthesized by literature methods (12-phosphodivanadomolybdic acid (HPV2Mo), 18-diphosphotungstic acid (18-HP2W), 21-diphosphotungstic acid (21-HP2W), and 21-diarsenotungstic acid (21-HAs2W)).

Nafion® 112 or 117 sheets were obtained from Ion Power, Inc. The Nafion® was cleaned by refluxing in 3% H_2O_2 for 1 h, deionized (DI) water for 1 h, 0.5 M H_2SO_4 for 1 h, and finally DI water for 1 h. It was then rinsed and stored in DI water in the dark. The Nafion® was doped with HPAs by refluxing in an aqueous solution of each HPA overnight. The Nafion® was placed in a mixed refluxed solution of 50 g of HPA and 250 ml of DI water for 24 h.

Infrared spectra were collected on a KRS-5 ATR attachment in a Thermo-Nicolet Nexsus 670 FT-Infrared spectrometer. Proton diffusion measurements were obtained on a Chemagnetics Infinity 400 NMR spectrometer operating at 400 MHz for ^1H using a 5mm Doty Scientific, Inc. #20-40 z-gradient pulsed-field gradient NMR probe. The stimulated-echo pulse sequence was used.[9] Spectra were recorded as a function of gradient pulse current using a 90° radio frequency excitation pulse of 6.5 μs, a gradient pulse width of 1.0 ms and a gradient pulse spacing of 3.2 ms. Spectra were recorded for 40 equally spaced values of gradient coil currents between 0.3 mA and 15 A in a random array by signal averaging 16 transients.

Membrane electrode assemblies (MEAs) were constructed using electrodes were purchased from E-Tek (ELAT) V2.2 hand fabricated, single sided coatings with 0.5 mg/cm^2 20% Pt on carbon. A 5% Nafion® 1100 solution was painted on each electrode until the loading was in the 0.4-0.5 mg/cm^2 range. The electrodes were then hot pressed at 150 °C and 80 psi for 5 min. Electrodes were then placed on the HPA doped Nafion® 112 and hot pressed at 145 °C for 90 sec.

Results and Discussion

The HPA interact strongly with polar molecules and so are expected to interact strongly with PFSA polymers.

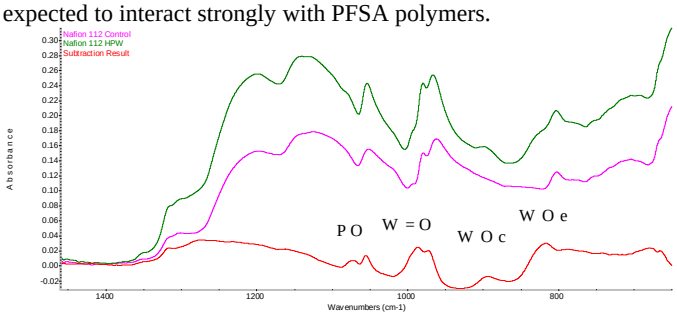

Figure 2. ATR IR of vacuum dried Nafion® 112 with and without 12-HPW and the subtracted spectrum.

The Infrared spectrum of vacuum dried Nafion® 12-HPW doped Nafion® is shown in Figure together with the result of subtracting the control spectrum from the doped spectrum. In the subtraction

result the four expected bands for the υ(PO), υ(W=O), υ(WO_c), and υ(WO_e) are clearly seen. Interestingly both the υ(PO), and υ(W=O) bands are split indicating bonding that bonding to the W=O of this Keggin anion is important. Obviously, these dry membranes in which the HPA bands are more obvious do not reflect the state of membranes hydrated in an actual fuel cell. On addition of water to the membrane further splitting of these IR bands is observed.

The effect on proton self-diffusion coefficients of doping Nafion® 112 with HPA are shown in Figure and Table 1. The maximum diffusion coefficient, $1.1x10^{-5}$ cm^2s^{-1}, for the Nafion® control is seen at 90°C. 12-HPW lowers this maximum temperature to 80°C, but increases the diffusion coefficient to $1.6x10^{-5}$ cm^2s^{-1}. With the exception of 21-HAs2W and 18-HP2W, all the other HPA increase the temperature of maximum diffusion, 21-HP2W to 100°C and HSiW to 130°C.

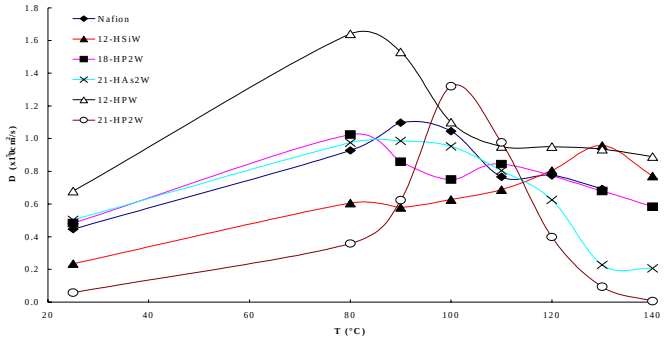

Figure 3. PFGSE data for the protons not associated with liquid water in HPA doped Nafion® 112 showing temperature vs. proton diffusion coefficient.

In Table 1 the activation energies for proton diffusion before the maximum temperature of diffusion are given. In general the E_a are all *ca.* 12 KJ mol^{-1} which is close to the literature value for diffusion in dry or nearly dry Nafion®.[10] Only 21-HP2W dramatically increases the Ea under these dry conditions, 21-HAsW21 decreases the E_a slightly.

Table 1. PFGSE data for the protons not associated with liquid water in HPA doped Nafion® 112 showing temperature vs. proton diffusion coefficient.

HPA	Max diffusion coefficent x 10^{-6} cm^2s^{-1}	Temperature of maximum D, °C	Ea before Max T, kJ mol^{-1}
Control	11	90	12
12-HPW	16	80	14
12-HSiW	10	130	13
18-HP2W	10	80	12
21-HAs2W	10	80	10
21-HP2W	13	100	31
11-HSiW	2.5	100	17

These changes to the Nafion® membranes are generally not reflected in the fuel cell testing of the corresponding MEAs. In general at 90°C or below the HPA doped membranes do as well as the undoped control or slightly worse. At 120°C slight improvements are seen for the commercial Keggin HPW and HSiW and the synthesized 21-HP2W doped Nafion®s. When the MEAs are constructed with no Nafion® in the electrodes dramatic improvements are seen in the performance of the doped Nafion® MEAs at 120°C.

From this data we deduced that we were actually seeing an improvement to the electrode/membrane interface in the doped MEAs. To test this hypothesis a Pt loaded ELAT anode was doped with the HV2MoP HPA. As can be seen, Figure , the improvement between the control MEA and the HPA anode doped MEA is dramatic. Examination of the data reveals that the biggest improvement in the polarization curve is in the ohmic region as the interfacial resistance has been dramatically reduced. It should be pointed out that additional contributions to this phenomenon on the fuel cell anode will also occur as the HPA when reduced by H_2 acts as a mixed protonic/electronic conductor.

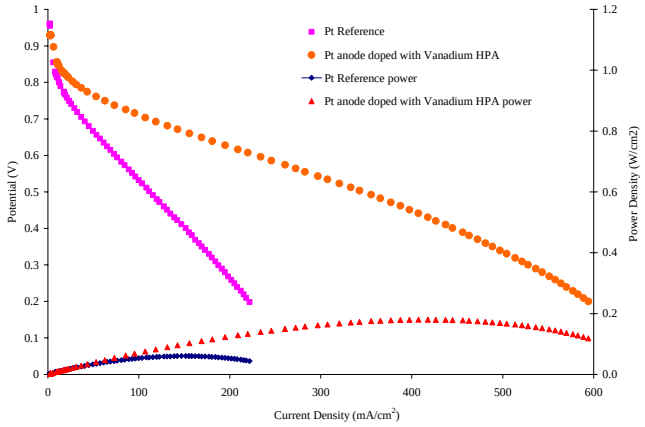

Figure 4. Polarization curves for a Nafion® 112 MEA with ELAT electrodes, both Pt control and Pt doped with $H_5[PMo_{10}V_2O_{40}]$ on the anode at 80**°C**.

Conclusions

HPA interact strongly with PFSA polymers and this interaction can be tailored to improve the proton conducting properties of these membranes. As unmodified HPA are water soluble and mobile their effect on an MEA actually occurs at the membrane/electrode interface, the interfacial resistance of which can be dramatically improved.

Acknowledgement. We would like to thank the DOE for financial support from award No. DE-FC02-0CH11088.

References

(1) Honma, I.; Nakajima, H.; Nishikawa, O.; Sugimoto, T.; Nomura, S. *J. Electrochem. Soc. 150*, (2003), A616.
(2) Honma, I.; Takeda, Y.; Bae, J. M. *Solid State Ionics 120*, (1999), 255.
(3) Vernon, D.; Meng, F.; Dec, S. F.; Williamson, D. L.; Turner, J. A.; Herring, A. M. *Journal of The Electrochemical Society submitted*, (2004).
(4) Kim, Y. S.; Wang, F.; Hickner, M.; Zawodzinski, T. A.; McGrath, J. E. *J. Membr. Sci. 212*, (2003), 263.
(5) Ramani, V.; Kunz, H. R.; Fenton, J. M. *J. Membr. Sci. 232*, (2004), 31.
(6) Staiti, P. *Journal of New Materials for Materials for Electrochemical Systems 4*, (2001), 181.
(7) Pope, M. T.; Müller, A., Eds. *Polyoxometalate Chemistry: From Topology Via Self-Assembly to Applications*; Kluwer Academic Publishers: Dordrecht, 2001.
(8) Nakamura, O.; Kodama, T.; Ogino, I.; Miyake, Y. *Chemistry Letters 1*, (1979), 17.
(9) Tanner, J. E. *The Journal of Chemical Physics 52*, (1970), 2523.
(10) Cappadonia, M.; Erning, J. W.; Stimming, U. *Journal of Electroanalytical Chemistry 376*, (1994), 18.

NANOCOMPOSITE NAFION® CONTAINING SULFONATED PARTICLES FOR PEMFC APPLICATION

Philippe Bébin, Magaly Caravanier, Hervé Galiano

Commissariat à l'Energie Atomique
Le Ripault Research Center, BP 16
37260 Monts, France

Introduction

Membranes commonly used in PEMFC are perfluorinated polymers containing sulfonic acid groups on side chains, like for example Nafion® manufactured by Dupont. However, for fuel cell application, this kind of membranes needs a high water content to reach satisfying proton conduction. Moreover, for temperature higher than 80°C, the proton conduction of Nafion® is unstable. To improve the fuel cell efficiency, the polymer electrolyte should have better water retention properties especially in hard conditions like, for example, temperatures around 100°C. The improvement of the membrane water retention should help keeping a significant proton conductivity under dehydrating conditions.

For last years, attention has been focused on organic-inorganic hybrid material to enhance the hydration properties of the membrane at high temperatures (near 100°C)[1-3]. Amongst the inorganic compounds suitable with a proton conductive organic matrix, the clay family is a promising candidate because of its advantageous hydrophilic properties and good thermal stability[4,5]. Laponite and Montmorillonite, due to their ionic sheets structure, allow the absorption of water with good retention capacity. These fillers used in Nafion® should then prevent the loss of the hydration water at high temperature but also under low relative humidity conditions.

In this work, the synthetic Laponites (Lp) are used because they can have a reproducible composition and a high level of purity[6]. The corresponding hybrid membranes are obtained by mixing the perfluoro-sulfonated polymer (Nafion®) with the synthetic inorganic particles. Nevertheless, the addition of clay, which is a poor proton conductor, inside Nafion®, which is highly proton conductive, can lead to a reduction of the global proton conductivity of the membrane. To enhance the proton conductivity of the hybrid material without loosing the benefits brought by the inorganic particles, some proton conductive groups are chemically bonded to the Laponite surface. The corresponding treatment and its efficiency are discussed, and the results, coming from chemical and electrochemical analysis for hybrid membranes prepared with both, unmodified (Lp) and grafted clay (Lp-g), are presented and compared to Nafion® ones. The influence of the hybrid membrane on the efficiency of PEMFC is also evaluated.

Experimental

Nanocomposite membrane preparation. Nafion® membranes, and Nafion® solutions (20wt.% of Nafion® in water/alcohols mixtures) are purchased from DuPont, and Laponite RD is purchased from Rockwood Industries. The surface of the clay, after being activated with an helium plasma, is chemically grafted with sulfonated styrene moieties using a DMF solution of p-styrene sulfonate (purchased from Aldrich). The corresponding dispersion is kept for 48 hours at reflux before washing the modified clay powder in DMF to remove all the monomers and oligomer moieties not attached to the Laponite particles. A pre-formed membrane of Nafion® is dissolved in a 15% (w/v) DMF clay suspension and the mixture is stirred at room temperature until complete dissolution. The mixture is then poured on a glass support using a Hand-Coater (Braive Instrument) in a clean laminar flow environment. The membrane is then heated in an oven at 120°C for 10 hours to enhance its mechanical properties. Finally, the membrane is soaked in a 3wt.% H_2O_2 solution at 80°C for 1 hour to oxidize the organic impurities. After 1 hour in pure water, the membrane is activated using a 0,5 M H_2SO_4 solution at 80°C for 1 hour before being rinsed again in de-ionized water for 1 hour. The sample is then stored in de-ionized water at room temperature until use.

Analysis. The proton conductivity measurements are performed using an impedance cell with two platinum disk electrodes of 0,5 cm in diameter. The cell containing the sample to analyze is placed in a Weiss WK 11180 climatic room that enables a controlled environment with relative humidity levels ranging from 0 to 98% and with temperatures ranging from RT to 95°C. The measurement conditions, i.e. the relative humidity and the temperature, are kept constant for at least three hours before performing the impedance analysis with an AC impedancemeter (Solartron SI 1260 Impedance/Gain Phase Analyser). The impedance spectra are recorded from 10 MHz to 1 Hz with a perturbation voltage amplitude of 10 mV.

Fuel cell tests are performed with an Electrochem fuel cell test station (RBL 488-50-150-800). The membrane electrode assemblies (MEAs) are prepared sandwiching the membrane between two E-Tek electrodes (0,35 mg Pt/cm^2) without hot pressing. The electrode area is 25 cm². The performance of the single cell is evaluated in the range of 80°C to 120°C with 3 and 4 bars of gas pressure. Hydrogen gas and oxygen or air are fully humidified passing through a bubble-type chamber.

Results and discussion

The good water retention properties of clays are expected to improve the proton conduction of Nafion® under low humidity levels. **Figure 1** shows the relationship between the proton conductivity and the relative humidity (from 50 to 98% RH) for Nafion®115 and for the nanocomposite membranes at 25°C.

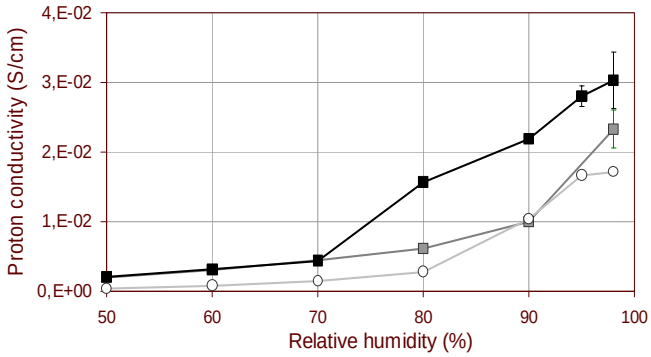

Figure 1. Variation of proton conduction at 25°C with relative humidity for Nafion®115 (○) and hybrid Nafion® containing 10wt.% of unmodified Laponite (Nafion®/Lp (■)) and containing 10wt.% of styrene-sulfonated Laponite (Nafion®/Lp-g (■))

As seen on Figure 1, the proton conductivity of the Nafion®/Lp-g membrane is higher than the one of the Nafion®115 whatever the relative humidity level. It is also higher than the proton conductivity of the Nafion®/Lp between 70 and 98% RH. The use of some proton conductive clay particles (Lp-g) as a filler for Nafion® induces a more significant effect on the proton conduction of the membrane than the use of non conductive clay particles. A 10^{-2} S/cm proton conduction level is then reached for a minimum of 75% RH with Lp-

g while it needs 90% RH when non conductive fillers are used. This level of humidity is, on the other hand, similar to the one needed when Nafion® is used without inorganic additives. An improvement of the working conditions is then expected for this kind of nanocomposite Nafion®, and, to evidence it, the levels of temperature and relative humidity needed to reach a 10^{-2} S.cm^{-1} conductivity are determined. The corresponding lines are presented in **Figure 2** as proton conductive maps for Nafion® and for the nanocomposite membrane (Nafion/Lp-g).

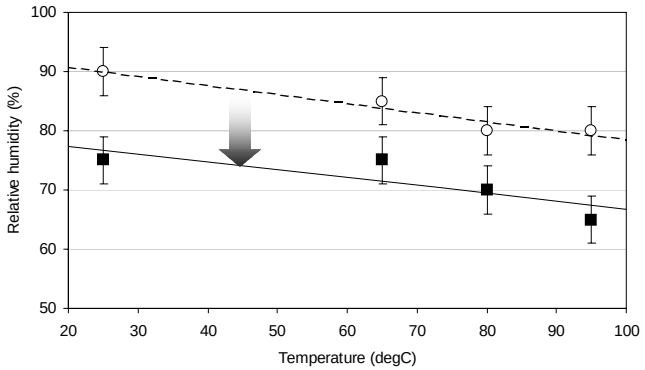

Figure 2. Temperature and relative humidity relationship for a 10^{-2} S.m^{-1} proton conductivity, for Nafion®115 (open circle and dotted line) and for Nafion®/Lp-g 10wt.% (black square and plain line) membranes

In Figure 2, a proton conductivity higher than 10^{-2} S/cm is obtained above the linear regression, while lower proton conductivity values are obtained below the corresponding lines. The relationships between temperature and humidity levels are linear and parallel for the two kinds of membranes with a decrease of the humidification level needed for the proton conduction when the temperature is increasing. The only difference between Nafion® and hybrid Nafion® is then the minimum level of humidity needed to have a satisfying proton conduction, which is about 10% lower for the nanocomposite Nafion® (Nafion®/Lp-g) compared to the pure Nafion®. The positive influence of the proton conductive filler is comparable on all the temperature range studied (25 to 95ºC).

The improvement of the hybrid membrane behavior can also be evidenced by fuel cell experiment. Nanocomposite Nafion® (Nafion®/Lp-g membranes) are tested in a fuel cell test station at different operation conditions, changing the cell temperatures (80-120°C), the reactant gases (H_2/O_2 and H_2/air), and the gas pressures (3-4 bars) in order to evidence the benefit brought by the particular formulation of the material. Good operation conditions, corresponding to fully hydrated fuel cell, are obtained at 80°C using H_2/O_2 gases under 4 bars. The hard operation conditions, corresponding to dehydrated fuel cell conditions, are obtained at 120°C using H_2/air gases under 3 bars. The polarization curves are presented on **Figure 3** for Nafion® and for nanocomposite Nafion® for the two working conditions.

In the good operation conditions, the use of Nafion® enables to reach about 600 mA.cm^{-2} of electronic current produced at 0.6 V, while the use of a Nafion®/Lp-g membrane leads to the production of about 720 mA.cm^{-2} at the same voltage. This difference corresponds to a 20% improvement in power density with the nanocomposite membrane (430 mW.cm^{-2} vs 360 mW.cm^{-2}). This gain decreases to 15% at 0,7 V. In the hard operation conditions, a Nafion® membrane can deliver 390 mA.cm^{-2} of current at 0,6 V while the nanocomposite one (Nafion®/Lp-g) can reach 500 mA.cm^{-2}. A 30% improvement in power density is then possible at 0,6 V, changing the commercial membrane for an hybrid one. This gain is about 25% at 0,7 V.

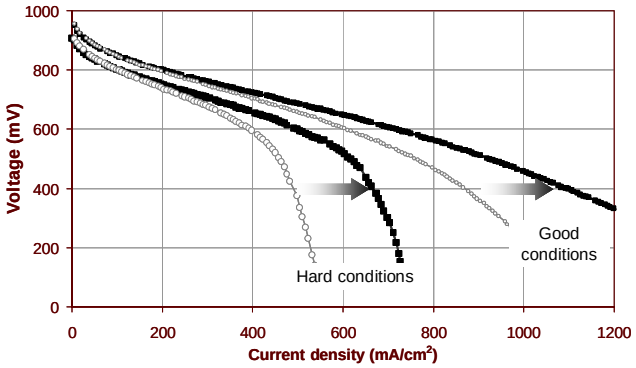

Firgure 3. Polarization curves of Nafion®115 and nanocomposite Nafion® (Nafion®/Lp-g (90/10 w/w)) under good operation conditions (80°C, H_2/O_2, 4 bars) and hard operation conditions (120°C, H_2/air, 3 bars).

Then, hybrid Nafion® presents a better behavior than the commercial Nafion®, whatever the operation conditions. Nevertheless, the gain in power density is always more significant under difficult humidification conditions than under fully humidification condititons. This improvement in fuel cell work has to be related to the good water retention of the inorganic filler while the sulfonic acid groups grafted to the particles surface enhance the global proton conductivity of the membrane.

Conclusions

The modification of clay particles by bonding styrene-sulfonic moieties at their surface has a significant positive effect on the behavior of a Nafion® membrane containing these particles. Indeed, the dispersion of this kind of fillers in Nafion® enhances both the water retention of the nanocomposite material and its proton conductivity.

Acknowledgements

The authors thank F. Bergaya from CNRS-Orléans and F. Poncin-Epaillard from CNRS-LeMans for their contribution in this project. S. Escribano from the Fuel Cell Laboratory of CEA is also acknowledged for her technical support on fuel cell experiments and analysis. The financial support of Région Centre was greatly appreciated for this project.

References

(1) Shao, Z.G.; Joghee, P.;Hsing,I.M., *J. Membrane Sci.*, **2004**, *229*, 242

(2) Chang, J.H.; Park, J.H.; Park, G.G.; Kim, C.S.;Park, O.O., *J. Power Sources*, **2003**, *124*, 18

(3) Kim, K.H.; Ahn, S.Y.; Oh, I.H.; Ha, H.Y.; Hong, S.A.; Kim, M.S.; Lee, Y.; Lee, Y.C., *Electrochimica Acta*, **2004**, *50*, 574

(4) Damay, F.; Klein, L.C.; *Solid State ionics*, **2003**, *162-163*, 261

(5) Greaves, C.R.; Bond, S.P.; McWhinne, W.R., *Polyhedron*, **1995**, 14 (23-24), 3635

(6) Qi, Y.; Al-Mulkhar, M.; Alcover, J.F.; Bergaya, F., *Applied Clay Sci.*, **1996**, *11*, 185

PREPARATION AND CHARACTERIZATION OF FLUORINE-CONTAINING POLY(ETHER KETONE)S WITH SULFONATED BIPHENYLENE UNIT

Yoshimitsu Sakaguchi[1], Shigenori Nagahara[1], Kota Kitamura[1], Masahiro Yamashita[1], Satoshi Takase[1], Kazushi Omote[2], Ai Nishichi[2], and Yoshinobu Asako[2]

[1]Toyobo Research Center, Toyobo Co., Ltd.
1-1 Katata 2-Chome, Ohtsu 520-0292, Japan
[2]Nippon Shokubai Co., Ltd.
5-8 Nishi Otabi-cho, Suita 564-0034, Japan

Introduction

As a new power source for transportation, stationary and mobile power applications from the viewpoint of environmental and new energy issues, solid polymer electrolyte membrane fuel cell is attracting much attention. Sulfonic acid-containing aromatic condensation polymers have been studied as possible candidates for the alternative of perfluorosulfonic acid polymer membranes, such as Nafion®, because their backbone structures are generally heat- and solvent-resistant with good mechanical properties. In many cases, however, perfluorosulfonic acid polymers are still used as a binder polymer for membrane electrode assembly, and it may cause problems in adhesion or delamination between the hydrocarbon membranes and the electrodes. A proton exchange membrane derived from partially fluorinated polymers may show good affinity with the perfluorosulfonic polymer binders and a binder made of partially fluorinated polymers also may show good affinity with nonfluorinated hydrocarbon polymer membranes with improved chemical stability.

Based on the above background, we have reported about preparation and properties of fluorine-containing sulfonated poly(ether ketone)s shown in **Figure 1**.[1] These polymers showed good proton conductivity by introducing adequate quantity of sulfonic groups, however, they showed pretty large swelling at the same time under higher humidified conditions. In this study, biphenylene structure is selected as a sulfonated segment instead of diphenyl fluorene unit in the figure to improve the dimensional stability of resulting membranes.

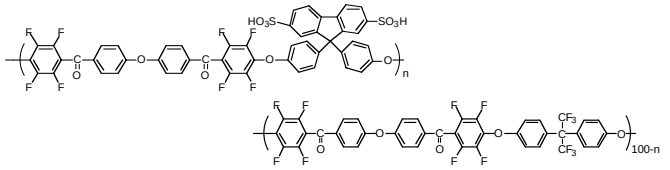

Figure 1. Sulfonic group-containing partially fluorinated poly(ether ketone) copolymers (S-HF-n).

Experimental

Preparation of sulfonated poly(ether ketone) copolymers (S-BP). Fluorine-containing poly(ether ketone) copolymers derived from 4,4'-bis(2,4,5,6-pentafluorobenzoyl)diphenylether (BPDE) and mixed diols of 4,4'-biphenol (BP) and 2,2-bis(4-hydroxyphenyl)-1,1,1,3,3,3-hexafluoropropane (6FBA) were prepared by aromatic nucleophilic substitution reaction with potassium carbonate in N-methl-2-pyrrolidone (NMP) according to a previous paper.[2] Sulfonation was carried out by dissolving the copolymers in concentrated sulfuric acid and stirred for designated time at room temperature. After the reaction, the reaction mixture was poured into water to precipitate the product. The sulfonated polymers thus obtained were washed with water until the washings were neutralized, and then dried under vacuum.

Preparation of films. Two grams of sulfonated polymers were dissolved in 10ml of NMP, and cast onto a glass plate on a hot plate to form films. The films obtained were placed in water overnight, then treated with 1M H_2SO_4 solution and pure water at 80°C for 1 hour, respectively, and then dried.

Characterization. Inherent viscosities were measured at a concentration of 0.5 g/dL in NMP at 30°C. Thermogravimetric analysis (TGA) was conducted at a heating rate of 10°C/min under flowing argon, using a Shimadzu TGA-50 thermogravimetric analyzer. Ionic conductivities of the films were measured at 80°C and 95%RH by using a Solartron 1250 Frequency Response Analyzer over the frequency range from 1Hz to 65KHz, and calculated based on the complex impedance plot. Ion exchange capacities of the films were measured by the back-titration with hydrochloric acid solution after the films were treated with sodium hydroxide aqueous solution. Methanol permeability was measured by monitoring the concentration of methanol with gas chromatograph using a H-shaped cell in which water and 5M-methanol aqueous solution are separated by a sample membrane.

Results and Discussion

Fluorine-containing poly(ether ketone)s were prepared by nucleophilic aromatic substitution reaction between BPDE and mixed diols of BP and 6FBA as shown in **Figure 2** (a copolymer containing n mol% of biphenol is abbreviated as BP-n). The previous paper[1] showed 6FBA unit in the copolymers was not sulfonated by concentrated sulfuric acid at room temperature, therefore, BP unit is expected as only one activated part for sulfonation in the copolymers. In general, sulfonated aromatic polycondensation polymers showed similar proton conductivity with Nafion® when their ion exchange capacity (IEC) is around 1.9 meq/g. Therefore, fluorine-containing poly(ether ketone) copolymer with BP:6FBA = 85:15 was prepared (BP-85).

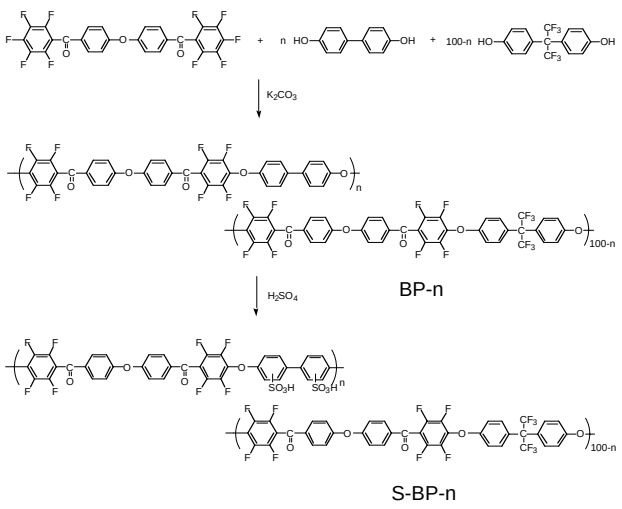

Figure 2. Synthesis of sulfonated poly(ether ketone) copolymers containing biphenylene unit (S-BP-n).

BP-85 was sulfonated in concentrated sulfuric acid at room temperature. Sulfonation for BP unit was slower than that for diphenyl fluorene unit (two hours is long enough for quantitative sulfonation for HF polymer), and complete sulfonation, two sulfonic

groups in one BP unit, was achieved for 62 hours reaction (measured IEC for the polymer was 1.98 and calculated IEC for complete sulfonation is 1.97). IR spectra before and after sulfonation are shown in **Figure 3**. Absorption peaks due to sulfonic groups are found in 1240 and 1100 cm^{-1}. ^{1}H NMR spectrum is shown in **Figure 4**. It is found that sulfonation was occurred on each benzene ring in biphenylene unit quantitatively. As sulfonation reaction was slow in this reaction system, a partially sulfonated polymer with 1.46 of IEC was also obtained by shorter reaction time of 17 hours.

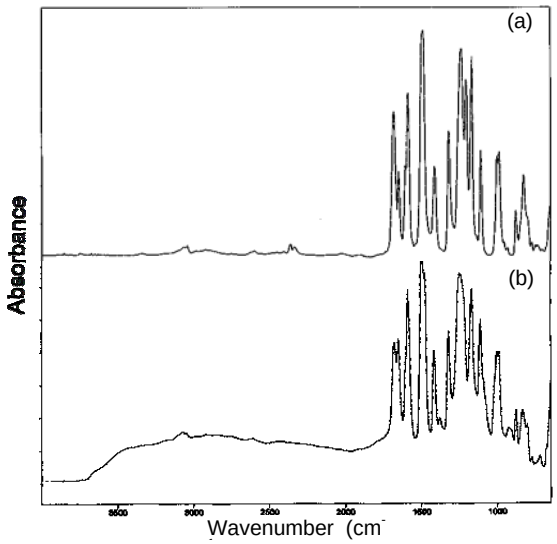

Figure 3. IR spectra of S-BP85 (a) before sulfonation and (b) after sulfonation for 62 hours.

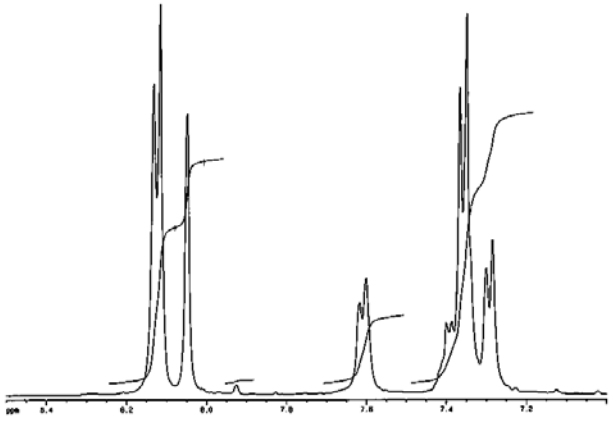

Figure 4. 1H NMR spectrum of S-BP85 sulfonated for 62 hours.

Table 1. Preparation of S-BP

Reaction time	IEC (meq/g)	η_{inh} (dl/g)		3% Weight loss temperature
		Before sulfonation	After sulfonation	
62hr	1.98	2.80	2.72	339°C
17hr	1.48	2.80	2.93	334°C

S-BP85(IEC=1.98) and S-BP85(IEC=1.48) showed lower swelling to water at higher temperature compared to S-HF100 and S-HF68, respectively. It is confirmed that replacement of diphenyl fluorine unit by biphenylene unit was effective to improve the dimensional stability of sulfonated poly(ether ketone) membranes. S-BP85 membranes also showed lower methanol permeability than corresponding S-HF membranes as shown in Table 2.

Table 2. Properties of S-BP85 and S-HF membranes

Polymer	IEC (meq/g)	S at 80°, 95%RH (S/cm)	MeOH permeability (μmol/m•s)
S-BP85(1.98)	1.98	0.29	0.25
S-BP85(1.48)	1.48	0.12	0.16
S-HF100	1.95	0.24	0.36
S-HF68	1.48	0.13	0.31

As it was possible to control the degree of sulfonation by changing the reaction time, sulfonation of BP100 was tried to improve dimensional stability further by eliminating flexible 6FBA unit. Sulfonated polymers having similar IEC to S-BP85 were obtained, however, their swelling properties and methanol permeabilities were almost the same as those of S-BP85 as shown in **Table3**.

Table 3. Properties of S-BP100 membranes.

Polymer	IEC (meq/g)	S at 80°, 95%RH (S/cm)	MeOH permeability (μmol/m•s)
S-BP100(1.91)	1.91	0.28	0.24
S-BP100(1.52)	1.52	0.17	0.17

Sulfonated poly(ether ketone) copolymers having partially fluorinated segments in this study showed improved performance as proton conductive membranes. As these polymers may show good adhesion with both aromatic hydrocarbon polymers and perfluorinated polymers, application of these polymers as a binder for MEA as well as a membrane is expected.

References

(1) Sakaguchi, Y., Kaji, A., Nagahara, S., Kitamura, K., Takase, S., Omote, K., Asako, Y., Kimura, K., ACS Polym. Prepr., **2003**, 45(1), 56.

(2) Kimura, K.; Tabuchi, Y.; Yamashita, Y.; Cassidy, P.E.; Fitch III, J.W.; Okumura, Y. Polym. Adv. Tech., **2000**, 11(8-12), 757.

MULTIBLOCK SULFONATED-FLUORINATED POLY(ARYLENE ETHER)S MEMBRANES FOR A PROTON EXCHANGE MEMBRANE FUEL CELL

Hossein Ghassemi, Tom A. Zawodzinski, Jr.

Case Advanced Power Institute and Department of Chemical Engineering, Case Western Reserve University, Cleveland, OH 44106

Introduction

Proton exchange membrane fuel cells (PEMFCs) offer potential advantages of clean and efficient energy conversion systems for automobiles, portable applications, and power generation. The primary demands on the hydrated proton exchange membrane (PEM) are high proton conductivity (above 0.01 S cm), low fuel and oxygen permeability, and high chemical, thermal and mechanical stability. Conventional PEMFCs typically operate with Nafion membranes, which offer quite good performance below 80 ◦C. However, to decrease the complexity and increase the efficiency and CO-tolerance of the PEMFC system, there is a strong need for PEMs capable of sustained operation above 100 ◦C and/or at decreased relative humidity of gases. Unfortunately, the proton conductivity of Nafion suffers greatly at temperatures above 80 ◦C due to loss of water. These factors, in addition to the high cost of Nafion, have triggered an extensive search for alternative PEM materials (1), some relying on other species than water to assist proton conduction.(2)

Sulfonated aromatic polymers have been recently studied (3-12) and in some cases showed satisfactory chemical and electrochemical stability for fuel cell applications. Among these polymers, sulfonated Poly(arylene ether sulfone)s have been extensively investigated for high temperature fuel cell applications. They are prepared by direct polymerization of the sulfonated activated halide with a bisphenol using otherwise nucleophilic substitution condensation polymerization conditions that are fairly similar to “polysulfone” preparation condiitons. These random copolymers display a hydrophilic/hydrophobic phase separated morphology that varies depending on the degree of sulfonation. The conductivity and water uptake of this series of copolymers also increase with degree of sulfonation. However, once the degree of sulfonation reaches 60 mole %, a semicontinuous hydrophilic phase is observed and the membranes swell dramatically, forming a hydrogel that is not useful as a proton exchange membrane.

Segmented multiblock (MB) copolymers are synthesized in order to create 'tailor-made materials' showing a combination of properties of the homopolymers. The combination of supramolecular phase separation in MB with self-ordering occurring on a molecular scale is assumed to provide interesting features changing the properties more than random copolymers. Multiblock copolymers composed of two or more long, contiguous sequences of chemically dissimilar repeat units, are able to spontaneously assemble into a wide variety of nanostructures, such as spherical or cylindrical micelles, bicontinuous channels, coalternating layers, and complex combinations.

In this article, we report new multiblock copolymers containing perfluorinated poly(arylene ether) as a hydrophobic segment and highly sulfonated poly(arylene ether sulfone) as a hydrophilic segment with the aim of providing polymeric materials with a highly phase-separated morphology. The phase formed by the hydrophobic block should enable good mechanical stability under fully hydrated state whereas the hydrophilic block should provide a high proton conductivity. The objective of this work is to produce thermally and hydrolytically stable, flexible membrane films with high proton conductivity even at lower water contents. We also report morphology of these MB copolymers using AFM. All polymers are characterized in terms of water-uptake and ion-exchange capacity.

Experimental

Materials. A series of multiblock copolymers **3** were synthesized from hydroxyl-terminated fully sulfonated poly(arylene ether) sulfones **1** and fluorine-terminated perfluorinated poly(arylene ether)s **2** according to a procedure reported elsewhere. (13)

Characterization. Conductivity measurements were performed on the acid form of the membranes using a Solatron SI 1280B Impedance analyzer. IR spectra are taken by a Perkin Elmer FT-IR Spectrum GX instrument using a ATR cell. Tapping mode atomic force microscopy (TM-AFM, Digital Instruments, Nanoscope IV) was performed in air.

Results and Discussion

As depicted in Figure 1, multiblock copolymers were prepared by the reaction of the dialkali metal salt of bisphenol-terminated disulfonated poly(arylene ether sulfone)s **1** with decafluorobiphenyl-terminated poly(arylene ether)s **2** in a polar aprotic solvent. The reaction was rapid and produced copolymers with light yellow color in high yield. The dialkali metal salts of bisphenol-terminated disulfonated poly(arylene ether sulfone) **1** were generated using 3,3’-disulfonated-4,4’-dichlorodiphenylsulfone and excess amount of biphenol in the presence of potassium carbonate at 180^{o}C. By controlling the amount of biphenol monomer samples with target molecular weight of 2.5K, 5K and 15K was prepared. The sulfonated copolymers were used in the next step without isolation. Similarly, decafluorobiphenyl-terminated poly(arylene ether)s **2** were synthesized using 6F-BPA and excess amount of decafluorobiphenyl in DMAc-benzene mixed solvent. It is known that perfluoroaromatic monomers are highly reactive toward the nucleophilic aromatic substitution reaction and high molecular weight polymers form at relatively low temperature and short period of time (9-11). Several fluorinated oligomers **2** were synthesized with molecular weights ranging from 2.8K to 60K. Low molecular weight samples formed white powder-like product after isolation, whereas the high molecular weight sample formed white fibrous material. The molecular structure of polymer **2** was confirmed by ^{19}F NMR in CDCl3, and compared with 6F-BPA and decafluorobiphenyl. Glass transition temperature for high molecular weight perfluorinated polymer **2** was traced by DSC and determined around 175◦C. Detection of Tg’s for the multiblock copolymers **3** has not been easy possibly due to the interfere of two separate phases.

Reaction of the preformed sulfonated **1** with the fluorinated oligomer **2** proceeded rapidly as evidenced by sharp increase in viscosity of reaction solution mixture in the first few hours. Dilution of the reaction mixture had little effect in lowering the viscosity of the solution. After isolation, products were treated in boiling water and boiling THF separately, in order to purify the product from unreacted starting oligomers. Multiblock copolymers **3** formed transparent films cast from solution. Films were flexible when fully hydrated and became brittle as their water content decreased.

The successful introduction of the sulfonate groups was confirmed by FT-IR spectra (Figure 2), where strong characteristic peaks at 1027 and 1097 cm-1 assigned to symmetric and asymmetric stretching of sulfonate groups were observed for all copolymers. The densities of these two peaks increase with higher ratio of sulfonated block to fluorinated block. The MB membranes were tested for ion exchange capacity by titrating with sodium hydroxide standard solution (Table 1). The multiblock copolymers had high water uptake both in salt and acid form. Conductivity of these materials in their

fully hydrated form in liquid water showed values between 0.08-0.32 S/cm (Table 1).

It was noticed that in spite of their relatively high water uptake (Table 1) the surface of the MB films is quite hydrophobic. This hydrophobicity further increased as the relative humidity decreased. It was observed that in several cases the proton conductivity of the membranes above water in various RH and temperature was surprisingly low. A highly fluorinated surface of these membranes might act as an insulator between the electrode and the proton conductive region of the membrane. More work is in progress to determine the contact angle of the MB membrane under different conditions and also to find a way to control their surface properties.

Figure 3 shows the representative morphology of Nafion 112, BPSH-40 and MB-150 derived from TM-AFM. BPSH-40 is a poly(arylene ether) sulfone random copolymer containing 40% sulfonated and 60% unsulfonated monomer (4, 12). All TM-AFM micrographs shown here were taken under partial hydration. Images from Nafion 112 and BPSH-40 suggest that the hydrophilic groups aggregate as isolated domains with some local connection of hydrophilic domains as evidenced by the proton exchange membrane's good conductivity. In the case of MB the hydrophilic blocks (dark area) clearly show the formation of the continuously connected nano-channels of about 10 nm average width. Furthermore, nano-structures of the hydrophobic domains (light regions) appear as lamellar/ cylindrical with average width of about 50 nm. This is direct evidence of well-ordered and continuous ionic channels formed by microphase separation between hydrophilic domains containing sulfonate groups and perfluorinated hydrophobic domains. Protons transfer through these nano-channels of MBs is most likely the reason for high proton conductivity of the multiblock copolymers.

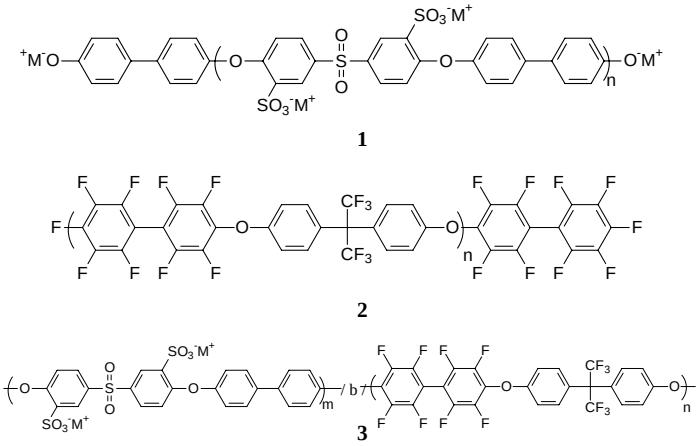

Figure 1. decafluorobiphenyl-terminated poly(arylene ether)s

Table I. Characterization of multiblock copolymers

Sample	Block size (Kg/mol)[1] S	F	IEC (meq/g)[2] Calc.	Exp.	Water Uptake (%)	Conductivity[3] (S.cm-1)
MB-229	5	2.8	2.05	2.29	470	0.32
MB-210	5	2.8	2.05	2.10	360	
MB-150	5	5	1.55	1.50	130	0.12
MB-117	5	5	1.55	1.17	115	
MB-095	3.2	5.3	1.17	0.95	41	0.08
Nf-1135	-	-	-	0.89	38	0.10

(1) Target value, (S) represents the sulfonated block and (F) represents the fluorinated block. (2) Samples were acidified in 0.5 M boiling sulfuric acid for 2 h and boiling deionized water for 2 h. (3) measured at room temperature in liquid water.

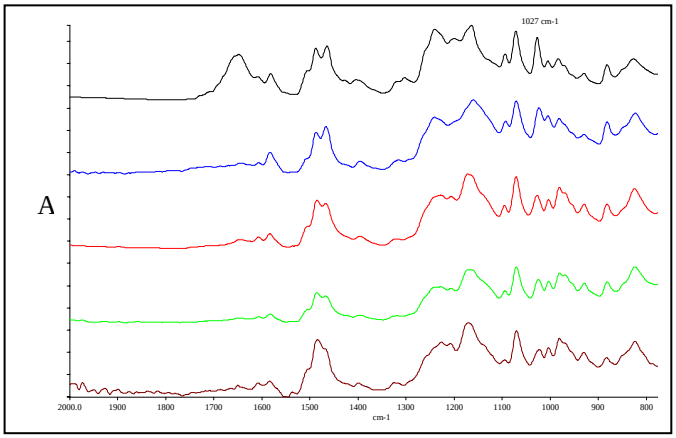

Figure 2. Influence of the relative size of sulfonated block on FT-IR of MB copolymers (sulfonated block size decrease from top to bottom)

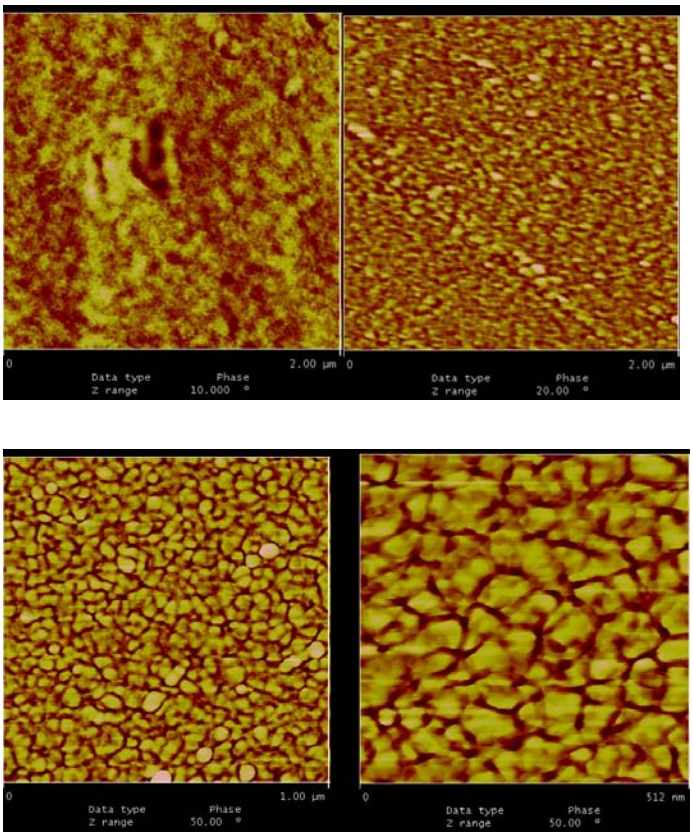

Figure 3. AFM tapping phase image for Nafion 112 (upper left), BPSH-40 (upper right) and multiblock MB-150 (bottom images)

Acknowledgement. The authors would like to thank the Department of Energy for support of this research effort.

References

(1) Michael A. Hickner, Hossein Ghassemi, James E. McGrath "Alternate Polymer Systems for Proton Exchange Membranes" Chemical Review**, 2004,** 104(10), 4587-4611

(2) Kreuer, K.D. "On the development of proton conducting membranes for hydrogen and methanol fuel cells". J Membr Sci 2001;185:29 – 39.

(3) Kobayashi, T.; Rikukawa, M.; Sanui, K.; Ogata, N. *Solid State Ionics* **1998**, 106, 219-225.

(4) Bae, J. M.; Honma, I.; Murata, M.; Yamamoto, T.; Rikukawa, M.; Ogata, N. *Solid State Ionics* **2002**.

(5) Kerres, J.; Ullrich, A.; Meier, F.; Haring, T. *Solid State Ionics* **1999**, 125, 243-249

(6) Wang, F.; Hickner, M.; Kim, Y. S.; Zawodzinski, T. A.; McGrath, J. E. *J. Membrane Science* **2002**, 197, 231-242.

(7) Cooper, J.E. *J. Polym. Sci. Part A; Polym. Chem*. **1971**, 9, 2361.

(8) (a) Hruszka, P.; Jurga, J.; Brycki, B. *Polymer* **1992**, 33, 248; (b) Miyatake, K.; Shouji, E.; Yamamoto, K.; Tsuchida, E. *Macromolecules* **1997**, 30, 2941.

(9) Iqbal, M.; Wightman, J. P.; Lloyd, D. R.; McGrath, J. E., *J Polym Sci Polym Chem Ed* **1984**, 22, 721.

(10) Ghassemi, H.; McGrath, J. E. *Polymer*, **2004,** 45(17), 5847-5854.

(11) Harrison, W. L.; Wang, F.; Mecham, J. B.; Bhanu, V. A.; Hill, M.; Kim, Y. S.; McGrath, J. E. *J. Polym. Sci. Part A; Polym. Chem*. **2003**, 41, 2264-2276.

(12) Ghassemi, H.; Grace, N.; McGrath, J. E. *Polymer*, **2004,** 45(17), 5855-5862.

(13) Ghassemi, H.; Harrison, W. L; Zawodzinski, T. A; McGrath, J.E.; Polym. Priprint, **2004**, 45(1).

HYDROCARBON AND PARTIALLY FLUORINATED SULFONATED COPOLYMER BLENDS AS FUNCTIONAL MEMBRANES FOR FUEL CELLS

*Natalie Y. Arnett, William L. Harrison, Limin Dong, and J.E. McGrath**

Virginia Polytechnic Institute and State University
Macromolecules and Interfaces Institute and the Department of Chemistry
*jmcgrath@vt.edu

Introduction

Polymer blends are recognized as a valuable technique to combine the properties of two different polymers[1], and has been the topic of several scientific reviews[2]. Polymer blending has been shown to improve many characteristics including impact strength, thermal behavior, and surface character[3]. One obvious advantage is that new polymers do not have to be synthesized to obtain novel materials. Several sulfonated copolymer blends have been investigated as candidates for application in proton exchange membrane fuel cells (PEMFCs). In general, these studies report that the unsulfonated copolymer reduces the aqueous swelling of the sulfonated polymer. However, it has been well documented that the majority of polymer pairs are thermodynamically immiscible[4]. Therefore, many polymer-blend pairs macrophase separate yielding poor adhesion at the interphase of the two polymers. Furthermore, due to the different possible microstructures within the blend, the surface composition can be significantly different from the bulk composition. However this possibility is not always undesirable as in the case of blends of fluorinated polymers that are interesting materials due to their hydrophobic surface properties.

The major objective of this research project is to develop membranes with interesting surface properties and characteristics through controlled polymer blending of fluorinated copolymers and non-fluorinated poly (arylene ether sulfone) copolymers (i.e., BPSH). The chemical structure and intrinsic viscosities of these copolymers are presented in **Figure 1** and **Table 1**, respectively. The partially fluorinated poly (arylene ether sulfone) copolymers (6FBPA-00, 6FS-35 or 6FS-60) have the potential to adhere favorably to Nafion electrode layers, while BPS-35 have mechanical and dimensional stability and good proton conductivity. This research was done in an effort to improve the adhesion and reduce interfacial resistance to commercially available Nafion® electrodes in alternative proton exchange based membrane fuel cells.

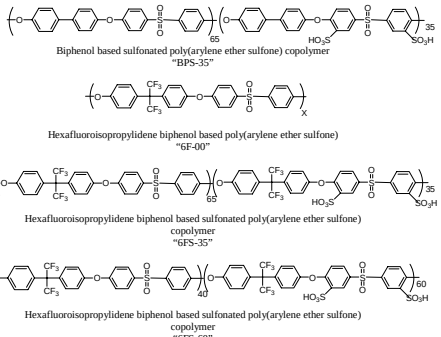

Biphenol based sulfonated poly(arylene ether sulfone) copolymer
"BPS-35"

Hexafluoroisopropylidene biphenol based poly(arylene ether sulfone)
"6F-00"

Hexafluoroisopropylidene biphenol based sulfonated poly(arylene ether sulfone) copolymer
"6FS-35"

Hexafluoroisopropylidene biphenol based sulfonated poly(arylene ether sulfone) copolymer
"6FS-60"

Figure 1. Chemical structures of the directly copolymerized poly(arylene ether sulfone) disulfonated random copolymers utilized.

Table 1. Intrinsic Viscosities of directly copolymerized poly(arylene ether sulfone) disulfonated random copolymers.

Copolymers	[η]
BPS-35	1.14*
6F-00	0.57**
6FS-35	0.52*
6FS-60	0.45**

*NMP with 0.5 M LiBr @ 25°C
**NMP @ 25°C

Experimental

Direct Copolymerization. A typical copolymerization for all sulfonated copolymers is shown in Figure 2 and will be described using the 6F-BPA, 4, 4'dichlorodiphenyl sulfone, and 60 mole percent 3, 3' disulfonated 4, 4'-dichlorodiphenyl sulfone (DCDPS). Firstly, 5.5 mmol 6F-BPA, 2.2 mmol DCDPS, and 3.3 mmol SDCDPS were added to a 3-neck flask equipped with an overhead mechanical stirrer, nitrogen inlet and a Dean Stark trap. Potassium carbonate (6.3 mmol), and sufficient DMAc (18 mL) were introduced to afford a 20% (w/v) solids concentration. Toluene (usually DMAc/Toluene = 2/1, v/v) was used as an azeotroping agent. The reaction mixture was refluxed at 150ºC for 4 hours to dehydrate the system. The temperature was raised slowly to 190ºC by controlled removal of the toluene. The reaction was allowed to proceed for 30 hours, during which the solution became very viscous. The solution was cooled to room temperature and diluted with enough DMAc to allow easier filtering. After filtering through filter paper to remove most of the salts, the copolymer was isolated by coagulation in stirred deionized water. The precipitated copolymer was also washed several times with deionized water to attempt to completely remove salts, and then extracted in deionized water at 60°C overnight. Finally, it was vacuum dried at 120ºC for 24 hours. The BPS-35, 6FS-35 and the 6F-00 were prepared using similar procedure with appropriate monomers and comonomer ratios.

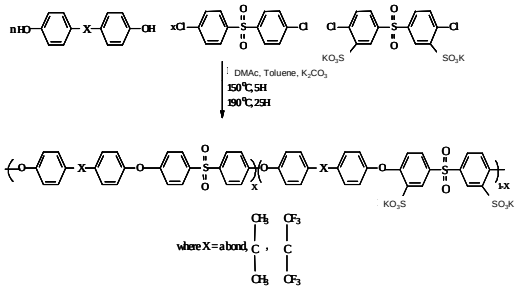

Figure 2. Synthesis of Disulfonated Poly (arylene ether sulfone) copolymers via direct copolymerization

Polymer Blending and Membrane Preparation

Polymer blends were prepared using several methods. Firstly, the potassium salt form by first redissolving approximately 1g of BPS-35 in 10 mL of DMAc (10% w/v). The desired amounts of 6F homopolymer or copolymers were added and the solutions were then stirred at room temperature for 24 hours. Solutions were filtered through a 0.45mm disk onto glass plates. The films were dried gradually via heating lamp with increasing intensity under nitrogen atmosphere. The films were released from the glass substrates by a razor blade. These films were not acidified.

The blending, casting, and drying procedures in the second method were the same as mentioned in the first blending technique. However, these blends were acidified.

In the third method, films of the copolymers were formed by casting transparent solutions (10% w/v) of the copolymers onto glass plates through a 0.45mm disk. The films were dried gradually via a

heating lamp with increasing intensity under nitrogen atmosphere. The films were released from the glass substrates by razor blade and were acidified before blending. The blending casting and drying procedures were the same as described above.

Acidification of Polymer Blend Membrane. The blended poly(arylene ether sulfone) copolymer films were acidified by first boiling in 0.5 M H_2SO_4 for 1hour and immediately followed by extraction in boiling deionized water for 1 hour as described earlier[5].

Characterization

Thermogravimetric Analysis (TGA). The thermal stability (weight loss) of the films in the acid form (5 to 10mg) was determined using a TA Instruments TGA Q 500. The films were first vacuum dried for at least 12 hours and then kept in TGA furnace at 150°C in nitrogen atmosphere for 30 minutes before TGA characterization. The samples were evaluated over the range of 30 to 700°C at a heating rate of 10°C/min in air.

Differential Scanning Calorimetry. The glass transition temperatures (Tg) of the films in the salt form were obtained on a TA Instrument DSC Q 1000. Scans were conducted under nitrogen at a heating rate of 10°C/min. Second heat Tg values are reported as the midpoint of the change in the slope of the baseline.

Contact Angle. The instantaneous (1-5 secs) contact angle measurements were obtained on a First Ten Angstroms (FTA 32) instrument that utilized the "sessile" method. Contact angle was a quantitative method used to determine the hydrophobicity or hydrophilicity of the film surface.

Specific Conductivity. A Hewlett-Packard 4129A LF impedance/gain phase analyzer was used to measure the resistance of each film in the acid form over a frequency range of 10Hz to 1MHz under fully hydrated conditions. The resistance of each film was measured at ~25°C using the conductivity cell.

Results and Discussion

Two partially fluorinated poly (arylene ether sulfone) copolymers were, respectively, blended at different weight fractions with a wholly aromatic, biphenol-based disulfonated poly (arylene ether sulfone) copolymers (BPS-35). Blended films were analyzed in both the salt and acidified form and clarity and miscibility observations were conducted visually. At low weight percentages (0-5 wt%) of the 6F homopolymers and copolymers in BPS-35 transparent films were observed. As the amount of 6F moiety increased, some white discoloration was seen predominately on the peripheral of the cast film. Moreover, at 30 wt% 6F-00 and the 6FS-60 films were opaque and showed large macrophase separation. However, at 30 wt% 6FS-35 a transparent, ductile film was obtained.

The surface characteristics of these solution cast copolymer blends were evaluated via contact angle. Surface enrichment of the fluorinated component revealed by a 26° change in the water-surface contact angle when 10wt% 6FBPA-00 (106°) was added to BPS 35 (80°).

The thermal properties (T_g) of the blends as a function of composition were investigated using DSC. It is well known that ion containing polymers display complex thermal transitions due to the presence of aggregates by the sulfonic acid (of varying sizes) and the influence to the 'normal' polymer transitions[6, 7]. Figure 3 shows selected DSC thermoscans (2nd heat). As shown, the 30wt% 6FS-60 blends displayed two weak, but detectable T_gs. The thermoscan suggested only partial miscibility because the T_gs of the blend was different from the 6FS-60 and BPS-35 copolymers.

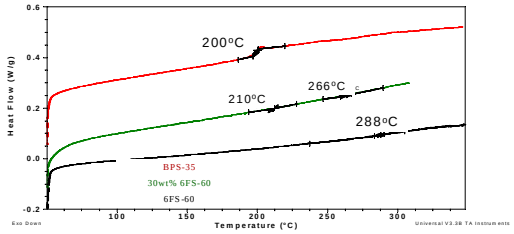

Figure 3. Influence of 6FS-60 blend composition on thermal transition (film in salt form)

Thermo-oxidative investigations of the 6F-00 in BPSH-35 displayed an increase with increasing 6F-00 incorporation. Conversely, the 6FSH-60 : BPSH-35 blends exhibited decreasing thermo-oxidative stability due to the increasing presence of the relatively unstable pendant sulfonic acid group.

Conclusions

A series of copolymer blends composed of varying weight percent BPS-35 with 6F-00, 6FS-35, and 6FS-60 have been made. The polymer blends were characterized via water uptake, conductivity, contact angle, DSC and TGA. The apparent miscibility is a function of blend's composition and copolymer chemical composition.

Current and Future Research

Titration of the polymer blends' actual ion exchange capacities (IEC), which may explain the consequence the blend fraction on the water uptake and conductivity data are ongoing. X-ray photoelectron spectroscopy (XPS) analyses on polymer blends are needed to acquire a better understanding on the surface properties and phenomena. Preparing blends using different copolymer compositions are being investigated as well as additional blending of the copolymers in the acid forms, which will introduce hydrogen bonding that, may improve miscibility. Membrane electrode assemblies (MEA) and voltage-current and durability tests are in progress.

References

1. D. R. Paul and C. B. Bucknall, Eds. Polymer Blends. John Wiley & Sons Ltd, New York, 2000, pp. 1217.
2. For example see: (a) JE Yoo and CK Kim *Polym Int.*, **2004**, **53**,1950; (b) Moon-Sung Kang, Jong Hak Kim, Jongok Won, Seung-Hyeon Moon and Yong Soo Kang, *J. Membr. Sci.*, **2004**.
3. Noshay, A.; McGrath, J. E. Block Copolymers: Overview and Critical Survey; Academic Press: New York, 1977.
4. Charoensirisomboon, P., Inoue, T., Solomko, S.I, Sigalov, G.M., Weber, M. *Polymer* **2000**, 41 7033-7042
5. Y.S. Kim, F. Wang, M. Hickner, S. McCartney, Y.T. Hong, T.A. Zawodzinski, and J.E. McGrath, *Journal of Polymer Science, Part B: Polymer Physics*, **2003,** 41(22).
6. Ehramann, M.; Muller, R.; Galin, J.C.; Bazuin, C.G., *Macromolecules.* **1993**, 26, 4910.
7. Eisenberg, A.; Kim, J., Introduction to Ionomers, Wiley-Interscience Pub., 1998; (b) Wilkes, G. L.; Tant, M. R.; Mauritz, K. A., Eds. Ionomers: Synthesis, Structure, Properties and Applications; Blackie Acadamic and Professional: New York, 1997.